UNIVERSIDAD DE GRANADA

ESCUELA TÉCNICA SUPERIOR DE INGENIEROS DE CAMINOS, CANALES Y PUERTOS

SISTEMAS DE RETENCIÓN DE TIERRAS PARA LA REDUCCIÓN DE LA ENERGÍA DE CONSTRUCCIÓN

TESIS DOCTORAL

JUAN FRANCISCO CARBONELL MÁRQUEZ

Ingeniero de Caminos, Canales y Puertos

2014

Editor: Editorial de la Universidad de Granada
Autor: Juan Francisco Carbonell Márquez
D.L.: GR 1877-2014
ISBN: 978-84-9083-061-1

DEPARTAMENTO DE MECÁNICA DE ESTRUCTURAS E INGENIRÍA HIDRÁULICA

PROGRAMA OFICIAL DE DOCTORADO EN INGENIERÍA CIVIL Y ARQUITECTURA

ESCUELA TÉCNICA SUPERIOR DE INGENIEROS DE CAMINOS, CANALES Y PUERTOS

SISTEMAS DE RETENCIÓN DE TIERRAS PARA LA REDUCCIÓN DE LA ENERGÍA DE CONSTRUCCIÓN

JUAN FRANCISCO CARBONELL MÁRQUEZ

Ingeniero de Caminos, Canales y Puertos

DIRECTOR DE TESIS

ENRIQUE HERNÁNDEZ MONTES

Doctor Ingeniero de Caminos, Canales y Puertos

2014

A Luisa, mi madre

Índice

LISTADO DE FIGURAS **VII**

LISTADO DE TABLAS **XI**

AGRADECIMIENTOS **XIII**

RESUMEN **XVII**

ABSTRACT **XIX**

1.INTRODUCCIÓN **1**
1.1. Objetivos 2
1.2. Metodología 2

2. DISEÑO A FLEXIÓN EN ROTURA DE ELEMENTOS ESTRUCTURALES **5**
2.1. Diseño de secciones rectangulares 8
2.2. Diseño de secciones circulares 12
2.3. Conclusiones 12

3. NUEVAS APORTACIONES AL DISEÑO A FLEXIÓN EN ROTURA DE ELEMENTOS ESTRUCTURALES **15**
3.1. Introducción 15
3.2. Los diagramas de armado óptimo a flexión 16
3.3. El Teorema del Armado Óptimo a Flexión (TAF) 22
3.4. Los dominios de armado óptimo a flexión 24
3.4.1. Los dominios y sus fronteras 25

3.4.2. Representación gráfica de los dominios 30
3.5. Límites al diseño en rotura de losas y elementos placa de hormigón armado 31
3.5.1. El procedimiento propuesto por Brondum – Nielsen [13] 32
3.5.2. El bloque de compresiones del hormigón 34
3.5.3. Distribución de deformaciones plana en estado límite último para losas y placas de hormigón armado en flexión y torsión 36
3.6. Conclusiones 38

4. OPTIMIZACIÓN DE PILOTES DE CONTENCIÓN DE TIERRAS EN ESTADO LÍMITE ÚLTIMO 41
4.1. Introducción 41
4.2. Diagramas de interacción axil – momento flector 44
4.3. Prescripciones normativas relativas al armado longitudinal de pilotes de hormigón 47
4.4. El proceso de optimización 48
4.5. Ejemplo 51
4.6. Pilotes "bi-simétricos" 55
4.7. Conclusiones 58

5. BENEFICIOS ECONÓMICOS Y MEDIOAMBIENTALES DE LOS PILOTES CON ARMADURA ASIMÉTRICA 61
5.1. Introducción 61
5.2. Coste medioambiental del acero 64
5.3. Ejemplo: Línea de Alta Velocidad Madrid – Barcelona – frontera francesa; Tramo Sants – La Sagrera (Barcelona) 65
5.4. Conclusiones 71

6. CONCLUSIONES 73

CONCLUSIONS 77

REFERENCIAS 81

ANEXO 1 87

ANEXO 2 119

ANEXO 3 145

ANEXO 4 169

Listado de figuras

Fig. 2.1. Distribuciones de deformación de la sección en rotura de acuerdo con el Eurocódigo 2[19] 8

Fig. 2.2. Estado límite último en flexo-compresión de una sección rectangular de hormigón armado: (a) Deformaciones; (b) Tensiones; (c) Equilibrio entre acciones exteriores e esfuerzos interiores 9

Fig. 2.3. Procedimiento habitual en el dimensionamiento a rotura de secciones rectangulares sometidas a flexo-compresión uniaxial. Adaptado de [23] 11

Fig. 2.4. Sección circular con armado tradicional 12

Fig. 3.1. Ejemplo de problema de diseño en rotura del armado de una sección rectangular de hormigón armado sometida a flexo-compresión uniaxial 17

Fig. 3.2. Diagrama RSD correspondiente a las soluciones de armado en rotura para la sección de la Fig. 3.1 18

Fig. 3.3. Diagrama LCRD para cuatro combinaciones de cargas en una sección cuadrada de 457 mm de lado. Adaptado de [30] 19

Fig. 3.4. RSD-Biaxial: (a) Deformaciones a nivel de sección en flexión biaxial; (b) Problema ejemplo; (c) Diagrama RSD-Biaxial del problema ejemplo 21

Fig. 3.5. Sección transversal, A_t, en función de la altura del alma, d_w y del espesor de las alas, t_f. Adaptado de [34] 22

Fig. 3.6. Flexo-compresión uniaxial: ambos sistemas (a) y (b) son equivalentes si $e_0 = N_d/M_d$ 25

Fig. 3.7. Estados límite últimos con armado óptimo para secciones rectangulares de hormigón sometidas a flexo-compresión uniaxial. Adaptado de [28] 29

Fig. 3.8. Diagrama de flujo del procedimiento basado en la excentricidad para el armado óptimo de secciones rectangulares de hormigón sometidas a flexo-compresión. Adaptado de [28] 30

Fig. 3.9. Gráfico e_0/h - ν correspondiente a secciones rectangulares con acero B 500 S y recubrimientos de h/10. Extraído de [28] 31

Fig. 3.10. Método de Brondum – Nielsen: (a) acciones aplicadas; (b) geometría de las capas; (c) descomposición en fuerzas de membrana de las cargas aplicadas 32

Fig. 3.11. Equilibrio de fuerzas en el elemento fisurado: (a) fuerzas en el armado para equilibrar las fuerzas normal y tangencial; (b) fuerza principal de compresión en el hormigón 33

Fig. 3.12. Momento flector y axil actuando en la dirección dominante 35

Fig. 3.13. Descomposición de las deformación impuesta por la compresión en la capa *k* según las direcciones del armado de la capa *j* 37

Fig. 3.14. Posiciones del armado para cada capa 38

Fig. 4.1. Armado tradicional de una sección circular 42

Fig. 4.2. Sección transversal según Weber y Ernst [55] 43

Fig. 4.3. Diagramas adimensionales de interacción axil – flector presentes en la literatura clásica: (a) extraído de [2]; (b) extraído de [5]; (c) extraído de [1] 44

Fig. 4.4. Geometría de la sección con armado asimétrico: (a) distribución de deformaciones; (b) bloque de compresiones del hormigón 45

Fig. 4.5. Diagramas de interacción axil – flector para pilotes de radio 600 mm construidos con hormigón HA – 30 y acero B – 500 – S con armado (a) simétrico y (b) asimétrico 47

Fig. 4.6. Efecto de la concentración de barras en la resistencia a flexión simple: (a) Definición de las zonas 1 y 2 en la sección transversal; (b) evolución de la resistencia a flexión simple con la concentración de barras en la zona 2; (c) evolución del diagrama axil – flector con la concentración de barras 49

Fig. 4.7. Proceso de optimización con diámetro de barras constante – $Ø_1 = Ø_2 = Ø$ –. Adaptado de [56] 50

Fig. 4.8. Proceso de optimización con diámetro de barras constante – $Ø_1 < Ø_2$ –. Adaptado de [56] 51

Fig. 4.9. Iteraciones llevadas a cabo en la optimización con $Ø_1 = Ø_2 = 20$ mm 52

Fig. 4.10. Iteraciones llevadas a cabo en la optimización con $Ø_1 = 16$ mm y $Ø_2 = 20$ mm 53

Fig. 4.11. Iteraciones llevadas a cabo en la optimización con $Ø_1 = 16$ mm y $Ø_2 = 25$ mm 54

Fig. 4.12. Iteraciones llevadas a cabo en la optimización con $Ø_1 = 16$ mm y $Ø_2 = 32$ mm 55

Fig. 4.13. Sistemas de riostra empleados en pantallas: (a) puntales horizontales en la construcción de los túneles de Ashford, Gran Bretaña, tomado de [60]; (b) puntal inclinado provisional proyectado en la construcción de los túneles del AVE en el tramo Barcelona Sants – La Sagrera 56

Fig. 4.14. Pilotes "bi-simétricos": (a) los máximos valores de la envolvente de flectores tiene valores similares pero distinto signo; (b) solución a emplear cuando el máximo valor del flector en un sentido es mayor que el máximo en el otro 57

Fig. 4.15. Pilote armado asimétricamente con varios niveles de armado distintos en su longitud 57

Fig. 4.16 Fabricación industrial del armado de un pilote 58

Fig. 5.1. Ciclo de vida útil del acero desde su fabricación hasta su empleo 63

Fig. 5.2. Evolución diaria y media anual del precio de los EUA. Fuente: SendeCO_2 [73] 65

Fig. 5.3. Traza del tramo Sants - La Sagrera. Fuente: ADIF [74] 65

Fig. 5.4. (a) Planta general del falso túnel de enlace entre la estación de Sants y el túnel excavado con tuneladora; (b) Localización de los pilotes asimétricos ejecutados 66

Fig. 5.5. Sección transversal del túnel en el pozo de extracción de tierras 67

Fig. 5.6. Pilote con armadura asimétrica empleado en el tramo Sants- La Sagrera 68

Fig. 5.7. Diagrama interacción axil – momento flector para pilotes simétrico y asimétrico. Flexión positiva 69

Fig. 5.8. Diagrama interacción axil – momento flector para pilotes simétrico y asimétrico. Flexión negativa 69

Listado de tablas

Tabla 4.1 Área de la armadura longitudinal mínima recomendada en pilotes perforados hormigonados in situ 47

Tabla 4.2 Solución original de armado y distintas opciones de búsqueda de armado óptimo 55

Tabla 5.1. Momentos de diseño del pilote 68

Tabla 5.2. Armado longitudinal de los pilotes simétrico y asimétrico 69

Tabla 5.3. Coste del armado simétrico original 70

Tabla 5.4. Coste del armado asimétrico optimizado 70

Tabla 5.5. Resumen de costes para las soluciones simétricas y asimétricas 71

Agradecimientos

Dice el refrán que *"es de biennacido el ser agradecido"* y por ello las primeras páginas de mi tesis doctoral van dirigidas a aquellos que, incluso sin voluntad expresa, han aportado o me han ayudado en algo a completar este trabajo. Si me olvido de alguien, espero que me perdone.

Quisiera acordarme en primer lugar de mis padres, espejo en el cual me he querido mirar siempre por ser ejemplo de trabajo, esfuerzo y superación en el día a día. Creo firmemente que ni una coma de este trabajo hubiese sido escrita sin contar con su ayuda y aliento. También tengo que darle las gracias a mi hermana, María Dolores, cuyos ánimos también han sido indispensables en esta carrera de fondo.

A mi director/jefe/mentor/¡amigo! Enrique Hernández Montes le estaré agradecido toda mi vida por acercarme al apasionante y, a la vez, duro mundo de la investigación en estructuras. ¡Y por tener una paciencia conmigo de mil demonios!: siempre se ha prestado a ayudarme sin reservas. Sus enseñanzas técnicas y, en especial, humanas quedarán grabadas en mi mente y mi corazón para siempre.

A Luisa María Gil Martín le agradezcor su incesante ayuda y colaboración. Por motivos administrativos no ha podido figurar como co-directora de esta tesis pero sus indicaciones me han servido de guía en todo el proceso de redacción de este trabajo.

Mis compañeros durante estos años de trabajo: Andrés Gil, Alejandro Hernández, Francisco García y Alejandro Fernández han hecho que las horas de trabajo se hayan pasado volando. No quisiera dejar de mencionar la ayuda desinteresada de Santiago Díaz en el Laboratorio de Estructuras, ni la del profesor José Rodríguez Montero y sus ayudantes Lázaro Bailón y Javi Luna, ni la del personal de la Biblioteca de la Escuela de Caminos de Granada en la búsqueda de bibliografía que sustenta esta tesis.

No puedo olvidarme de mis amigos durante los estudios en Granada, en especial de mis compañeros en el Colegio Mayor Albayzín: Alfonso Fernández, Alberto Sánchez, Migue Conde, Iván Ruíz, Santi Rubí, Fede Pulido, José Ángel López y su esposa Ana Ramírez, Carlos Lorenzo, Pablo Castillo, Juanfran Merino, Javi Murciano; a todos ellos gracias por los buenos momentos de estudio, camaradería, deporte y, llamémosle, esparcimiento que hemos pasado y por la amistad inquebrantable que se ha forjado entre todos nosotros.

Doy las gracias desde aquí también a la gente de Toronto en especial a Felipe Llano y Mateo Rodríguez porque sin su ayuda no hubiese podido acceder a muchos artículos que forman parte de la bibliografía de esta tesis. También al profesor Oh Sung Kwon que me acogió con gran amabilidad y paciencia asiáticas durante los tres meses que estuve trabajando bajo su supervisión en la Universidad de Toronto.

Y dejo reservadas estas últimas líneas para darle las gracias de todo corazón a mi novia, Blanca, que con su paciencia, cariño y compresión se ha prestado a escucharme hablar sobre hormigón y *tension stiffening* en los momentos de euforia tras obtener buenos resultados y que me ha sabido sacar una sonrisa que borraba cualquier atisbo de cansancio en los momentos duros de trabajo. Sus ánimos en los últimos días de redacción de esta tesis han sido cruciales. Fruto de las horas que hemos estado estudiando juntos, ella Nutrición Humana, yo Hormigón, he aprendido

muchísimas cosas útiles en el día a día relacionadas con la salud; me temo que a ella, en cambio, de poco le va a servir saber que integrando la curvatura se obtiene la deflexión en una viga. Sin embargo, se prestó pacientemente a escucharme cuando, espontáneamente, me ponía a explicarle cosas sobre estructuras de hormigón que a ella no le interesaban y que incluso le hacían perder el tiempo. Creo sinceramente que este trabajo ha servido para unirnos más si cabe.

Resumen

En elementos estructurales como pilares, en los que se pueden emplear secciones circulares, es preciso proveer la suficiente capacidad a la sección de manera que se tengan en cuenta posibles cambios en el sentido de las fuerzas horizontales, tales como el viento o el sismo; para este tipo de secciones la adopción de una disposición de armado longitudinal con simetría radial parece la más adecuada. Sin embargo, otro tipo de estructuras, tales como sistemas de contención de tierras construidos en obras civiles lineales o en obras de edificación como aparcamientos subterráneos, estarán sometidas a envolventes de momentos flectores que variarán mínimamente durante la vida útil de la estructura, ya que su origen se encuentra en la acción que las tierras ejercen sobre la pantalla. En estos casos, parece lógico pensar que soluciones asimétricas de armado longitudinal resulten más adecuadas.

Los elementos estructurales de hormigón lineales como pilotes de contención de tierras son diseñados para cumplir las prescripciones impuestas por el estado límite último de rotura por flexión. La solución a problemas de ese mismo tipo han sido planteadas en los libros de hormigón clásicos desde mediados del siglo pasado, pero la mayoría de ellas implican procedimientos de prueba y error y aproximaciones no válidas universalmente

Recientes estudios de investigación del grupo TEP 190 de la Universidad de Granada hacen énfasis en el armado óptimo de elementos estructurales de hormigón sometidos a estado límite último de flexión. La idea principal introducida por estos trabajos de investigación es que existe un número infinito de soluciones que dotan a la sección de la resistencia adecuada para soportar la flexo-compresión uniaxial en rotura; este hecho permite al ingeniero escoger el armado óptimo teniendo en cuenta factores estructurales o de otra índole, como por ejemplo, facilidad de construcción. Además, dichos trabajos componen un método analítico y sistemático de estudio de la rotura de secciones con aplicaciones tan amplias que van desde el armado óptimo de pilotes para contención de tierras hasta el diseño del armado de elementos losa o placa de hormigón sometidos a acciones en el plano junto con flexión y torsión, procedimientos ambos que se explican en esta tesis.

Así pues, dada su importancia, se presenta en este trabajo una revisión de los procedimientos de armado a flexión en rotura de secciones de hormigón sometidas a flexo-compresión, haciendo hincapié en los estudios realizados por el grupo TEP – 190.

Como resultado de dichos trabajos se expone un procedimiento sistemático de optimización del armado longitudinal de secciones circulares de hormigón, presentando diversos tipos de soluciones asimétricas. El empleo de este procedimiento de optimización no solo supone importantes ahorros económicos, sino que también evita la emisión de grandes cantidades de CO_2 a la atmósfera provenientes de la industria del acero.

Abstract

Due to the fact that it is precise to provide enough flexural capacity in the presence of potentials reversals of horizontal forces such as wind or earthquake loading, it is common to use central symmetrical reinforcement arrangements for cross sections employed in columns members. However, other type of structures such as earth retaining systems built in civil linear works or excavations for parkings are subjected to invariant-in-time bending moment laws which have a clear direction since they are due to the retained earth pressures. In these cases, it is logical to think that an asymmetric solution for the longitudinal reinforcement arrangement is suitable.

Linear concrete members such as beams or the piles above mentioned are designed to observe the prescriptions given by the ultimate state of bending. The solution of these kind of problems are been given in the classical concrete books since mid-century but most of them involve trial-and-error procedures or approximations that are not valid universally.

Recent research studies of group TEP 190 at the University of Granada provide a new approach to optimal design of reinforcement in concrete members subjected to ultimate bending. The main contribution of those works is to recognize that an infinite number of reinforcement solutions can provide a section with adequate strength; this knowledge allows an engineer to choose an optimal combination of reinforcement considering structural and non – structural –

e.g. construction-related – issues. What is more, these works compound an analytic and systematic method of study the ultimate strength of concrete sections with broad applications that range from the optimal design of the reinforcement for concrete piles to the computation of the needed reinforcing steel in concrete slab or shell members subjected to in-plane actions together with flexure and torsion; both procedures are explained within this thesis.

Therefore, a revision of the common procedures to design the longitudinal reinforcement of concrete cross sections is made, emphasizing in the studies proposed by the cited group TEP – 190.

As a result of those works, a systematic optimization procedure for the design of the longitudinal reinforcement of circular concrete cross sections is explained in detail, providing various types of asymmetrical solutions. The employment of this optimization procedure represent not only economic savings but it also avoids the emission of important amounts of CO_2 to the atmosphere coming from the steel industry.

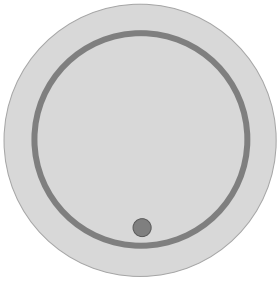

1. Introducción

El sector de la construcción es muy rígido y tradicionalista a la hora de adoptar nuevos criterios de cálculo y soluciones estructurales sin claros beneficios implícitos, tanto más si los criterios y soluciones actualmente aplicados están contrastados y no admiten controversia alguna.

El diseño en rotura de secciones de hormigón sometidas a flexión uniaxial y a acción axil – tracción o compresión – está resuelto desde los años 50 del siglo pasado y está ampliamente recogido en la literatura [1]–[7]. No obstante, dado que el problema está gobernado por numerosas variables, las soluciones ofrecidas por la literatura anteriormente referenciada están basadas en simplificaciones o procedimientos de prueba y error, sin que una solución analítica y universal haya sido propuesta.

Un problema similar a éste, aunque en dos dimensiones, es el armado a flexión, acción axil en el plano y torsor de elementos placa o losa de hormigón. Este problema ha sido abordado por numerosos autores [8]–[12], aunque la solución que ha trascendido en mayor medida ha sido la una de las primeras propuestas, la de Brondum – Nielsen [13], incluso incluida en software comercial de cálculo. Tal es la rigidez del mundo ingenieril que han pasado 40 años para que dicha solución haya tenido que ser revisada por Hernández – Montes et al. [14]

Volviendo al problema lineal, el armado de secciones circulares empleadas en sistemas de contención de tierras se ha venido realizando tradicionalmente disponiendo la armadura longitudinal – constituida por barras de igual diámetro – en el perímetro de la sección transversal a una separación constante. Es claro que la envolvente de momentos flectores a la que estos elementos estructurales se ven sometidos es asimétrica, debido principalmente al empuje de las tierras contenidas. Por tanto, a priori cabe pensar que la solución de armado óptima para este tipo de elementos es un armado asimétrico, tal y como se hace en secciones de vigas, las cuales presentan envolventes de flectores con un marcado carácter asimétrico.

1.1. Objetivos

El objetivo principal de esta tesis es la presentación de un procedimiento de optimización de secciones circulares de pilotes empleados en sistemas de contención de tierras. Como objetivos particulares se encuentran:

a) Exponer los métodos tradicionales del armado a flexión de secciones de hormigón presentado en los libros de hormigón clásicos y explicados en las escuelas de ingeniería

b) Describir un método analítico de cálculo de secciones en rotura que conduce tanto al armado óptimo de secciones circulares de hormigón sometidas a flexión como al armado óptimo de elementos losa o placa bajo acciones de normales en su plano

c) Enunciar un procedimiento sistemático de optimización del dimensionamiento de secciones circulares en rotura a flexión y presentar diferentes opciones de armado óptimo.

d) Cuantificar los beneficios económicos y medioambientales de dicha optimización

1.2. Metodología

En primer lugar, el Capítulo 2 presenta una revisión de la optimización en rotura a flexión de secciones de hormigón armado. Posteriormente, el Capítulo 3 incluye las nuevas aportaciones realizadas por el grupo de investigación TEP-190 de la UGR – donde se enmarca el presente

trabajo – relativas al dimensionamiento a rotura por flexión de elementos estructurales de hormigón armado. El Capítulo 4 presenta la optimización del armado secciones circulares de hormigón, incluyendo varios tipos de soluciones de tipo asimétrica. A continuación, en el Capítulo 5 explica el concepto de coste ambiental derivado del Protocolo de Kioto y se evalúa el ahorro económico y ambiental que supondría el empleo de soluciones de armado optimizadas en una obra real.

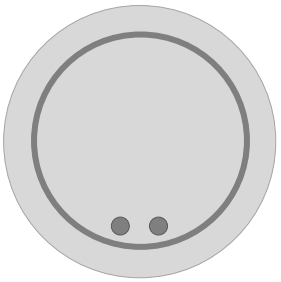

2. Diseño a flexión en rotura de elementos estructurales

La característica más importante de cualquier miembro estructural es su resistencia, la cual debe ser suficiente para soportar, con cierto margen de seguridad, todas las cargas que previsiblemente pueden ejercer algún tipo de acción durante la vida útil de la estructura en la que el miembro se integra. Es lógico, por tanto, dimensionar los elementos estructurales, es decir, seleccionar la geometría y propiedades materiales adecuadas, de manera que la resistencia del elemento sea la idónea para soportar las acciones resultantes de ciertos estados hipotéticos de sobrecarga que resultarán significantemente superiores a los niveles de carga que son realmente esperables durante el uso habitual de la estructura, en otras palabras, el estado de servicio [3].

El comportamiento de los materiales empleados normalmente en construcción – hormigón y acero – ante cargas cercanas a la de rotura del material es eminentemente inelástico y no lineal, es decir, se encuentra fuera del rango donde las tensiones son proporcionales a las deformaciones. Así pues, se entiende cómo la resistencia nominal de un elemento estructural

debe ser calculada teniendo en cuenta el comportamiento inelástico que pueda presentar los materiales que constituyen el citado elemento.

Sin embargo, desde principios del siglo XX se había adoptado el elástico como criterio diseño convencional. Este criterio conducía a una formulación matemática más sencilla y, además, se había comprobado que el empleo de la teoría elástica con una elección cuidadosa para los esfuerzos permisibles de trabajo conducía a un diseño estructural que mostraba comportamientos adecuados bajo las cargas de servicio y que tenía un margen de seguridad suficiente contra el colapso [15]. De esta manera, el criterio elástico dio lugar al denominado "*diseño por esfuerzo de trabajo"*, en inglés *"allowable stress desing"*, que ha permanecido vigente durante décadas. Según el diseño por esfuerzo de trabajo, las secciones de los elementos estructurales son dimensionadas asumiendo comportamiento elástico de los materiales asegurando que, bajo las cargas de servicio, los esfuerzos en los materiales no exceden determinados esfuerzos permisibles de trabajo. El criterio de diseño por esfuerzo de trabajo considera todas las cargas sin realizar ningún tipo de distinción por variabilidad o incertidumbre en su aparición. Además, dado que el comportamiento en rotura de los materiales es inelástico y el cálculo de las tensiones según este método se realiza asumiendo elasticidad, no se puede establecer una evaluación clara del margen de seguridad que posee el diseño realizado.

Tras más de medio siglo de investigación en laboratorio y de experiencia en el campo práctico, sumado a la aparición de los equipos informáticos, se ha logrado conocer en profundidad el complejo comportamiento real de materiales, como por ejemplo el hormigón, dejando además en evidencia los diseños llevados a cabo mediante la aplicación de la teoría elástica. De esta manera, a mediados de los años 50 del siglo pasado el diseño basado en la resistencia máxima se introdujo como alternativa al diseño por esfuerzo de trabajo. El "*diseño por resistencia máxima*" o *"strength design"* considera distintos factores multiplicadores de carga en función del tipo y probabilidad de ocurrencia de la acción considerada y coeficientes reductores de la resistencia que se ajustan en función del tipo de esfuerzo solicitante. Un elemento estructural dimensionado según el diseño por resistencia máxima debe además mostrar un comportamiento

adecuado bajo cargas de servicio, en otras palabras, se debe controlar la deformación experimentada por el elemento o sus vibraciones, así como su posible fisuración en el caso de estructuras de hormigón. De esta manera, los Eurocódigos [16] recogen la distinción entre el cálculo de estructuras en estados límite últimos y los estados límite de servicio. Los estados límites últimos se refieren a la seguridad de las personas y de la estructura y deben verificarse cuando pueda producirse la pérdida de equilibrio o estabilidad de la estructura o una porción de la misma, cuando pueda ocurrir fallo por deformación excesiva o transformación de la estructura en un mecanismo. Por otra parte, los estados límite de servicio son referidos al funcionamiento de la estructura bajo uso normal, a la comodidad de las personas o a la apariencia de las construcciones, entendida esta apariencia como flecha excesiva y/o fisuración extendida.

El dimensionamiento de pilotes de hormigón armado suele realizarse en estado límite último, normalmente sin prestar atención a las comprobaciones relativas al estado límite de servicio, es decir, a las deflexiones y a la fisuración. Cuando se diseña un miembro estructural que estará sometido a flexo-compresión, entre otros estados límite últimos, como ocurre en el caso de los pilotes, hay que comprobar que no se supera el de rotura por tensiones normales a la sección transversal. En otras palabras, este límite último no se superará si no se alcanza un plano de deformación de la sección que produzca rotura. La rotura por flexión es en muchos casos el estado límite más restrictivo, entre otros motivos, debido a que sus coeficientes de seguridad son mucho mayores que los de los estados límite de servicio. No obstante, habrá casos en los que sea preciso prestar atención a los estados límite de servicio de deformación y a la fisuración, algo que comúnmente se obvia en el cálculo de pilotes de contención de tierras [17].

Uno de los motivos que puede justificar la no comprobación de los estados límite de servicio en pilotes es la falta de tratamiento de secciones circulares por los códigos y la normativa de diseño de estructuras de hormigón, de ahí que existan nuevos trabajos de investigación relativos al comportamiento en estado de servicio – fisuración y deformación – de este tipo de secciones[18] (Anexo 1).

En el presente capítulo se introducen y explican las procedimientos habituales recogidos por la bibliografía clásica de estructuras de hormigón para el cálculo en rotura por flexo – compresión uniaxial de secciones de hormigón armado. Primero se presentan el diseño de secciones rectangulares y posteriormente las secciones circulares.

2.1. Diseño de secciones rectangulares

Imagínese que es necesario determinar el acero necesario en las partes inferior y superior, A_s y A'_s, para armar una sección trasversal rectangular. Para obtener la solución al problema, será necesario plantear las ecuaciones de equilibrio de axiles y flectores en la sección trasversal – Eqs –, de manera que se dispondrán de dos ecuaciones, pero tres incógnitas: A_s, A'_s y x, la profundidad de la fibra neutra.

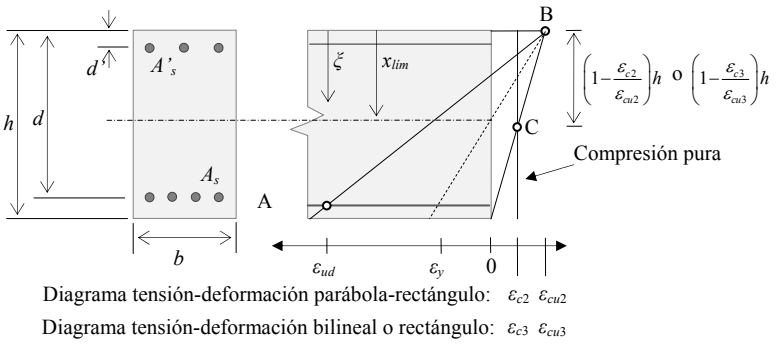

Fig. 2.1. Distribuciones de deformación de la sección en rotura de acuerdo con el Eurocódigo 2[19]

$$N_d = \int_{Ac} \sigma_c dA_c + \int_{A's} \sigma'_s \, dA'_s + \int_{As} \sigma_s dA_s$$
$$M_d = \int_{Ac} \sigma_c y dA_c + \int_{A's} \sigma'_s \, y dA'_s + \int_{As} \sigma_s y dA_s \qquad (2.1)$$

En Eqs. (2.1), σ_c es la tensión en el hormigón σ'_s y σ_s son las tensiones en el acero superior e inferior respectivamente, y es el brazo del área considerada respecto del punto donde se ha referenciado el par $M_d - N_d$ y A_c es el área de hormigón.

De acuerdo con las distribuciones de deformaciones presentadas en la Fig. 2.1, y asumiendo como válida la hipótesis de Bernouilli, según la cual cualquier sección transversal plana de un elemento estructural permanece plana tras la deformación de dicho elemento, y la perfecta adherencia entre hormigón y acero, la deformación de rotura en cualquier fibra situada a una

distancia ξ desde la fibra superior de la sección puede en términos de una sola variable: la posición de la fibra neutra, *x*. Si se considera para el acero un diagrama de tensión-deformación bilineal sin endurecimiento por deformación, el pivote A en la Fig. 2.1 desaparece; en este caso, y considerando el diagrama tensión-deformación rectangular del hormigón propuesto por el Eurocódigo 2 (EC2)[19], la deformación de rotura en la sección viene dada por:

$$\varepsilon(\xi,x)=\begin{cases}\varepsilon_{cu3}\dfrac{x-\xi}{x} & \text{si} \quad 0\le x<h\\ \varepsilon_{c3}\dfrac{x-\xi}{x-\Xi} & \text{si} \quad x\ge h\end{cases} \tag{2.2}$$

donde $\Xi=h\left(1-\varepsilon_{c3}/\varepsilon_{cu3}\right)$. Si se considerase el pivote A, la deformación de rotura, Eq. (2.2), estaría definida por tres tramos en vez de dos. Aprovechando la definición de la deformación en cualquier fibra en términos de *x* dada por Eq. (2.2), realizando una composición de funciones tal y como se propone en Gil – Martín et al. [20], las tensiones en el hormigón y acero pueden ser expresadas también en términos de *x*:

$$\begin{aligned}\varepsilon_c(x)=\varepsilon(\xi,x) \quad &\rightarrow \quad \sigma_c(x)=\sigma_c\left(\varepsilon_c(x)\right)=\left(\sigma_c\circ\varepsilon_c\right)(x)\\ \varepsilon'_s(x)=\varepsilon(d',x) \quad &\rightarrow \quad \sigma'_s(x)=\sigma'_s\left(\varepsilon'_s(x)\right)=\left(\sigma'_s\circ\varepsilon'_s\right)(x)\\ \varepsilon_s(x)=\varepsilon(d,x) \quad &\rightarrow \quad \sigma_s(x)=\sigma_s\left(\varepsilon_s(x)\right)=\left(\sigma_s\circ\varepsilon_s\right)(x)\end{aligned} \tag{2.3}$$

En Eqs. (2.4) las tensiones en el hormigón y del acero, σ_c, σ'_s y σ_s, han sido expresadas como función de *x* aprovechando el hecho de que la deformación en cualquier fibra de la sección puede ser expresada en términos de la posición de la fibra neutra, tal y como dicta la Eq. (2.2)

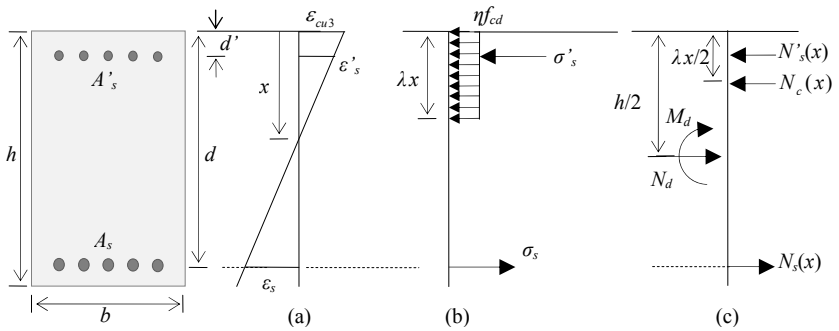

Fig. 2.2. Estado límite último en flexo-compresión de una sección rectangular de hormigón armado: (a) Deformaciones; (b) Tensiones; (c) Equilibrio entre acciones exteriores e esfuerzos interiores

De esta manera, tomando el diagrama rectángulo para el hormigón – Fig. 2.2 –, las Eqs. (2.1), pueden simplificarse como:

$$\begin{aligned} N_u &= N_c(x) + A_s\sigma_s\left(x\right) + A'_s\sigma'_s\left(x\right) \\ M_u &= N_c(x)\left(h_{cg} - z_c\left(x\right)\right) + A_s\sigma_s\left(x\right)\left(h_{cg} - d\right) + A'_s\sigma'_s\left(x\right)\left(h_{cg} - d'\right) \end{aligned} \tag{2.4}$$

donde h_{cg} es la posición del centro de gravedad de la sección transversal con respecto a la fibra superior, $N_c(x)$ la resultante del bloque de compresiones puede expresarse en función de la posición de la fibra neutra x como:

$$N_c(x) = \begin{cases} \eta f_{cd}\, b\, \lambda x & \text{si } 0 \le x < h/\lambda \\ \eta f_{cd}\, b\, h & \text{si } x \ge h/\lambda \end{cases} \tag{2.5}$$

donde f_{cd} es el valor de cálculo de la resistencia a compresión del hormigón, h y b son el canto y el ancho de la sección transversal y λ y η son parámetros definidos por EC2 en función de la resistencia del hormigón.; z_c es la posición del centro de compresiones del hormigón también con respecto a la fibra superior, definida para una sección rectangular como:

$$z_c\left(x\right) = \begin{cases} \dfrac{\lambda\, x}{2} & \text{si } 0 \le x < h/\lambda \\ \dfrac{h}{2} & \text{si } x \ge h/\lambda \end{cases} \tag{2.6}$$

Así pues, el sistema de ecuaciones constituido por Eqs. (2.4) es indeterminado, es decir, al disponer solo de dos ecuaciones y tres incógnitas, el sistema posee infinitas soluciones. Recurriendo a la bibliografía clásica que explica la práctica técnica, el armado de una sección rectangular suele seguir el procedimiento expuesto en la Fig. 2.3. Dicho procedimiento lleva implícito un método de optimización avalado por la práctica, en el cual el parámetro de importancia es la profundidad límite de la fibra neutra, $x_{lím}$, que es el valor de x para el cual el acero tiene una deformación de ε_y – Fig. 2.1 –:

$$x_{lím} = \frac{\varepsilon_{cu}}{\varepsilon_{cu} + \varepsilon_y} d \tag{2.7}$$

Como indica la Fig. 2.3, el dimensionamiento en rotura por flexo-compresión uniaxial de secciones rectangulares de hormigón armado se ha apoyado tradicionalmente en el método de grandes o pequeñas excentricidades de Whitney [21] o en el método denominado por Walther y Mielhbradt [22] de Wuczkowsky o por Jiménez Montoya et al. [5] de Ehlers. No obstante, Páez [6] previene que la generalización del uso del citado método puede conducir al descontrol sobre la entrada en plasticidad de la armadura, haciéndose inviable su aplicación y empleo.

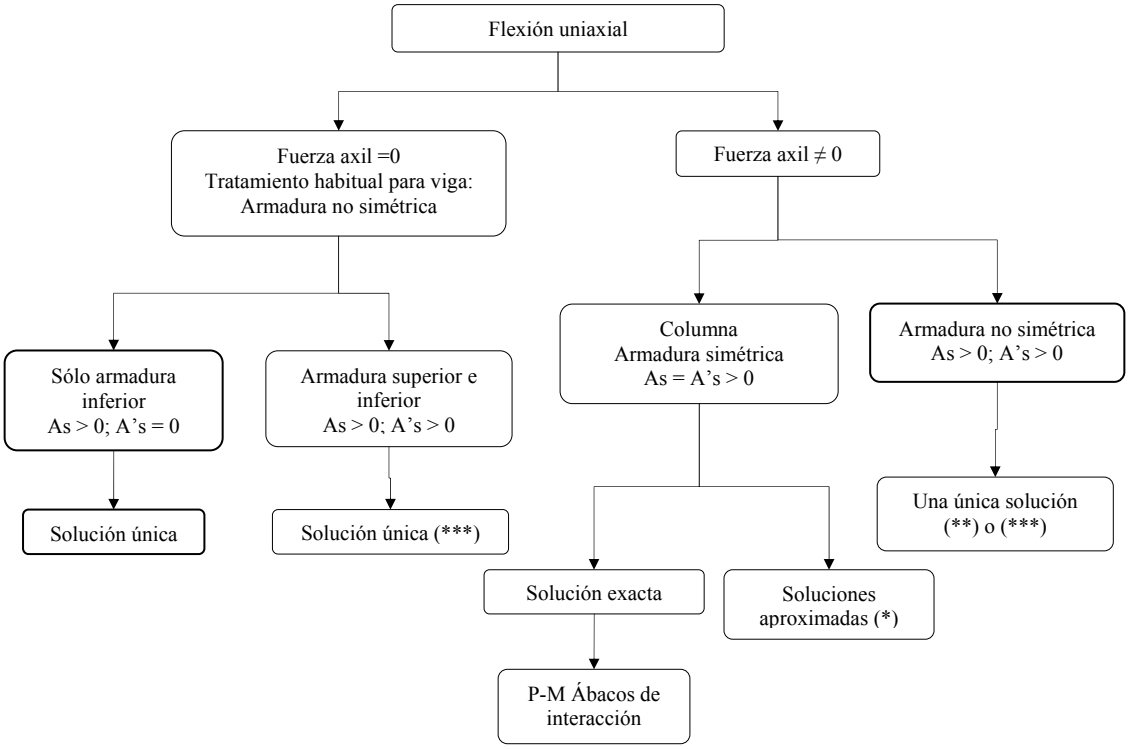

(*) Expresiones aproximadas de Whitney para secciones rectangulares
(**)Método de grandes y pequeñas excentricidades de Whitney junto con el método de Wuczkowsky (o de Elhers) para grandes excentricidades.
(***) Método de la profundidad límite.

Fig. 2.3. Procedimiento habitual en el dimensionamiento a rotura de secciones rectangulares sometidas a flexo-compresión uniaxial. Adaptado de [23]

Hernández – Montes et al. [24] demostraron que puede establecerse un Teorema de Armado a Flexión (TAF) que caracteriza las soluciones óptimas del armado de secciones de hormigón rectangulares sometidas a flexo – compresión uniaxial. El TAF, que será expuesto en el Capítulo 3 de este trabajo, establece cinco condiciones de armado mínimo relativas a la posición de la fibra neutra x y a las áreas de armado inferior y superior, A_s y A'_s.

2.2. Diseño de secciones circulares

En el caso de secciones rectangulares, el concepto de $x_{lím}$ va asociado a la existencia de armadura principal de flexión, A_s, en una posición fija d (canto útil). Tal y como establece el enunciado del TAF, el que A_s esté en fase elástica o plástica es determinante en el dimensionamiento óptimo de la sección.

El hecho de que la armadura de una sección circular se sitúe en un anillo de radio R-r_m, con r_m el recubrimiento mecánico de la armadura – Fig. 2.4 –, hace que el concepto de $x_{lím}$ no tenga una aplicación tan inmediata como sucedía en las secciones rectangulares. En este caso el esquema de la Fig. 2.3 ya no es aplicable y, por tanto, desde el punto de vista de diseño la sección circular y la rectangular son bastante diferentes.

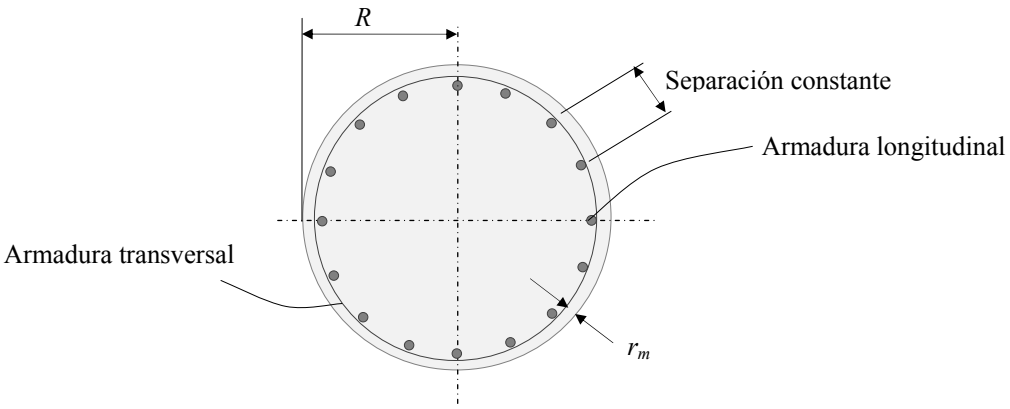

Fig. 2.4. Sección circular con armado tradicional

Tradicionalmente la sección circular se ha armado mediante barras de diámetro único a separación constante – Fig. 2.4 –. El problema así planteado tiene una solución única dado que basta con aumentar el diámetro de las barras o reducir la separación de las mismas hasta alcanzar el momento flector (o el par axil-flector) que solicita a la sección.

2.3. Conclusiones

Aunque inicialmente las estructuras se diseñaban según el criterio de diseño por esfuerzo de trabajo, hoy en día el dimensionamiento estructural se realiza bajo el criterio de resistencia máxima. Este criterio queda recogido en la normativa de diseño estructural de mayor aplicación – Eurocódigos y normativa americana [25] –. Según esta filosofía de diseño, los miembros

estructurales diseñados no pueden rebasar ciertas limitaciones de carácter último – rotura – y de servicio.

Los pilotes empleados en sistemas de contención de tierras han sido tradicionalmente calculados imponiendo las limitaciones correspondientes a estados límite últimos y las limitaciones impuestas por los estados de servicio no son comúnmente comprobadas. Uno de los motivos que justifica este hecho es la falta de tratamiento de secciones circulares por los códigos y la normativa de diseño de estructuras de hormigón, de ahí que existan nuevos trabajos de investigación relativos al comportamiento en estado de servicio – fisuración y deformación – de este tipo de secciones.

Entre los estados límites últimos a cumplir por los pilotes de contención de tierras se encuentra el de rotura por flexión uniaxial. Las bases para el diseño del armado de secciones de hormigón en rotura sometidas a axil y a flexión uniaxial fueron establecidas a mediados del siglo pasado. Muchas de las soluciones derivadas de dichas bases siguen todavía siendo de aplicación pero otras, en cambio, ha podido quedar ya obsoletas y podrían ser sustituidas por otras más económicas u óptimas teniendo en cuenta la facilidad de construcción, ductilidad de la sección o aspectos medio ambientales, entre otros. Además, el gran desarrollo en el campo de la informática ha permitido a la ingeniería estructural hacer uso de complejas técnicas de optimización que eran impensables a la hora de abordarse a mano, sobre todo en secciones distintas a las rectangulares, como las circulares, donde no el nivel de armado de tracción depende de las acciones que solicitan dichas secciones.

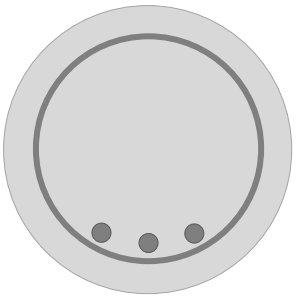

3. Nuevas aportaciones al diseño a flexión en rotura de elementos estructurales

3.1. Introducción

Durante los últimos años, los miembros del grupo de investigación TEP-190 de la Universidad de Granada, principalmente los profesores Hernández-Montes y Gil-Martín, junto con el profesor Aschheim de la Universidad de Santa Clara, en California, ha llevado a cabo tareas investigadoras en el campo del armado óptimo de secciones de hormigón sometidas a flexión y a acción axil (de tracción o compresión) en estado límite último. Fruto de estas investigaciones ha sido la propuesta de un procedimiento de armado óptimo de secciones de hormigón sometidas a flexión compuesta. Los métodos clásicos, incluyendo la división entre pequeñas y grandes excentricidades descritas por Whitney [4], han sido incluidos de una manera gráficamente clara en los Diagramas de Armado Óptimo (RSD, del inglés *Reinforcement Sizing Diagrams*) [26][27], los Dominios de Armado Óptimo [28][29], el Teorema de Armado Óptimo a Flexión (TAF o TOSR, del inglés *Theorem of Optimal Section Reinforcement*) [24][30]. Además, estos fundamentos se aplican también a combinaciones múltiples de carga en [31] o al problema de flexión biaxial [32]. La idea básica bajo todo el trabajo anteriormente citado es que

existen infinitas soluciones de armado que proporcionan una sección con la resistencia adecuada, de manera que el ingeniero a cargo del diseño de la estructura puede seleccionar la solución que más se ajuste a sus necesidades, teniendo en cuenta la minimización del acero empleado, coste total, ductilidad final de la sección, etc.

Aunque el procedimiento de armado óptimo de secciones rectangulares establecido ha quedado principalmente como una aportación académica y sus aplicaciones son limitadas en la práctica, sigue siendo la base teórica que fundamenta el armado óptimo de secciones circulares sometidas a flexo-compresión. Por este motivo, a continuación se explican detalladamente los principios básicos que fundamentan este procedimiento: los Diagramas RSD, los Dominios de Armado Óptimo a Flexión y el Teorema del Armado Óptimo a Flexión. Además, se explica en este Capítulo la revisión al método de Brondum – Nielsen [13] para el dimensionamiento del armado de losas y placas de hormigón realizado por Hernández – Montes et al. [14].

3.2. Los diagramas de armado óptimo a flexión

Los diagramas de armado óptimo a flexión, RSD, fueron introducidos por los profesores Hernández-Montes, Gil-Martín y Aschheim [26][27] como una herramienta para presentar todas las posibilidades de armado a rotura en flexo-compresión de una sección de hormigón. De esta manera, los diagramas RSD permiten al ingeniero a cargo del diseño de la sección seleccionar la opción de armado más conveniente en función de distintos objetivos como el económico o la facilidad de construcción de la sección diseñada.

3.2.1. El diseño de la sección transversal

De la mera observación de la Eq. (2.4) expuesta en el anterior capítulo se puede llegar a la conclusión de que el problema de diseño del armado de una sección de hormigón es un problema indeterminado. Al imponer que $N_u(x)$ iguale al axil N_d y que se cumpla el equilibrio de flectores, $M_d = M_u(x)$, se nos presentan dos ecuaciones pero tres incógnitas: las áreas de armado inferior A_s y superior A'_s y la profundidad de la fibra neutra, x. De esta manera las posibles soluciones al problema son infinitas.

Considérese el caso de la sección transversal de hormigón armado mostrada en la Fig. 3.1. Esta sección se encuentra sometida a un axil de compresión N_d = 1700 kN aplicado el centro de gravedad de la sección bruta y a un momento flector M_d = 2000 kN·m y es necesario determinar el área de armado a disponer en los niveles superior, A'_s, e inferior, A_s, a fin de soportar las acciones anteriormente citadas en estado límite último.

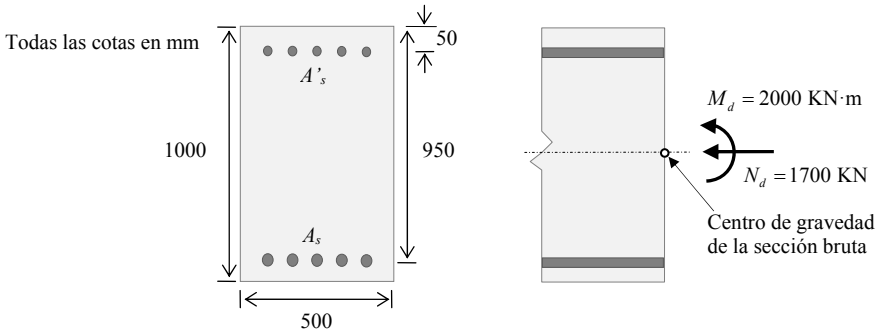

Fig. 3.1. Ejemplo de problema de diseño en rotura del armado de una sección rectangular de hormigón armado sometida a flexo-compresión uniaxial

Si se plantea el equilibrio de momentos con respecto al centro de gravedad de la armadura superior e inferior, los valores de A_s y A'_s, respectivamente, pueden ser expresados como función de la profundidad de la fibra neutra, x, según Eq. (3.1) y pueden ser representados gráficamente en un diagrama RSD tal y como se muestra en la Fig. 3.2.

$$A_s(x) = -\frac{M_d - N_d\left(h_{cg} - d'\right) - N_c(x)\left(d' - z_c(x)\right)}{\sigma_s(x)\left(d - d'\right)}$$

$$A_s'(x) = \frac{M_d - N_d\left(h_{cg} - d'\right) - N_c(x)\left(d - z_c(x)\right)}{\sigma_s'(x)\left(d - d'\right)} \tag{3.1}$$

Así pues, la solución simétrica en este caso correspondería a unas áreas de acero para los armados superiores e inferiores de $A_s = A'_s$ = 4723 mm^2 (6Ø32, 4825 mm^2). En cambio, la solución óptima de armado contaría con un armado superior igual a A'_s = 1616 mm^2 (9Ø16, 1810 mm^2) e inferior A_s = 6187 mm^2 (8Ø32, 6434 mm^2). Esta solución ocurre para el valor límite de la profundidad de la fibra neutra, $x_{lím}$, en la que la deformación en la fibra superior de la sección es ε_{cu3} y la deformación en el armado inferior es ε_y, es decir, el acero se encuentra en

su límite plástico. Si la profundidad de la fibra neutra supera el valor límite, $x > x_{lím}$, la deformación en el acero de la capa inferior de armado es menor que la correspondiente al límite plástico de tal manera que el acero se encuentra en régimen elástico.

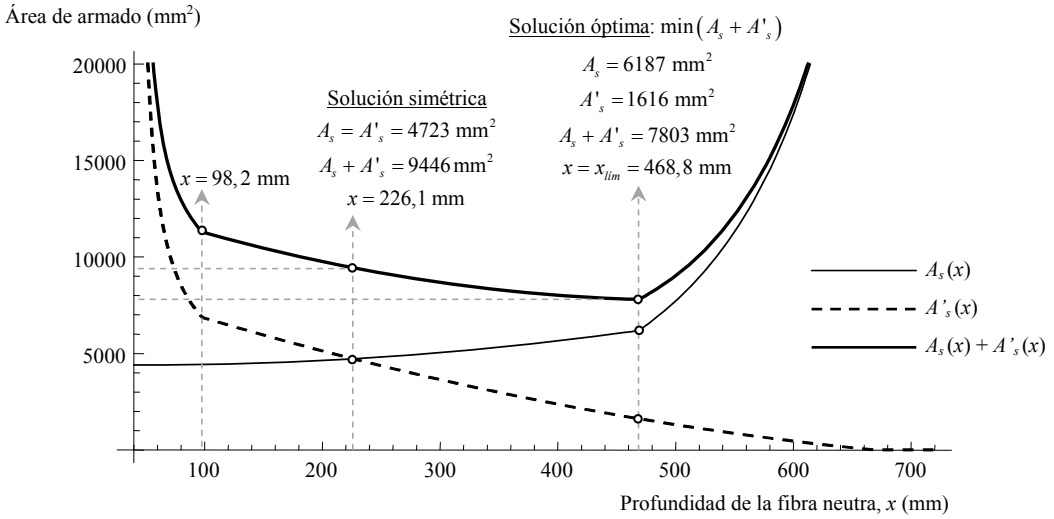

Fig. 3.2. Diagrama RSD correspondiente a las soluciones de armado en rotura para la sección de la Fig. 3.1

La Fig. 3.2 muestra claramente como las necesidades de armado inferior aumentan a medida que *x* crece una vez superada $x_{lím}$; la pérdida de tensión en el acero hace necesaria la presencia de una mayor área para obtener una resultante de tracciones que compense a la resultante del creciente bloque de compresiones. Se puedo observar otro punto singular en el diagrama RSD presentado en la Fig. 3.2, el correspondiente a un valor de la profundidad de la fibra neutra de *x* = 98,2 mm. Para fibras neutras con profundidades inferiores a ésta, el armado superior tiene una deformación de compresión inferior a su límite plástico, ocurriendo el mismo fenómeno que ha sido explicado para la armadura inferior en tracción. Podría así establecerse, tal y como señalan Lee et al. [31], que las soluciones en la franja en el diagrama RSD de la Fig. 3.2 con $x < 98{,}2$ mm está controlada por la tracción y que la franja con $x > x_{lím} = 468{,}8$ mm está controlada por la compresión.

3.2.2. Distintas aplicaciones de los diagramas RSD

Los diagramas RSD tal y como han sido hasta ahora expuestos son de aplicación en el armado de secciones de hormigón rectangulares sometidas a flexo-compresión uniaxial. Lee et al. [31]

introducen los Diagramas de Armado para Combinaciones de Carga (LCRD del inglés, *Load Combination Reinforcement Diagram*), los cuales conjugan los diagramas RSD junto con técnicas de optimización no lineales para determinar la distribución óptima de armado en secciones de este tipo pero sometidas a múltiples combinaciones de axiles y flectores, bajo los criterios de diseño establecidos en la normativa americana ACI-318 [25]. La Fig. 3.3 muestra un ejemplo de diagrama LCRD, contenido en [31] para una sección cuadrada de 457 mm de lado sometida a cuatro combinaciones de axil y flector distintas.

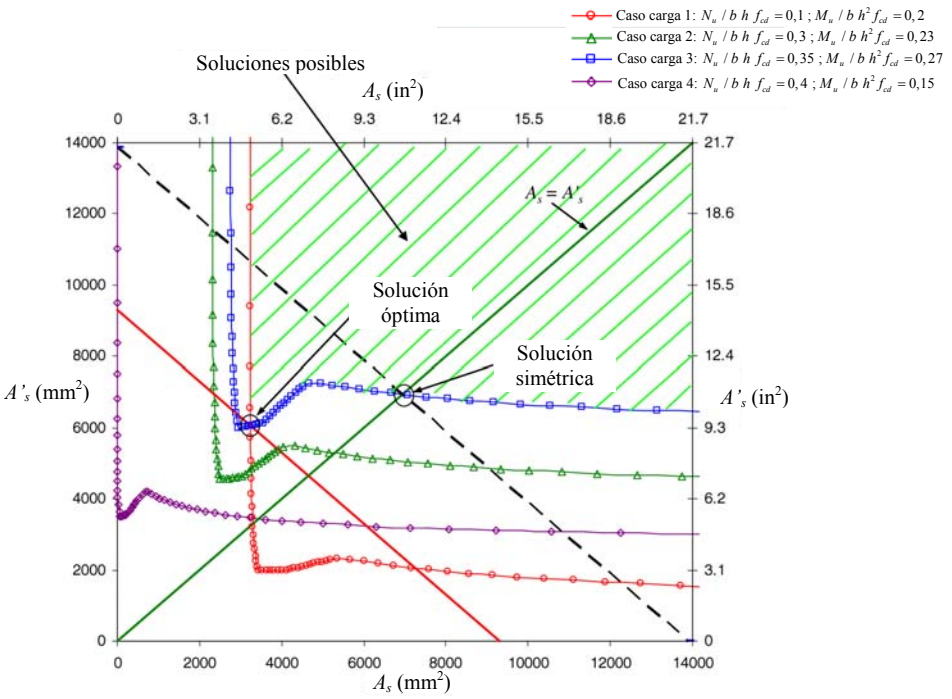

Fig. 3.3. Diagrama LCRD para cuatro combinaciones de cargas en una sección cuadrada de 457 mm de lado. Adaptado de [31]

Otro trabajo de Gil-Martín et al. [32] recoge la aplicación de los diagramas RSD en el armado óptimo de secciones rectangulares de elementos de hormigón sometidos a flexión biaxial y a acción axil. Este procedimiento se plantea como una alternativa al dimensionamiento tradicional de este tipo secciones, en las que las soluciones típicas consisten en barras equidistantes a lo largo del perímetro de la sección con diámetro constante. Las principales diferencias con respecto al caso uniaxial que se presentan al abordar este tipo de problemas son:

i. En el caso de flexión biaxial existen dos momentos flectores aplicados a la sección, cuyas direcciones coinciden con la de los ejes principales de inercia de la sección. Por

tanto, aparecerán tres ecuaciones de equilibrio: una para el axil y una para cada momento flector aplicado

ii. Al contrario que en la flexión uniaxial, en la flexión biaxial la posición de la fibra neutra se define mediante dos variables, ξ y φ, Fig. 3.4(a)

iii. Normalmente es habitual colocar armado en las cuatro caras de la sección empleando un mismo diámetro de barra Ø. De esta manera, para caracterizar el armado resulta solamente necesario conocer la separación de las barras

Para construir los diagramas RSD-Biaxial, se consideran dos separaciones distintas por cada par de caras paralelas (s_h y s_v, Fig. 3.4(b)) con el objetivo de conservar la simetría de la armadura. De esta manera, las incógnitas presentes en el problema son cuatro: ξ y φ, Ø y el ratio s_h/s_v y las tres las ecuaciones:

$$\begin{aligned} N_d &= \sum N_u\left(\xi,\varphi,Ø,s_h/s_v\right) \\ M_{xd} &= \sum M_{xu}\left(\xi,\varphi,Ø,s_h/s_v\right) \\ M_{yd} &= \sum M_{yu}\left(\xi,\varphi,Ø,s_h/s_v\right) \end{aligned} \tag{3.2}$$

Finalmente, la variable independiente que se adopta en el procedimiento es la suma del área de armado colocado en dos caras paralelas, quedando así como variable dependiente el área total de armadura a disponer. La Fig. 3.4(c) muestra el diagrama RSD-Biaxial para una sección rectangular de hormigón sometida a 200 kN de compresión y a unos momentos flectores de 300 kN·m en la dirección del eje fuerte y 250 kN·m en la dirección del débil.

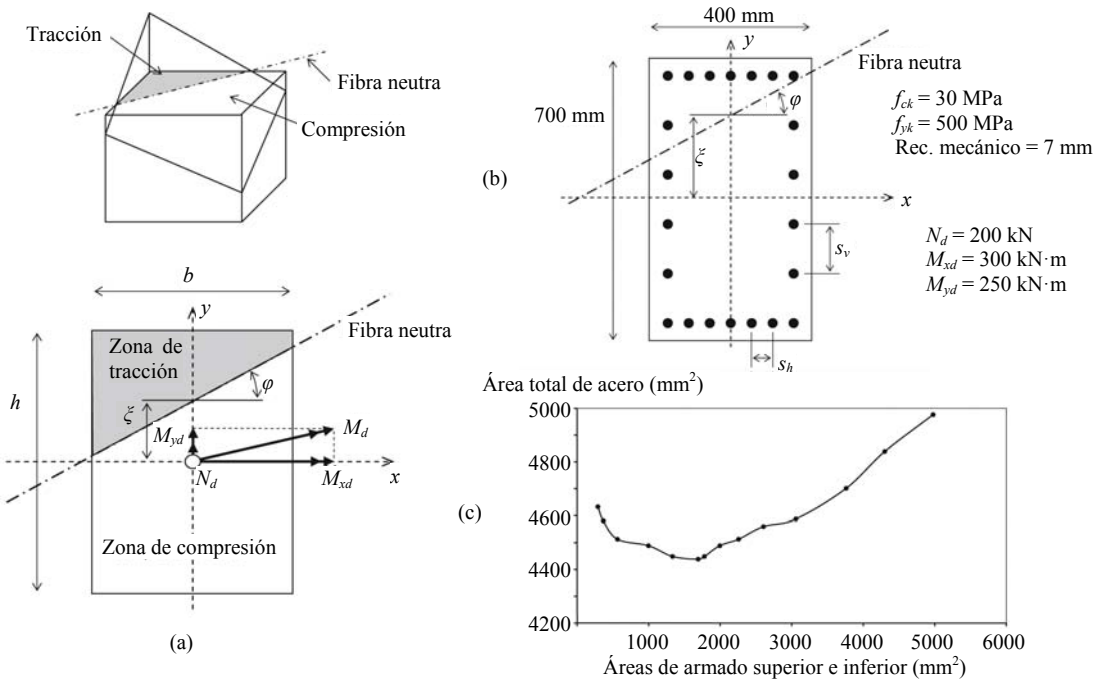

Fig. 3.4. RSD-Biaxial: (a) Deformaciones a nivel de sección en flexión biaxial; (b) Problema ejemplo; (c) Diagrama RSD-Biaxial del problema ejemplo

Por último y como una de las últimas aplicaciones de la técnica RSD, cabe destacar que dicho método de optimización no ha sido solamente de utilidad en el campo del hormigón armado. Así, este método ha sido empleado para la optimización de secciones metálicas armadas en doble-T; primero para secciones en Clase 1 (secciones compactas) según el Eurocódigo 3 (EC3) [33] y posteriormente este trabajo ha sido completado para todo el rango de Clases [34] recogidas en EC3 [35]. En estos trabajos, se parte de un predimensionamiento planteando el agotamiento plástico de las alas, consideradas inicialmente iguales. Posteriormente, para distintos valores de la altura del alma de la sección, el ancho y el espesor de las alas se altera iterativamente hasta encontrar la sección con menor área. En todo el proceso se tienen en cuenta posibles inestabilidades globales o locales por compresión. La Fig. 3.5 presenta las distintas soluciones posibles para armar una sección en doble-T que soporta las mismas cargas que agotan una sección laminada HEB-600 a flexo-compresión uniaxial. Otros ejemplos de la aplicación del RSD en el dimensionamiento de elementos metálicos pueden encontrarse en el Anexo 2 del presente trabajo.

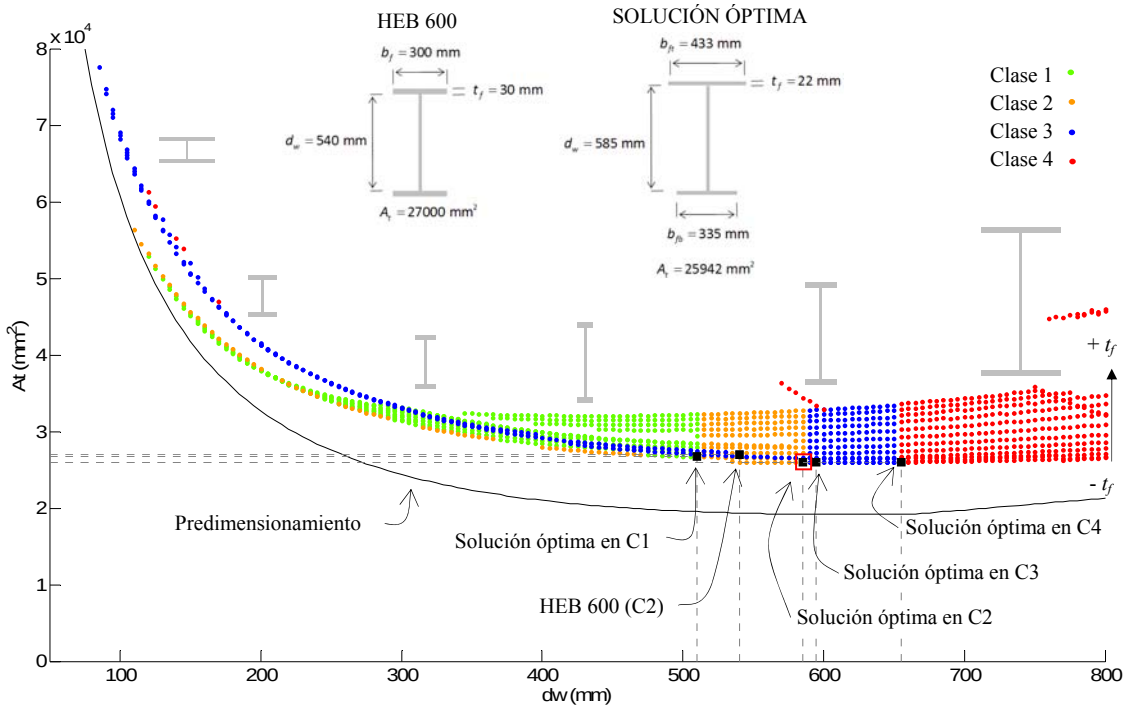

Fig. 3.5. Sección transversal, A_t, en función de la altura del alma, d_w y del espesor de las alas, t_f. Adaptado de [34]

3.3. El Teorema del Armado Óptimo a Flexión (TAF)

Tras la presentación de los diagramas RSD, Hernández-Montes et al. demostraron en [24] que puede establecerse un Teorema de Armado a Flexión que caracterizaba las soluciones óptimas del armado de secciones de hormigón rectangulares sometidas a flexión compuesta, bajo los preceptos de diseño recogidos en el EC2. Posteriormente, el TAF quedó demostrado también aplicando los criterios establecidos en la norma americana ACI-318 [30].

- Teorema:

  En el caso de secciones transversales rectangulares con dos niveles de armadura, A_s y A'_s, se verifica que, de entre las infinitas soluciones de armado de la sección en rotura sometida ésta a flexo-compresión, el mínimo total de armadura, $A_s + A'_s$, se obtiene con una de las siguientes soluciones:

  i. $A_s = A'_s = 0$

  ii. $A_s = 0$ o $A'_s = 0$

iii. x igual o ligeramente superior a su valor límite $x_{lím}$

iv. Deformación de tracción constante en toda la sección transversal igual al máximo de deformación de tracción del acero, ε_{ud} – Fig. 2.2 –, si se considera el endurecimiento por deformación del acero

v. Deformación de compresión constante en toda la sección transversal igual al máximo de deformación de compresión ε_{c3} – Fig. 2.2 –.

Este teorema se demostró numéricamente en [24] según EC2 y en [30] según ACI-318 para un rango de valores habituales en la práctica para las variables implícitas en el proceso: geometría de la sección, características resistentes del hormigón y el acero y cargas aplicadas. Como corolario del TAF, se establece:

- Corolario:

  El armado óptimo en rotura de secciones de hormigón armado con dos niveles de armadura puede resolverse empleando alguna de las siguientes condiciones:

  a. Armadura simétrica ($A_s = A'_s$), solución tradicionalmente empleada en columnas en las que el conjunto de pares $N_d - M_d$ a soportar presenta una simetría clara respecto al eje de N_d

  b. Ausencia del armado superior ($A'_s = 0$), solución apropiada para vigas sometidas a flexión simple con un momento inferior o igual al denominado Momento Límite, $M_{lím}$, que es el momento que produce en la sección una profundidad de fibra neutra igual a $x_{lím}$

  c. Fijar el valor de una de las variables o una relación entre ambas (A_s / A'_s = cte.), quedando el problema determinado al disponer de dos ecuaciones y dos incógnitas

  d. Imponer un valor de la profundidad de la fibra neutra igual al su valor límite ($x = x_{lím}$)

e. Calcular las armaduras necesarias para los cinco casos expuestos en el teorema y comprobar cuál de ellos proporciona la armadura total mínima a disponer

f. Expresar las armaduras superior e inferior en función de x tal y como se presenta en la Eq (3.1), representar el diagrama RSD y seleccionar la solución más adecuada para el caso concreto de estudio

3.4. Los dominios de armado óptimo a flexión

El TOSR expuesto anteriormente proporciona cinco soluciones posibles al problema de armado entre las cuales se encuentra la óptima, en términos de área total de acero. Sin embargo, tal y como el corolario enuncia, el ingeniero tendría que comprobar los cinco casos expuestos en el teorema u obtener el diagrama RSD correspondiente a fin de obtener la solución óptima.

Aschheim et al. [28] presentaron una serie de dominios en coordenadas $N - M$ que proporcionan la condición a imponer en las ecuaciones de equilibrio para obtener el armado óptimo de una sección de hormigón rectangular sometida a acción axil y a flector uniaxial.

López-Martín et al. [29] afrontan el problema de la flexo-compresión uniaxial expresando las solicitaciones en forma de axil excéntrico, tal y como Whitney [21] plantea al hacer la distinción entre problemas de grandes y pequeñas excentricidades; la carga axil aplicada respecto al centro de gravedad de la sección bruta N_d y el momento flector M_d exteriormente aplicados pueden ser equivalentemente por el mismo axil anterior actuando a una excentricidad e_0 respecto a dicho centro de gravedad, de tal manera que (Fig. 3.6):

$$e_0 = \frac{M_d}{N_d} \tag{3.3}$$

De esta manera, las condiciones anteriormente expuestas en el TOSR para el armado óptimo de secciones rectangulares de hormigón pueden ser explicadas en términos de la excentricidad e_0 y la carga de compresión N_d. Así pues, planteando el equilibrio de momentos en distintos puntos de la sección transversal y estableciendo un sistema de coordenadas $N_d - e_0$, pueden establecerse

ciertas regiones o dominios en dicho sistema correspondientes a la condición más adecuada para obtener el armado óptimo de la sección en cuestión.

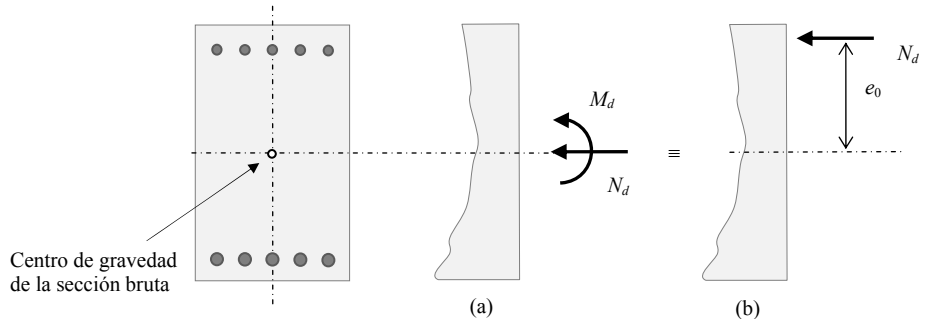

Fig. 3.6. Flexo-compresión uniaxial: ambos sistemas (a) y (b) son equivalentes si $e_0 = N_d/M_d$

3.4.1. Los dominios y sus fronteras

Los pares de valores $N_d - e_0$ para los cuales una sección de hormigón puede permanecer sin armado, esto es $A_s = A'_s = 0$ (dominio 0), pueden ser determinados a partir de la Fig. 3.7(a). Sea una sección cuya fibra superior tiene una deformación de compresión igual a la límite para el hormigón, ε_{cu3}, y una deformación en la fibra inferior que no llega al valor límite de la deformación de rotura del hormigón a tracción, ε_{ctm}. En esta situación, la sección no precisaría ningún tipo de armado ya que el hormigón por sí mismo es capaz de soportar las acciones exteriores. La Fig. 3.7(a) muestra como para estos casos la excentricidad debe permanecer en el rango $0 \le e_0 < h/2$ de tal manera que las siguientes condiciones pueden ser establecidas:

$$N_d = \eta f_{cd} \lambda x b \tag{3.4}$$

$$e_0 = \frac{h}{2} - \frac{\lambda}{2} x \tag{3.5}$$

La combinación de las Eqs. (3.4) y (3.5) conduce al valor de la excentricidad límite, e_{0c}, por debajo de la cual no se precisa armado en la sección ($A_s = A'_s = 0$):

$$e_{0c} = \frac{1}{2}\left(h - \frac{N_d}{\eta f_{cd} b} \right) \tag{3.6}$$

Aunque este caso es teóricamente posible, en la práctica siempre se tendrá que disponer un mínimo de armado, tal y como prescribe la normativa al respecto, por ejemplo EC2 § 9.3.1.1 (1).

Supóngase ahora una solución en el dominio 1 en el que la condición del TOSR a imponer es que $x = +\infty$, es decir, deformación de compresión constante en toda la sección transversal igual al máximo de deformación de compresión ε_{c3}, con lo que la excentricidad e_0 del axil N_d será baja. En algunos casos, el equilibrio en la sección puede hacer necesaria la presencia de armado inferior de compresión ($A_s \neq 0$). El valor frontera de la excentricidad, e_{0h}, que separa los casos en que $A_s = 0$ y $A_s \neq 0$ se calcula en la Eq. (3.7). Estableciendo equilibrio de momentos en el centro de gravedad del armado superior en la situación presentada en la Fig. 3.7(b), pero imponiendo $A_s = 0$, se obtiene que:

$$e_{0h} = \left(\frac{h}{2} - d'\right) - \frac{\eta f_{cd}\, h\, b\left(\frac{h}{2} - d'\right)}{N_d} \tag{3.7}$$

Para los casos en el dominio 1, para los cuales ambos niveles superior e inferior de armado son necesarios ($A_s \neq 0$ y $A'_s \neq 0$), el armado óptimo se obtiene imponiendo la condición 5 del TOSR ($\varepsilon = \varepsilon_{c3}$ en toda la sección). El equilibrio de momentos a nivel del armado superior y el equilibrio de axiles (Fig. 3.7(b)) en la sección permiten obtener las áreas de acero necesarias:

$$A_s = \frac{\left(\frac{h}{2} - d' - e_0\right) N_d - \eta f_{cd} h\, b\left(\frac{h}{2} - d'\right)}{\left(d - d'\right)\sigma_s\left(x = +\infty\right)} \tag{3.8}$$

$$A'_s = \frac{N_d - \left[\eta f_{cd} h\, b + A_s \sigma_s\left(x = +\infty\right)\right]}{\sigma'_s\left(x = +\infty\right)} \tag{3.9}$$

El valor frontera e_{0h} separa los dominios 1 y 2. En el dominio 2, la condición adicional a imponer en las ecuaciones de equilibrio presentadas en Eq. (2.4) para obtener la solución óptima de armado es $A_s = 0$. En este dominio, la sección puede estar parcial o completamente

comprimida, esto es $x \le h/\lambda$, y el área de armado superior necesaria se puede obtener imponiendo equilibrio de axiles en la Fig. 3.7(c):

$$A'_s = \frac{N_d - \eta f_{cd} \lambda x\, b}{f_{yd} - \eta f_{cd}} \tag{3.10}$$

La profundidad de la fibra neutra, x, a introducir en la Eq. (3.10) puede obtenerse del equilibrio de momentos en la posición del armado superior (Fig. 3.7(c)):

$$\left(\frac{h}{2} - d' - e_0\right) N_d = \eta f_{cd} \lambda x\, b \left(\frac{\lambda x}{2} - d'\right) \tag{3.11}$$

En el dominio 3, la condición a imponer en el TOSR se corresponde con $x = x_{lím}$. En este caso, la deformación en la armadura inferior coincide con la correspondiente al límite elástico del acero. El valor de la excentricidad e_0 que separa los dominios 2 y 3, $e_{0lím}$, se calcula a partir del equilibrio en la Fig. 3.7(d) imponiendo que $A_s = 0$ (dominio 2) y que $x = x_{lím}$ (dominio 3):

$$e_{0lím} = \left(\frac{h}{2} - d'\right) - \frac{\eta f_{cd}\ \lambda x_{lím} b \left(\frac{\lambda x_{lím}}{2} - d'\right)}{N_d} \tag{3.12}$$

El valor de la excentricidad $e_{0lím}$, marca la clásica frontera entre problemas de grandes y pequeñas excentricidades [4].

En el dominio 3, tanto el nivel superior como el inferior de armado son necesarios. Tomando momentos respecto al nivel inferior de armado y estableciendo el equilibrio de axiles (Fig. 3.7(d)) se obtienen los valores de las áreas de armado a disponer en la sección:

$$A'_s = \frac{\left(e_0 + d - \frac{h}{2}\right) N_d - \eta f_{cd} \lambda x_{lím} b \left(d - \frac{\lambda x_b}{2}\right)}{\left(f_{yd} - \eta f_{cd}\right)\left(d - d'\right)} \tag{3.13}$$

$$A_s = \frac{\eta f_{cd} \lambda x_{lím} b + A'_s \left(f_{yd} - \eta f_{cd}\right) - N_d}{f_{yd}} \tag{3.14}$$

El último dominio a considerar es el dominio 4, Fig. 3.7(e), en el que el armado superior no es necesario ($A'_s = 0$). El valor frontera de la excentricidad, e_{02} que separa los dominios 3 y 4 se deduce considerando el equilibrio en la Fig. 3.7(d) imponiendo $A'_s = 0$:

$$e_{02} = -\left(d - \frac{h}{2}\right) + \frac{\eta f_{cd}\ \lambda x_{lím} b\left(d - \frac{\lambda x_{lím}}{2}\right)}{N_d} \tag{3.15}$$

Para obtener el área de armadura inferior a disponer en soluciones en el dominio 4 resulta necesario conocer el valor de la profundidad de la fibra neutra, valor que es calculado estableciendo el equilibrio de momentos al nivel de la armadura inferior, Eq. (3.16). Una vez x es conocido, el equilibrio de acciones axiles proporciona el área de acero a disponer en el nivel inferior, Eq. (3.17).

$$\left(e_0 + d - \frac{h}{2}\right) N_d = \eta f_{cd} \lambda x\ b\left(d - \frac{\lambda x}{2}\right) \tag{3.16}$$

$$A_s = \frac{\eta f_{cd} \lambda x\ b - N_d}{f_{yd}} \tag{3.17}$$

Tal y como se ha mostrado anteriormente, el cálculo de los distintos valores de la excentricidad que marcan la frontera entre unos dominios de armado y otros son fácilmente calculables; el único cálculo auxiliar que necesitan es el del valor límite de la profundidad de la fibra neutra, $x_{lím}$, algo que, a su vez, tampoco conlleva mucha complejidad. Así pues, el ingeniero puede calcular la excentricidad del axil de cálculo y, por comparación con los valores fronteras, conocer que condición ha de imponer en las ecuaciones de equilibrio de momentos y de axiles en la sección, Eq. (2.4). El diagrama de flujo de la Fig. 3.8 resume el procedimiento que podría llegar a seguirse.

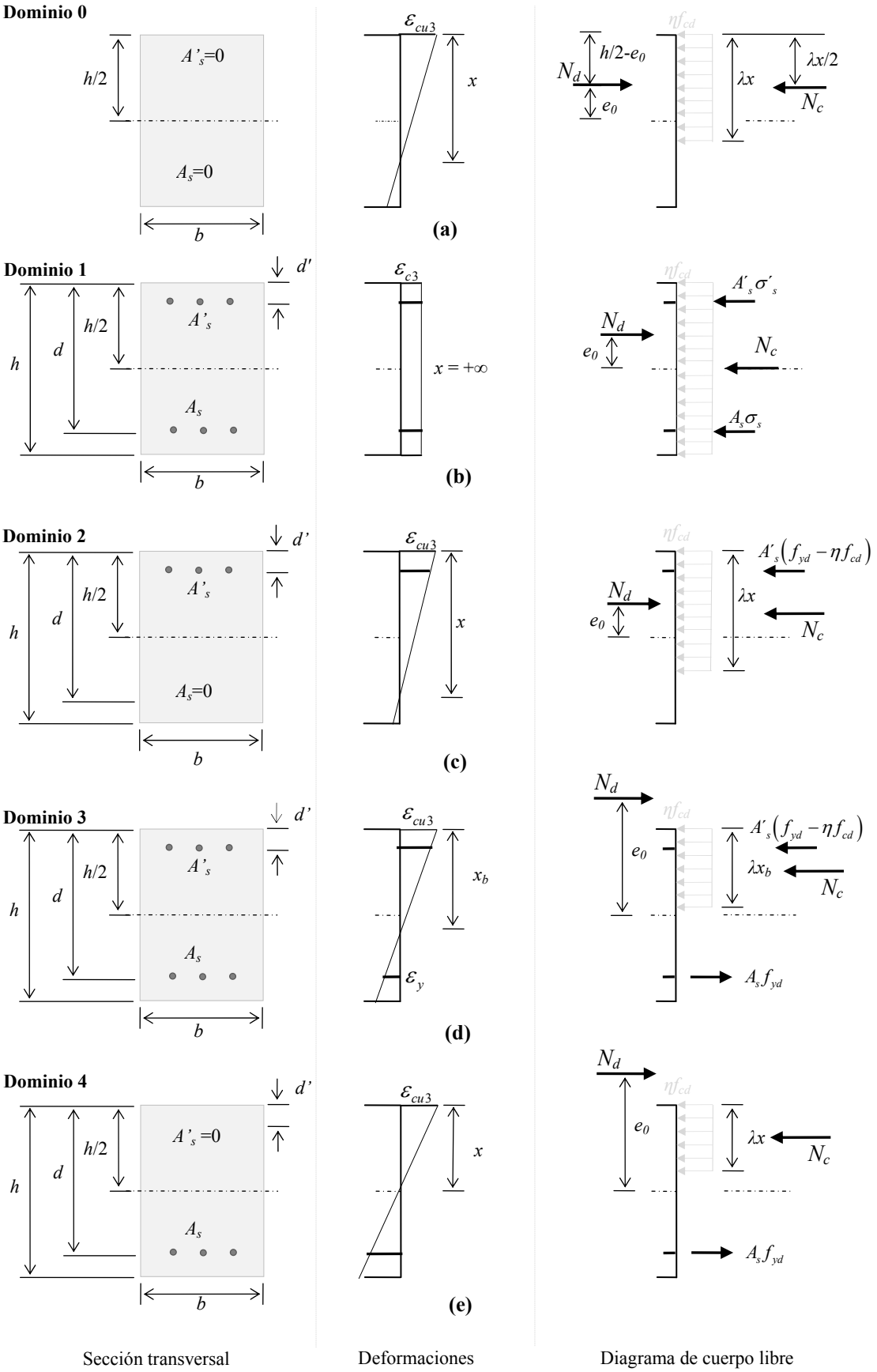

Fig. 3.7. Estados límite últimos con armado óptimo para secciones rectangulares de hormigón sometidas a flexo-compresión uniaxial. Adaptado de [29]

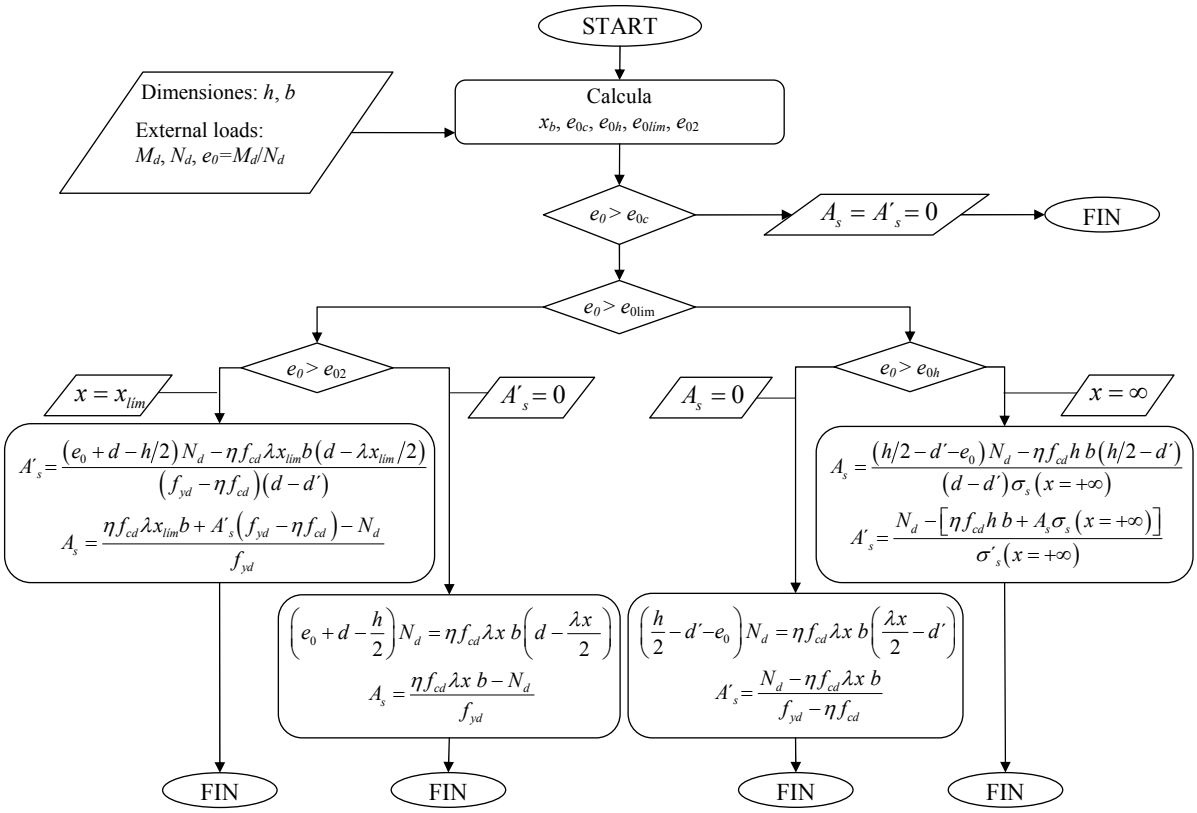

Fig. 3.8. Diagrama de flujo del procedimiento basado en la excentricidad para el armado óptimo de secciones rectangulares de hormigón sometidas a flexo-compresión. Adaptado de [29]

3.4.2. Representación gráfica de los dominios

Una manera alternativa para representar las anteriores fronteras y dominios que permiten obtener el armado óptimo de secciones rectangulares de hormigón es usar un gráfico como el representado en la Fig. 3.9. En este gráfico el valor del ratio e_0/h (ratio entre la excentricidad del axil y el canto de la sección) se representa como una función del axil reducido $\upsilon = N_d / (\eta f_{cd} bh)$. La principal ventaja que presenta este gráfico es que, si los recubrimientos superior e inferior y el límite acero no cambia, el gráfico no depende del problema tratado. La región horizontal marcada en la gráfica de la Fig. 3.9 se corresponde con $e_0/h < 1/30$; esta zona debe ser excluida de acuerdo con las prescripciones de EC2 § 6.1 (4) [19] relativas a limitaciones de excentricidades mínimas.

Ejemplos de aplicación de los dominios de rotura pueden encontrarse en el Anexo 3 del presente trabajo.

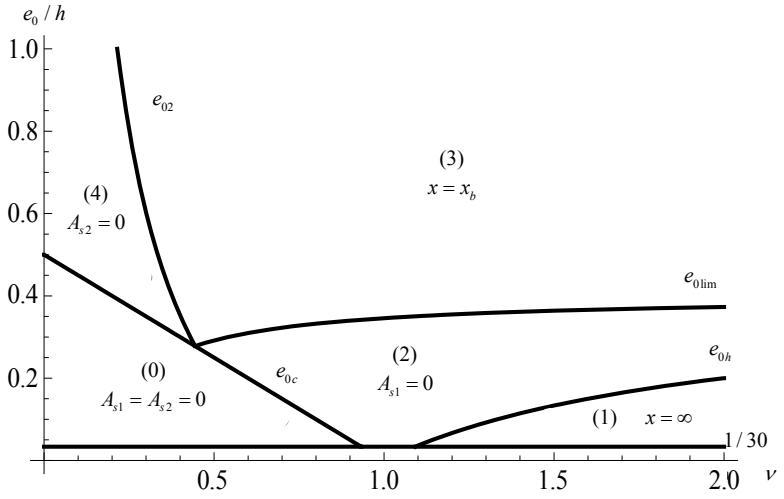

Fig. 3.9. Gráfico e_0/h - ν correspondiente a secciones rectangulares con acero B 500 S y recubrimientos de h/10. Extraído de [29]

3.5. Límites al diseño en rotura de losas y elementos placa de hormigón armado [14]

El problema del diseño del armado de una placa o losa de hormigón armado en estado límite último para soportar fuerzas de membrana junto con esfuerzos axiles y torsores no ha sido resulto universalmente. Existen en la literatura muchas aportaciones que tratan de obtener una solución general. Una de los primeros procedimientos prácticos que han sido aceptados como válidos es el propuesto por Bromdum – Nielsen [13], que trata el elemento 2D como si se estuviese compuesto por tres capas, siendo las externas las responsables de soportar los esfuerzos de membrana. Este procedimiento es acorde a las sugerencias propuestas en el Código Modelo 2010 [36] en las que se establecen: "*los elementos placa pueden ser modelizados como si estuviesen compuestos por tres capas. Las capas exteriores proporcionan resistencia a los efectos en el plano producidos por el flector y por las cargas axiles en el plano, mientras que la capa interior proporciona la transferencia del cortante entre la capas exteriores*."

Las aportaciones anteriormente mencionadas [9]–[13], [37], [38] tienen en común la división en capas del elemento placa o losa, que las tensiones de compresión son distribuidas de manera uniforme a través del espesor de la capa considerada –el bloque de compresiones de Whitney en vigas – y que el acero en tracción se supone que ha entrado en deformación plástica – su tensión de tracción es f_y –.

Esta última hipótesis relativa a la entrada del acero en tracción en cedencia es la que parece a priori cuestionable. De manera similar a como ocurre en el armado en estado límite último por flexión de elementos lineales, la entrada en cedencia del acero en tracción de una capa debiera estar ligada a la profundidad del bloque de compresiones de la capa opuesta, bajo las hipótesis de que las secciones planas permanecen planas tras la deformación.

3.5.1. El procedimiento propuesto por Brondum – Nielsen [13]

El elemento placa o losa de espesor h considerado tiene que soportar unas fuerzas normales N_x y N_y, el cortante en su plano N_{xy}, los momentos flectores M_x y M_y y el momento torsor M_{xy}, dadas dichas acciones por unidad de longitud y consideras positivas de acuerdo a como se indica en Fig. 3.10 (a). Si el elemento se divide en capas tal y como muestra la Fig. 3.10 (b), todas las acciones aplicadas pueden descomponerse en fuerzas de membrana aplicadas al nivel de la superficie media de cada una de las capas de acuerdo con las Eqs. (3.18). La Fig. 3.10 (c) muestra dicha descomposición.

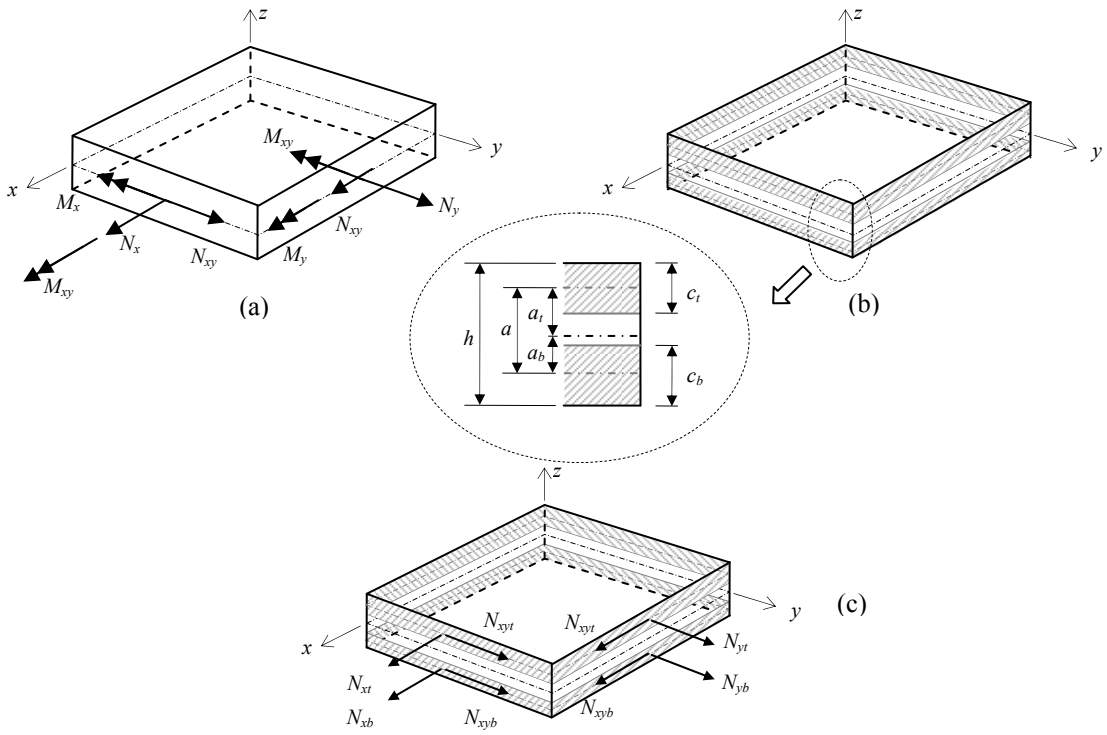

Fig. 3.10. Método de Brondum – Nielsen: (a) acciones aplicadas; (b) geometría de las capas; (c) descomposición en fuerzas de membrana de las cargas aplicadas

$$N_{xt} = N_x \frac{a_b}{a} - \frac{M_x}{a} \qquad N_{xb} = N_x \frac{a_t}{a} + \frac{M_x}{a}$$
$$N_{yt} = N_y \frac{a_b}{a} - \frac{M_y}{a} \qquad N_{yb} = N_y \frac{a_t}{a} + \frac{M_y}{a} \tag{3.18}$$
$$N_{xyt} = N_{xy} \frac{a_b}{a} - \frac{M_{xy}}{a} \qquad N_{xyb} = N_{xy} \frac{a_t}{a} + \frac{M_{xy}}{a}$$

A su vez, estas fuerzas de membrana deben ser resistidas por el hormigón y el acero de cada una de las capas. Para calcular las fuerzas resultantes de compresión en el hormigón y de tracción en el acero, y para cada una de las capas, se imponen el equilibrio de fuerzas en una porción de la capa cuyos dos de sus lados son paralelos a las direcciones *x* e *y* y el tercero se corresponde con una grieta en la capa, con longitud igual a 1 y formando un ángulo α_k con la dirección *x* – Fig. 3.11 –. El armado óptimo de la capa *k*, siendo *k* = *t* para la capa superior y *k* = *b* para la inferior, ocurre cuando α_k = 45º. En este caso, las fuerzas de tracción en el armado para las direcciones *x* e *y*, N_{xak} y N_{yak}. ,y la fuerza de compresión en el hormigón N_{ck} son:

$$N_{xak} = N_{xk} + \left|N_{xyk}\right|$$
$$N_{yak} = N_{yk} + \left|N_{xyk}\right| \tag{3.19}$$
$$N_{ck} = 2\left|N_{xyk}\right|$$

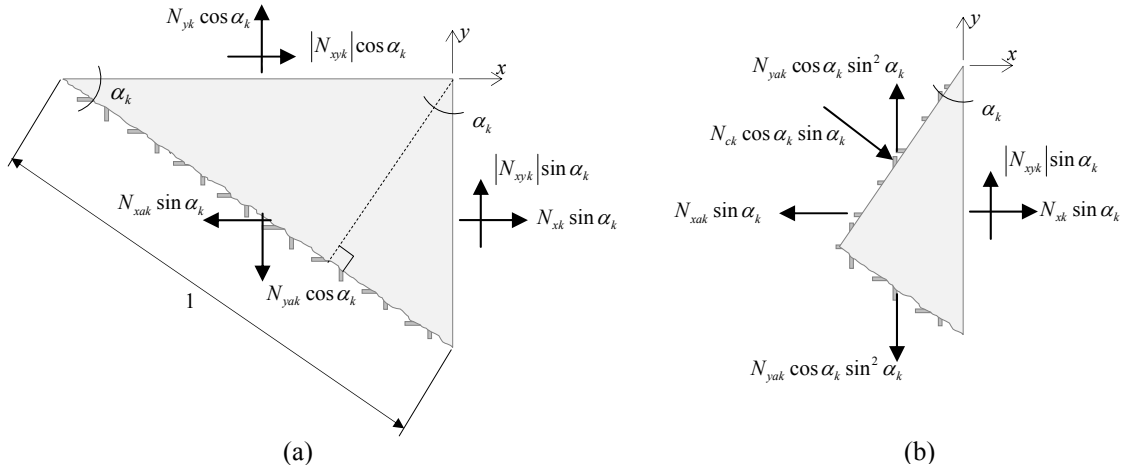

Fig. 3.11. Equilibrio de fuerzas en el elemento fisurado: (a) fuerzas en el armado para equilibrar las fuerzas normal y tangencial; (b) fuerza principal de compresión en el hormigón

La anterior solución es válida si las fuerzas en el armado en las dos direcciones, *x* e *y*, son de tracción. Si esta condición no se cumple, considerando las fuerzas de tracción como positivas, entonces aparece la siguiente casuística:

a) Si $N_{xk} < -\left|N_{xyk}\right|$ y $N_{yk} \geq -\left|N_{xyk}\right|$, el armado en la dirección *x* está comprimido. En esa situación se impone que $N_{xak} = 0$ – no se dispone armadura en *x* – y el ángulo α_k determina el valor de la tracción en el armado en dirección *y* y en de la compresión en el hormigón:

$$\begin{aligned} \alpha_k &= \arctan\left(\frac{\left|N_{xyk}\right|}{-N_{xk}}\right) \\ N_{yak} &= N_{yk} + \left|N_{xyk}\right| \tan\alpha_k \\ N_{ck} &= \left|N_{xyk}\right|\left(\tan\alpha_k + \cot\alpha_k\right) \end{aligned} \tag{3.20}$$

b) Si $N_{yk} < -\left|N_{xyk}\right|$ y $N_{xk} \geq -\left|N_{xyk}\right|$, el armado en la dirección *y* está comprimido. En esa situación se impone que $N_{yak} = 0$ – no se dispone armadura en *y* – y el ángulo α_k determina ahora el valor de la tracción en el armado en dirección *y* y nuevamente la compresión en el hormigón:

$$\begin{aligned} \alpha_k &= \arctan\left(\frac{-N_{yk}}{\left|N_{xyk}\right|}\right) \\ N_{xak} &= N_{yk} + \left|N_{xyk}\right| \cot\alpha_k \\ N_{ck} &= \left|N_{xyk}\right|\left(\tan\alpha_k + \cot\alpha_k\right) \end{aligned} \tag{3.21}$$

c) Por último si $N_{xk} < -\left|N_{xyk}\right|$ y $N_{yk} < -\left|N_{xyk}\right|$ ambas direcciones de armado están comprimidas y, por tanto, no será necesario disponerlas en la capa *k*. La compresión en el hormigón queda:

$$N_{ck} = \frac{1}{2}\left(N_{xk} + N_{yk}\right) - \frac{1}{2}\sqrt{\left(N_{xk} - N_{yk}\right)^2 + 4N_{xyk}} \tag{3.22}$$

3.5.2. El bloque de compresiones del hormigón

Si las dimensiones de las capas se conocieran de antemano, el problema quedaría resuelto sin mayores dificultades. Sin embargo, la determinación de las fuerzas anteriormente explicada no tiene validez si dichas dimensiones no se conocen. Por ello, es necesario establecer un

procedimiento iterativo de prueba y error para determinar la geometría de las capas y conocer las fuerzas que actuarán en el hormigón y las necesidades de armado. No obstante, se consideran conocidas los niveles del armado en ambas capas y en cada dirección fruto de un predimensionamiento inicial.

El procedimiento iterativo selecciona la dirección, *x* o *y*, en la cual actúa el momento flector, *M*, de mayor magnitud. Este momento comprimirá una capa y provocará tracciones en la otra capa del elemento. La superficie media de la capa traccionada se coloca en la posición de la armadura de tracción correspondiente a la dirección del momento flector. Es decir, si el mayor de los flectores aplicados es $M = M_x$ y éste provoca compresiones en la capa superior, la superficie media de la capa inferior se supondrá colocada al nivel del armado inferior en la dirección *x*. De esta manera, si en la dirección del momento *M* actúa un axil de tracción *N*, la resultante de momentos M_a a nivel del armado en la capa inferior es – Fig. 3.12–:

$$M_a = M - N\, e_j \tag{3.23}$$

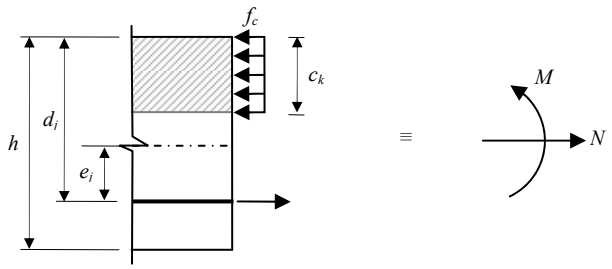

Fig. 3.12. Momento flector y axil actuando en la dirección dominante

En la Eq. (3.23) e_j es la distancia entre la superficies media del elemento placa y de la capa inferior. El momento M_a debe quedar equilibrado con el bloque de compresiones en la capa superior de profundidad c_k. Utilizando este planteamiento de equilibrio, se puede obtener una primera estimación de la profundidad de la capa *k*, en este caso, la superior, $k = t$. Como se ha supuesto que la superficie media de la capa inferior – capa $j = b$ – se sitúa a nivel del armado en *x* en dicha capa, los valores de las fuerzas de membrana según dados por las Eqs. (3.18) pueden calcularse, así como las fuerzas en cada dirección de armado y en el hormigón para cada capa, según Eqs. (3.19) - (3.22). Por último, una vez conocidas las fuerzas de compresión en el

hormigón para cada capa, se puede determinar si las profundidades supuestas al inicio del procedimiento son adecuadas dado que:

$$c_k = \frac{N_{ck}}{f_c} \tag{3.24}$$

con f_c la resistencia del hormigón a compresión. Si la profundidad obtenida del equilibrio del bloque de compresiones y el momento M_a no resulta suficiente, dicho parámetro se incrementará y se realizarán las iteraciones pertinentes hasta que se obtenga el valor adecuado.

3.5.3. Distribución de deformaciones plana en estado límite último para losas y placas de hormigón armado en flexión y torsión

Una vez que la geometría de las capas ha sido determinada según el proceso iterativo explicado anteriormente, conocidas las fuerzas de tracción en el acero, será necesario proveer del acero suficiente en cada dirección y en cada capa a fin de que se resistan las citadas fuerzas. El trabajo original de Brondum – Nielsen [13] simplemente toma dicha fuerzas por la resistencia de diseño del acero empleado, f_y. No obstante, este procedimiento puede reconsiderarse ya que el estado real de tensiones del acero en una capa debería depender de la profundidad del bloque de compresiones en el otro, de manera similar a como se procede en el cálculo y diseño de vigas de hormigón armado; en el caso de las losas y placas, se tienen en cuenta las siguientes hipótesis para la distribución de deformaciones plana para el diseño en estado límite último de losas y placas de hormigón armado en flexión y torsión:

1. La resistencia a rotura de losas y placas de hormigón armado sometidas a flexión y torsión con o sin fuerzas axiles se corresponde con una distribución plana de deformaciones.

2. La orientación de la distribución de deformaciones planas de rotura en el plano del elemento placa o losa viene definida por la dirección principal de compresión en el hormigón.

Dado que estas hipótesis se emplearán en el proceso de diseño, el Teorema del Límite Superior garantiza que las fuerzas obtenidas con dichas hipótesis son un límite superior de las verdaderas fuerzas que provocan el colapso.

Así pues, teniendo en cuenta la definición de $x_{lím}$ dada por la Eq. (2.7) y sabiendo que el bloque de compresiones relativo a dicha fibra neutra es $c_{lím} = \lambda x_{lím}$, con $\lambda = 0.8$ para hormigones con resistencias características f_{ck} menores a 50 MPa – de acuerdo con EC2 –, puede relacionarse la profundidad del bloque de compresiones de una capa con la deformación en el acero en la capa opuesta. Siguiendo las hipótesis expuestas anteriormente, la dirección principal de compresión en una capa coincide con la dirección principal de tracción en la capa opuesta – Fig. 3.13 –. De esta manera, la deformación de cedencia del acero colocado en la capa *j* en cada dirección, *x* e *y*, se corresponde con una deformación en la dirección principal de las compresiones, α_k, en la capa *k* opuesta dada por:

$$\begin{aligned} x: \quad & \varepsilon_{j-x\,\mathrm{lim}-\alpha k} = \frac{\varepsilon_y}{\cos\alpha_k} \\ y: \quad & \varepsilon_{j-y\,\mathrm{lim}-\alpha k} = \frac{\varepsilon_y}{\sin\alpha_k} \end{aligned} \tag{3.25}$$

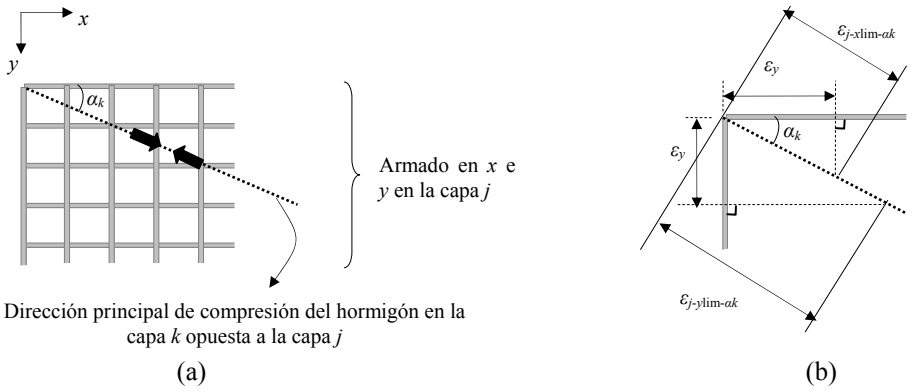

Fig. 3.13. Descomposición de las deformación impuesta por la compresión en la capa *k* según las direcciones del armado de la capa *j*

De esta manera, el valor máximo del espesor de la capa *k* para el cual se produce la cedencia del acero en la capa *j* para cada dirección de armado se obtiene como:

$$x: \quad c_{kx\lim} = \lambda \cdot d_{jx} \cdot \frac{\varepsilon_{cu}}{\varepsilon_{j-x\lim-\alpha k} + \varepsilon_{cu}}$$
$$y: \quad c_{ky\lim} = \lambda \cdot d_{jy} \cdot \frac{\varepsilon_{cu}}{\varepsilon_{j-y\lim-\alpha k} + \varepsilon_{cu}} \tag{3.26}$$

donde d_{jx} y d_{jy} es la distancia entre el centro de gravedad del armado en la dirección x e y y la fibra de la capa k más lejana – Fig. 3.14 –.

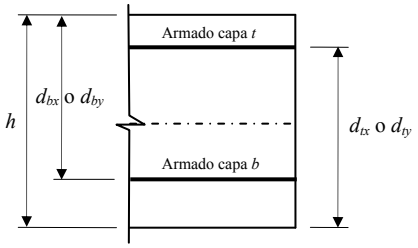

Fig. 3.14. Posiciones del armado para cada capa

Una vez que los valores límites para las profundidades de las capas han sido calculados, estos deben ser comparados con los valores de la profundidad de las capas obtenidos con el procedimiento de Brondum – Nielsen. Si para la capa k, c_k resulta menor que el mínimo de $c_{klímx}$ y $c_{klímy}$ entonces se puede afirmar que el acero en la capa j ha cedido en ambas direcciones. En caso contrario, la geometría de la losa debe ser alterada de manera que se consiga la cedencia del acero a disponer en cada una de las direcciones de cada capa.

Hernández – Montes et al [14] muestran como el ejemplo proporcionado en el trabajo original de Brondum – Nielsen no cumple los anteriores requisitos relativos a la cedencia del acero para una de las direcciones de armado. Éste y otros ejemplos pueden ser consultados en el Anexo 4 del presente trabajo.

3.6. Conclusiones

Las investigaciones llevadas a cabo por el grupo TEP-190 del Departamento de Mecánica de Estructuras e Ingeniería Hidráulica de la Universidad de Granada han realizado importantes aportaciones a la optimización del armado de secciones de hormigón sometidas a flexo-compresión o flexo-tracción uniaxial. Entre dichas aportaciones quedan los diagramas RSD, el TOSR o el procedimiento de armado óptimo basado en los dominios de excentricidad del axil.

Tanto como si resultan de aplicación en la práctica ingenieril como si no, dichas aportaciones son de gran ayuda desde el punto de vista didáctico a obtener un mejor entendimiento del problema de flexión compuesta en secciones de hormigón armado en rotura. No obstante, como resultado de su aplicación práctica se encuentran los pilotes de contención de tierras con armadura simétrica cuyo comportamiento es estudiado en el presente trabajo de investigación.

Por otra parte, el conocimiento adquirido del dimensionamiento en rotura en flexión de elementos de hormigón armado ha hecho posible también otra importante aportación, esta vez en el diseño del armado de losas y placas de hormigón, proponiendo ciertos límites a la aplicación del método de Brondum – Nielsen [13] de aplicación muy extendida.

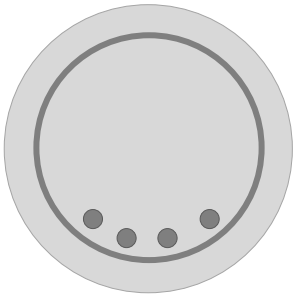

4. Optimización de pilotes de contención de tierras en estado límite último

4.1. Introducción

Las aplicaciones de los diagramas RSD, del TAF y de los Dominios Óptimos de Armado a Flexión son limitadas para secciones rectangulares. Sin embargo, estos principios sí tienen una aplicación ventajosa en el diseño de secciones circulares sometidas a flexión uniaxial, como pueden ser los pilotes empleados en la construcción de muros de contención de tierras.

Debido a que es necesario proporcionar capacidad a flexión ante posibles cambios de las acciones horizontales ocasionadas por el viento o por sismos, la utilización de disposiciones asimétricas de armado no es muy frecuente en columnas; en estos casos, el armado necesario para secciones circulares ha de poseer simetría central [39]. De hecho, normalmente, las soluciones de armado longitudinal empleadas en el diseño de secciones circulares consisten en un número de barras del mismo diámetro separadas entre sí una distancia fija a lo largo del perímetro de la sección – Fig. 4.1 –. Así, la mayoría de programas comerciales de diseño – Sap2000®[40], CYPE®[41], Tricalc®[42], Prontuario Informático del Hormigón Estructural[43] – proporcionan este tipo de soluciones automáticamente.

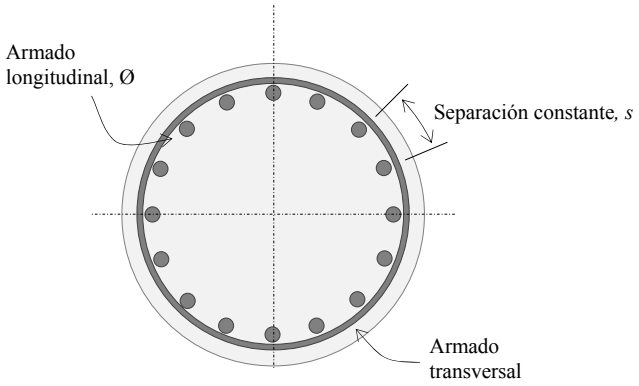

Fig. 4.1. Armado tradicional de una sección circular

La optimización del armado de secciones de hormigón en rotura es un tema muy tratado en la bibliografía. Estudios recientes ponen énfasis en el estudio del armado óptimo de una sección de hormigón en rotura, empleando para ello diversas técnicas de optimización. Kanagasudaram y Karihaloo [44]–[46] emplean las programaciones secuenciales lineal y convexa para abordar el diseño óptimo en términos de coste económico de vigas con múltiples vanos y columnas teniendo en cuenta aspectos como la estabilidad del elemento, resistencia, deformación, durabilidad y resistencia al fuego. Ceranic y Fryer [47] hacen uso del Método de Multiplicadores Lagrangianos para estudiar el coste mínimo de diseño del armado de secciones rectangulares de hormigón en estado límite último. Otros como Barros et al. [48] estudian la optimización del coste de una sección rectangular de hormigón armado empleando el modelo no lineal de tensión – deformación del hormigón propuesto en el Código Modelo 90 [49] teniendo en cuenta el coste de cada componente de la sección (hormigón y acero– . Barros et al. [50] investigan el problema de optimización óptima en términos de coste de una sección rectangular en flexión simple donde la función objetivo es el coste de los materiales aislados y las variables son el canto de la sección y las áreas de armado necesarias. Camp et al. [51] y Lee y Ahn [52] aplican algoritmos genéticos para llevar a cabo una optimización discreta del diseño de pórticos de hormigón armado, ambos incluyendo costes de material y de construcción.

En 1988, Davalath y Madugula [53] proponen un método numérico para la optimización de secciones circulares sometidas a flexo-tracción o flexo-compresión uniaxial bajo los criterios de diseño de la normativa ACI-318 [25]. Su procedimiento determina armados uniformemente

distribuidos a lo largo del perímetro para cualquier tamaño de sección circular dada, o la combinación óptima de armado y diámetro de la sección, todo ello para minimizar el coste. Las soluciones obtenidas mediante este procedimiento están basadas en barras del mismo diámetro, repartidas equidistantemente a lo largo del perímetro de la sección. Şahin [54] presenta un modelo matemático para el diseño integral de pilotes de hormigón armado, de tal manera que tanto el armado como la longitud del pilote sean óptimos. Sin embargo, los pilotes diseñados por este método son empleados como cimentación y, por este motivo, las soluciones de armado son siempre simétricas. Uno de los primeros intentos de armado asimétrico de secciones circulares se debe a Weber y Ernst [55]. En este trabajo, los autores desarrollaron diagramas de interacción axil – flector para secciones circulares de hormigón con distribución asimétrica de armado, considerando los armados principal y secundarios como placas continuas perimetrales con distinto espesor. Definidos estos espesores, la variable a determinar es el ángulo α abarcado por el armado principal – Fig. 4.2 –.

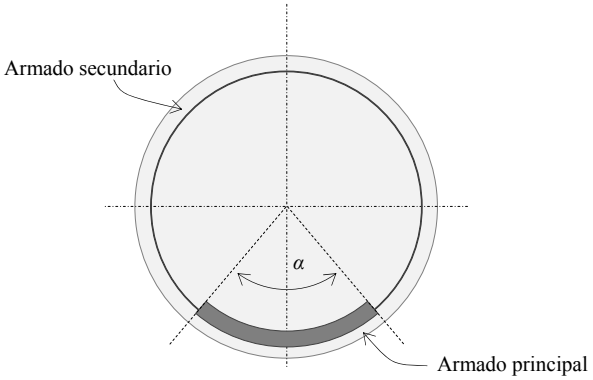

Fig. 4.2. Sección transversal según Weber y Ernst [55]

Con la publicación de los trabajos de Gil-Martín et al. [56] y de Hernández-Montes et al. [39] se presenta una metodología clara y concisa para el armado óptimo de secciones circulares sometidas a flexo-compresión uniaxial. Este método, basado en los conceptos explicados en el Capítulo 2 del presente trabajo, permite conseguir soluciones de armado asimétrico que implican ahorros incluso del 30% con respecto al armado simétrico. En el presente capítulo se detallará dicho procedimiento de armado óptimo. Para ello, se siguen empleando las hipótesis

de Bernouilli, el modelo rectangular del hormigón y el modelo bilineal de acero recogidos en el EC2[19].

4.2. Diagramas de interacción axil – momento flector

Para el diseño óptimo del armado de secciones circulares se emplearán aquí los diagramas de interacción axil – momento flector. Estos diagramas, introducidos por Whitney [21] y estudiados en profundidad por Morán [57], proporcionan el valor del axil y el momento flector que provocan el agotamiento de la sección [58], y han sido tradicionalmente presentados en ábacos empleados para el dimensionamiento de elementos sometidos a acción axil y a flector uniaxial – Fig. 4.3 –.

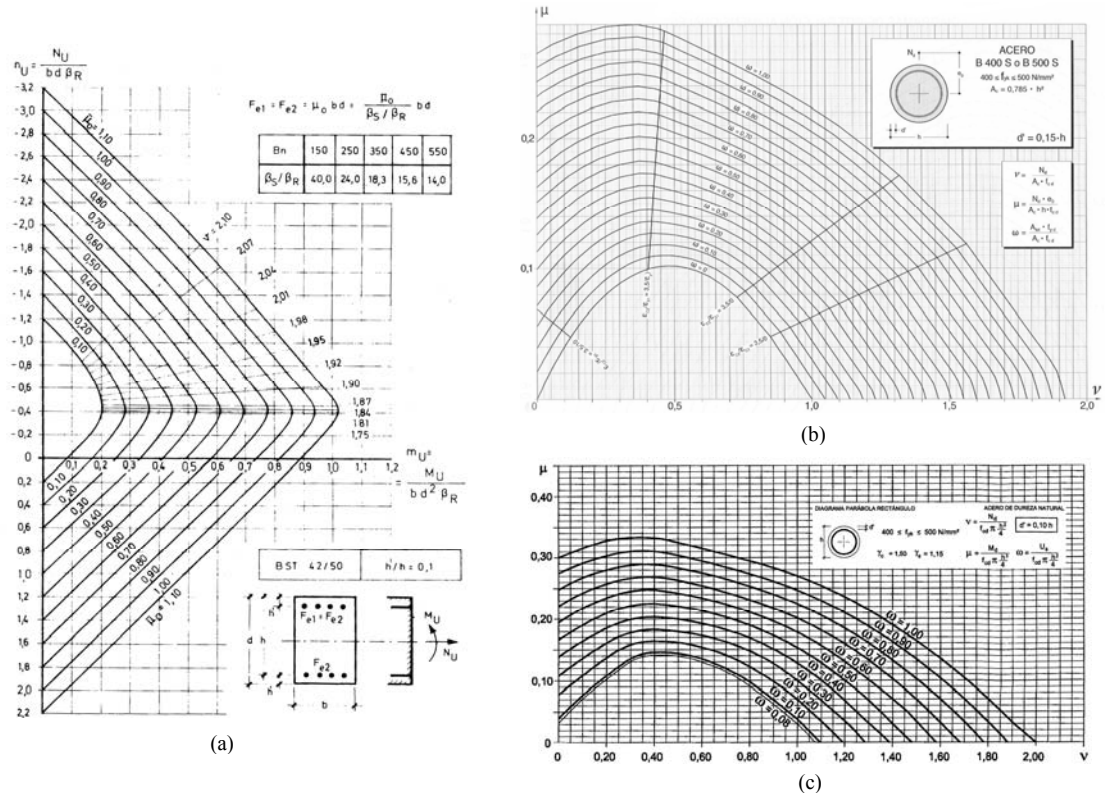

Fig. 4.3. Diagramas adimensionales de interacción axil – flector presentes en la literatura clásica: (a) extraído de [2]**; (b) extraído de** [5]**; (c) extraído de** [1]

Así pues, si se conocen la geometría de la sección transversal, esto es, el diámetro y la posición de cada barra – Fig. 4.4 – y considerando que las acciones exteriores están aplicadas en el centro de gravedad de la sección bruta, el planteamiento del equilibrio en rotura a flexo-compresión de la sección conducirá a un conjunto de ecuaciones similares a Eq. (2.4). Dado que en este caso el

armado está constituido por n_1 barras longitudinales con diámetro $Ø_1$ y n_2 con diámetro $Ø_2$ y que las mismas no están dispuestas en el mismo nivel, las ecuaciones de equilibrio quedan:

$$\begin{aligned} N_u &= N_c(x) + \sum_{i=1}^{n_1} A_{Ø_1}\sigma_s(x,y_i) + \sum_{i=1}^{n_2} A_{Ø_2}\sigma_s(x,y_i) \\ M_u &= M_c(x) + \sum_{i=1}^{n_1} A_{Ø_1}\sigma_s(x,y_i)\,y_i + \sum_{i=1}^{n_2} A_{Ø_2}\sigma_s(x,y_i)\,y_i \end{aligned} \tag{4.1}$$

donde $N_c(x)$ y $M_c(x)$ son el axil y el momento respecto al centro de gravedad de la sección bruta resultantes de las compresiones en el hormigón, $A_{Ø_1}$ y $A_{Ø_2}$ el área de las barras de diámetros $Ø_1$ y $Ø_2$ respectivamente e y_i la posición vertical de la barra i con respecto al centro de gravedad de la sección bruta – Fig. 4.4 –.

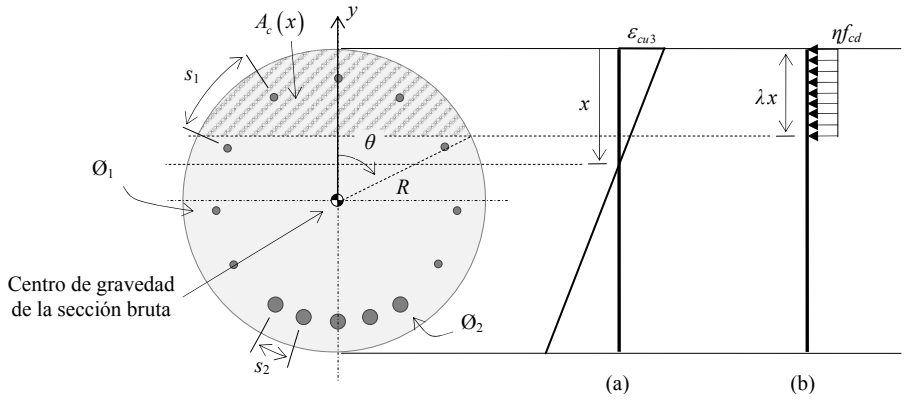

Fig. 4.4. Geometría de la sección con armado asimétrico: (a) distribución de deformaciones; (b) bloque de compresiones del hormigón

Para determinar los valores de $N_c(x)$ y $M_c(x)$ resulta útil expresar el valor de la profundidad del bloque de compresiones, λx, como:

$$\lambda x = R(1-\cos\theta) \tag{4.2}$$

donde θ es el ángulo que delimita el bloque de compresiones, medido desde el eje de simetría de la sección, tal y como se indica en la Fig. 4.4. De esta forma, el valor de dicho ángulo θ puede expresarse en función de la profundidad de la fibra neutra, x, como:

$$\theta = \theta(x) = \begin{cases} 0 & \text{si} \quad x < 0 \\ \arccos\left(1 - \dfrac{\lambda x}{R}\right) & \text{si} \quad 0 \le x < \dfrac{h}{\lambda} \\ \pi & \text{si} \quad x \ge \dfrac{h}{\lambda} \end{cases} \tag{4.3}$$

De esta manera, $N_c(x)$ queda:

$$N_c(x) = \begin{cases} \eta f_{cd} A_c(x) & \text{si} \quad 0 \le x < \dfrac{h}{\lambda} \\ \eta f_{cd} \pi R^2 & \text{si} \quad x \ge \dfrac{h}{\lambda} \end{cases} \tag{4.4}$$

con $A_c(x) = R^2(\theta - \sin\theta\cos\theta)$, y $M_c(x)$:

$$M_c(x) = N_c(x) y_{cgc}(x) \tag{4.5}$$

donde $y_{cgc}(x)$ es la distancia entre el centro de gravedad del bloque de compresiones y el de la sección bruta, dada por:

$$y_{cgc}(x) = \frac{2R}{3} \frac{(\sin\theta)^3}{\theta - \sin\theta\cos\theta} \tag{4.6}$$

Determinadas todas estas expresiones, los distintos pares $N_u - M_u$ que agotan la sección pueden obtenerse simplemente evaluando la Eq. (4.1) para valores de x comprendidos entre 0 e ∞. La Fig. 4.5 muestra un ejemplo del cálculo de un diagrama de interacción axil – flector para dos secciones circulares, una simétrica y la otra asimétrica. Cualquier par de valores $N_d - M_d$ situado entre los ejes coordenados y el diagrama de interacción puede ser soportado por la sección sin llegar a la rotura. Si este par $N_d - M_d$ se sitúa justo en la traza del diagrama de interacción, la sección agotará; si el par se encuentra en la parte exterior del diagrama, la sección no podrá soportar dichas cargas.

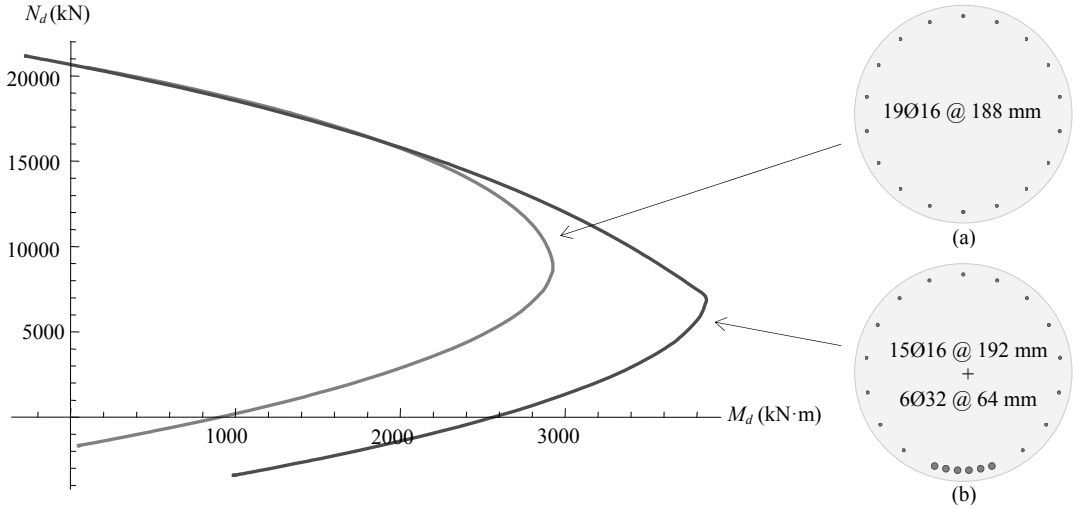

Fig. 4.5. Diagramas de interacción axil – flector para pilotes de radio 600 mm construidos con hormigón HA – 30 y acero B – 500 – S con armado (a) simétrico y (b) asimétrico

4.3. Prescripciones normativas relativas al armado longitudinal de pilotes de hormigón

El EC2 §9.8.5 dispone que en pilotes perforados:

- Se debería disponer una armadura longitudinal mínima de área $A_{s,bpmín}$ en relación con la sección transversal del pilote A_c, según se indica en la Tabla 4.1:

Tabla 4.1 Área de la armadura longitudinal mínima recomendada en pilotes perforados hormigonados in situ

A_c	$A_{s,bpmín}$
$A_c \leq 0.5$ m^2	$A_s \geq 0.005\ A_c$
0.5 m^2 < $A_c \leq$ 1.0 m^2	$A_s \geq 25$ cm^2
$A_c >$ 1.0 m^2	$A_s \geq 0.0025\ A_c$

- El diámetro mínimo de las barras longitudinales no debería ser menor que 16 mm

- Los pilotes deberían tener al menos 6 barras longitudinales

- La distancia libre no debería superar los 200 mm medida a lo largo del contorno del pilote –$s_{máx}$ = 200 mm–

En general, el EC2 §8.2 dispone que la distancia libre horizontal entre barras aisladas paralelas no debe ser menor que el máximo entre el diámetro de la barra (Ø– , el tamaño máximo del árido – d_g– más 5 mm o 20 mm:

$$s_{mín} = \min\left[Ø,\ d_g + 5 \text{ mm}, 20 \text{ mm} \right] \tag{4.7}$$

Por otra parte, la norma UNE-EN 1536 "*Ejecución de trabajos geotécnicos especiales – pilotes perforados*" [59] establece en §7.5.2.10 que para pilotes circulares se deberían evitar las jaulas asimétricas, aunque, a su vez, también indica que si las barras longitudinales no están espaciadas uniformemente, se requieren métodos especiales para conservar el posicionamiento correcto de la jaula de armadura durante la instalación y el hormigonado, los cuales se suponen disponibles.

4.4. El proceso de optimización

4.4.1. Efecto de la concentración de barras

Previamente a la definición de los proceso de optimización ideados en este trabajo, se presenta mediante un claro ejemplo el efecto en la resistencia a flexión simple que produce la concentración de barras en una zona de la sección. Sea un pilote de diámetro 500 mm fabricado con un hormigón HA – 30 y un acero B – 500 – S. El armado del pilote consta de 16 barras de 18 mm de diámetro – 16Ø18 – distribuidos uniformemente a lo largo del perímetro – con un recubrimiento mecánico de 60 mm –. El área total de armado es 3418.05 mm^2 y el momento último que agota la sección a flexión simple es 619.14 kN·m.

La sección transversal del pilote puede separarse en dos zonas, 1 y 2, de tal manera que cada una de estas zonas contenga el mismo número de barras que la otra – Fig. 4.6 (a) –. Sea ξ el ángulo que abarca la zona 1 – mitad de la sección –, de tal manera que ξ = 90º corresponde al armado simétrico. Un aumento del valor de ξ conllevará una mayor concentración de barras en la zona 2 y una mayor distancia entre barras en la zona 1. Así pues, la evolución de la capacidad a flexión simple de la sección, con respecto al incremento de ξ se presenta en la Fig. 4.6 (b).

Este ejemplo muestra claramente como simplemente modificando la disposición de las barras en la sección transversal del pilote, manteniendo la cuantía del armado, se pueden obtener mayores resistencias a flexión simple. En este caso, la solución simétrica agota con un momento flector

de 619.14 kN·m, mientras que la solución correspondiente a un ángulo de zona 1 de 150º agota con un flector de 884.65 kN·m.

El procedimiento hasta aquí presentado ha mostrado como, manteniendo la misma cuantía, la sección puede ver incrementada su resistencia a flexión simple por el mero cambio de disposición del armado. A continuación se presentan dos procesos de optimización en los que se pretende obtener la cuantía de armado óptima para soportar unas solicitaciones de flexión determinadas. Ambos procedimientos concentran la armadura en la zona donde la sección ha de soportar mayores solicitaciones de tracción. De esta manera, en dicha zona las barras se dispondrán separadas a la distancia mínima permitida por la normativa, mientras que en el resto de la sección las barras se dispondrán a la separación máxima prescrita.

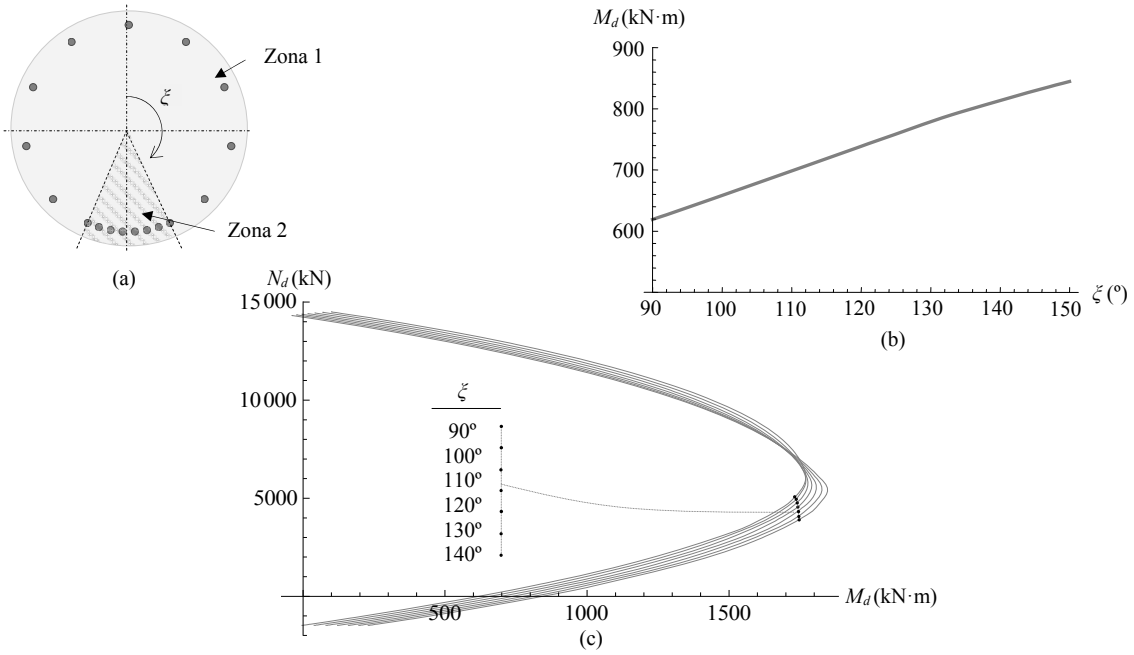

Fig. 4.6. Efecto de la concentración de barras en la resistencia a flexión simple: (a) Definición de las zonas 1 y 2 en la sección transversal; (b) evolución de la resistencia a flexión simple con la concentración de barras en la zona 2; (c) evolución del diagrama axil – flector con la concentración de barras

4.4.2. Proceso 1: optimización manteniendo el diámetro de las barras – $Ø_1 = Ø_2$ –

Los pasos de este procedimiento de optimización se muestran en la Fig. 4.7. Dado un diámetro de pilote, D, el recubrimiento mecánico de las barras, r_m, y el diámetro de barra para armar – $Ø_1$

= $Ø_2$ = Ø –, se determinan primero las separaciones entre barras máxima s_1 y mínima s_2 – Fig. 4.4 –. Posteriormente, se calcula el número máximo de barras, n_1, a colocar a separación s_1:

$$n_1 = \frac{2\pi\left(\frac{D}{2} - r_m\right)}{s_1} \tag{4.8}$$

Así pues, conociendo estas distancias, se añaden progresivamente barras en la zona de tracción separadas por la distancia s_2 hasta que el par de diseño N_d – M_d quede sobre la traza o en el interior del diagrama de interacción de la sección. A medida que se añaden las barras en la zona de tracción – zona 2 – será necesario eliminar barras del resto de la sección e incluso modificar la separación s_1 de manera que ninguna barra de dicha zona quede entre dos barras de la zona de tracción y que las limitaciones de separaciones máximas y mínimas se cumplan en todo momento.

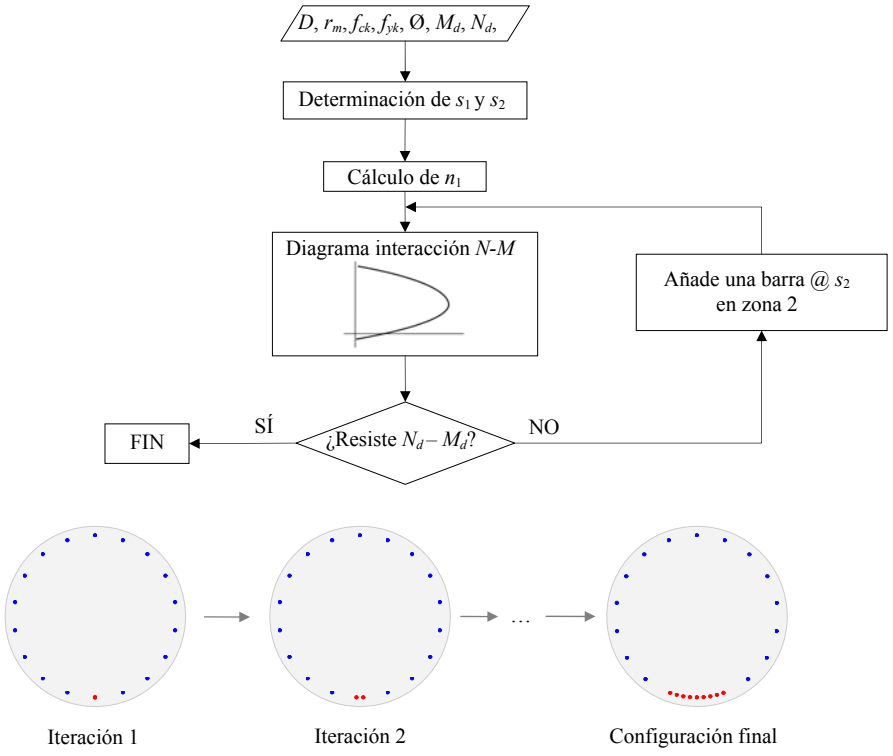

Fig. 4.7. Proceso de optimización con diámetro de barras constante – $Ø_1$ = $Ø_2$ = Ø –. Adaptado de [56]

4.4.3. Proceso 2: optimización con distinto diámetro de barras – $Ø_1$ < $Ø_2$ –

Al igual que en el caso anterior, los pasos que describen este procedimiento se presentan en la Fig. 4.8. Nuevamente, las separaciones s_1 y s_2 corresponderán a la máxima y mínima permitidas. En este caso el armado se realiza de tal manera que para las barras de la zona traccionada – zona 2 – se emplea el mayor diámetro posible – $Ø_2$– o aceptable y el resto de la sección – zona 1– se arma con el diámetro menor aceptado según normativa. Con estas prescripciones, se añaden sucesivamente barras en la zona 2 hasta que el par de diseño $N_d - M_d$ quede sobre la traza o en el interior del diagrama de interacción de la sección. Como ocurría en el caso anterior, hay que eliminar barras de diámetro $Ø_1$ a medida que se añaden barras a la zona 2, de manera que se cumplan las limitaciones de separación y que no exista ninguna barra de diámetro $Ø_1$ dentro de la zona 2.

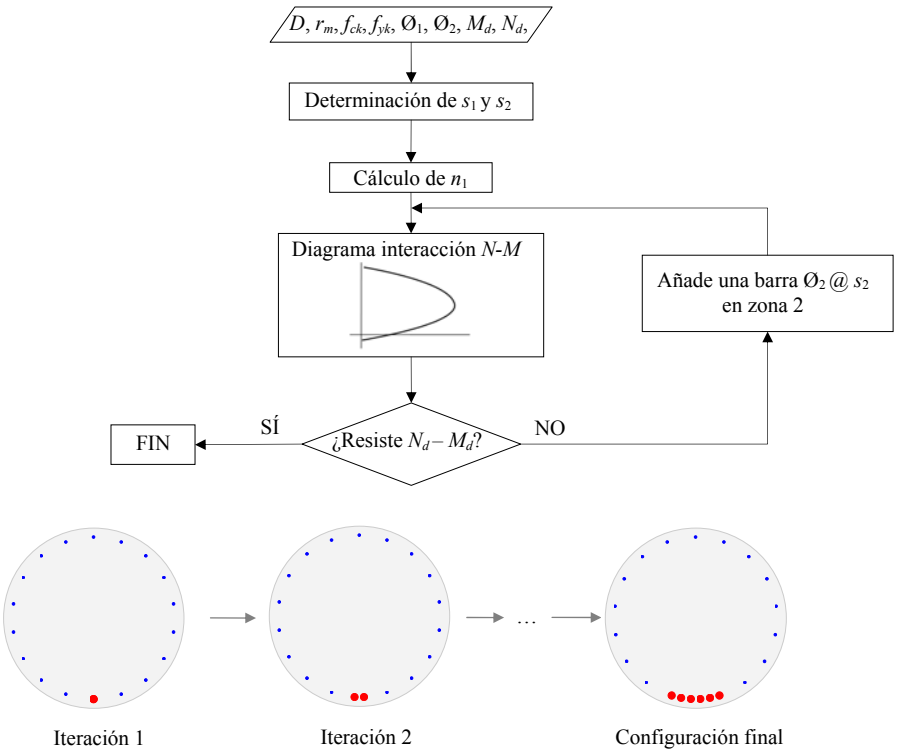

Fig. 4.8. Proceso de optimización con diámetro de barras constante – $Ø_1 < Ø_2$ –. Adaptado de [56]

4.5. Ejemplo

Sea una pantalla de contención de tierras construida mediante pilotes de hormigón armado HA-30. La sección de los pilotes tiene 0.5 m de radio y cuenta con 20 barras de acero B – 500 – S de diámetro 20 mm – 20Ø20 – para soportar una solicitación de flexión simple de M_d = 1050

kN·m, con un recubrimiento mecánico, r_m, de 60 mm. El área total de armado longitudinal resulta 6283.19 mm^2, el 0.8% de la sección bruta.

Empleando un diámetro de barra constante – $Ø_1 = Ø_2$ – y separación también constante e igual a la separación máxima permitida – $s_1 = s_2 = s_{máx} = 200$ mm –, el armado que proporciona una resistencia a flexión simple adecuada se corresponde con 14Ø25, que supone un área total de armado de 6872.23 mm^2 – 0.875% de la sección bruta – , mayor que el armado original de 20Ø20.

Si optamos nuevamente por mantener el diámetro de barra constante y, en este caso, igual al original – $Ø_1 = Ø_2 = 20$ mm –, pero con separaciones s_1 y s_2 distintas – $s_1 \leq s_{máx} = 200$ mm, $s_2 = s_{mín} = 45$ mm – la solución óptima se corresponde con 13Ø20 separadas a 198 mm más 4Ø20 separadas a 45 mm. Esta solución supone un área total de armado de 5340.71 mm^2 – cuantía sobre sección bruta: 0.68% – que resulta en un 15% menos de acero que la solución original de 20Ø20. La Fig. 4.9 muestra los diagramas de interacción obtenidos para distintas iteraciones del proceso de optimización.

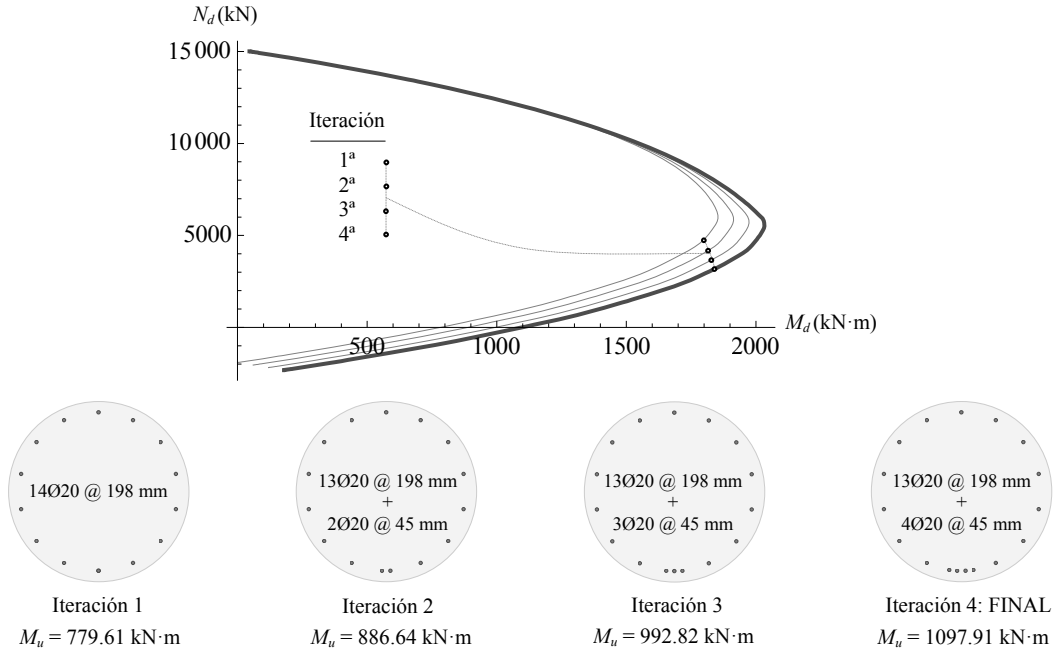

Fig. 4.9. Iteraciones llevadas a cabo en la optimización con $Ø_1 = Ø_2 = 20$ mm

La optimización puede llevarse a cabo empleando diámetros distintos, de tal manera que para $Ø_1$ se selecciona el mínimo permitido por las prescripciones normativas – $Ø_1$ = 16 mm – y para $Ø_2$ se prueba con tres diámetros distintos – 20 mm, 25 mm y 32 mm – para evaluar que opción proporciona el armado con menor área de acero. La Fig. 4.10 muestra los diagramas de interacción obtenidos para cada iteración utilizando $Ø_2$ = 20 mm. La solución de armado óptimo utilizando este diámetro se corresponde 13 barras de diámetro $Ø_1$ = 16 mm separadas a 198 mm y 6 barras de diámetro $Ø_2$ = 20 mm separadas a 45 mm – Fig. 4.10 –. El área total de armado resulta 4498.76 mm^2 – cuantía sobre área bruta de 0.57% – y supone un ahorro de acero de 28.40% sobre el armado original de 20Ø20. La Fig. 4.10 muestra diferentes secciones para iteraciones intermedias en el proceso así como la sección correspondiente a la solución óptima.

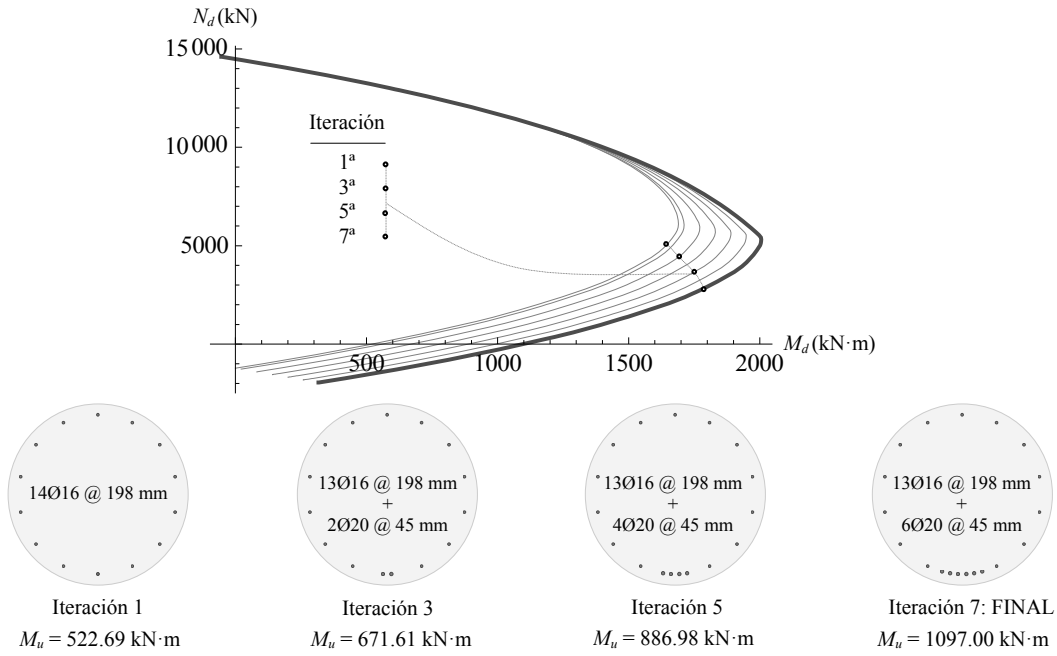

Fig. 4.10. Iteraciones llevadas a cabo en la optimización con $Ø_1$ = 16 mm y $Ø_2$ = 20 mm

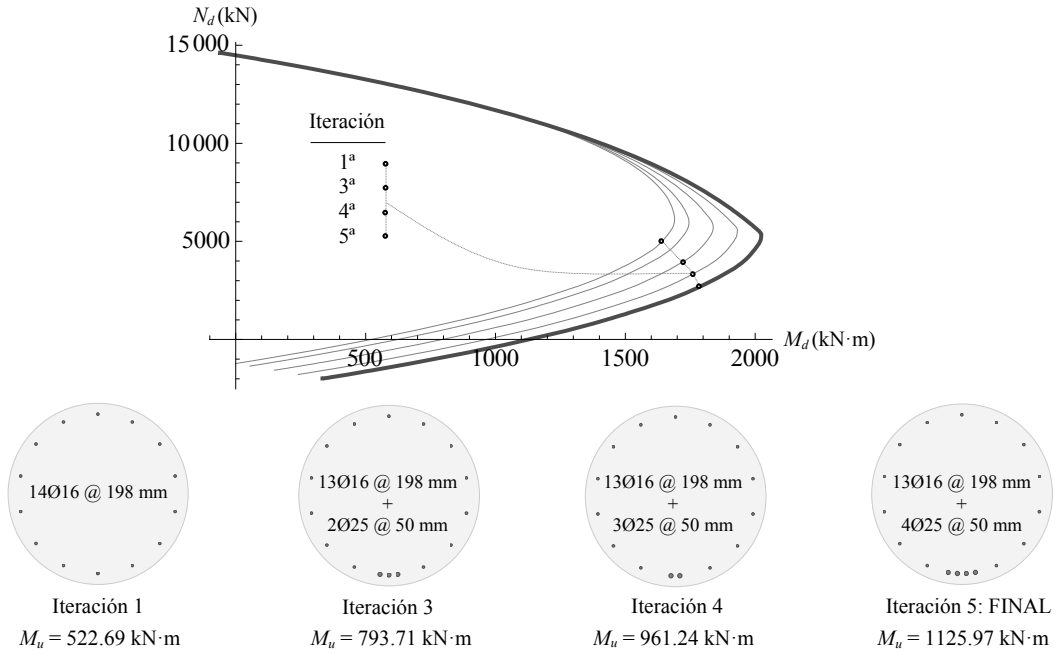

Fig. 4.11. Iteraciones llevadas a cabo en la optimización con $Ø_1$ = 16 mm y $Ø_2$ = 25 mm

Si ahora $Ø_2$ = 25 mm, se necesitan menos iteraciones en el proceso de optimización, logrando la solución óptima en 5 iteraciones. La Fig. 4.11 muestra los diagramas de interacción obtenidos para cada iteración utilizando $Ø_2$ = 25 mm. La solución de armado óptimo utilizando este diámetro se corresponde 13 barras de diámetro $Ø_1$ = 16 mm separadas a 198 mm y 4 barras de diámetro $Ø_2$ = 25 mm separadas a 50 mm. El área total de armado en este caso es 4577.30 mm^2 – cuantía sobre área bruta de 0.58% – y supone un ahorro de acero de 27.15% sobre el armado original de 20Ø20. La Fig. 4.11 presenta las secciones correspondientes a la primera y tres últimas iteraciones.

Por último, en la Fig. 4.12 se presentan los diagramas de interacción obtenidos para cada iteración con $Ø_2$ = 32 mm. La solución de armado óptimo utilizando este diámetro se corresponde 13 barras de diámetro $Ø_1$ = 16 mm separadas a 198 mm y 3 barras de diámetro $Ø_2$ = 32 mm separadas a 64 mm. Con esta armadura, el área total de armado es 5026.55 mm^2 – cuantía sobre área bruta de 0.64% – y supone un ahorro de acero de 20.00% sobre el armado original de 20Ø20.

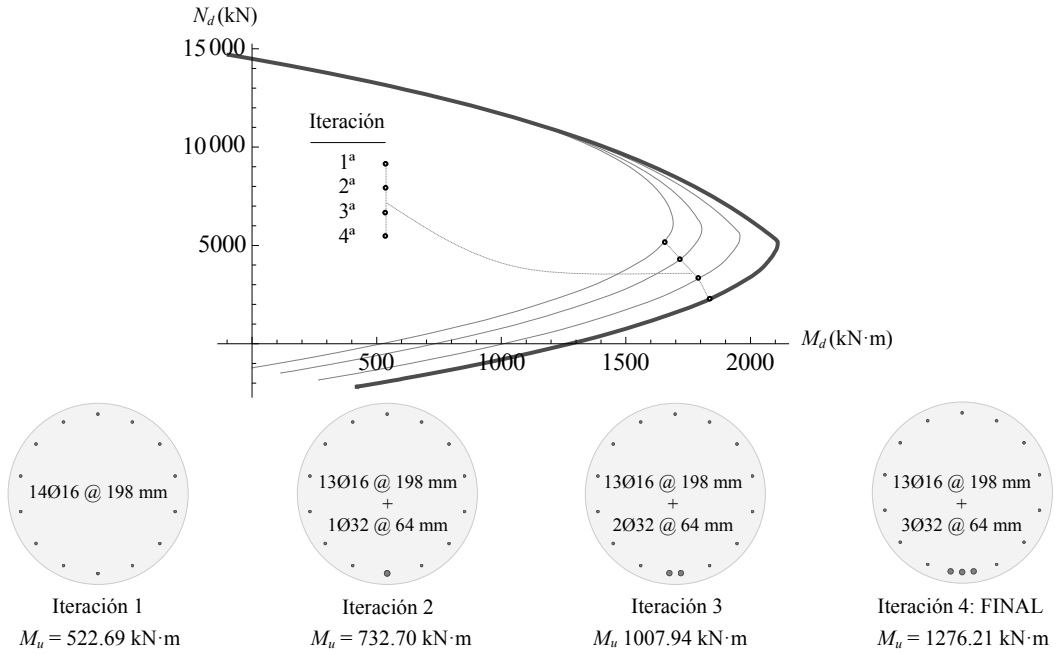

Fig. 4.12. Iteraciones llevadas a cabo en la optimización con $Ø_1$ = 16 mm y $Ø_2$ = 32 mm

Evaluadas todas las distintas opciones anteriores, el armado que proporciona la resistencia a flexión adecuada con menor área de armado longitudinal es el correspondiente a 13Ø16 separados a 198 mm y 6Ø20 separados a 45 mm. La Tabla 4.2 muestra un resumen de las opciones de armado obtenidas.

Tabla 4.2 Solución original de armado y distintas opciones de búsqueda de armado óptimo

	Armado longitudinal	M_u (kN·m)	A_t [1](mm^2)	Cuantía sobre sección bruta	Ahorro	
Original	20Ø20@138 mm	1078.76	6283.19	0.800%	-	
	14Ø25@198 mm	1166.80	6872.23	0.875%	-9.38%	
	13Ø20@198 mm + 4Ø20@45 mm	1097.91	5340.71	0.680%	15.00%	
	13Ø16@198 mm + 6Ø20@45 mm	1097.00	4498.76	0.573%	**28.40%**	Óptimo
	13Ø16@198 mm + 4Ø25@50 mm	1125.97	4577.30	0.583%	27.15%	
	13Ø20@198 mm + 3Ø32@64 mm	1276.21	5026.55	0.640%	20.00%	

4.6. Pilotes "bi-simétricos"

Todas las soluciones asimétricas presentadas anteriormente son válidas en los casos en que el funcionamiento de la pantalla de contención de tierras corresponda a un voladizo; este tipo de estructura se mantendrá estable si se proporciona la profundidad adecuada a los pilotes de manera que se garantice el empotramiento a lo largo de la porción de pilote que se encuentra

[1] A_t se refiere en Tabla 4.2 al área de armado longitudinal total

bajo el nivel de excavación. A medida que la altura de tierras a contener supera los 3 – 5 metros, consideraciones de índole económica requieren de la instalación de riostras horizontales en uno o varios niveles de la pantalla. Estas riostras pueden materializarse desde el interior de la excavación – puntales horizontales instalados desde un lateral de la excavación hasta el otro para excavaciones profundas, Fig. 4.13 (a), o apeos diagonales para el caso de excavaciones de menor profundidad, Fig. 4.13 (b) – o mediante el uso de anclajes de la pantalla al terreno. Estas riostras horizontales intermedias hacen que la penetración de los pilotes en bajo el nivel de excavación sea menor, suponiendo ahorros en la ejecución de los mismos. En el caso de pantallas riostradas, los pilotes actúan como vigas continuas verticales provocando cambios de sentido en la ley de momentos flectores.

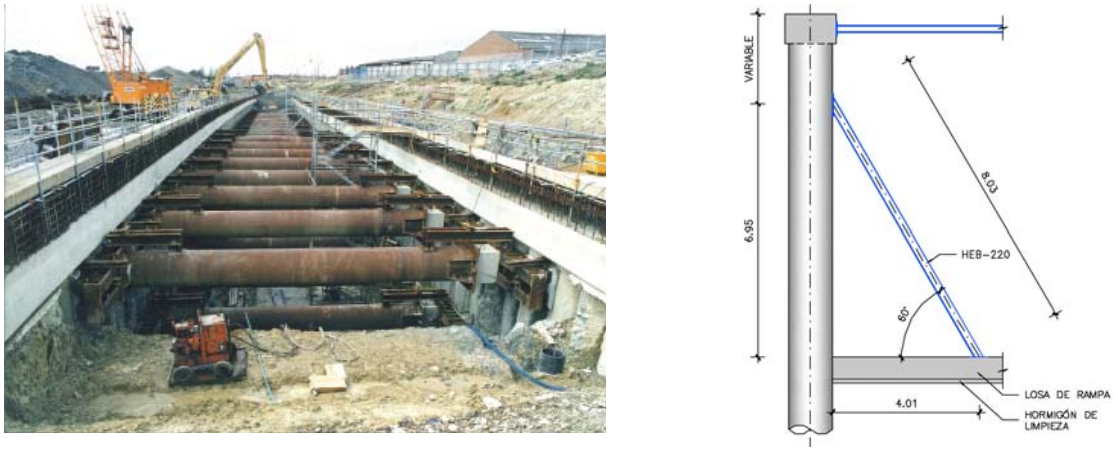

(a) (b)

Fig. 4.13. Sistemas de riostra empleados en pantallas: (a) puntales horizontales en la construcción de los túneles de Ashford, Gran Bretaña, tomado de [60]**; (b) puntal inclinado provisional proyectado en la construcción de los túneles del AVE en el tramo Barcelona Sants – La Sagrera**

El cambio de sentido en la ley de momentos flectores soportada por los pilotes hace que el uso de las soluciones hasta ahora presentadas no sea válido. No obstante, existen otras soluciones óptimas que también emplean armado asimétrico – Fig. 4.14 –. Es claro que las configuraciones de armado presentadas en la Fig. 4.14 son adecuadas para casos donde el sentido del momento flector cambia, como ocurre en el caso de pantallas de pilotes ancladas al terreno o con riostras. Para casos donde los valores máximos del flector en ambos sentidos sean similares se emplearán soluciones como la mostrada en Fig. 4.14 (a), mientras que si el máximo de la

envolvente de flectores es significantemente mayor en un sentido que en el otro, se emplearán soluciones del tipo de la Fig. 4.14 (b).

Fig. 4.14. Pilotes "bi-simétricos": (a) los máximos valores de la envolvente de flectores tiene valores similares pero distinto signo; (b) solución a emplear cuando el máximo valor del flector en un sentido es mayor que el máximo en el otro

El procedimiento de optimización de este tipo de secciones es similar al del pilote asimétrico original. Primero se optimiza la armadura dispuesta para el momento máximo en un sentido y posteriormente se hace lo mismo con el otro sentido, esta vez teniendo en cuenta la armadura con diámetro $Ø_2$. En estos casos, los resultados teóricos arrojan unos ahorros de armadura del orden del 20 al 30% con respecto al armado simétrico convencional. Si el pilote cuenta con una longitud importante se podrían llegar ahorros todavía más significativos si la armadura se hace variar a de su longitud – Fig. 4.15 –, de manera que, conociendo la ley envolvente de momentos flectores, se optimice la armadura en varias secciones del pilote, tal y como se realiza el armado en otros elementos estructurales como vigas.

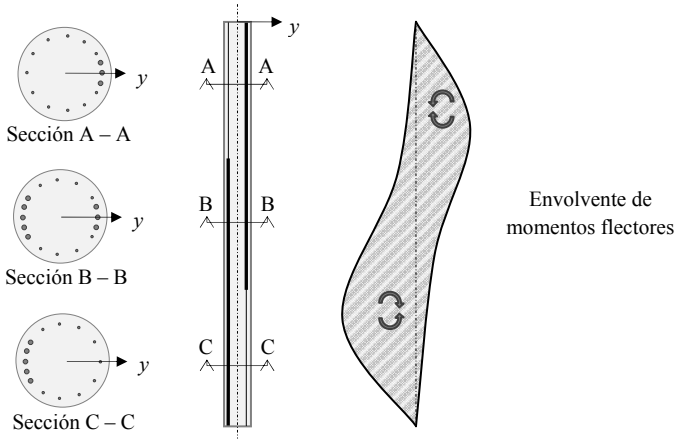

Fig. 4.15. Pilote armado asimétricamente con varios niveles de armado distintos en su longitud

El inconveniente más inmediato que puede presentar una solución como la expuesta en la Fig. 4.15 es su montaje en fábrica. Los pilotes convencionales, asimétricos y bisimétricos son fabricados por tramos en fábrica colocando las barras longitudinales entre dos "platos" enfrentados y soldando la armadura transversal a su alrededor, tal y como muestra la Fig. 4.16.

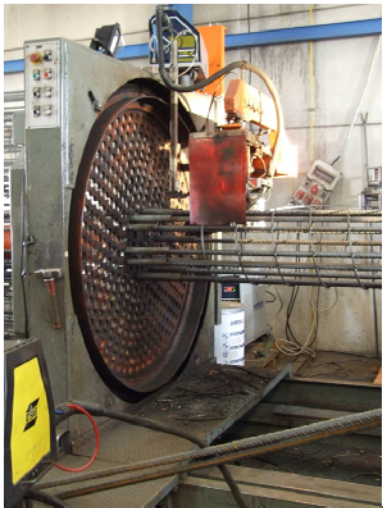

Fig. 4.16 Fabricación industrial del armado de un pilote

Un pilote con distinto armado en su longitud haría difícil o inaplicable este procedimiento automatizado de fabricación, aumentando los costes.

4.7. Conclusiones

El armado longitudinal de secciones circulares de elementos de hormigón armado longitudinales suele realizarse de manera simétrica, disponiendo barras de acero del mismo diámetro separadas a una distancia constante a lo largo del perímetro de la sección. Cuando las solicitaciones a las que se ve sometido el elemento durante su vida útil poseen dirección y sentido predominantes el armado con simetría radial tradicional pierde eficacia. Este es el caso de las pantallas de contención de tierras ejecutadas mediante pilotes de hormigón armado, las cuales soportan los empujes provenientes de las tierras contenidas.

Para este tipo de estructura se han propuesto varios métodos de optimización de armado que pueden conducir a importantes ahorros en la cantidad de acero a disponer en la sección. Los procedimientos de optimización explicados concentran la armadura en la zona de la sección que resistirá las tracciones producidas por el momento flector; en el resto de la sección se dispone la

armadura mínima prescrita por la normativa aplicable. El primer método de optimización mantiene constante el diámetro de las barras mientras que el segundo emplea un diámetro mayor para las barras colocadas en la zona de tracción.

Por otra parte, en situaciones donde la envolvente de momentos flectores presente valores importantes del flector en ambos sentidos, las secciones asimétricas con armadura concentrada en un sector no resultan adecuadas. Se ha descrito otro tipo de solución asimétrica que concentra la armadura en dos sectores diametralmente opuestos, de manera que los valores máximos del flector en distintos sentidos determinan la cantidad de acero a disponer en cada sector. Además, pueden disponerse distinto armado en la longitud del pilote, pero dicha solución dificulta la fabricación automática del módulo de armadura.

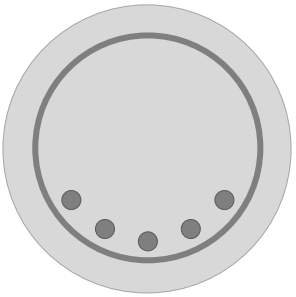

5. Beneficios económicos y medioambientales de los pilotes con armadura asimétrica

5.1. Introducción

La polémica relativa al cambio climático es un tema de gran actualidad e importancia durante las últimas décadas. Es bien conocido que una de las principales causas de este fenómeno global es el efecto invernadero provocado por las emisiones de gas realizadas principalmente por la industria y el transporte, asociadas a la quema de combustibles fósiles.

En 1992 se establece la Convención Marco de las Naciones Unidas sobre el Cambio Climático [61] cuyo fin es estabilizar las concentraciones gases efecto invernadero (GEI) para reducir las interferencias de la acción del hombre en el cambio climático. El Protocolo de Kioto de 1997 [62] estableció las obligaciones legales para la mayoría de países desarrollados para reducir sus emisiones de GEI, de media, un 6 – 8% por debajo de los niveles de 1990, en el período entre 2008 y 2012 [63].

Los GEI son gases cuya presencia en la atmósfera contribuye al efecto invernadero y los cuatro tipos más importantes generados por la actividad humana son: dióxido de carbono (CO_2),

metano (CH_4), óxido nitroso (N_2O) y halocarbonos – gases que contienen flúor, cloro o bromo – . De entre los anteriores, el CO_2 es con diferencia el más importante. Tanto es así que las emisiones de GEI son convertidas a equivalentes de CO_2 (CO_2 – e) a la hora de elaborar estadísticas y estudios en esta temática.

La industria de la construcción lleva asociados importantes niveles de emisiones de CO_2. La producción de cemento Portland empleado en la fabricación de hormigón lleva asociada valores cercanos a un 8% de las emisiones globales de CO_2. Aproximadamente la mitad de las emisiones de este gas están relacionadas con el proceso de quema de combustibles fósiles para alcanzar las altas temperaturas requeridas para calcinar la caliza y producir cemento. Además, el proceso mismo de calcinación de caliza conlleva emisiones adicionales de CO_2. Así pues, la cantidad CO_2 implícita en el hormigón queda en principalmente en función de la cantidad de cemento incluida en la mezcla. Más allá del proceso de calcinación de la caliza, el resto de procesos asociados con la fabricación de cemento y hormigón y su puesta en obra requieren relativamente cantidades bajas de energía y emisiones de CO_2. Las emisiones de CO_2 asociadas a la fabricación de un hormigón típicamente usado en obras convencionales, con una resistencia a compresión normal (20-30 MPa), varían entre 0.29 y 0.32 Tn CO-e/m^3 [64].

La otra fuente de emisiones de CO_2 relacionada con la construcción se encuentra en la industria del acero. Las plantas de fabricación de acero tienen la infraestructura necesaria para elaborar sus productos a partir de materiales brutos – principalmente mineral hierro y carbón –. Muchos de los procesos implicados en la producción de acero conllevan altas temperaturas o al aplicación de grandes fuerzas para conformar el producto. Todos esos procesos con tan alta demanda de energía tienen un claro impacto sobre el medio ambiente, es decir, en el aire, agua o suelo. No obstante, la porción de acero reciclado que se emplea en la producción de nuevos productos de este metal permite el ahorro de energía en la manipulación del hierro puro, pero nuevamente las altas temperaturas necesarias para la fabricación de acero reciclado y el uso de caliza para purificar los óxidos de hierro conducen a importantes emisiones de CO_2 a la

atmósfera. Según datos de ArcelorMittal, la mayor compañía en la industria del acero, en 2012 se produjeron una media de 2,13 Tn de CO_2 – e por tonelada de acero fabricada [65].

Motivada por razones económicas y medioambientales, la industria del acero ha hecho uso de tecnología modernizada y también costosa con el objetivo de controlar los procesos de fabricación de sus productos de manera más eficiente, reduciendo así los impactos medioambientales. Este hecho ha conducido a reducciones en el consumo de energía y al tratamiento de los residuos generados durante la producción de acero. Sin embargo, incluso así, las emisiones de GEI siguen siendo un tema clave que la industria internacional del acero ha de afrontar y que, en la actualidad, están motivando a la realización de muchos trabajos de investigación en el campo de la valoración del ciclo de vida del acero, Fig. 5.1 – "*steel life cycle assessment*" –, y de la reducción de emisiones por su producción [66]–[70].

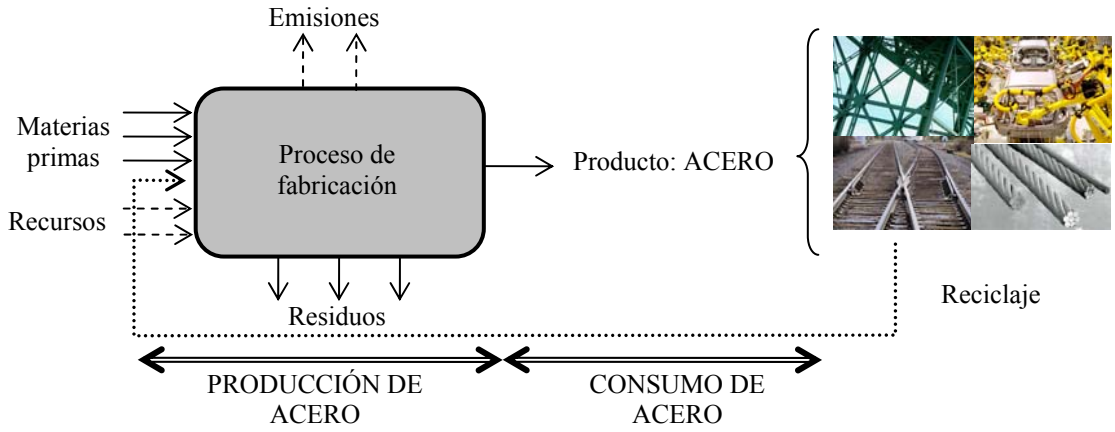

Fig. 5.1. Ciclo de vida útil del acero desde su fabricación hasta su empleo

Sin embargo, la sostenibilidad para la industria del acero no sólo concierne a la producción del material – considerando el reciclaje del acero al final de su vida útil –, sino que también atañe al desarrollo de usos más eficiente del material. La concienciación de los ingenieros sobre métodos racionales de diseño que conlleven un uso más eficiente del acero puede lograr evitar usos innecesarios de este material, con los beneficios económicos y medioambientales que esto aporta.

5.2. Coste medioambiental del acero

Los Créditos de Carbono son uno de los tres mecanismos propuestos en el Protocolo de Kioto para reducir las emisiones que causan el cambio climático. Un Crédito de Carbono, o Bono de Carbono, representa el derecho a emitir una tonelada de CO_2. Las reducciones en emisiones de GEI son contabilizadas mediante los Certificados de Emisiones Reducidas (CER) en toneladas de CO_2–e. Este sistema proporciona incentivos para motivar a la industria reducir las emisiones de GEI generadas por sus procesos de producción, de tal manera que los Créditos de Carbono pueden ser vendidos entre compañías y países.

Desde 2005, el sistema conocido como Régimen Europeo de Comercio de Derechos de Emisión – o EU ETS, del inglés *European Union Emissions Trading Scheme* – [71] regula el comercio de derechos de emisión – EUA, del inglés *European Union Allowance* – entre los países de la Unión Europea. Los EUAs son los Créditos de Carbono en este sistema. El objetivo principal del EU ETS es ayudar a los Estados miembros de la Unión Europea a cumplir sus compromisos para limitar o reducir las emisiones de GEI en términos económicos, permitiendo a las compañías a comprar o vender EUAs. El EU ETS establece un techo de emisiones, que es el volumen total de EUAs en circulación. Este techo determina el objetivo medioambiental y da valor económico a las EUAs al crear escasez [72], permitiendo obtener beneficios económicos aquellas empresas que optan por reducir o eliminar sus emisiones, mientras que fuerza a comprar EUAs a las empresas que sobrepasan sus emisiones inicialmente permitidas. La Fig. 5.2 muestra la evolución del valor diario y su media anual de las EUAs según SendeCO_2 [73], el sistema electrónico de negociación de derechos de emisión de dióxido de carbono, desde 2008 hasta la actualidad. Así pues, considerando que por cada tonelada de acero producida se emiten 2 Tn de CO_2–e, el coste medioambiental asociado con la producción de este material puede evaluarse de manera sencilla y ser incorporado al presupuesto de la estructura diseñada.

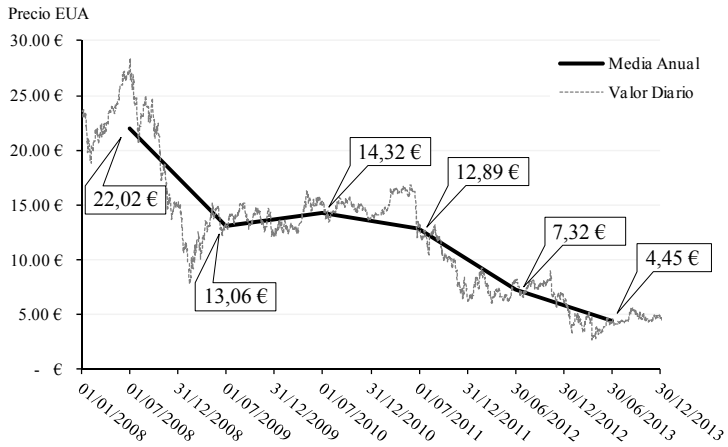

Fig. 5.2. Evolución diaria y media anual del precio de los EUA. Fuente: SendeCO_2 [73]

5.3. Ejemplo: Línea de Alta Velocidad Madrid – Barcelona – frontera francesa; Tramo Sants – La Sagrera (Barcelona)

5.3.1. Breve descripción de las obras

Las obras donde se ejecutan por primera vez los pilotes de contención de tierras con armadura asimétrica son las de la Línea de Alta Velocidad Madrid – Barcelona – frontera francesa, concretamente en el tramo Sants – La Sagrera, en la ciudad de Barcelona. Este tramo consiste en un túnel de longitud 5781 m, 5095 de los cuales se ejecutan mediante el empleo de tuneladora y los 686 m correspondientes a los extremos que enlazan con la estación de Sants y La Sagrera se realizan mediante la construcción de pantallas de pilotes y posterior vaciado de las tierras – "*cut & cover*" –. Todo el túnel ejecutado en esta obra discurre bajo las calles de la ciudad de Barcelona en ningún caso pasando bajo edificaciones existentes

Fig. 5.3. Traza del tramo Sants - La Sagrera. Fuente: ADIF [74]

A modo experimental, se sustituyen cinco pilotes convencionales por cinco pilotes asimétricos en el tramo de "*cut & cover*" que hace de enlace entre el túnel excavado con tuneladora y la estación de Sants Fig. 5.4(a), concretamente en la intersección entre el Carrer de Provença y el Carrer de Vilmarí Fig. 5.4(b).

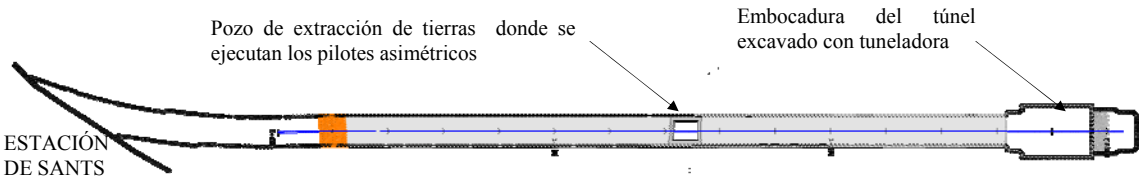

(a)

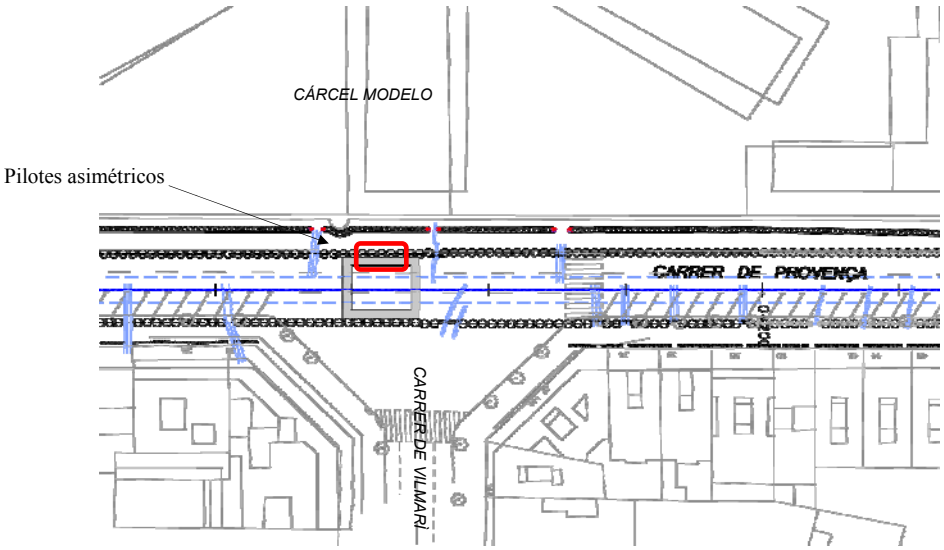

(b)

Fig. 5.4. (a) Planta general del falso túnel de enlace entre la estación de Sants y el túnel excavado con tuneladora; (b) Localización de los pilotes asimétricos ejecutados

La excavación cuenta con una profundidad máxima de 13.5 m entre pantallas de pilotes de 18.5 m de profundidad, diámetro 1.20 m y separados sus centros 1.40 m. En dicho punto de la obra se encuentra un pozo de extracción de tierras, de tal manera que los pilotes quedan arriostrados durante las obras por la viga perimetral que constituye el marco del pozo y por un puntal provisional a una profundidad de 5 m. La Fig. 5.5 muestra la sección transversal del falso túnel en el pozo de extracción de tierras anteriormente referido.

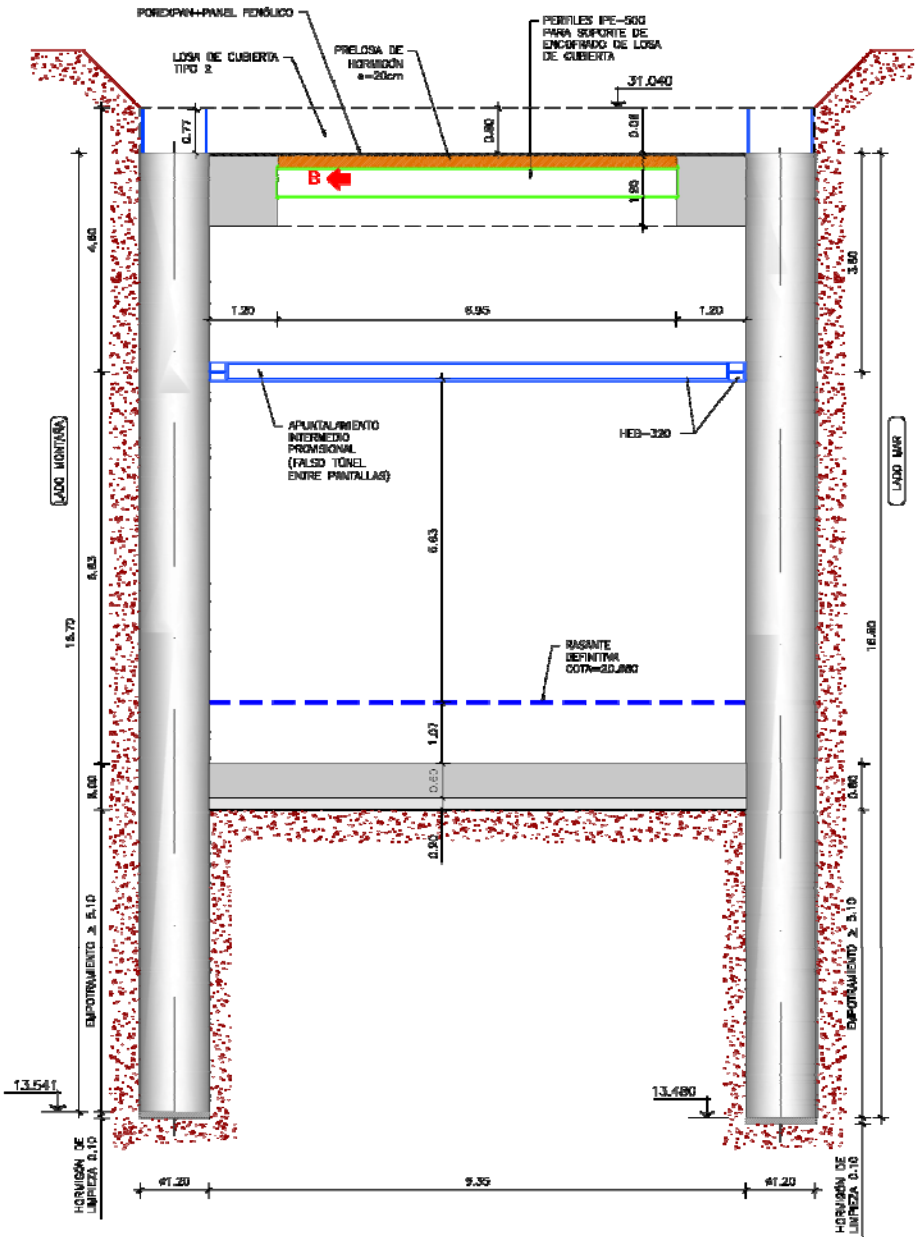

Fig. 5.5. Sección transversal del túnel en el pozo de extracción de tierras

5.3.2. Características de los pilotes

Los pilotes tienen un diámetro de 1.20 m. El hormigón empleado es un HA-30 y el acero utilizado en el armado de los mismos es B – 500 – S. Los flectores de diseño se indican en la Tabla 5.1. El armado longitudinal de los pilotes simétricos convencionales a sustituir se resuelve mediante 27 barras de acero de 25 mm de diámetro (27Ø25), con un área total de acero de 13256.30 mm^2, resultando una cuantía sobre el área transversal bruta del pilote de 2.34%. Por su parte, la solución asimétrica cuenta con 9 barras de diámetro 32 mm separadas 64 mm entre centros, dispuestas en la zona de pilote en contacto con las tierras y 11 barras de diámetro 12

mm, separadas 196 mm y repartidas por el resto de la sección para cumplir los requisitos de cuantía mínima. El área total de acero longitudinal es 8482.30 mm^2, resultando un ahorro del 36.01% sobre el área de acero longitudinal de la solución simétrica. La Fig. 5.6 muestra una imagen de la armadura acopiada en obra. El armado transversal en ambos casos fue resuelto mediante cercos circulares de diámetro 12 mm colocados cada 12 m – cØ25 @ 120 mm–. El gráfico de la Fig. 5.7 representa en discontinuo el diagrama de interacción axil – momento flector positivo de la sección simétrica, que posee un resistencia a flexión simple de 2683.83 kN m. El gráfico con trazo continuo de la Fig. 5.7 representa el diagrama de interacción axil – momento positivo flector de la sección asimétrica. La resistencia a flexión simple de esta sección es 2992.15 kN m, mayor que la correspondiente a la solución simétrica. Por su parte, la Fig. 5.8 muestra los diagramas interacción axil – flector negativo de ambas soluciones. La Tabla 5.2 recoge un resumen de todos estos resultados.

Tabla 5.1. Momentos de diseño del pilote

M_d (kN·m) +	M_d (kN·m) –
2176.16	428.51

Fig. 5.6. Pilote con armadura asimétrica empleado en el tramo Sants- La Sagrera

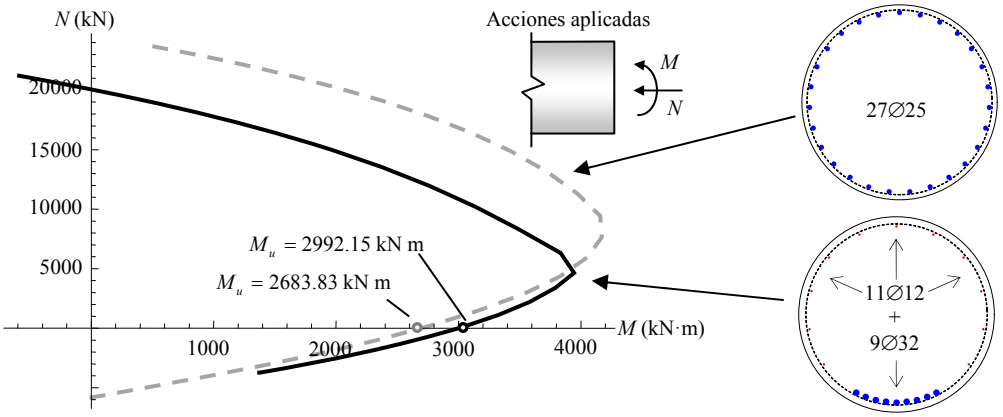

Fig. 5.7. Diagrama interacción axil – momento flector para pilotes simétrico y asimétrico. Flexión positiva

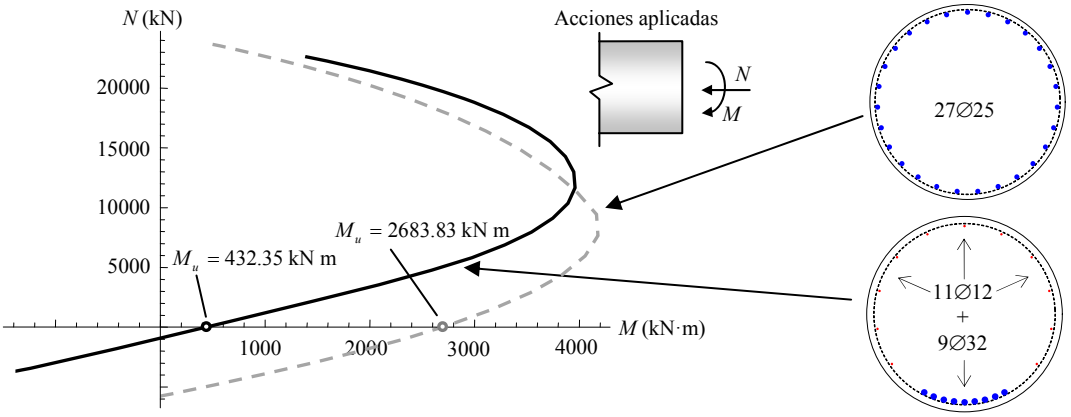

Fig. 5.8. Diagrama interacción axil – momento flector para pilotes simétrico y asimétrico. Flexión negativa

Tabla 5.2. Armado longitudinal de los pilotes simétrico y asimétrico

Configuración	Armado longitudinal	Área armado longitudinal (mm^2)	M_u (kN·m) +	M_u (kN·m) –
Simétrica	27∅25	13253.60	2683.83	
Asimétrica	9∅32@64 mm +11∅12@196 mm	8482.30	2992.15	432.35

5.3.3. Análisis de ahorro ambiental

Gracias a la empresa SACYR, constructora del tramo de obras descrito anteriormente, se dispone de la descripción de los pilotes instalados en el falso túnel presentado en la Fig. 5.4 (a). Considerando precios del año 2013, el coste por kg de acero es 0.81€, según la Base de Costes de la Construcción de Andalucía [75]. Por otra parte, considerando que por cada tonelada de acero producido se emiten 2 Tn de CO_2–e y que el coste medio de los EUA de 2013 es 4.45€ – Fig. 5.2 –, la Tabla 5.3 recoge el coste material – acero –, ambiental y la suma de ambos para las soluciones de armado simétrico originalmente adoptadas en proyecto. El peso de acero en los pilotes ha sido calculado empleando una densidad de 7850 kg/m^3

Tabla 5.3. Coste del armado simétrico original

Tipo	Nº Pilotes	Long (m)	Armado	Coste		
				Acero	Ambiental	Total
1	31	16.26	27 Ø 20	27186.33 €	298.71 €	27485.04 €
2	14	16.26	29 Ø 32	33759.12 €	370.93 €	34130.05 €
3	212	18.5	27 Ø 25	330518.62 €	3631.62 €	334150.24 €
4	34	15.85	20 Ø 20	21529.94 €	236.56 €	21766.50 €
5	11	15.6	20 Ø 20	6855.70 €	75.33 €	6931.03 €
6	5	15.6	20 Ø 20	3116.23 €	34.24 €	3150.47 €
7	9	15.75	20 Ø 20	5663.14 €	62.22 €	5725.37 €
8	1	15.75	24 Ø 32	1933.02 €	21.24 €	1954.26 €
9	14	15.75	20 Ø 20	8809.34 €	96.79 €	8906.13 €

Aplicando el procedimiento de optimización explicado en el capítulo 4 de este trabajo, se ha optimizado la armadura de las soluciones expuestas la Tabla 5.3. Ahora, la Tabla 5.4 recoge los resultados obtenidos para las soluciones asimétricas.

Tabla 5.4. Coste del armado asimétrico optimizado

Tipo	Armado optimizado	Coste		
		Acero	Ambiental	Total
1	3 Ø 32 + 17 Ø 16	18688.08 €	205.34 €	18893.42 €
2	13 Ø 32 + 13 Ø 16	18916.75 €	207.85 €	19124.60 €
3	6 Ø 32 + 15 Ø 16	195549.50 €	2148.63 €	197698.13 €
4	3 Ø 25 + 17 Ø 16	16758.36 €	184.14 €	16942.50 €
5	3 Ø 25 + 17 Ø 16	5336.31 €	58.63 €	5394.94 €
6	3 Ø 25 + 17 Ø 16	2425.59 €	26.65 €	2452.25 €
7	3 Ø 25 + 17 Ø 16	4408.05 €	48.43 €	4456.48 €
8	10 Ø 32 + 15 Ø 16	1107.46 €	12.17 €	1119.63 €
9	3 Ø 25 + 17 Ø 16	6856.97 €	75.34 €	6932.31 €

Finalmente la Tabla 5.5 recoge el ahorro por pilote y el ahorro total que se habría conseguido en este tramo de obra si la armadura hubiese sido optimizada con disposiciones asimétricas. Así, el tipo de pilote que produce mayor ahorro unitario al ser optimizado es el pilote tipo 2, que originalmente está armado con 29Ø32 y al ser optimizado se arma con 13Ø32+13Ø16, suponiendo un ahorro del 44%. El pilote con mayor presencia en la obra es 3, con 212 unidades. El armado original de este pilote consta de 27Ø25 – A_s = 13253.59 mm^2 – y al ser optimizado pasa a ser armado con 6Ø32+15Ø16 – A_s = 7841.42 mm^2 –, con un ahorro económico del 41% incluyendo los costes ambientales.

Tabla 5.5. Resumen de costes para las soluciones simétricas y asimétricas

Tipo	Coste Total		Ahorro
	Solución simétrica	Solución asimétrica	
1	27485.04 €	18893.42 €	31.26%
2	34130.05 €	19124.60 €	43.97%
3	334150.24 €	197698.13 €	40.84%
4	21766.50 €	16942.50 €	22.16%
5	6931.03 €	5394.94 €	22.16%
6	3150.47 €	2452.25 €	22.16%
7	5725.37 €	4456.48 €	22.16%
8	1954.26 €	1119.63 €	42.71%
9	8906.13 €	6932.31 €	22.16%
Total	444199.09 €	273014.26 €	38.54%

Así pues, las soluciones simétricas conllevan unas emisiones de 1084.87 Tn de CO_2–e, mientras que las soluciones asimétricas evitarían unas emisiones a la atmósfera de 418.08 Tn de CO_2–e, con un total de 666.78 Tn. En términos monetarios, el ahorro ambiental no resulta muy importante – del orden del 1% respecto al ahorro material – debido a la devaluación de los EUA en estos últimos años de crisis económica en los que la producción industrial ha descendido. No obstante, la cantidad en Tn de emisiones de CO_2 que se evitarían al emplear la optimización del acero pone en valor el impacto ambiental beneficioso de los pilotes con armadura longitudinal asimétrica.

5.4. Conclusiones

El Protocolo de Kioto de 1997 estableció las obligaciones legales para la mayoría de países desarrollados para reducir sus emisiones de gases efecto invernadero, de media, un 6 – 8% por debajo de los niveles de 1990, en el período entre 2008 y 2012. Entre las medidas adoptadas para lograr los objetivos establecidos se crean los Créditos del Carbono, que dan derecho a la emisión de una tonelada de CO_2. En la Unión Europea se crea el Régimen Europeo de Comercio de Derechos de Emisión que regula el comercio de los derechos de emisión o Créditos del Carbono, de tal manera que se cree escasez y dichos derechos de emisión adquieran valor económico.

El sector de la construcción es responsable de grandes emisiones de CO_2 y las producidas por la industria del acero es una parte importante de dichas emisiones. A día de hoy, por cada tonelada de acero producida, se emiten dos toneladas de CO_2 a la atmósfera, cuyo valor en términos económicos en 2013 es de 4.45€/Tn.

Así pues, el procedimiento de optimización de secciones circulares expuesto en este trabajo no solo supondrá beneficios económicos, si no que la optimización de las secciones se traducirá en menores emisiones de gases efecto invernadero a la atmósfera.

Se ha presentado un ejemplo de una obra real donde se han ejecutado por primera vez, a modo de prueba, los pilotes asimétricos. Además, se ha realizado la optimización de todos los pilotes empleados en el tramo presentado y se han evaluado, en términos económicos, los beneficios materiales y ambientales que supone el empleo de pilotes asimétricos frente a los armados simétricamente.

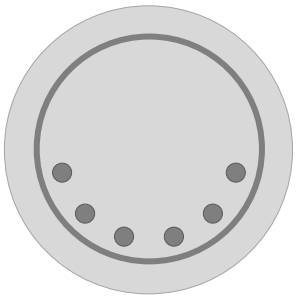

6. Conclusiones

Prestando atención a los objetivos establecidos en el Capítulo 1 del presente trabajo y recapitulando las conclusiones parciales expuestas en cada Capítulo, se puede concluir:

I. Los pilotes empleados en sistemas de contención de tierras han sido tradicionalmente calculados imponiendo las restricciones correspondientes a estados límite últimos, entre los que se encuentra el de flexión, y las limitaciones impuestas por los estados de servicio no son comúnmente comprobadas. Uno de los motivos que justifica este hecho es la falta de tratamiento de secciones circulares por los códigos y la normativa de diseño de estructuras de hormigón, de ahí que existan nuevos trabajos de investigación relativos al comportamiento en estado de servicio – fisuración y deformación – de este tipo de secciones.

II. Las soluciones de armado óptimo en estado límite de flexo – compresión uniaxial son bien conocidas desde mediados del siglo pasado para secciones rectangulares o semejantes. Sin embargo, el diseño de las secciones circulares se ha realizado tradicionalmente empleado soluciones que distan en gran medida de las óptimas.

III. Existen novedosas aportaciones relativas al armado óptimo de secciones rectangulares de hormigón sometidas a flexo – compresión como los Diagramas RSD, el Teorema del Armado Óptimo a Flexión o los Dominios de Armado Óptimo. La idea principal introducida por estos trabajos de investigación es que existe un número infinito de soluciones que dotan a la sección de la resistencia adecuada para soportar la flexo-compresión uniaxial en rotura; este hecho permite al ingeniero escoger el armado óptimo teniendo en cuenta factores estructurales o de otra índole, como por ejemplo, facilidad de construcción.

IV. El método analítico y sistemático de análisis de secciones en rotura permite formular soluciones de armado óptimo a problemas tan amplios como el diseño óptimo del armado de secciones de hormigón y de las dimensiones de secciones de acero sometidas a flexo-compresión uniaxial como la determinación del armado de elementos de hormigón tipo placa o losa sometidos a flexión, torsión y a acciones en el plano.

V. Dentro de la aplicación del método de secciones en rotura, se han presentado límites al procedimiento de diseño del armado de elementos losa y placa propuesto por Brondum – Nielsen [13], ampliamente aceptado

VI. El empleo del procedimiento de optimización del armado de secciones circulares presentado puede traducirse en grandes ahorros económicos, dando lugar a secciones que pueden llegar a emplear un 30% menos de acero. Además, dichas disposiciones de armado facilitan su puesta en obra y manipulación. Se presentan soluciones para pantallas voladizo y pantallas ancladas o con riostras intermedias, en las que pueden aparecer valores máximo del momento en ambos sentidos. Por último, se explica la solución con cambio de armadura longitudinal en la longitud del pilote.

VII. Además de los ahorros de material, el empleo de disposiciones asimétricas para el armado longitudinal de pilotes de contención de tierras supone un importante ahorro de

costes ambientales, ya que se evitan la emisión de apreciables cantidades de CO_2 a la atmósfera provenientes de la industria de fabricación del acero.

Conclusions

According to the objectives established in Chapter 1 of this work and summarizing the main conclusions given for each Chapter, it may be concluded:

I. The pile members employed in earth retaining systems have been traditionally designed taking into account the ultimate strength prescriptions, amongst which is the corresponding to ultimate bending. By the other hand, the limitations imposed by the serviceability are not considered commonly. One of the reasons for this is the lack of treatment of circular cross sections in the current codes of reinforced concrete design. Therefore, new research work are been conducted in order to get a better knowledge of the behavior of circular cross sections under service conditions – cracking and deformations –.

II. Optimal solutions for the reinforcement of rectangular concrete cross sections subjected to uniaxial bending and compression are well known since mid-century. However, the design of circular cross sections under those kinds of loads has been traditionally done employing solutions far away from the optimal ones.

III. There are recent and new research works relating the optimal reinforcement of rectangular concrete cross sections subjected to uniaxial bending and compression, as RSD Diagrams, the Theorem of Optimal Reinforcement for Reinforced Concrete Cross – Sections and the Optimal Domains. The main contribution of those works is to recognize that an infinite number of reinforcement solutions can provide a section with adequate strength; this knowledge allows an engineer to choose an optimal combination of reinforcement considering structural and non – structural – e.g. construction-related – issues.

IV. The analytic and systematic method of study of ultimate strength of sections allows to solve a wide range of problems such as the optimal design of the reinforcement of concrete sections or the dimensions of steel sections, both subjected to combined uniaxial flexion and compression, or to the problem of the reinforcement determination in concrete shell or slabs elements under flexure, torsion and in-plane actions.

V. A modification of the commonly accepted Brondum – Nielsen [13] procedure of designing the reinforcement of concrete shell and slab elements has been proposed, providing limits to the application of the original method.

VI. The employment of the presented optimization procedure when designing the reinforcement of circular cross sections leads to suppose relevant economic savings of around 30% of the original symmetric solution. In addition to this, the optimized asymmetrical reinforcement is much easy to manage at the work place, offering more advantages than the economic one. Solutions for piles employed in cantilever – type earth retaining systems are given as well as solutions for anchored or propped walls, in which maximum values of bending moment can be found in both directions. Finally, solutions where longitudinal reinforcement layout changes along the pile are also introduced.

VII. An important aspect presented within this work is the environmental profits than the optimized design offers. Important amounts of CO_2 emissions coming from steel industry are avoided when employing the asymmetrically reinforced concrete piles.

Referencias

[1] J. Calavera, *Proyecto y cálculo de estructuras de hormigón: en masa, armado, pretensado*, 2ª ed. Madrid: INTEMAC, 2008, p. 2116.

[2] F. Leonhardt, *Estructuras de hormigón armado Vol. 1*, 2ª ed. Buenos Aires: El Ateneo, 1993.

[3] A. H. Nilson, D. Darwin, C. W. Dolan, *Design of concrete structures*, 13th ed. New York: McGraw-Hill, 2004, p. 780.

[4] E. G. Nawy, *Reinforced concrete: a fundamental approach*, 5th ed. Upper Saddle River, New Jersey: Prentice-Hall, 2003, p. 821.

[5] P. Jimenez Montoya, Á. García Meseguer, F. Morán Cabré, J. C. Arroyo Portero, *Jiménez Montoya: hormigón armado*, 15ª ed. Barcelona: Gustavo Gili, 2009, p. 629.

[6] A. Páez, *Hormigon Armado, Vol 1*. Barcelona: Reverté, 1986, p. 635.

[7] R. Saliger, *El hormigón armado: su cálculo y formas constructivas*, 6ª ed. Barcelona: Labor, 1943, p. 740.

[8] J. Kolleger, "Computer programme for consistent design of surface structures," *IABSE reports*, vol. 62, pp. 507–512, 1991.

[9] P. B. Lourenço, J. A. Figueiras, "Solution for the Design of Reinforced Concrete Plates and Shells," *Journal of Structural Engineering*, vol. 121, no. 5, pp. 815–823, 1995.

[10] C. Min, "Design and ultimate behavior of RC plates and shells," *Nuclear Engineering and Design*, vol. 228, no. 1–3, pp. 207–223, 2004.

[11] A. Tomás, P. Martí, “Design of reinforcement for concrete co-planar shell structures using optimization techniques,” *Meccanica*, vol. 45, no. 5, pp. 657–669, 2009.

[12] G. Bertagnoli, S. Mancini, “Design and optimization of skew reinforcement in concrete shells,” *Structural Concrete*, vol. 13, no. 4, pp. 248–258, 2012.

[13] T. Brondum-Nielsen, “Optimum Design of Reinforced Concrete Shells and Slabs,” Copenhagen, 1974.

[14] E. Hernández-Montes, J. F. Carbonell-Márquez, L. M. Gil-Martín, “Limits to the strength design of reinforced concrete shells and slabs,” *Engineering Structures (In press)*, 2014.

[15] R. Park, T. Paulay, *Reinforced Concrete Structures*. New York: John Wiley & Sons, Ltd., 1975, p. 796.

[16] Comité Europeo de Normalizacion, *Eurocódigos. Bases de cálculo de estructuras. UNE-EN 1990*. Bruselas: Comité Europeo de Normalización, 2003, p. 84.

[17] I. A. Tegos, N. C. Giannakas, T. A. Chrysanidis, “Serviceability cracking check of circular section piers,” *Bridge Structures - Assessment, Design & Construction*, vol. 7, no. 1, pp. 43–52, 2011.

[18] J. F. Carbonell-Márquez, L. M. Gil-Martín, E. Hernández-Montes, “Effective area in tension stiffening of reinforced concrete piles subjected to flexure according to Eurocode 2,” *Enviado para publicación a Engineering Structures*.

[19] Comité Europeo de Normalizacion, *Eurocódigo 2: Proyecto de estructuras de hormigon. Parte1-1: Reglas generales y reglas para edificación. UNE-EN 1992-1-1*. Bruselas: Comité Europeo de Normalización, 2010, p. 244.

[20] L. M. Gil-Martín, D. López-Martín, E. Hernández-Montes, M. Aschheim, “Dimensionamiento en rotura a flexión de secciones de hormigón armado. Un planteamiento compacto,” *Informes de la Construcción*, vol. 64, no. 528, pp. 497–505, 2012.

[21] C. S. Whitney, E. Cohen, “Guide for Ultimate Strength Design of Reinforced Concrete,” *ACI Journal Proceedings*, vol. 53, no. 11, pp. 455–490, 1956.

[22] R. Walther, M. Miehlbradt, *Dimensionnement des structures en béton: bases et technologie*. Lausanne: Presses Polytechniques et Universitaires Romandes, 1990, p. 388.

[23] E. Hernández-Montes, L. M. Gil-Martín, M. Aschheim, “Pilotes asimétricos para contención de tierras,” *Revista de Obras Públicas*, vol. 157, no. 3, pp. 31–38, 2010.

[24] E. Hernández-Montes, L. M. Gil-Martín, M. Pasadas-Fernández, M. Aschheim, “Theorem of optimal reinforcement for reinforced concrete cross sections,” *Structural and Multidisciplinary Optimization*, vol. 36, no. 5, pp. 509–521, 2007.

[25] ACI Commitee 318, *318-08: Builiding Code Requirements for Structural Concrete and Commentary*. Detroit: American Concrete Institute, ACI, 2008, p. 473.

[26] E. Hernández-Montes, M. Aschheim, L. M. Gil-Martín, “Impact of optimal longitudinal reinforcement on the curvature ductility capacity of reinforced concrete column sections,” *Magazine of Concrete Research*, vol. 56, no. 9, pp. 499–512, 2004.

[27] E. Hernández-Montes, L. M. Gil-Martín, M. Aschheim, “Design of Concrete Members Subjected to Uniaxial Bending and Compression Using Reinforcement Sizing Diagrams,” *ACI Structural Journal*, vol. 102, no. 1, pp. 150–158, 2005.

[28] M. Aschheim, E. Hernández-Montes, L. M. Gil-Martín, “Optimal domains for strength design of rectangular sections for axial load and moment according to Eurocode 2,” *Engineering Structures*, vol. 29, no. 8, pp. 1752–1760, 2007.

[29] D. López-Martín, J. F. Carbonell-Márquez, L. M. Gil-Martín, E. Hernández-Montes, “Eccentricity-Based Optimization Procedure for Strength Design of RC Sections under Compression and In-Plane Bending Moment,” *Journal of Structural Engineering*, pp. 1–9, 2012.

[30] L. M. Gil-Martín, M. Aschheim, E. Hernández-Montes, M. Pasadas-Fernández, “Recent developments in optimal reinforcement of RC beam and column sections,” *Engineering Structures*, vol. 33, no. 4, pp. 1170–1180, 2011.

[31] H. J. Lee, M. Aschheim, E. Hernández-Montes, L. M. Gil-Martín, “Optimum RC column reinforcement considering multiple load combinations,” *Structural and Multidisciplinary Optimization*, vol. 39, no. 2, pp. 153–170, 2008.

[32] L. M. Gil-Martín, E. Hernández-Montes, M. Aschheim, “Optimal reinforcement of RC columns for biaxial bending,” *Materials and Structures*, vol. 43, no. 9, pp. 1245–1256, 2009.

[33] L. M. Gil-Martín, M. Aschheim, E. Hernández-Montes, “Proportioning of steel beam–column members based on RSD optimization methodology,” *Engineering Structures*, vol. 30, no. 11, pp. 3003–3013, 2008.

[34] J. F. Carbonell-Márquez, L. M. Gil-Martín, E. Hernández-Montes, “Strength design optimization of structural steel members according to Eurocode 3,” *Journal of Constructional Steel Research*, vol. 80, no. 2013, pp. 213–223, 2013.

[35] Comité Europeo de Normalizacion, *Eurocódigo 3: Proyecto de estructuras de acero. Parte 1-1: Reglas generales y reglas para edificios. UNE-EN 1993-1-1*. Bruselas: Comité Europeo de Normalización, 2008, p. 106.

[36] fib-Special Activity Group 5, *fib Bulletin 65: Model Code 2010 - Final Draft*. Lausanne: International Federation for Structural Concrete (fib), 2012.

[37] A. K. Gupta, “Combined Membrane and Flexural Reinforcement in Plates and Shells,” *Journal of Structural Engineering*, vol. 112, no. 3, pp. 550–557, 1986.

[38] D. Fall, K. Lundgren, R. Rempling, K. Gylltoft, “Reinforcing tailor-made concrete structures: Alternatives and challenges,” *Engineering Structures*, vol. 44, pp. 372–378, 2012.

[39] E. Hernández-Montes, P. Alameda-Hernández, L. M. Gil-Martín, “Strength design criterion for asymmetrically reinforced RC circular cross-sections in bending,” *Computers and Concrete*, vol. 11, no. 6, pp. 571–585, 2013.

[40] Computers and Structres Inc., *SAP2000: Integrated software for structural analysis and design*. 2009.

[41] Cype Ingenieros S.A., *Software for architecture, engineering and construction*. 2011.

[42] Arktec S.A., *Tricalc 8.0*. .

[43] H. Corres Peiretti, J. León González, A. Pérez Caldentey, J. C. Arroyo Portero, J. C. López Agüí, *Prontuario informático del hormigón estructura V. 3.0*. Madrid: Instituto Español del Cemento y sus Aplicaciones, 2001, p. 96.

[44] S. Kanagasundaram, B. L. Karihaloo, “Minimum cost design of reinforced concrete structures,” *Structural optimization*, vol. 2, no. 3, pp. 173–184, 1990.

[45] S. Kanagasundaram, B. L. Karihaloo, “Minimum-cost reinforced concrete beams and columns,” *Computers & Structures*, vol. 41, no. 3, pp. 509–518, 1991.

[46] S. Kanagasundaram, B. L. Karihaloo, “Minimum-cost design of reinforced concrete structures,” *Computers & Structures*, vol. 41, no. 6, pp. 1357–1364, 1991.

[47] B. Ceranic, C. Fryer, “Sensitivity analysis and optimum design curves for the minimum cost design of singly and doubly reinforced concrete beams,” *Structural and Multidisciplinary Optimization*, vol. 20, no. 1996, pp. 260–268, 2000.

[48] M. H. F. M. Barros, R. A. F. Martins, A. F. M. Barros, “Cost optimization of singly and doubly reinforced concrete beams with EC2-2001,” *Structural and Multidisciplinary Optimization*, vol. 30, no. 3, pp. 236–242, 2005.

[49] Commitee for The Model Code 1990, “CEB Bulletin No. 213/214: CEB-FIP Model Code 90.” Tomas Telford, Lausanne, p. 460, 1993.

[50] A. F. M. Barros, M. H. F. M. Barros, C. C. Ferreira, “Optimal design of rectangular RC sections for ultimate bending strength,” *Structural and Multidisciplinary Optimization*, vol. 45, no. 6, pp. 845–860, 2012.

[51] C. V. Camp, S. Pezeshk, H. Hansson, “Flexural Design of Reinforced Concrete Frames Using a Genetic Algorithm,” *Journal of Structural Engineering*, vol. 129, no. 1, pp. 105–115, 2003.

[52] C. Lee, J. Ahn, “Flexural Design of Reinforced Concrete Frames by Genetic Algorithm,” *Journal of Structural Engineering*, vol. 129, no. 6, pp. 762–774, 2003.

[53] G. S. R. Davalath, M. K. S. Madugula, “Analysis/Design of Reinforced Concrete Circular Cross Sections,” *ACI Structural Journal*, vol. 85, no. 6, pp. 617–623, 1988.

[54] A. Şahin, “Mathematical models and solution algorithms for computational design of RC piles under structural effects,” *Applied Mathematical Modelling*, vol. 35, no. 7, pp. 3611–3638, 2011.

[55] K. Weber, M. Ernst, “Entwicklung von Interaktionsdiagrammen für asymmetrisch bewehrte Stahlbeton-Kreisquerschnitte.,” *Beton- und Stahlbetonbau*, vol. 84, no. 7, pp. 176–180, 1989.

[56] L. M. Gil-Martín, E. Hernández-Montes, M. Aschheim, “Optimization of piers for retaining walls,” *Structural and Multidisciplinary Optimization*, vol. 41, no. 6, pp. 979–987, 2010.

[57] F. Morán Cabré, “Monografía n^{o}. 304: Cálculo de secciones de hormigón armado, sometidas a solicitaciones normales, en el estado límite último,” Consejo Superior de Investigaciones Científicas, Patronato de Investigación Científica y Técnica Juan de la Cierva ,, Madrid, 1972.

[58] E. Hernández-Montes, L. M. Gil-Martín, *Hormigón Armado y Pretensado - Concreto Reforzado y Preesforzado* -, 1^{a} ed. Granada: Grupo de Investigación TEP-190 Ingeniería e Infraestructuras, Universidad de Granada, 2007, p. 402.

[59] Comité Europeo de Normalizacion, *Ejecución de trabajos geotécnicos especiales. Pilotes perforados. UNE-EN 1536*. Bruselas: Comité Europeo de Normalización, 2011, p. 89.

[60] H. Roscoe, D. Twine, “Design and performance of retaining walls,” *Proceedings of the ICE - Geotechnical Engineering*, vol. 163, no. 5, pp. 279–290, 2010.

[61] ONU, “Convención Marco de las Naciones Unidas sobre el cambio climático,” vol. 62301. Organización de las Naciones Unidas (ONU), Nueva York, 1992.

[62] ONU, “Protocolo de Kyoto de la Convención Marco de las Naciones Unidas sobre el cambio climático,” vol. 61702. Organización de las Naciones Unidas (ONU), Nueva York, 1998.

[63] W. Fang, S. M. Miller, “The effect of ESCO s on carbon dioxide emissions,” *Applied Economics*, vol. 45, no. 34, pp. 4796–4804, 2013.

[64] D. J. M. Flower, J. G. Sanjayan, “Green house gas emissions due to concrete manufacture,” *International Journal of Life Cycle Assessment*, vol. 12, no. 5, pp. 282–288, 2007.

[65] ArcelorMittal, “Tackling climate change.” [Online]. Available: http://corporate.arcelormittal.com/corporate-responsibility/environment/climate-change-and-energy/performance. [Accessed: 26-Oct-2013].

[66] T. E. Norgate, S. Jahanshahi, W. J. Rankin, “Assessing the environmental impact of metal production processes,” *Journal of Cleaner Production*, vol. 15, no. 8–9, pp. 838–848, 2007.

[67] R. van Berkel, “Eco-efficiency in primary metals production: Context, perspectives and methods,” *Resources, Conservation and Recycling*, vol. 51, no. 3, pp. 511–540, 2007.

[68] M. Yellishetty, G. M. Mudd, P. G. Ranjith, “The steel industry, abiotic resource depletion and life cycle assessment: a real or perceived issue?,” *Journal of Cleaner Production*, vol. 19, no. 1, pp. 78–90, 2011.

[69] M. Yellishetty, G. M. Mudd, P. G. Ranjith, A. Tharumarajah, “Environmental life-cycle comparisons of steel production and recycling: sustainability issues, problems and prospects,” *Environmental Science & Policy*, vol. 14, no. 6, pp. 650–663, 2011.

[70] D. Burchart-Korol, “Life cycle assessment of steel production in Poland: a case study,” *Journal of Cleaner Production*, vol. 54, pp. 235–243, 2013.

[71] The European Parliament and the Council of the European Union, “Directive 2003/87/EC of the European Parliament and of the Council of 13 October 2003 establishing a scheme for greenhouse gas emission allowance trading within the Community and amending Council Directive 96/61/EC,” *Official Journal of the European Union L275*, vol. 46, no. 25.10.2003, pp. 32–46, 2003.

[72] Ministerio de Agricultura Alimentación y Medio Ambiente, Gobierno de España, “¿Qué es el comercio de derechos de emisión?” [Online]. Available: http://www.magrama.gob.es/es/cambio-climatico/temas/comercio-de-derechos-de-emision/que-es-el-comercio-de-derechos-de-emision/default.aspx. [Accessed: 27-Oct-2013].

[73] Sistema Electrónico de Negociación de Derechos de Emisión de Dióxido de Carbono, “La Bolsa de SendeCO2.” [Online]. Available: http://www.sendeco2.com/. [Accessed: 27-Oct-2013].

[74] ADIF, “Túnel de Alta Velocidad Sants-La Sagrera.” [Online]. Available: http://www.adif.es/es_ES/comunicacion_y_prensa/fichas_de_actualidad/ficha_actualidad_00056.shtml. [Accessed: 27-Oct-2013].

[75] *Base de Costes de la Construcción de Andalucía*. Consejería de Fomento y Vivienda, Junta de Andalucía, 2013.

Anexo 1

Effective area in tension stiffening of reinforced concrete piles subjected to flexure according to Eurocode 2

Juan F. Carbonell-Márquez[1], Luisa. M. Gil-Martín[2], M. Alejandro Fernández-Ruíz[3] and Enrique Hernández-Montes[4]

ABSTRACT

There is a need of improvement in circular cross sections in the current codes of design of reinforced concrete structures. Asymmetric arrangement of reinforcement in concrete pile members employed as retaining earth systems has been recently introduced. The study of the behavior of those members under service loads requires the study of tension stiffening in circular cross sections under flexure. In order to apply tension stiffening, an effective area of concrete in tension is to be defined. General expressions to evaluate the effective area of concrete in tension are given and tested in full scale experiments of members with circular cross sections symmetrically and asymmetrically reinforced.

KEYWORDS:

Reinforced concrete; tension stiffening; effective area; asymmetric reinforcement; serviceability

NOTATION

A_c	Area of concrete
$A_{c,eff.}$	Effective area of concrete in tension
A_s	Area of steel
E_c, E_{cm}	Concrete elastic modulus

[1] PhD Candidate, Department of Structural Mechanics, University of Granada (UGR). Campus Universitario de Fuentenueva s/n. 18072 Granada, Spain. (corresponding author). Email jfcarbonell@ugr.es. Tel.: +34 958249965; fax: +34 958249959

[2] Associate Professor, Department of Structural Mechanics, University of Granada (UGR). Campus Universitario de Fuentenueva s/n. 18072 Granada, Spain. mlgil@ugr.es.

[3] PhD Candidate, Department of Structural Mechanics, University of Granada (UGR). Campus Universitario de Fuentenueva s/n. 18072 Granada, Spain. malejandrofr@ugr.es

[4] Professor, Department of Structural Mechanics, University of Granada (UGR). Campus Universitario de Fuentenueva s/n. 18072 Granada, Spain. emontes@ugr.es.

E_s	Steel elastic modulu
I_1, I_2	Second moments of area of the uncracked and fully cracked transformed cross sections about the horizontal principal axis of inertia
M	Bending moment
N	Axial load
R	Cross section radius
R_{int}	Radius of the circle that contains the center of gravity of the rebar
$R_{hc,effint}$, $R_{hc,effext}$	Radius of the internal and external circles that limit the circular strip of $A_{c,eff}$.
TSz	Tension Stiffening zone, height of the portion of cross section below the fiber whose deformation is ε_{ctm}
TSz_{top}	Portion of TSz located between the mechanical cover and the fiber whose deformation is ε_{ctm}
c	Mechanical cover
$h_{c,eff}$	Width of the circular strip composing the effective area of concrete in tension
$h_{c,effint}$, $h_{c,effext}$	Each of two portions in which $h_{c,eff}$ is divided interior and exterior
f_{ck}	Characteristic concrete compressive strength
f_{cm}	Average concrete compressive strength
f_{ctm}	Average concrete tensile strength
f_y	Steel yield limit stress
x	Position of neutral fiber in the cross section
y	Vertical coordinate measured from center of gravity of gross section
$\alpha_{\varepsilon ctm}$	Angular coordinate of the fiber whose strain is ε_{ctm}
$\alpha_{hc,effint,}$ $\alpha_{hc,effext}$	Angular coordinate of the radio vector fo the intersection of the interior/exterior circle defining $A_{c,eff}$ and the fiber whose strain is ε_{ctm}
ε	Strain
ε_{ap}	Apparent yield strain
ε_{cg}	Strain at center of gravity of the gross section
ε_{ctm}	Concrete limit strain of cracking
ε_y	Steel yield limit strain
ϕ	Curvature

Ø	Rebar diameter
θ	Angular coordinate
ρ	Reinforcement ratio
σ_c	Uncracked concrete stress
σ_{cTS}	Concrete tension stiffening stress
σ_s	Steel stress

1. Introduction

Traditionally, the reinforcement layout employed in the cross section of circular concrete members has been symmetric, even though the direction of loading had a clear direction, as in the case of pile walls built to retain earth in excavations. Recent works of TEP-190 research group at the University of Granada [1]–[3] have presented the strength design of asymmetrically reinforced concrete (RC) members with circular cross section under flexure – Fig. 1 –. However, behavior in service, i.e., cracking and deformation, of that type of members is still under study.

Fig. 1. Asymmetrical reinforcement for wall pile at construction site

When studying the short term deformation under flexure of RC members is essential to know the relationship between curvature and bending moment, $\phi - M$, for any particular cross section of the member. Once the $\phi - M$ relationship is obtained, the deformation of the entire member is computed by integration of the $\phi - M$.

To compute the full $\phi - M$ relationship of a RC cross section (for constant values of the axial force), the strain distribution which causes axial equilibrium has to be found for a particular value of the curvature, ϕ; employing that strain distribution, the value of the bending moment

M can be computed by integration of the corresponding normal stress distribution. Therefore, the stress – strain distributions for the materials composing the section – concrete and steel – have to be known.

Eurocode 2 (EC2) [4] or, equivalently, CEB-fib Model Code 2010 (MC2010) [5] propose concrete and steel stress – strain relationships but do not provide an explicit expression to model the tension stiffening behavior of RC of type $\sigma_{cTS} = \sigma_{cTS}(\varepsilon)$, that is, the average tensile behavior of the member after cracking. Instead of that, those codes contain an expression to evaluate the strain, curvature, or deflection which takes into account tension stiffening by interpolating the computed parameter between the corresponding to the uncracked and fully cracked states of the section.

$$\alpha = \zeta\alpha_2 + \beta\left(1-\zeta\right)\alpha_1 \tag{1}$$

In Eq. (1) α is the strain, curvature, or deflection after the section has cracked; α_1 y α_2 are the values of α computed for the uncracked and fully cracked conditions respectively; ζ is an interpolation coefficient that takes into account the effect of tension stiffening at a section that will be described below and β is a parameter that takes into account the duration of load and its repeatability. As short term processes are considered within this work, $\beta = 1.0$.

However, Hernández – Montes et al. [6] deduced a $\sigma_{cTS}(\varepsilon)$ relationship from the tension stiffening model included in "CEB Design Manual on Cracking and Deformations" [7] which is the same interpolation expression given in EC2 and MC2010:

$$\sigma_{cTS}\left(\varepsilon\right) = -\frac{\rho}{2}E_s\varepsilon + \sqrt{\left(\frac{\rho}{2}E_s\varepsilon\right)^2 + f_{ctm}^2\left(1+n\rho\right)} \tag{2}$$

where ρ is the reinforcement ratio, $n = E_s/E_c$, E_s and E_c are the elastic modulus of steel and concrete, respectively, and f_{ctm} is the tensile strength of concrete. Nevertheless, this $\sigma_{cTS}(\varepsilon)$ tension stiffening expression has to be applied to a particular portion of the cross section under tensile stress; since tension stiffening is due to bond between concrete and reinforcement, it

seems reasonable to apply the tension stiffening stress – strain relationship to a specific zone of the cross section around the reinforcing steel, that is, to an effective area of concrete in tension, $A_{c,eff}$. In fact, Bentz [8] suggests that average tension in the concrete will reduce to zero as the distance away from the bar reaches about half the crack spacing. According to this, he proposes a tension stiffening stress – strain relationship which varies along the depth of the cross section of the RC element. Originally, CEB-fib Model Code 1978 [9] proposes $A_{c,eff}$ to be the rectangular area tributary to and surrounding the bar of diameter Ø over an distance not exceeding 7.5Ø from the center of the bar [10], being this area truncated by geometrical limits of the member and without overlapping with the effective area of concrete corresponding to other bars – Fig. 2 –.

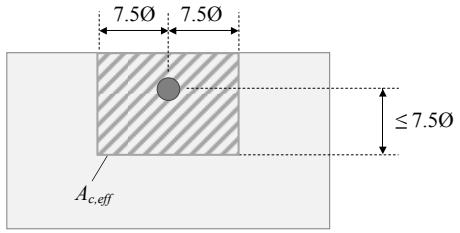

Fig. 2. Effective area of concrete in tension, $A_{c,eff}$, stiffened by the reinforcement steel bar [10]

The later versions of Model Code, MC90 [11] and MC2010 [5], change that definition of $A_{c,eff}$ to the values showed in Fig. 3; this definition is also proposed by EC2 [4].

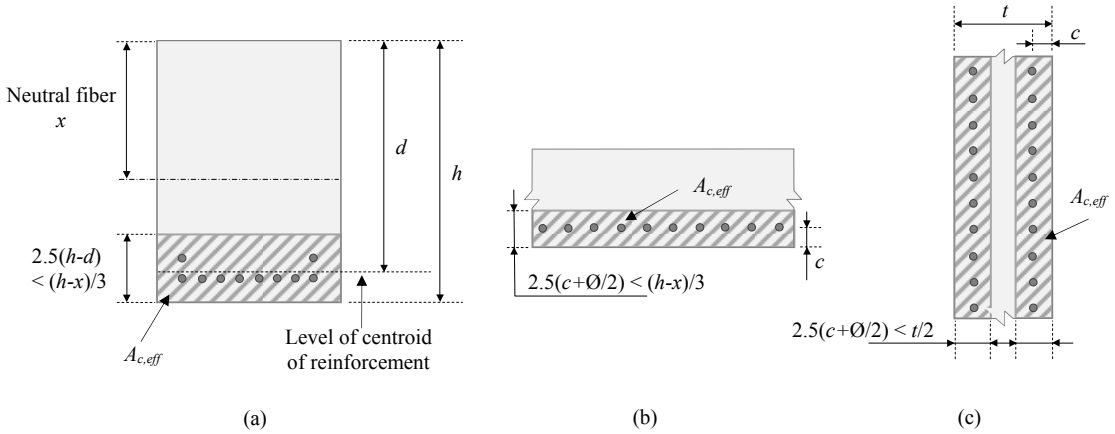

Fig. 3. Effective area of concrete in tension according to MC2010[5]**: (a) beam; (b) slab; (c) member in tension**

Manfredi and Pecce [12] present a refined fiber model for the analysis RC beams that include an explicit formulation of bond – slip relationship in which employ an effective area around the reinforcement that occupies the whole width of the section and has a height $h_{c,eff} = (c+8Ø)$, with

c being the concrete cover. Kwak and Song [13] set out in their cracking analysis of RC members that the effective area of concrete in tension can be represented by $A_{c,eff} \approx 1/4(1+n\rho)bh$, with *b* and *h* the width and height of the section respectively, $n = E_s/E_c$ and $\rho = A_s/bh$. Gilbert and Ranzi, in their book about time – dependent behavior of RC structures [14] present a method for predicting the maximum final crack width based on the Tension Chord Model of Marti et al. [15] and employ an effective area of concrete in tension equal to $A_{c,eff} = 1/2(h\text{-}x)b^*$, where b^* is the width of the section at the level of centroid of tensile steel but not greater than the number of bars in the tension zone multiplied by 12Ø. Castel et al. [16] propose a new value for $A_{c,eff}$ which is based on a multi-linear stress profile in the full depth of the concrete section between the flexural cracks, as shown in Fig. 4.

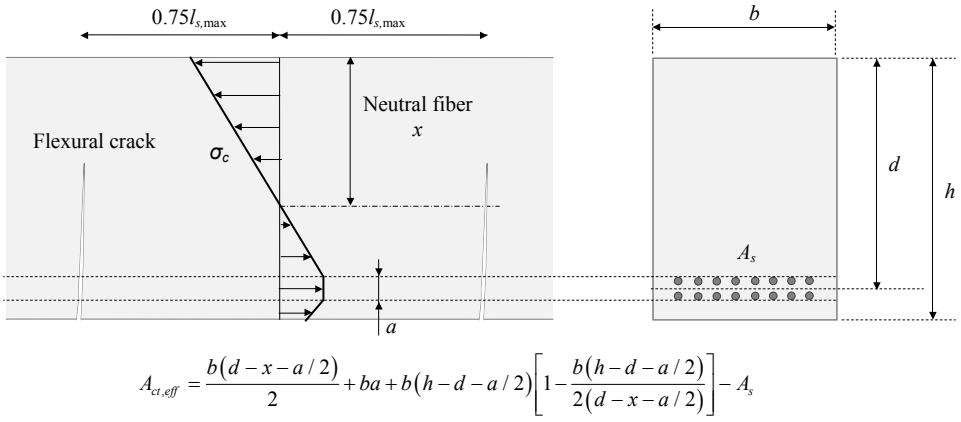

Fig. 4. Model of stress distribution in the concrete and effective area of concrete in tension proposed by Castel et al. [16]

Every above given expression for $A_{c,eff}$ has been applied to rectangular cross sections and the only found by the authors of this work related to circular cross sections is the one given by Wiese et al. [17]. The authors of that work deal with symmetrically reinforced cross sections and idealize the reinforcement as a continuous ring. The value of $A_{c,eff}$ that they employ is equal to the area of the circular strip which lies below the cross section neutral axis, i.e., in tension, whose width is $2.5(R\text{-}R_{int})$, where *R* is the radius of the section and R_{int} is the radius of the circle joining the reinforcement – Fig. 5 –.

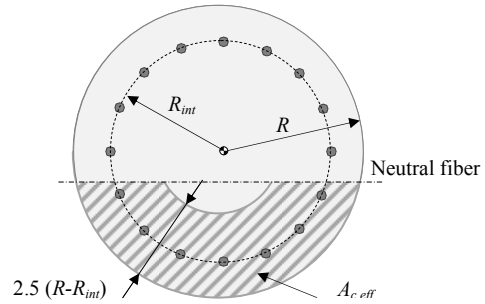

Fig. 5. Effective area of concrete in tension for circular cross sections proposed by Wiese et al. [17]

The present work presents a new definition of $A_{c,eff}$ in circular cross section for symmetric or asymmetric reinforcement layout, so that when integrating the $\sigma_{cTS}(\varepsilon)$ tension stiffening relationship, Eq. (2), given by Hernández–Montes et al. [6] – deduced from CEB Design Manual [7] – in the effective area of concrete in tension, the resulting $\phi - M$ relationship is the same as computing it with the interpolation equation Eq. (1) given in EC2 [4] or MC2010 [5] – Fig. 6–. Firstly, the expression of Hernández–Montes et al. [6] is presented in detail. Afterwards, the research of the proposed value of $A_{c,eff}$ is explained for circular sections and general expressions are given. The obtained ϕ–M relationships with the deduced $A_{c,eff}$ are compared with those from Eq. (1). Finally, the predictions of the deflection of some RC elements subjected to pure flexure are compared with the experimental results.

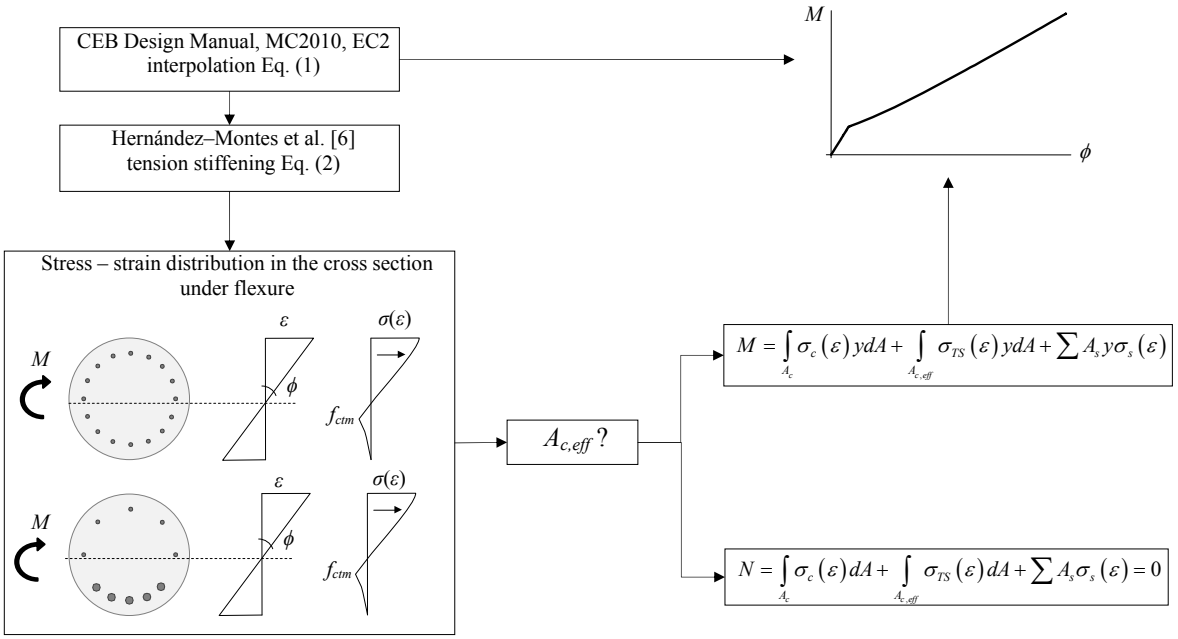

Fig. 6. Problem presentation

2. Previous considerations: hypothesis employed in this work and computation of the ϕ – M relationship

The numerical method employed by the authors in order to compute the ϕ–M relationship for a given RC section is a smeared crack approach and makes use of the Bernouilli's hypothesis that plane sections remain plane after deformation and assuming no slip of reinforcement so that the strain at any fiber of the section is given by:

$$\varepsilon(y, \varepsilon_{cg}, \phi) = \varepsilon_{cg} + y\,\phi \tag{3}$$

where ε_{cg} is the strain at the center of gravity of the gross section and y is the vertical coordinate of the fiber with its origin at that point of the section – Fig. 7 –. The former Eq. (3) can be also expressed in terms of the angle θ between the vertical principal axis of inertia of the section and the radio vector of the fiber where the strain is evaluated:

$$\varepsilon(\theta, \varepsilon_{cg}, \phi) = \varepsilon_{cg} + \phi\, R\cos\theta \tag{4}$$

In the present work, compression strain, stresses and forces are considered as positive as well as, bending moments which cause compression at top fiber.

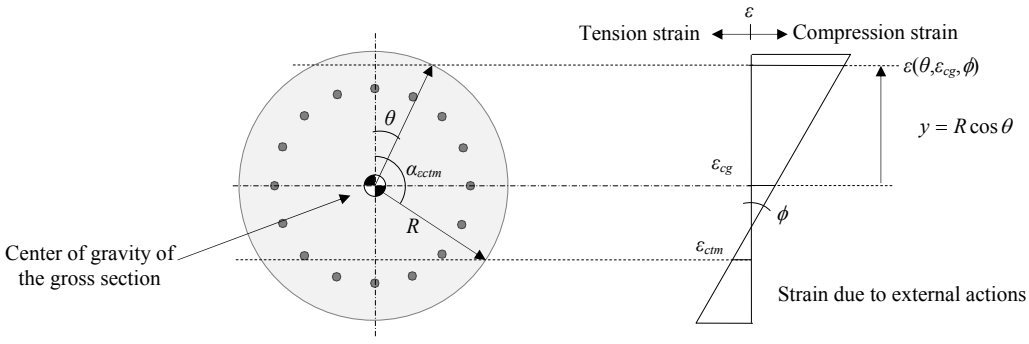

Fig. 7. Bernouilli's hyphotesis and strain at the cross section and nomenclature

In Fig. 7, $\alpha_{\varepsilon ctm}$ is the angle between the vertical principal axis of inertia and the radio vector of the fiber whose strain is the concrete limit strain of cracking, ε_{ctm}. Therefore, considering the stress–strain laws for concrete and steel, $\sigma_c(\varepsilon)$ and $\sigma_s(\varepsilon)$, given by EC2 and the tension stiffening

behavior of the concrete given by Eq. (2), the value of the resultant axial force N in the section for a given pair of values $\phi - \varepsilon_{cg}$ is:

$$N = 2\int_0^{\alpha_{\varepsilon ctm}} \left(R\sin\theta\right)^2 \sigma_c\left(\theta, \varepsilon_{cg,}\phi\right) d\theta + \int_{A_{c,eff}} \sigma_{cTS}\left(\theta, \varepsilon_{cg,}\phi\right) dA + \sum_j A_{\emptyset j}\sigma_s\left(y_j, \varepsilon_{cg,}\phi\right) \qquad (5)$$

where $A_{\emptyset j}$ and y_j are the cross sectional area and the vertical coordinate of each of the reinforcing steel bars, respectively. In Eq. (5), the stress–strain laws for concrete and steel, $\sigma_c(\varepsilon)$, $\sigma_{cTS}(\varepsilon)$ and $\sigma_s(\varepsilon)$, have been written directly as functions of the angle of the fiber, θ, the strain at the center of gravity of the section, ε_{cg}, and the curvature of the section, ϕ: $\sigma\left(\varepsilon\right) = \sigma\left(\varepsilon\left(\theta, \varepsilon_{cg}, \phi\right)\right) = \sigma\left(\theta, \varepsilon_{cg}, \phi\right)$.

Now, the ϕ–M relationship for the RC section is calculated in an iterative way: given a value of $\phi = \phi_i$, the strain at the center of gravity of the section, ε_{cgi}, which causes axial equilibrium is found employing the bisectional method. Once, ε_{cgi} is known, the strain at each fiber of the section can be obtained with Eq. (4), and the corresponding bending moment, M_i, is computed as:

$$M_i = \int_0^{\alpha_{\varepsilon ctm}} R^3 \sin^2\theta\cos\theta\sigma_c\left(\theta, \varepsilon_{cg,}\phi_i\right) d\theta + \int_{A_{c,eff}} \sigma_{cTS}\left(\theta, \varepsilon_{cg,}\phi_i\right) y dA + \sum_j A_{\emptyset j}\sigma_s\left(y_j, \varepsilon_{cg,}\phi_i\right) y_j \qquad (6)$$

A new value of ϕ is imposed and the process is repeated.

3. Material models employed in this work

3.1. Stress – strain model for uncracked concrete

The stress – strain model for uncracked concrete employed in this work is the one proposed by EC2. [4]. Therefore:

$$\sigma_c(\varepsilon)=\begin{cases} E_{cm}\varepsilon & \text{if} \quad \varepsilon_{ctm}\le\varepsilon<0 \\ f_{cm}\dfrac{k\eta(\varepsilon)-\eta(\varepsilon)^2}{1+(k-2)\eta(\varepsilon)} & \text{if} \quad 0\le\varepsilon<\varepsilon_{cu1} \end{cases} \tag{7}$$

where

$$\eta(\varepsilon)=\varepsilon/\varepsilon_{c1}$$

$$\varepsilon_{c1}=0.7f_{cm}^{\,0.31}<2.8 \quad [‰]$$

$$E_{cm}=22000\left(\frac{f_{cm}}{10}\right)^{0.3} \quad [\text{MPa}]$$

$$f_{cm}=f_{ck}+8 \quad [\text{MPa}]$$

$$\varepsilon_{ctm}=f_{ctm}/E_{cm}$$

$$f_{ctm}=\begin{cases} -0.3f_{ck}^{\,2/3} & f_{ck}\le 50\text{MPa} \\ -2.12\log\left(1+\dfrac{f_{cm}}{10}\right) & f_{ck}>50\text{MPa} \end{cases}$$

$$k=1.05E_{cm}\frac{\varepsilon_{c1}}{f_{cm}}$$

$$\varepsilon_{cu1}=\begin{cases} 3.5 & f_{cm}<50\text{MPa} \\ 2.8+27\left(\dfrac{(98-f_{cm})}{100}\right)^4 & f_{cm}\ge 50\text{MPa} \end{cases} \quad [‰]$$

3.2. The concrete tension stiffening model implicit in CEB Design Manual on Cracking and Deformation [7]

The model given in CEB Design Manual [7] considers tension stiffening as an increment of stiffness in the steel. This phenomenon of tension stiffening can most easily be understood by considering the mechanism of cracking of a reinforced concrete prism reinforced by a sole bar and subjected to pure tension. According CEB Design Manual [7] model, the stress–strain relationship for the reinforcement is given in terms of an average strain which is an intermediate value between the strain corresponding to an uncracked section, $\varepsilon_{s,1}$, and the corresponding to a fully cracked section, $\varepsilon_{s,2}$, that is, the bare bar. The values of $\varepsilon_{s,1}$ and , $\varepsilon_{s,2}$ are given by:

$$\varepsilon_{s,1} = \frac{N}{A_s E_s + A_{c,eff} E_c}$$
$$\varepsilon_{s,2} = \frac{N}{A_s E_s} \tag{8}$$

where N is the tensile axial load, A_s and $A_{c,eff}$ are the areas and E_s and E_c the elastic modulus of steel and concrete, respectively. Here it is assumed that the whole cross section of the member contributes to tension stiffening, so that $A_c = A_{c,eff}$.

Once N is greater than the cracking tensile force, N_{cr}, the average strain in the RC member is expressed as:

$$\varepsilon_{sm} = \frac{\Delta l}{l} = \varepsilon_{s,2} - \Delta\varepsilon_s \tag{9}$$

where $\Delta\varepsilon_s$ is the tension stiffening contribution of concrete which, according to CEB Design Manual, is given by:

$$\Delta\varepsilon_s = \Delta\varepsilon_{s\max} \frac{\sigma_{sr}}{\sigma_{s,2}} \tag{10}$$

In Eq. (10), σ_{sr} is the tensile stress in the steel assuming a fully cracked section under the load that causes tensile stress in the concrete equal to its maximum tensile strength, f_{ctm}:

$$\sigma_{sr} = f_{ctm} \frac{\left(1 + n\rho_{eff}\right)}{\rho_{eff}} \tag{11}$$

being $n = E_s / E_c$ and $\rho_{eff} = A_s / A_{c,eff}$; $\sigma_{s,2}$ in Eq. (10) is the stress at the reinforcement with fully cracked section:

$$\sigma_{s,2} = \frac{N}{A_s} \tag{12}$$

and $\Delta\varepsilon_{s\max}$ is the strain difference between the uncracked and fully cracked states just at the beginning of the cracking process:

$$\Delta\varepsilon_{s\max} = \varepsilon_{s,2} - \varepsilon_{s,1} \tag{13}$$

All these parameters can be easily understood by observing Fig. 8.

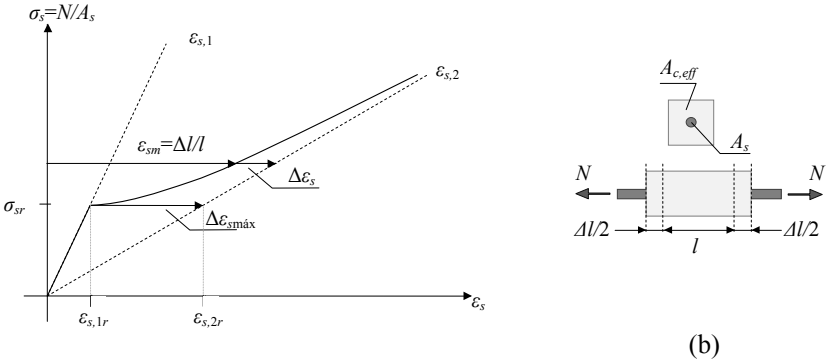

Fig. 8. Tension stiffening model proposed by CEB Design Manual on Cracking and Deformation [7]**: (a) stress –strain model for the reinforcement; (b) RC prism subjected to tensile force**

By introducing Eqs. (10) and (13) into Eq. (9), the average strain ε_{sm} remains:

$$\varepsilon_{sm} = \varepsilon_{s,2} - \left(\varepsilon_{s,2r} - \varepsilon_{s,1r}\right)\frac{\sigma_{sr}}{\sigma_{s,2}} \tag{14}$$

From Fig. 8 the following relationships can be stated:

$$\begin{aligned} \frac{\varepsilon_{s,2r}}{\varepsilon_{s,2}} &= \frac{\sigma_{sr}}{\sigma_{s,2}} \\ \varepsilon_{s,1r} = \varepsilon_{s,1}\frac{\varepsilon_{s,2r}}{\varepsilon_{s,2}} &= \varepsilon_{s,1}\frac{\sigma_{sr}}{\sigma_{s,fis}} \end{aligned} \tag{15}$$

Therefore, introducing the relationships given in Eq. (15) into Eq. (14), the average strain finally is expressed as:

$$\varepsilon_{sm} = \varepsilon_{s,1}\left(\frac{\sigma_{sr}}{\sigma_{s,2}}\right)^2 + \varepsilon_{s,2}\left[1 - \left(\frac{\sigma_{sr}}{\sigma_{s,2}}\right)^2\right] \tag{16}$$

This expression is similar to the one given by EC2 [4] or MC2010[5] – Eq. (1) –, being the parameter ζ equal to:

$$\zeta = 1 - \left(\frac{\sigma_{sr}}{\sigma_{s,2}}\right)^2 \tag{17}$$

Hernández–Montes et al. [6] take Eq. (16) and get an expression $\sigma(\varepsilon)$ that describes the tension stiffening contribution of the concrete. Thus, introducing the definitions of ε_{s1}, ε_{s2}, σ_{sr} and σ_{s2} given by Eqs. (8), (11) and (12) into Eq. (16), ε_{sm} is:

$$\varepsilon_{sm} = \frac{N}{A_s E_s + A_{c,eff} E_c} \left(\frac{f_{ctm} \left(1 + n\rho_{eff}\right) \Big/ \rho_{eff}}{N \Big/ A_s} \right)^2 + \frac{N}{A_s E_s} \left[1 - \left(\frac{f_{ctm} \left(1 + n\rho_{eff}\right) \Big/ \rho_{eff}}{N \Big/ A_s} \right)^2 \right] \tag{18}$$

Knowing that:

$$\frac{\left(1 + n\rho_{eff}\right)}{\rho_{eff}} = \frac{A_s E_s + A_{c,eff} E_c}{A_s E_c} \tag{19}$$

and writing ε instead of ε_{sm}, the expression given by (18) can be rewritten as quadratic equation with N as unknown:

$$N^2 E_c - N E_c A_s E_s \varepsilon - A_s \left(A_s E_s + A_{c,eff} E_c \right) f_{ctm}^2 = 0 \tag{20}$$

Since N is greater thant N_{cr}, it can be defined as:

$$N = A_{c,eff} \sigma_{cTS} + A_s E_s \varepsilon \tag{21}$$

where σ_{cTS} is the tension stiffening stress in the concrete. Substituting N by Eq. (21) in Eq. (20), the unknown parameter now in the quadratic equation is σ_{cTS}:

$$\sigma_{cTS}^2 + \sigma_{cTS} \frac{A_s E_s}{A_{c,eff}} \varepsilon - f_{ctm}^2 \frac{A_{c,eff} E_c + A_s E_s}{A_{c,eff} E_c} = 0 \tag{22}$$

Finally, solving in Eq. (22), the tension stiffening contribution of concrete remains:

$$\sigma_{cTS}\left(\varepsilon\right) = -\frac{\rho_{eff}}{2} E_s \varepsilon + \sqrt{\left(\frac{\rho_{eff}}{2} E_s \varepsilon \right)^2 + f_{ctm}^2 \left(1 + n\rho_{eff}\right)} \tag{23}$$

As it has been aforementioned, tensile strains and stresses are considered negative in this work. Therefore, Eq. (23) has to be rewritten as:

$$\sigma_{cTS}(\varepsilon) = \frac{\rho_{eff}}{2} E_s |\varepsilon| - \sqrt{\left(\frac{\rho_{eff}}{2} E_s |\varepsilon|\right)^2 + f_{ctm}^2 \left(1 + n\rho_{eff}\right)} \tag{24}$$

This equation is valid just until steel at any crack in the element reaches its tensile yield strain – ε_y. The average strain at the member in that moment, the apparent yield strain, can be found by equilibrium – Fig. 9 –:

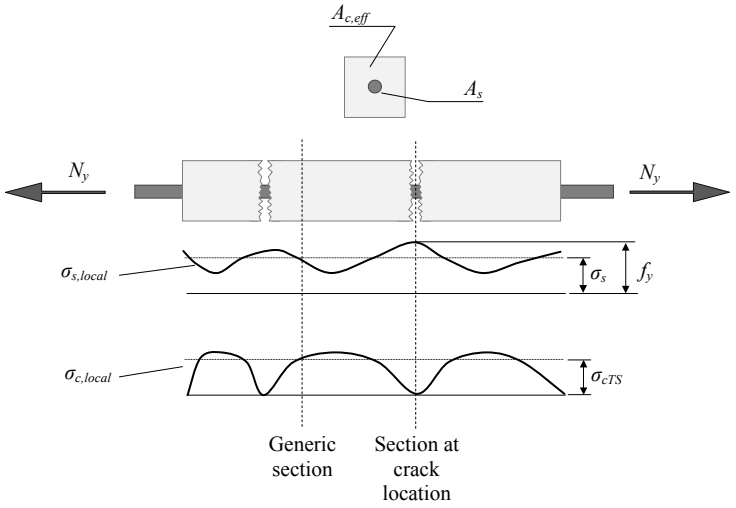

Fig. 9. Local and average stresses at the cracked prism

$$f_y A_s = \sigma_s(\varepsilon_{ap}) A_s + \sigma_{cTS}(\varepsilon_{ap}) A_{c,eff} \rightarrow \varepsilon_{ap} \tag{25}$$

If the strain keeps growing, the axial load will be constant and the average tensile stress in concrete will be reduced linearly until the average strain of the prism reaches ε_y – Fig. 10–.

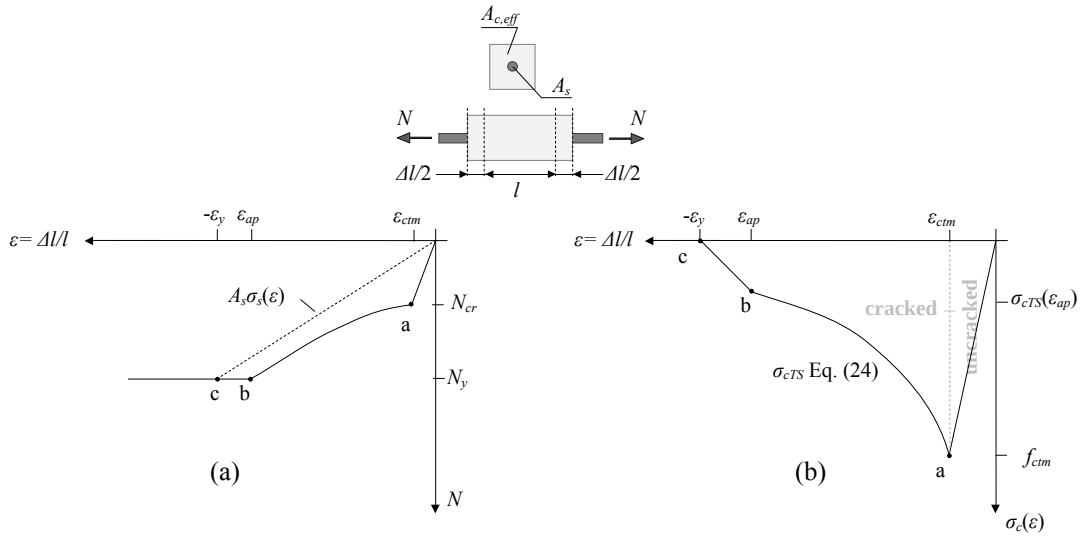

Fig. 10. RC prism subjected to axial tensile load: (a) load evolution versus average strain in the member; (b) stress – strain diagram of concrete in tension. Adapted from [18]

Therefore, the complete stress – strain expression for the cracked concrete is:

$$\sigma_{cTS}(\varepsilon) = \begin{cases} 0 & \text{if} \quad \varepsilon < -\varepsilon_y \\ \dfrac{\sigma_{cTS,ap}}{\varepsilon_y + \varepsilon_{ap}}\left(\varepsilon + \varepsilon_y\right) & \text{if} \quad -\varepsilon_y \le \varepsilon < \varepsilon_{ap} \\ \dfrac{\rho_{eff}}{2} E_s |\varepsilon| - \sqrt{\left(\dfrac{\rho_{eff}}{2} E_s |\varepsilon|\right)^2 + f_{ctm}^2\left(1 + n\rho_{eff}\right)} & \text{if} \quad \varepsilon_{ap} \le \varepsilon < \varepsilon_{ctm} \end{cases} \tag{26}$$

Eqs. (7) and (26) describe the complete behavior of concrete.

3.3. Reinforcing steel stress – strain model

For the steel of the reinforcement, the bilinear and symmetric model given in EC2[4] is employed. The hypothesis of symmetry is valid for the maximum spacing for the stirrups allowed by the majority of existing concrete codes [19]. According to this, the stress–strain relationship is given by:

$$\sigma_{cTS}(\varepsilon) = \begin{cases} -f_y & \text{if} \quad \varepsilon < -\varepsilon_y \\ E_s\varepsilon & \text{if} \quad -\varepsilon_y \le \varepsilon < \varepsilon_y \\ -f_y & \text{if} \quad \varepsilon \ge \varepsilon_y \end{cases} \tag{27}$$

being f_y the yield limit of the steel, $\varepsilon_y = f_y/E_s$, and E_s = 200 GPa.

4. Seeking the effective concrete area in tension stiffening

The stress–strain models for the materials composing the cross section of the member have been exposed, but still the axial force, N_{TS}, and bending moment, M_{TS}, produced by tension stiffening

$$\begin{aligned} N_{TS} &= \int_{A_{c,eff}} \sigma_{cTS}(\varepsilon)\, dA \\ M_{TS} &= \int_{A_{c,eff}} \sigma_{cTS}(\varepsilon)\, y dA \end{aligned} \tag{28}$$

cannot be computed since $A_{c,eff}$ is an unknown parameter.

As above mentioned, this work intends to find an expression for $A_{c,eff}$ so that the resulting ϕ–M relationship is the same as the one computed with Eq. (1). In that equation, the parameter that takes into consideration the tension stiffening, ζ, is defined by Eq. (17). However, EC2 [4] and MC2010 [5] allow to compute that parameter as follows, when the RC element is subjected to pure bending:

$$\zeta = 1 - \left(\frac{M_{cr}}{M}\right)^2 \tag{29}$$

where M_{cr} is the cracking moment and M is the moment to which the element is subjected. If this parameter is included in Eq. (1) and being α the curvature ϕ, it remains:

$$\phi = \left(1 - \left(\frac{M_{cr}}{M}\right)^2\right)\phi_2 + \left(\frac{M_{cr}}{M}\right)^2 \phi_1 \tag{30}$$

Writing the uncracked and fully cracked curvatures, ϕ_1 and ϕ_2, in terms of the bending moment M and the second moments of area of the uncracked and fully cracked transformed cross sections about the horizontal principal axis of inertia, I_1 and I_2, an expression of the type $M(\phi)$ can be obtained from Eq. (30) as:

$$M(\phi) = \frac{\phi E_{cm} I_2}{2} + \sqrt{\left(\frac{\phi E_{cm} I_2}{2}\right)^2 - M_{cr}^2 \left(\frac{I_2}{I_1} - 1\right)} \tag{31}$$

The expression given in Eq. (31) determines the values that have to be gotten for a particular value of ϕ when using the correct value for $A_{c,eff}$.

4.1. Adopted model for $A_{c,eff}$

In this work, it is assumed that, for a given strain distribution, that is, a pair of $\phi - \varepsilon_{cg}$, the effective area of concrete in tension, $A_{c,eff}$, is a circular strip whose width is $h_{c,eff}$ placed in the tensile side of the section below the horizontal fiber whose deformation is ε_{ctm} – Fig. 11 –. Other models have been intended to be used for effective area but the presented here is the one which gave better results.

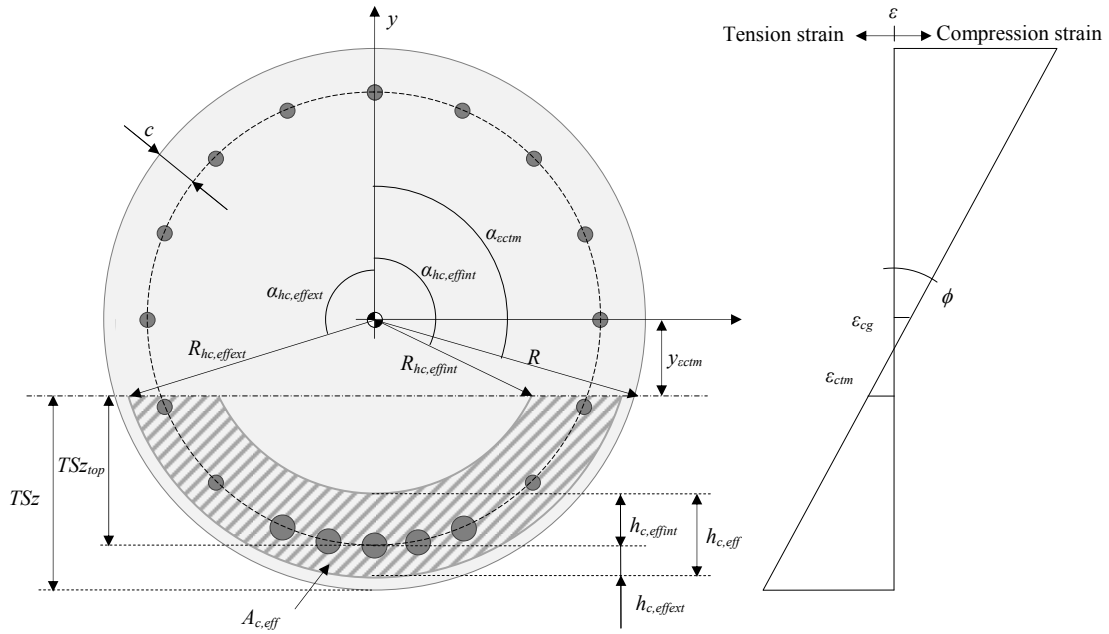

Fig. 11. Definition and nomenclature for $A_{c,eff}$

The width $h_{c,eff}$ is distributed around the circle that links the center of gravity of the bars. $h_{c,eff}$ is divided in two portions: interior ,$h_{c,effint}$, and exterior ,$h_{c,effext}$. This division is made taking into account the rate TSz_{top}/TSz; TSz – Tension Stiffening zone – is the distance that exists from the bottom fiber of the cross section and the fiber whose strain is ε_{ctm}, and TSz_{top} is TSz minus the mechanical cover of the reinforcement, c, – Fig. 11 –. Therefore:

$$h_{c,effint} = h_{c,eff}\frac{TSz_{top}}{TSz} \le R - c$$
$$h_{c.effext} = h_{c,eff} - h_{c,effint} \tag{32}$$

Once the distribution of $h_{c,eff}$ is known, the other parameters that define $A_{c,eff}$ can be computed: $R_{hc,effint}$ and $R_{hc,effext}$ are the radius of the internal and external circles that limit the circular strip; $\alpha_{hc,effint}$ is the angle between the vertical principal axis of inertia and the radio vector of the intersection of the interior circle defining $A_{c,eff}$ and the fiber whose strain is ε_{ctm}; $\alpha_{hc,effext}$ is defined equivalently for the exterior circle – Fig. 11 –. Knowing all the parameters that define $A_{c,eff}$, the integral expressions given in Eq. (28) become:

$$\begin{aligned} N_{TS} &= 2\left(R_{hc,effext}^2 \int_{\alpha_{hc,effext}}^{\pi} \sigma_{cTS}(\varepsilon)\sin^2 d\theta - R_{hc,effint}^2 \int_{\alpha_{hc,effint}}^{\pi} \sigma_{cTS}(\varepsilon)2\sin^2 d\theta \right) \\ M_{TS} &= 2\left(R_{hc,effext}^3 \int_{\alpha_{hc,effext}}^{\pi} \sigma_{cTS}(\varepsilon)\sin^2\theta\cos\theta d\theta - R_{hc,effint}^3 \int_{\alpha_{hc,effint}}^{\pi} \sigma_{cTS}(\varepsilon)\sin^2\theta\cos\theta d\theta \right) \end{aligned} \quad (33)$$

Therefore, if the strain distribution and the value of $h_{c,eff}$ are known, the axial load and the bending moment acting at the cross section can be computed. Now, assuming pure flexure, if the value of $A_{c,eff}$, that is, $h_{c,eff}$, that yields the same bending moment given by Eq. (31) for a particular value of ϕ, a bisectional method is followed taking as bottom and upper values for the width of $A_{c,eff}$: $h_{c,effb} = 0$ and $h_{c,efft} = R$; this process is finished when the difference from the moment computed with Eq. (31) and that computed with Eqs. (6) and (33) is less than 0.1 N·m – Fig. 12 –.

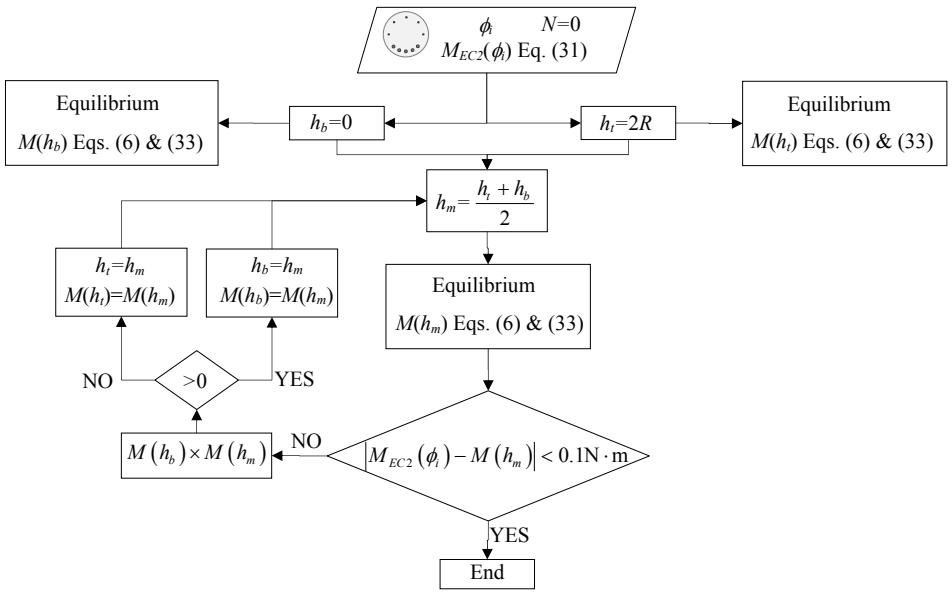

Fig. 12. Flow chart of the $h_{c,eff}$ finding process. For the sake of simplicity the bottom and upper values $h_{c,eff}$ in the bisectional method have been called h_b and h_t; the same has been applied to the middle value h_m

This procedure is repeated for monotonic values of the curvature greater than the one which causes cracking and within the elastic range of the materials, since Eq. (1) and so Eq.(31) are of application in it. Fig. 13 shows an example of asymmetric section and the evolution of $h_{c,eff}$ with the position of the neutral fiber in the section.

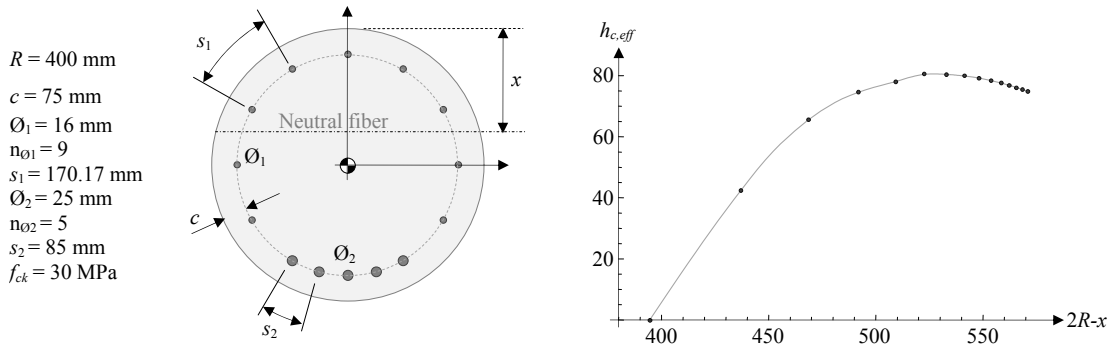

Fig. 13. Example of the evolution of $h_{c,eff}$ with the position of the neutral fiber for a RC pile with asymmetrical displacement of reinforcement

4.2. Selected pile sections and general expression for the evolution of $h_{c,eff}$ with the position of the neutral fiber, x

The same process as in the example presented in Fig. 13 is carried out in many different cross section configurations, both symmetric and asymmetric. The placement of reinforcement bars within the cross section is done according to the recommendations of the company Armatek® relating the automatized fabrication of the reinforcement assembly. Also, the prescriptions of EC2 [20] have been followed relating the maximum and minimum number of bars within the cross section. According to this:

- The maximum spacing between consecutive bars is 200 mm
- The minimum spacing between consecutive bars is the maximum value amongst: 2Ø, 5+d_g+Ø and Ø+20 mm, where d_g is the coarse aggregate size
- There will be a minimum of 6 bars
- The minimum diameter for the bars is $Ø_{min}$ = 16 mm

The values for the radius, R, of the piles are 300mm, 400 mm, 500 mm and 600 mm, all of them with a mechanical cover of c = 75 mm. For the symmetric reinforcement, bars of diameter, Ø, 20, 25 and 32 mm have been tested and for the asymmetric the main reinforcement diameters $Ø_2$ are 25 and 32 mm and the rest of bars are of diameter $Ø_1$ = 16 mm. The entire set of cross sections that have been utilized are presented in Appendix 1.

Fig. 14 shows the results for the evolution of $h_{c,eff}$ with the position of the neutral fiber, this being measured from the bottom fiber of the cross section. Not important changes are detected when using a different value for f_{ck}; for the sake of simplicity only the results of f_{ck} = 30 MPa are shown. The symmetric cases correspond to Fig. 14 (a) and the results for the unsymmetrical disposition of reinforcement are displayed in Fig. 14 (b). The results are similar for the same diameter of the pile cross-section.

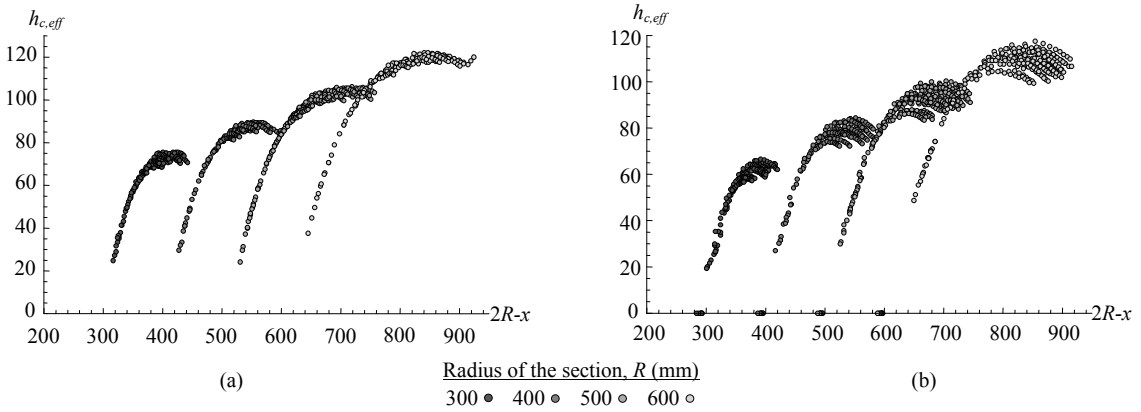

Fig. 14. Evolution of $h_{c,eff}$ with the position of the neutral fiber x for different cross section diameters: (a) symmetric cases; (b) asymmetric cases

The results for both cases, symmetric and asymmetric, can be clumped together if the system of coordinates is lightly modified: the original values of the abscissa are divided by the pile diameter and the ordinates are divided by $R^{2/3}$. By doing so, the numerically obtained values can be adjusted employing the least square method by a parabolic law with good adjustment. Fig. 15 shows the comparison between the numerical values and the adjustments for both cases, symmetric and asymmetric. If the coordinate system transformation is undone, the proposed general expressions which provide the evolution of $h_{c,eff}$ remain:

a) Symmetric case:

$$h_{c,eff} = \frac{1}{R^{4/3}}\left(-1.765R^2 + 11.343R \cdot x - 9.375x^2\right) \tag{34}$$

b) Asymmetric case:

$$h_{c,eff} = \frac{1}{R^{4/3}}\left(-1.117R^2 + 8.657R \cdot x - 7.132x^2\right) \tag{35}$$

In Eqs. (34) and (35) the values of $h_{c,eff}$, R and x are given in mm.

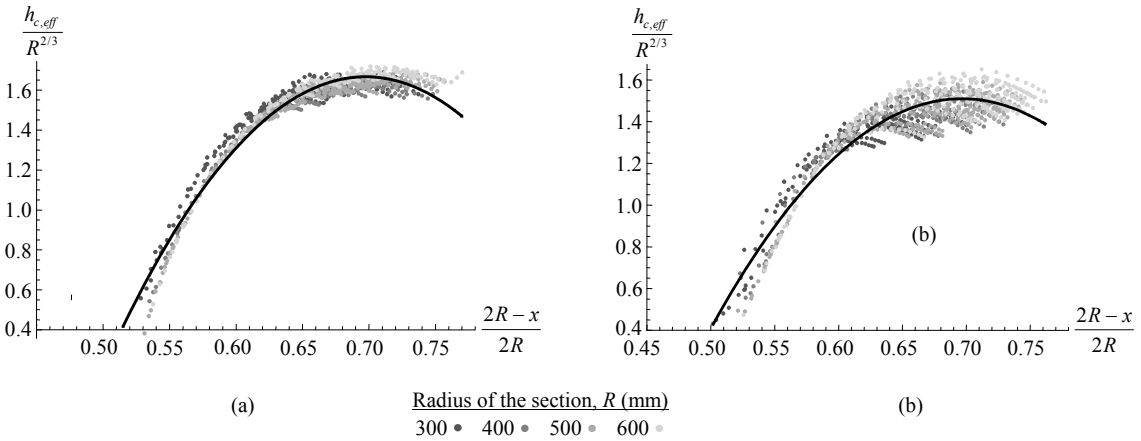

Fig. 15. Parabolic adjustment for $h_{c,eff}$ with the position of the neutral fiber x after the normalization: (a) symmetric cases; (b) asymmetric cases : (a) symmetric cases; (b) asymmetric cases

Although, as above mentioned, Eq. (31) is of application in the elastic range of concrete and steel, the deduced expressions for $h_{c,eff}$ are used, in this work, also out of that range when computing the ϕ–M relationship of the cross section.

5. Examples and applications

The above proposed expressions for the evaluation of $h_{c,eff}$ in terms of the position of the neutral fiber, x, are tested in two experiments with circular RC cross sections, one symmetric and other asymmetric. The experiments consist of two 4 m long piles subjected to 4–point bending – Fig. 16 –, with cross section diameter of 400 mm. The supports separation is 3.6 m and the distance from the application of the loads to the supports is 1.0 m, so that there is a central segment of the specimen being subjected to a bending moment of P KN·m, with P the applied load. Both structural elements are conduced to rupture without significant development of shear cracks. In both experiments, the deflection of the member at mid span is measured and strain gauges are

located at the reinforcement bars and at the same section level in order to measure the longitudinal strain of those bars and, subsequently, deduce the curvature of the section assuming plane sections remain plane after deformation.

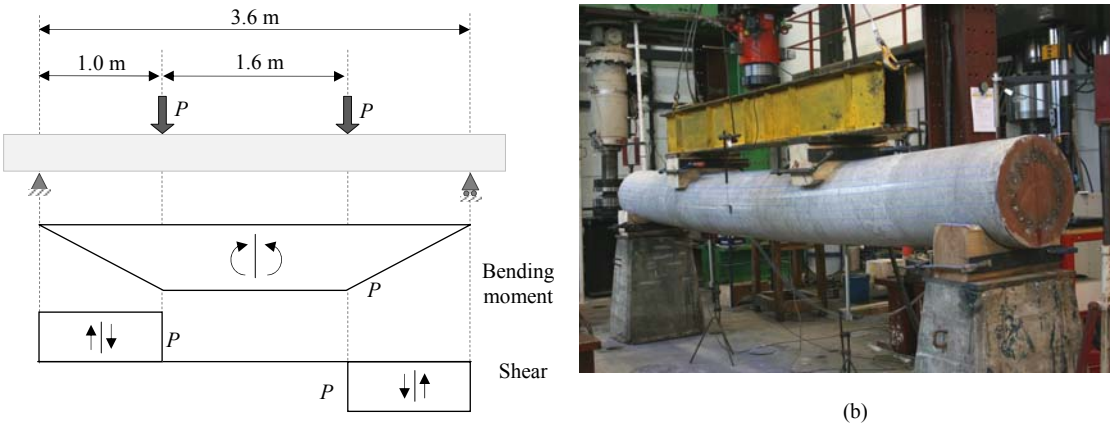

Fig. 16. 4 – point bending tests in RC piles: (a) experiment disposition; (b) specimen being tested

5.1. Symmetric cross section

The cross section of the first tested RC pile member consists of 16 bars of Ø 16 mm equally spaced with a mechanical cover c = 77 mm. Fig. 17 (a) shows the details of the cross-section and Fig. 17 (b) shows one of the ends of the element, where steel plates are placed to which the longitudinal bars are welded in order to guarantee the anchorage of the bars. Although the member is transversally reinforced with stirrups of Ø 10 mm each 200 mm, no confinement effect is taken into account in the concrete model, whose mean compressive strength f_{cm} is 34.8 MPa after 28 days. For the steel, values of f_y = 500 MPa and E_s = 200 GPa are used in the computations.

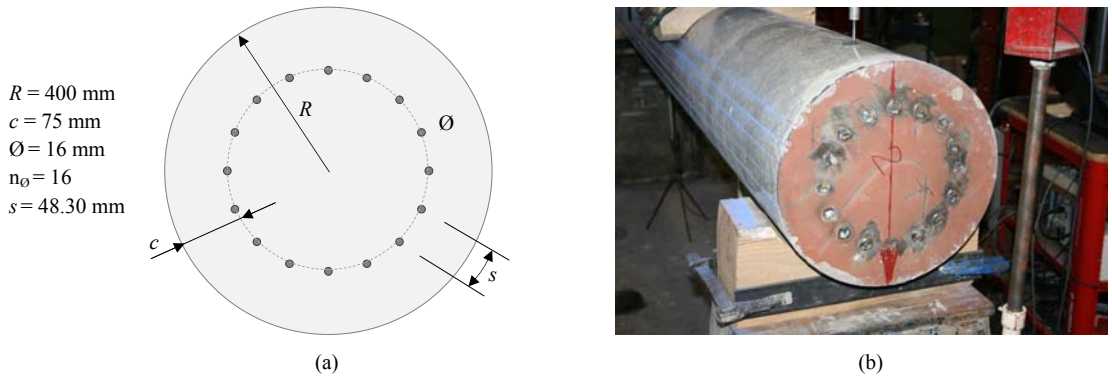

Fig. 17. Symmetric cross section: (a) cross section configuration; (b) steel plate at the end of the element to anchor the reinforcement

Fig. 18 (a) shows the comparison of the $\phi - M$ relationship obtained with Eq.(31) deduced from EC2 and that computed by integration of stresses according to the procedure explained in part 2 and making use of the $A_{c,eff}$ definition given in Fig. 11 and Eq (34). It can be observed the good agreement between both computations even though the mean value of concrete is not 30MPa, -the one employed to obtain Eq. (34)-. In the other hand, Fig. 18 (b) represents the measured ϕ – M relationship in a cross section of the tested element placed at the central segment with constant bending moment law and that relationship computed as above mentioned. The observed differences at the end of the graphic are due to the actual yield strain of the reinforcing steel, which is greater than the employed in the simulation. However, the agreement between the test and the simulation is very good in general. The consequences of this good agreement are observed in Fig. 18 (c) where is represented the deflection at mid-span of the tested element, which in the simulation is computed by integration of the curvature along the member.

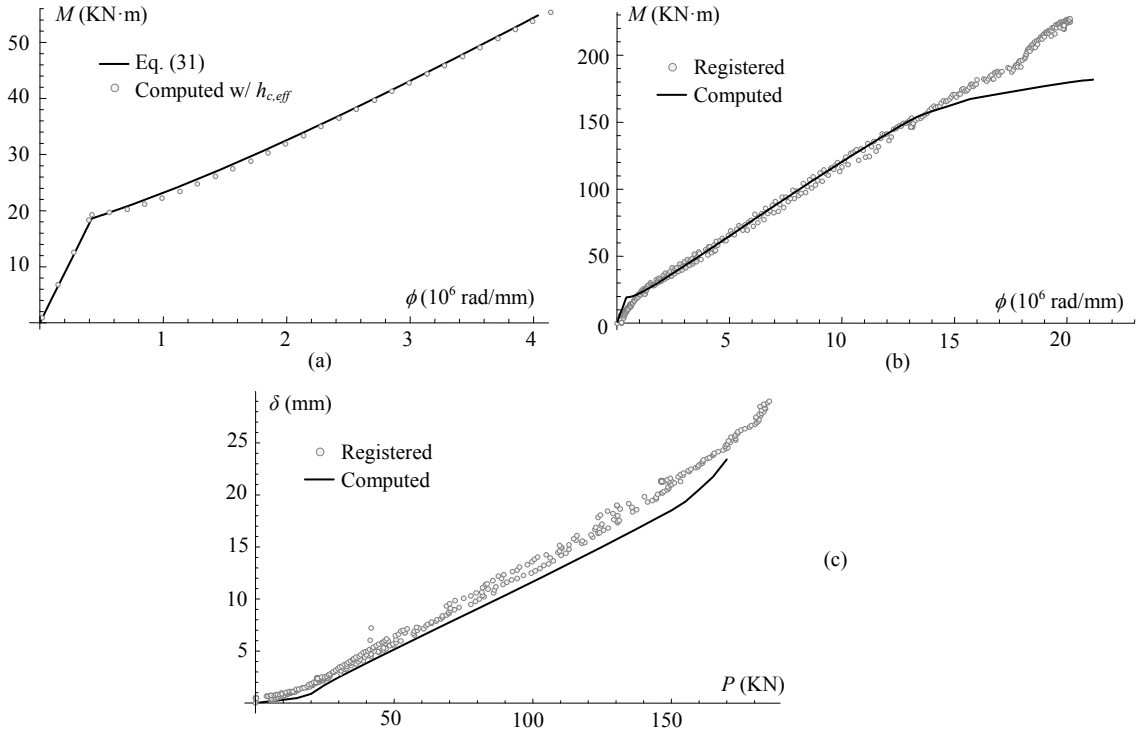

Fig. 18. Results for symmetric case: (a) comparison of the $\phi - M$ values obtained integrating the stresses at the section employing the definition of $h_{c,eff}$ given by Eq. (34) and the values obtained with EC2 Eq. (31); (b) $\phi - M$ relationships registered in the experiment and computed with the exposed method employing Eq. (34); (c) deflections at mid-span of the member with the increment of *P* registered at the experiment and computed by integration of the computed $\phi - M$ relationship.

For the asymmetric cross section, five bars of Ø 16 mm are placed at the bottom of the section, with the same mechanical cover as in the previous case, c = 77 mm, with a separation between bars of 41 mm, and the rest of the cross section is reinforced by means of 3 bars of Ø 10 mm separated 193.21 mm. In this case, Ø 10 mm stirrups are placed at a distance of 150 mm but, as in the previous case, no confinement effect is considered. The concrete mix in the asymmetric case has a mean compressive strength of f_{cm} = 31.2 MPa and the steel is the same as in the symmetric case.

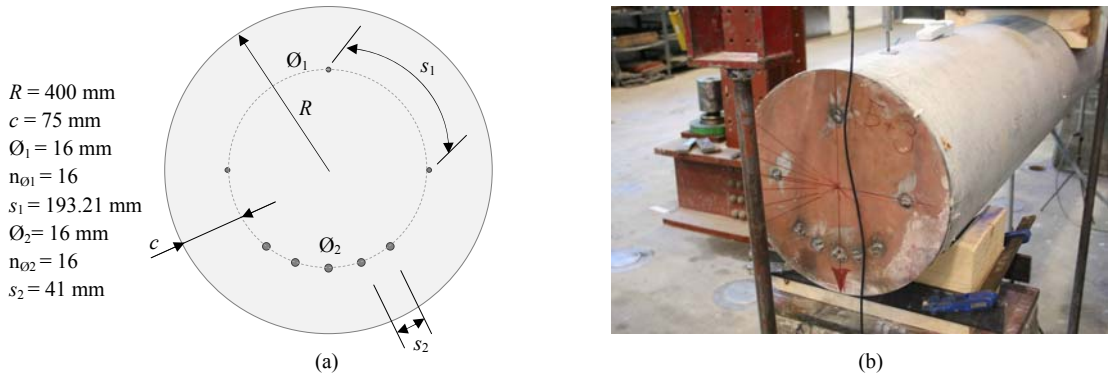

Fig. 19. Asymmetric cross section: (a) cross section configuration; (b) steel plate at the end of the element to anchor the reinforcement

Fig. 20 shows the results for the asymmetric case. As observed in Fig. 20 (a), the ϕ –M relationship computed taking into account the value of $h_{c,eff}$ given by Eq. (35) and the one calculated with Eq. (31) are almost the same. Furthermore, the registered and the computed ϕ – M relationships presented in Fig. 20 (b) have a good adjustment. Here again, as mentioned for the previous case, the differences between the assumed and actual yield strains of the reinforcement lead to deviations between registered and computed results. Fig. 20 (c) shows the deflection at the mid-span of the member. In this case, the differences between computed and registered results are greater than in the symmetric case. The reason for this phenomenon can be found in the shrinkage, which has not been taken into account in the computations. By observing the cross section configuration – Fig. 19–, it may be understood that concrete around bottom reinforcement is more limited to shrinkage strain than concrete in the rest of the section, leading to greater values of shrinkage that induce curvature. In the symmetric case, all concrete in the cross section is equally constricted to shrinkage and, therefore, its effect is less noticeable.

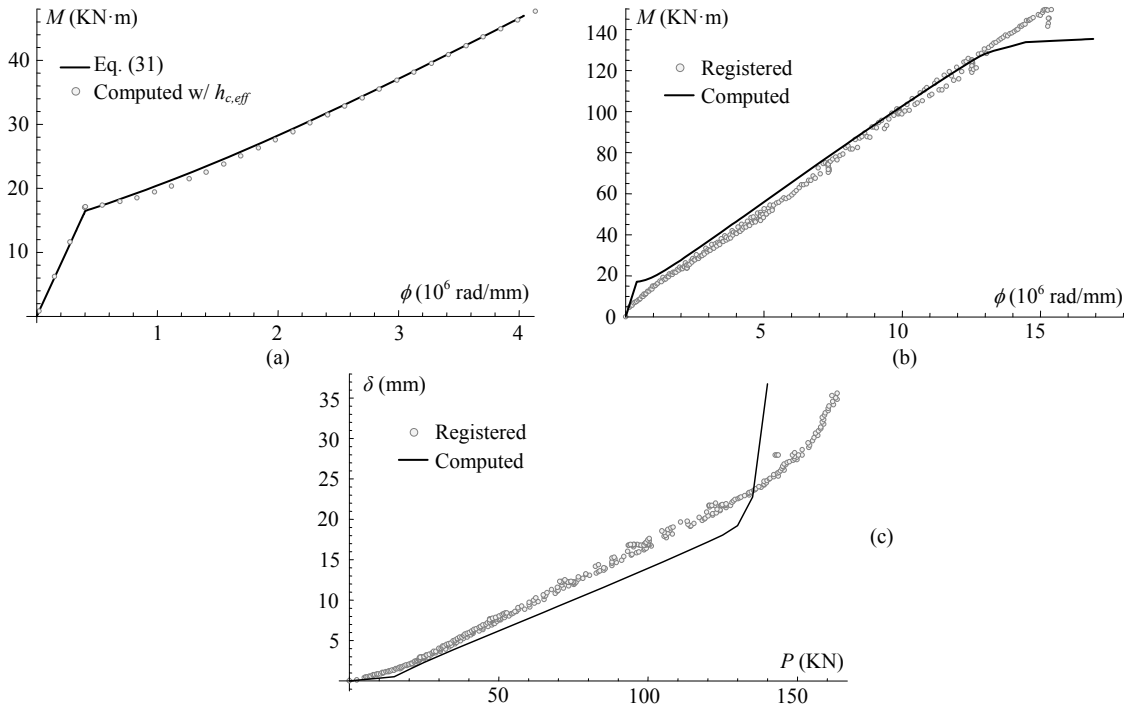

Fig. 20. Results for symmetric case: (a) comparison of the $\phi - M$ values obtained integrating the stresses at the section employing the definition of $h_{c,eff}$ given by Eq. (35) and the values obtained with EC2 Eq. (31); (b) $\phi - M$ relationships registered in the experiment and computed with the exposed method employing Eq. (35); (c) deflections at mid-span of the member with the increment of P registered at the experiment and computed by integration of the computed $\phi - M$ relationship.

6. Conclusions

Current codes of design of RC structures are oriented to rectangular and T-type cross section types and there is a clear lack of treatment of circular cross sections. In this context, the effective area of concrete in tension, $A_{c,eff}$, has been studied for rectangular or T-type sections at once with the tension stiffening effect, and codes of design, i.e., Eurocode 2 or CEB-fib Model Code 2010, suggest standard values for this effective area to be take into account in the serviceability computations of reinforced concrete structures. However, no treatment for circular sections is found.

A model to represent the evolution of the effective area in tension as cross sectional strain changes has been introduced. General expressions for the evolution of $A_{c,eff}$ with the neutral fiber of the section has been presented in this work for circular sections. These expressions have been deduced by obtaining the necessary values of $A_{c,eff}$ in order to get the same $\phi - M$ relationship

than the one given by the interpolation equation suggested by Eurocode 2. As asymmetric cross sections have been introduced in the construction of retaining earth structures, two different expressions have been presented: one for symmetric reinforced sections and another for asymmetric reinforced sections. The proposed expressions have been tested with real scale experiments of two RC piles, symmetric and asymmetric, and they showed to work properly in both cases.

In order to make the work self–contained, the employed computation process of ϕ–M relationship has been explained as well as the used material models, including the tension stiffening model implicitly included in CEB Design Manual for cracking and deformation.

7. Appendix 1

The sections employed in the study of the evolution of hc,eff with the position of x presented in part 4 of this work are exposed. Table 1 shows the radius, the diameter and the number of bars equally spaced in the symmetric solutions. In the other hand, Table 2 presents the employed asymmetrical cross sections; for this type of reinforcement, the radious of the pile, the diameter, number and space between bars of the same diameter are given for the two groups of bars.

Table 1. Symmetric cross sections with equally spaced bars employed in the study of the evolution of $h_{c,eff}$ with x

Section	R(mm)	Ø (mm)	N. Bars
1	300	20	8
2	300	20	10
3	300	20	12
4	300	20	20
5	300	20	24
6	300	25	8
7	300	25	10
8	300	25	12
9	300	25	20
10	300	25	24
11	300	32	8
12	300	32	10
13	300	32	12
14	300	32	20
15	400	20	12
16	400	20	18
17	400	20	20
18	400	20	24
19	400	25	12
20	400	25	18
21	400	25	20
22	400	25	24
23	400	32	12
24	400	32	18
25	400	32	20
26	400	32	24

Section	R(mm)	Ø (mm)	N. Bars
27	500	20	16
28	500	20	18
29	500	20	20
30	500	20	24
31	500	20	36
32	500	20	40
33	500	20	48
34	500	25	16
35	500	25	18
36	500	25	20
37	500	25	24
38	500	25	36
39	500	25	40
40	500	25	48
41	500	32	16
42	500	32	18
43	500	32	20
44	500	32	24
45	500	32	36
46	500	32	40
47	500	32	48
48	600	20	18
49	600	20	24
50	600	20	36
51	600	20	48
52	600	25	18
53	600	25	24
54	600	25	36
55	600	25	48
56	600	32	18
57	600	32	24
58	600	32	36
59	600	32	48

Table 2. Asymmetric cross sections with equally spaced bars employed in the study of the evolution of $h_{c,eff}$ with

Section	R(mm)	$Ø_1$ (mm)	N. Bars	s_1 (mm)	Ø2 (mm)	N. Bars	s_2 (mm)
1	300	16	9	141.37	25	3	70.69
2	300	16	7	176.71	25	3	58.90
3	300	16	7	141.37	25	5	70.69
4	300	16	7	176.71	25	5	58.90
5	300	16	7	141.37	25	7	70.69
6	300	16	5	176.71	25	7	58.90
7	300	16	9	141.37	32	3	70.69
8	300	16	7	176.71	32	3	58.90
9	300	16	7	141.37	32	5	70.69
10	300	16	7	176.71	32	5	58.90
11	300	16	7	141.37	32	7	70.69
12	300	16	5	176.71	32	7	58.90
13	400	16	15	113.45	25	3	113.45
14	400	16	11	170.17	25	3	85.08
15	400	16	13	113.45	25	5	113.45
16	400	16	9	170.17	25	5	85.08
17	400	16	11	113.45	25	7	113.45
18	400	16	9	170.17	25	7	85.08
19	400	16	15	113.45	32	3	113.45
20	400	16	11	170.17	32	3	85.08
21	400	16	13	113.45	32	5	113.45
22	400	16	9	170.17	32	5	85.08
23	400	16	11	113.45	32	7	113.45
24	400	16	9	170.17	32	7	85.08
25	500	16	21	111.26	25	3	111.26
26	500	16	17	148.35	25	3	74.18
27	500	16	19	133.52	25	3	66.76
28	500	16	19	111.26	25	5	111.26
29	500	16	15	148.35	25	5	74.18
30	500	16	17	133.52	25	5	66.76
31	500	16	17	111.26	25	7	111.26
32	500	16	15	148.35	25	7	74.18
33	500	16	17	133.52	25	7	66.76
34	500	16	15	111.26	25	9	111.26

Section	R(mm)	$Ø_1$ (mm)	N. Bars	s_1 (mm)	Ø2 (mm)	N. Bars	s_2 (mm)
35	500	16	13	148.35	25	9	74.18
36	500	16	15	133.52	25	9	66.76
37	500	16	21	111.26	32	3	111.26
38	500	16	17	148.35	32	3	74.18
39	500	16	19	133.52	32	3	66.76
40	500	16	19	111.26	32	5	111.26
41	500	16	15	148.35	32	5	74.18
42	500	16	17	133.52	32	5	66.76
43	500	16	17	111.26	32	7	111.26
44	500	16	15	148.35	32	7	74.18
45	500	16	17	133.52	32	7	66.76
46	500	16	15	111.26	32	9	111.26
47	500	16	13	148.35	32	9	74.18
48	500	16	15	133.52	32	9	66.76
49	600	16	21	137.44	25	3	137.44
50	600	16	17	183.26	25	3	91.63
51	600	16	23	137.44	25	3	68.72
52	600	16	19	137.44	25	5	137.44
53	600	16	15	183.26	25	5	91.63
54	600	16	21	137.44	25	5	68.72
55	600	16	17	137.44	25	7	137.44
56	600	16	15	183.26	25	7	91.63
57	600	16	21	137.44	25	7	68.72
58	600	16	21	137.44	32	3	137.44
59	600	16	17	183.26	32	3	91.63
60	600	16	23	137.44	32	3	68.72
61	600	16	19	137.44	32	5	137.44
62	600	16	15	183.26	32	5	91.63
63	600	16	21	137.44	32	5	68.72
64	600	16	17	137.44	32	7	137.44
65	600	16	15	183.26	32	7	91.63
66	600	16	21	137.44	32	7	68.72

8. Acknowledgments

Our gratitude to the industrial company Armatek for their assistance in the possible location of the reinforcing steel bars within the section. The present paper was financed by the Ministry of Science and Innovation under the research project IPT-2011-1485-420000. The first author is a Spanish Government PhD fellow (FPU grant AP 2010-3707). This support is gratefully acknowledged.

References

[1] L. M. Gil-Martín, E. Hernández-Montes, M. Aschheim, "Optimization of piers for retaining walls," *Structural and Multidisciplinary Optimization*, vol. 41, no. 6, pp. 979–987, 2010.

[2] L. M. Gil-Martín, E. Hernández-Montes, M. Shin, M. Aschheim, "Developments in excavation bracing systems," *Tunnelling and Underground Space Technology*, vol. 31, pp. 107–116, 2012.

[3] E. Hernández-Montes, P. Alameda-Hernández, L. M. Gil-Martín, "Strength design criterion for asymmetrically reinforced RC circular cross-sections in bending," *Computers and Concrete*, vol. 11, no. 6, pp. 571–585, 2013.

[4] Comité Europeo de Normalizacion, *Eurocódigo 2: Proyecto de estructuras de hormigon. Parte1-1: Reglas generales y reglas para edificación. UNE-EN 1992-1-1*. Bruselas: Comité Europeo de Normalización, 2010, p. 244.

[5] fib-Special Activity Group 5, *fib Bulletin 65: Model Code 2010 - Final Draft*. Lausanne: International Federation for Structural Concrete (fib), 2012.

[6] E. Hernández-Montes, A. Cesetti, L. M. Gil-Martín, "Discussion of 'An efficient tension-stiffening model for nonlinear analysis of reinforced concrete members', by Renata S.B. Stramandinoli, Henriette L. La Rovere," *Engineering Structures*, vol. 48, pp. 763–764, 2013.

[7] CEB, *CEB Design Manual on Cracking and Deformations, Bulletin d'information 158*. Paris: Comite Euro-International du Beton, 1985, p. 250.

[8] E. C. Bentz, "Sectional Analysis of Reinforced Concrete Members," University of Toronto, 2000.

[9] *CEB model code for concrete structures: International recommendation*, 3rd ed. London: Cement and Concrete Association, 1978.

[10] A. M. Hernández-Díaz, L. M. Gil-Martín, "Analysis of the equal principal angles assumption in the shear design of reinforced concrete members," *Engineering Structures*, vol. 42, pp. 95–105, 2012.

[11] Commitee for The Model Code 1990, "CEB Bulletin No. 213/214: CEB-FIP Model Code 90." Tomas Telford, Lausanne, p. 460, 1993.

[12] G. Manfredi, M. Pecce, "A refined R.C. beam element including bond–slip relationship for the analysis of continuous beams," *Computers & Structures*, vol. 69, no. 1, pp. 53–62, 1998.

[13] H.-G. Kwak, J.-Y. Song, "Cracking analysis of RC members using polynomial strain distribution function," *Engineering Structures*, vol. 24, no. 4, pp. 455–468, 2002.

[14] R. I. Gilbert, G. Ranzi, *Time-Dependent Behaviour of Concrete Structures*, 1st ed. New York: Spon Press, 2010, p. 447.

[15] P. Marti, M. Alvarez, W. Kaufmann, V. Sigrist, "Tension Chord Model for Structural Concrete," *Structural Engineering International*, vol. 8, no. 4, pp. 287–298, 1998.

[16] A. Castel, T. Vidal, R. François, "Effective Tension Active Cross-Section of Reinforced Concrete Beams After Cracking," *Materials and Structures*, vol. 39, no. 1, pp. 115–126, 2006.

[17] H. Wiese, M. Curbach, K. Speck, S. Weiland, L. Eckfeldt, T. Hampel, "Rißbreitennachweis für Kreisquerschnitte," *Beton- und Stahlbetonbau*, vol. 99, no. 4, pp. 253–261, 2004.

[18] R. S. B. Stramandinoli, H. L. La Rovere, "An efficient tension-stiffening model for nonlinear analysis of reinforced concrete members," *Engineering Structures*, vol. 30, no. 7, pp. 2069–2080, 2008.

[19] L. M. Gil-Martín, E. Hernández-Montes, M. Aschheim, S. J. Pantazopoulou, "Aproximate expressions for the simulated response of slender longitudinal reinforcement in monotonic compression," *Magazine of Concrete Research*, vol. 60, no. 6, pp. 391–397, 2008.

[20] Comité Europeo de Normalizacion, *Eurocódigo 3: Proyecto de estructuras de acero. Parte 1-1: Reglas generales y reglas para edificios. UNE-EN 1993-1-1*. Bruselas: Comité Europeo de Normalización, 2008, p. 106.

Anexo 2

Strength design optimization of structural steel members according to Eurocode3

Juan Francisco Carbonell-Márquez[1], Luisa María Gil-Martín[2], and Enrique Hernández-Montes[3]

Keywords: Steel Structures, Structural Optimization, Cross-Section Class, Local Buckling, Eurocode 3.

(Published in "Journal of Constructional Steel Research", Volume 80, January 2013, Pages 213–223)

http://dx.doi.org/10.1016/j.jcsr.2012.07.019

Abstract

In order to design a steel member subjected to a bending moment and an axial load, there are an infinite number of possible solutions I- or H- steel cross-sections, the doubly-symmetric solution being just one of them. This paper presents a procedure to obtain the optimal steel cross-section from the infinite number of possible solutions. The process is based on the Reinforcement Sizing Diagrams employed in reinforced concrete strength design. The procedure looks for any type of solution regarding compact or non-compact steel sections. All aspects related to local instabilities will be taken into account, as well as special considerations in order to address the global instabilities associated with the slenderness of the steel element.

Notation

A	Cross-section area employed to compute $N_{b,Rd}$
A_t	Cross-section area
A_{teff}	Effective cross-section area for cross-sections in Class 4
A_1	Top flange area
A_2	Bottom flange area
E	Steel elastic modulus
M_y	External in-plane bending moment

[1] Ph.D. candidate. University of Granada, Campus de Fuentenueva. 18072 Granada. Spain. jfcarbonell@ugr.es.
[2] Associate Professor, University of Granada, Campus de Fuentenueva. 18072 Granada. Spain. mlgil@ugr.es.
[3] Professor, University of Granada, Campus de Fuentenueva. 18072 Granada. Spain. emontes@ugr.es

$M_{b,Rd}$ Design buckling resistance moment of a laterally unrestrained beam

$M_{y,Ed}$ External in-plane bending moment applied to the section

$M_{y,Rk}$ Critical cross-section characteristic moment resistance about *y-y* axis

N External axial load

$N_{b,Rd}$ Design buckling resistance of a compression member

N_{Ed} External axial load applied to the section

N_{Rk} Critical cross-section characteristic resistance to normal force

$W_{eff,y}$ Effective section modulus about *y-y* axis, for Class 4 sections

$W_{el,y}$ Elastic section modulus about *y-y* axis

$W_{pl,y}$ Plastic section modulus about *y-y* axis

W_y Appropriate section modulus employed in the computation of $M_{b,Rd}$

b_{fcomp} Compressed flange width

b_{fb} Bottom flange width

b_{ft} Top flange width

d_w Web height

h Centroid height

f_y Specified steel yield strength

k Factor employed in the computation of the criterion to prevent the compression flange buckling in the plane of the web

l_b Unbraced length of the beam-column member

t_{fb} Bottom flange thickness

t_{ft} Top flange thickness

t_w Web thickness

χ Reduction factor for the relevant buckling mode in compression

χ_{LT} Reduction factor for lateral-torsional buckling

γ_{M1} Partial safety factor for the building ζ Interaction factor

1. Introduction

Typical sections for beam-column members in steel edifications are usually I- or H- rolled sections. However, in other fields of steel constructions such as civil bridges, the selected cross-sections may be welded, since the higher demands to be supported by the structure calls for

larger dimensions not possible for tabulated rolled sections. Whether edification or civil construction, designers tend to proportion their structures using symmetric sections, these being just one of the multiple solutions. Nevertheless, the optimal solution may not coincide with the symmetric one and important savings in the amount of steel used could be achieved. In this respect, environmental concerns constitute an important role because savings in steel consumption may be translated into significant reductions in greenhouse gas emissions.

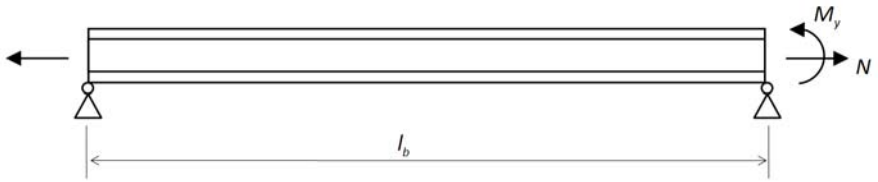

Figure 1. Conditions of the problem to be analyzed

The present work studies the optimal design of beam-column members subject to an external in-plane bending moment, M_y, and to an axial load, N, initially considered to be applied at the centroid of the web of the section (Figure 1). Figure 2 shows the employed nomenclature for the cross-section of the element and the sign criteria for the applied external loads. Bending moment, M_y, acting on the strong axis of the cross-section will be considered positive when compressing the top flange of the section. The applied axial load, N, will be considered positive in tension. For the sake of simplicity, the fillets in rolled sections and throat thickness in welded sections have been ignored in the process. The different elements of the section are proportioned to provide sufficient strength and stiffness to resist the external actions and avoid premature buckling of the member. For non-compact sections, the plastic capacity will not be reached, so elastic capacity will be employed.

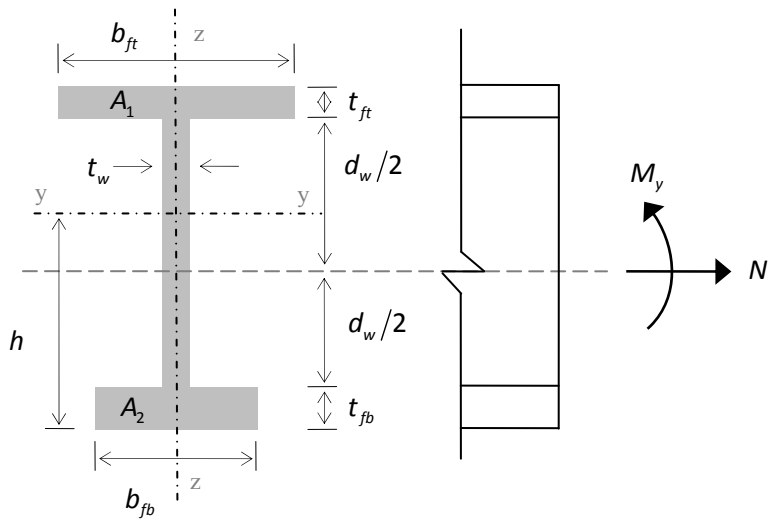

Figure 2. Nomenclature and sign criteria

The problem studied in this work has already been solved by Gil-Martín et al. [1] for Class 1 sections. Optimization was completed by using the RSD design approaches [2-3]. This methodology, originally conceived for reinforced concrete, represents the required reinforcement area for supporting a determined external loading as a function of depth of neutral axis in the concrete section (Figure 3). When applying RSD design approaches to optimization in steel sections, minor changes need to be made. Thereby, the graphics represent the cross-section area, A_t, as a function of the web height, d_w, and the optimal solution corresponds to the one with the lowest value for A_t (Figure 4).

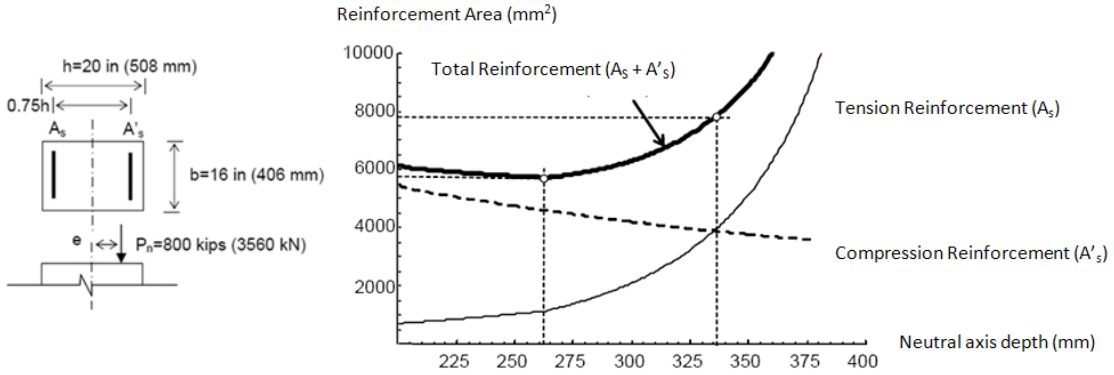

Figure 3. Example of RSD in a reinforced concrete section, from [4]

The present paper explains the well-developed process that was followed to obtain the optimal solution for any pair of (M_y , N). The process makes it possible for the designer to choose the Class of the adopted cross-section; this is either compact or non-compact. Selecting the Class of the section is very important, for example, when designing a building for earthquake resistance according to Eurocode 8 (EC8) [5]. EC8 states that, for any given building subjected to an earthquake, the relation between its resistance and capacity for dissipating energy is related to the section classification (see Table 6.3 in EC8). Generally speaking, the more ductility needed the more compactness is required for the cross-section.

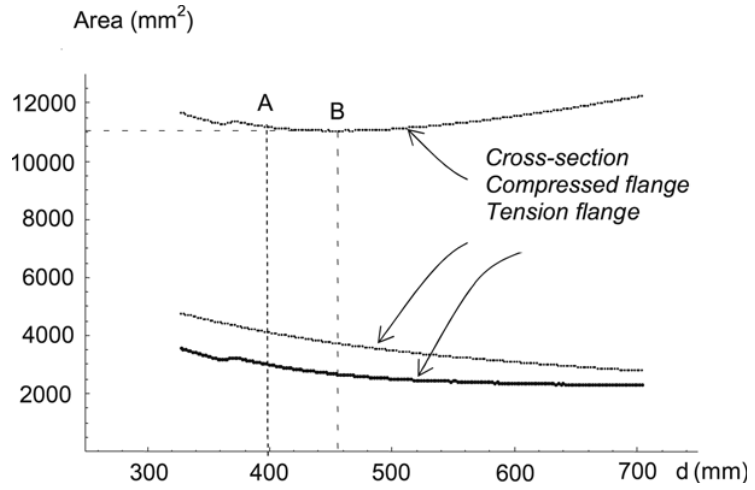

Figure 4. Example of RSD in a steel section: optimization of IPE500 under $M_{y,Ed}$ = 288 kN m and N_{Ed} = - 483 kN with t_f=16 mm and t_w=10,2 mm. Point A represents the optimal solution and point B corresponds to IPE500. Taken from [1]

In contrast to the previous case is a composite roadway or highway bridge. These kinds of bridges, which also called "twin-girder bridges", are composed of two longitudinal steel girders connected to the concrete slab of the deck by shear connectors. Twin-girder bridges are the most economical solution when covering span lengths in the range of 30 and 100 m [6], with special suitability between 60 and 80 m [7]. Considering these span lengths, self-weight becomes an important action to be withstood. Under this load, and beyond the complexity involving a composite section, cross-sections under positive moment at mid-span regions of composite bridges are usually in Class 1 or 2, since compression is carried mainly by the concrete deck. However, on internal supports, under negative moment, sections tend to be designed in Class 3 or 4 in order to avoid the excessive amount of steel that would be needed if those compressed sections were to be in Class 1 or 2 [8].

The typical section for these kinds of bridges is shown in Figure 5. The most usual range for *H/L,* being *H* the height of the I-section and *L* the covered span, is between 1/25 and 1/20 for highway or roadway bridges and 1/15 for railway bridges [6-7][9]. For a highway bridge with a span of 600 m, *H* would be between 2.5 and 3.0 m. This is due to the fact that the high dimensions of the sections do not allow the designer to choose them from the standard rolled sections and a welded design is needed. For these types of girders, the algorithm developed within this work lets the designer impose any constraint related to the dimensions of a particular element of the section, in this case, web height or even related to the Class of the cross-section.

The algorithm used to optimize the sections has been implemented in a computer program and some examples are presented here. The results obtained will be analyzed in order to test the validity of the process.

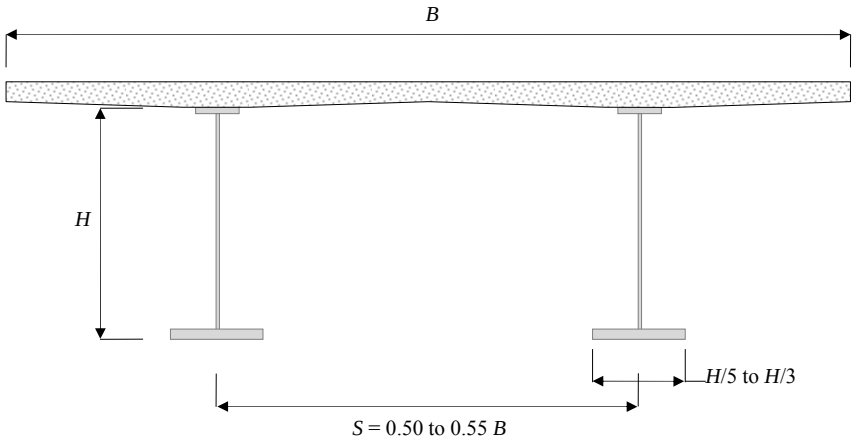

Figure 5. Typical section for a twin-girder composite bridge

2. The optimization procedure

As above explained, the optimization procedure to be presented in the current work is based on RSD methodology. This approach consists on the consideration of all the possible solutions for a design problem through a graphical representation that allows to choose the optimal one. In reinforced concrete members, usually the reinforcement area is represented in function of the neutral axis depth [2-3].

In steel construction, as was observed with reinforced concrete, an infinite number of solutions exist for the design of a steel cross-section subjected to combined loads N and M. These solutions can be presented using graphics similar to those used in the reinforced concrete RSD representation. In this case, the area of structural steel has been represented in function of the height of the web [1]. The main advantage of this procedure is that the engineering know all the possible cross-sections that resist a given combination of axial load and moment (N, M) making possible the choice, among all them, of the optimal one considering minimum weight, availability of steel shapes, simplicity on the job site, Class of the cross-section and so on.

The process followed during the optimization procedure is represented in the flow chart in Figure 6.

Section initial proportioning

The first step in the process is to select a fixed value for the web thickness, t_w, and a range of values for the height of the web, d_w. The range of d_w is obtained accounting both shear strength and shear buckling requirements. The flanges preliminary proportions are provided by equilibrium of forces acting on the cross-section, applying the axial load at the centroid of the web. The equilibrium is established by ignoring the web contribution and assuming that the forces carried by the top and bottom flanges act at the ends of the web and drive the flanges to the yield stress. Therefore, the sum of moments on either ends of the web results in Eq. 1:

$$A_1 \cdot f_y \cdot d_w + M_y - N \cdot \frac{d_w}{2} = 0$$
$$A_2 \cdot f_y \cdot d_w + M_y + N \cdot \frac{d_w}{2} = 0 \quad (1)$$

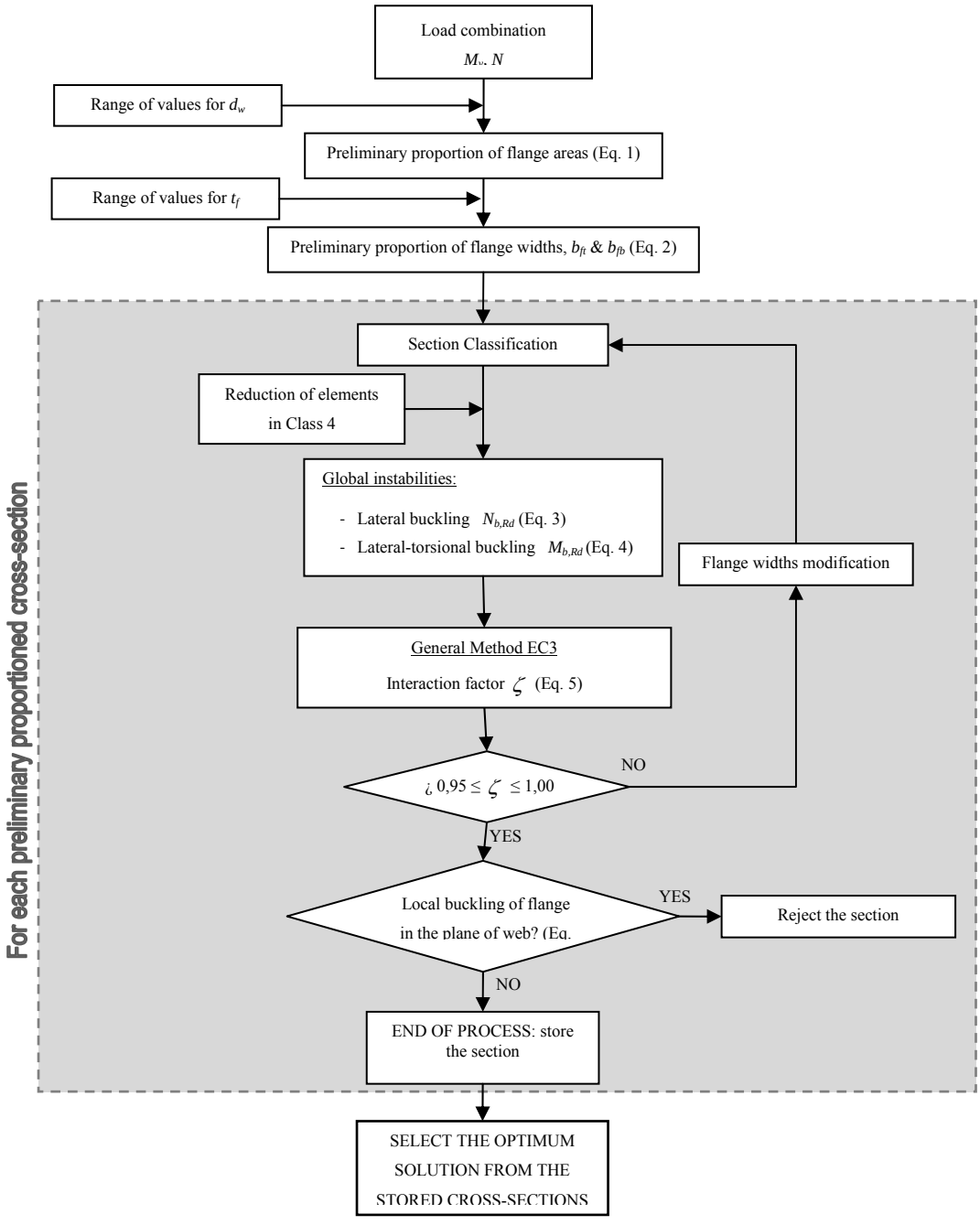

Figure 6. Flow chart explaining the entire process

Once A_1 and A_2 are known for each value of d_w, the next step is to choose another range of values for the flange thicknesses, t_{ft} and t_{fb}. Therefore, for each value of t_{ft} and t_{fb} the values of the flange widths can be obtained from Eq. 2:

$$b_{ft} = \frac{A_1}{t_{ft}} \text{ and } b_{fb} = \frac{A_2}{t_{fb}} \tag{2}$$

In the following, without lost of generality, the same thickness of both flanges has been considered, being, $t_{ft} = t_{fb} = t_f$.

Section classification

As described in Eurocode 3(EC3)[10] , the role of cross-section classification is to identify the extent to which the resistance and rotation capacity of the cross-section is limited by its local buckling resistance. The classification of a determined cross-section will depend on the slenderness, i.e. the width to thickness ratio, of the parts subject to compression.

According to EC3, there are four classes for steel sections: Class 1, which can form a plastic hinge with the rotation capacity required from plastic analysis without reduction of the resistance; Class 2, similar to class 1 but with limited rotation capacity due to local buckling; Class 3, those sections in which local buckling appears before forming a plastic hinge and are assumed to work with an elastic distribution of stresses reaching the yield strength; and Class 4, in which local buckling is reached before elastic limit [11]. This classification may also be found in other codes as AISC Steel Construction Manual [12] with other terminology and slenderness limit values. Thereby, according to AISC, Class 1 and 2 sections are called compact sections; Class 3 sections are equivalent to non-compact sections; and Class 4 sections are similar to slender sections.

The limit values for the slenderness of each component of the section are given by Tables 5.2-1 and 5.2-2, presented in section 5 of Part 1-1 in EC3. According to these standard codes, the cross-section is classified according to the highest (least favorable) class of its compression parts.

Widths of the elements of the cross-section in Class 4 have to be reduced in order to their effective dimensions according to Part 1-5 of EC3.

Global instabilities at member level

Once the class of the cross-section is determined, it is necessary to calculate the resistance of the beam-column member to lateral buckling and lateral-torsional buckling due to axial load and bending moment, respectively. Following the formulas given in EC3 [9], the design buckling resistance of a compression member should be taken as:

$$N_{b,Rd} = \frac{\chi \cdot A \cdot f_y}{\gamma_{M1}} \tag{3}$$

where $A=A_t$ for cross-sections in Classes 1, 2, or 3, and $A=A_{teff}$ for cross-sections in Class 4 when subjected to uniform compression. The parameter χ is the reduction factor for the relevant buckling mode, computed as indicated in section 6.3.1. in Part 1-1 of EC3.

On the other hand, Section 6.3.2 of EC3 [9] provides the formula to calculate the parameter χ_{LT}, i.e. the reduction factor for lateral-torsional buckling. According to this, the design buckling resistance moment of a laterally unrestrained beam should be taken as:

$$M_{b,Rd} = \frac{\chi_{LT} \cdot W_y \cdot f_y}{\gamma_{M1}} \tag{4}$$

Here, W_y is the appropriate section modulus, taken as $W_{pl,y}$ for Class 1 or 2 cross-sections, $W_{el,y}$ for Class 3 cross-sections, and $W_{eff,y}$ for Class 4 cross-sections when only moment about the relevant axis is applied.

When the buckling resistances of the member are calculated, the General Method for lateral and lateral torsional buckling of structural components is applied. This method, explained in Section 6.3.4 of EC3 [9], allows the verification of the resistance to the former global instabilities of single members subject to compression and mono-axial bending in the plane. The member must fulfill Eq. 5 in order to achieve stability.

$$\frac{N_{Ed}}{\chi \cdot N_{Rk}/\gamma_{M1}} + \frac{M_{y,Ed}}{\chi_{LT} \cdot M_{y,Rk}/\gamma_{M1}} \leq 1 \tag{5}$$

where N_{Rk} and $M_{y,Rk}$ are the critical cross-section characteristic resistance to normal force and moment resistance about *y-y* axis. In this work, applied loads N_{Ed} y $M_{y,Ed}$ are:

$$M_{y,Ed} = M_y + \left(e_0 + e_{N_y}\right) N \tag{6}$$

$$N_{Ed} = N \tag{7}$$

Being e_{Ny} the shift of the relevant centroidal axis of the cross-section due to the widths reduction in class 4 when the member is subjected to uniform compression and e_0 the distance between the mid-height of the web –where the axial load is supposed initially applied at the gravity center of the gross-section (Figure 7), calculated as:

$$e_0 = h - \left(d_w/2 + t_f\right) \tag{8}$$

In the above expression h is the height of the gravity centre of the cross-section.

In this work, the value for the sum presented in Eq. 5 has been called "interaction factor" and is represented by $\zeta = {}^{N_{Ed}}\!/_{\chi \cdot N_{Rk}/\gamma_{M1}} + {}^{M_{y,Ed}}\!/_{\chi_{LT} \cdot M_{y,Rk}/\gamma_{M1}}$.

Design adjustments

It is clear from the flow chart presented in Figure 6 that the proposed procedure is iterative. The dimensions of the cross-section are preliminary proportioned and classified. Afterwards, the General Method is applied to evaluate the stability of the member; because in most of the cases the preliminary cross-section will not be able to stand the applied loads without buckling, dimensions need to be modified. In this work, for each pair of values d_w-t_f, the width of the flanges, b_{ft} and b_{fb}, are adjusted until the member does not buckle, i.e. $\zeta \leq 1$. However, in order to gain optimal results, a lower limit has been imposed to ζ, so that the adjustments will be completed when $0.95 \leq \zeta \leq 1$. The adopted process for providing a cross-section of minimum cross-sectional area, fulfilling all the stability considerations, is similar to the one followed by [1], and is explained below:

1. If $\zeta < 0,95$ the section provides excess capacity. To reduce the cross-sectional area, the widths of both flanges are reduced until:

$$0,95 \le \zeta \le 1 \tag{9}$$

2. If $\zeta > 1$ the section behavior is governed by instability. To provide sufficient strength, the flange areas must be increased. The approach to increase one flange or another depends on axial force and bending moment:

   a. If $M_y = 0$ or $N = 0$, the section is symmetric from the initial proportioning given by Eq. 1. The area of both flanges are increased the same amount until the condition given by Eq. 9 is fulfilled.

   b. If $M_y \neq 0$ and $N \neq 0$, the section from Eq. 1, the section will initially be asymmetric. In this case, one of the flange areas is increased in order to reduce the eccentricity given by Eq. 8 until the formula given by Eq. 9 is fulfilled:

      i. If M_y and N have an equal sign, the top flange width will increase.

      ii. If M_y and N have a different sign, the bottom flange width will increase.

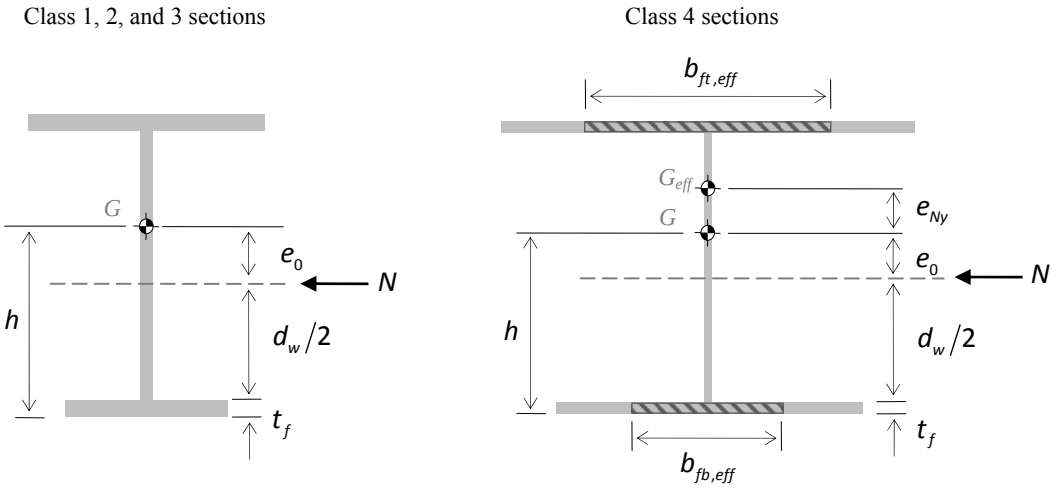

Figure 7. Values for the eccentricities e_0 and e_{Ny}

Once Eq. 9 is fulfilled for certain values of d_w - t_{ft} - t_{fc} (in this example t_f = t_{ft} = t_{fc}), the cross-section will be stored if the dimensions of the flanges in compression are sufficient to prevent local buckling in the plane of the web. According to section 8 in Part 1-5 of EC3 [13], the following criterion should be met:

$$\frac{d}{t_w} \le k\frac{E}{f_y}\sqrt{\frac{d_w \cdot t_w}{A_{fcomp}}} \Rightarrow b_{fcomp} \le \frac{k^2 \cdot E^2 \cdot t_w^3}{f_y^2 \cdot t_f \cdot d_w} \quad (10)$$

The value of k should be taken as follows:

- Plastic rotation utilized $k = 0,3$
- Plastic moment resistance utilized $k = 0,4$
- Elastic moment resistance utilized $k = 0,55$

All the cross-sections with their corresponding pairs of d_w-t_f are stored. These solutions are sorted by cross-sectional area and the minimum is identified as the optimal solution. It is important to notice that the process may provide some solutions with the same optimal cross-sectional area. In this case, the final selected solution will be that with the minimum value of interaction factor ζ .

Furthermore, the procedure provides an infinite number of solutions (depending on the established constraints). The optimum (i.e. minimum cross-sectional area) or the symmetric solution is just one of the possible cross-sections that may be chosen [1-3].

3. Examples

The validity and effectiveness of the process have been tested and can be seen in the following three examples; in order to obtain minimum cross-sectional solutions for three combinations of M_y and N with the conditions represented in Figure 1: a simple supported beam with end-fork conditions (i.e. pin supported end and free warping). The applied load combinations correspond to three points in the interaction equation (Figure 8) corresponding to a specimen made of steel Grade 235 ($f_y = 235\,\text{N/mm}^2$) with a cross-section HEB600 ($d_w = 540$ mm; $t_w = 15,50\ mm$, $t_f = 30$ mm; $b_{ft} = b_{fb} = 300$ mm; $A_t = 27000\ \text{mm}^2$) and an unbraced length, l_b, equals to 6,00 m. The load combinations are presented in Figure 8.

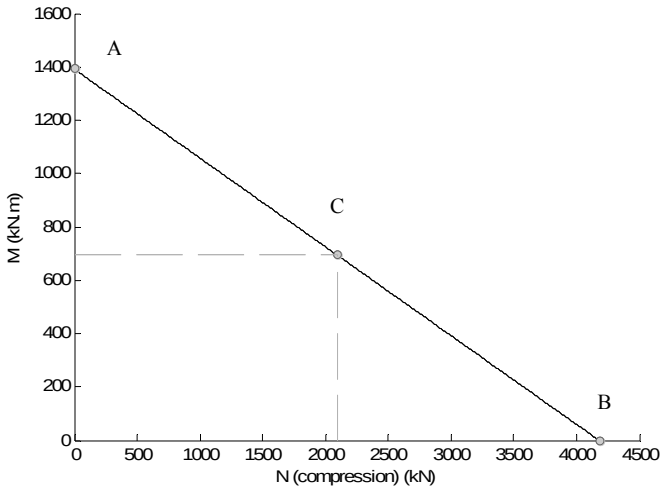

Figure 8. Interaction equation corresponding to HEB600, for f_y = 235 N/mm^2, l_b = 6 m and ψ = 0

3.1. Combination A: M_y=1391.60 kN.m –bending moment applied on the right support of the beam-

The first combination of loads corresponds to point A in Figure 8, simple strong axis bending with a value of $M_y = 1391,60\ kN \cdot m$. Figure 9 shows the obtained design solutions for different web depths, d_w, with a range from 50 mm to 2000 mm with a step of 5 mm. The adopted range of values for flange thicknesses, t_f, varies from 4 mm to 40 mm, with a step of 2 mm. The HEB 600 web thickness ($t_w = 15,50\ mm$) is adopted for every solution. According to Eq. 1, if $t_f = t_{ft} = t_{fc}$ all the obtained solutions are doubly-symmetric (i.e. $b_{ft} = b_{fb}$). The results from Eq. 1 are presented as a continuous line. Dots in Figure 9 correspond to the solutions obtained after the adjustment process for the four different Classes of the cross-section. To distinguish between each class different have been used, respectively. In Figure 9 the solution corresponding to the HEB section and the optimal ones obtained for each class using the optimization procedure have been identified. As may be observed from Figure 9, the initially proportioned dimensions for the elements of the cross-section given by Eq. 1 are subsequently modified by the adjustment process. In some cases, those dimensions have been overestimated since the contribution of the web was ignored in Eq. 1. However, many solutions have cross-sectional areas greater than initially estimated due to the fact that members turned out unstable and buckled and therefore dimensions need to be modified in order to get sufficient strength to withstand the applied loads.

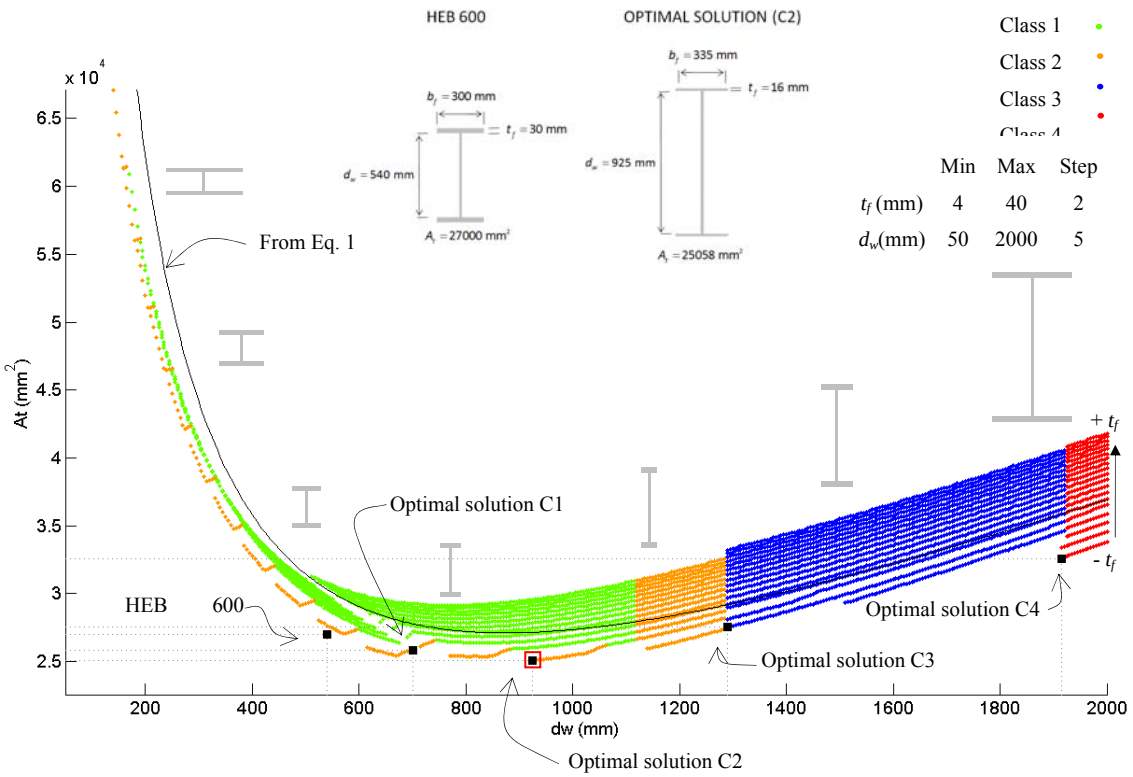

Figure 9. Cross-sectional area A_t of the solutions in terms of web depth d_w for strong axis bending moment

The solution with the lowest cross-sectional area corresponds to:

$$d_w = 925 \text{ mm};\ t_w = 15{,}50\ mm\ ;\ t_f = 16 \text{ mm};\ b_{ft} = b_{fb} = 335 \text{ mm};\ A_t = 25058 \text{ mm}^2$$

The web and top flange Classes are 1 and 2 respectively, leading to cross-section Class 2. The interaction factor is $\zeta = 0{,}9989$.

Figure 10 shows the optimal solution for each Class according to EC3 and compares their cross-sectional area with the one of HEB 600. The table in Figure 10 provides the dimensions for these optimal solutions. Class 1, 2, and 3 sections reduce the flange width, b_f, when increasing web depth, d_w, while in Class 4 b_f increases since web is reduced for local buckling. In this case, only compact solutions (Classes 1 and 2) provide less cross-sectional area than the standard HEB600. Figure 9 shows that a saving of 7,2 % with respect to the area of HEB600 can be obtained.

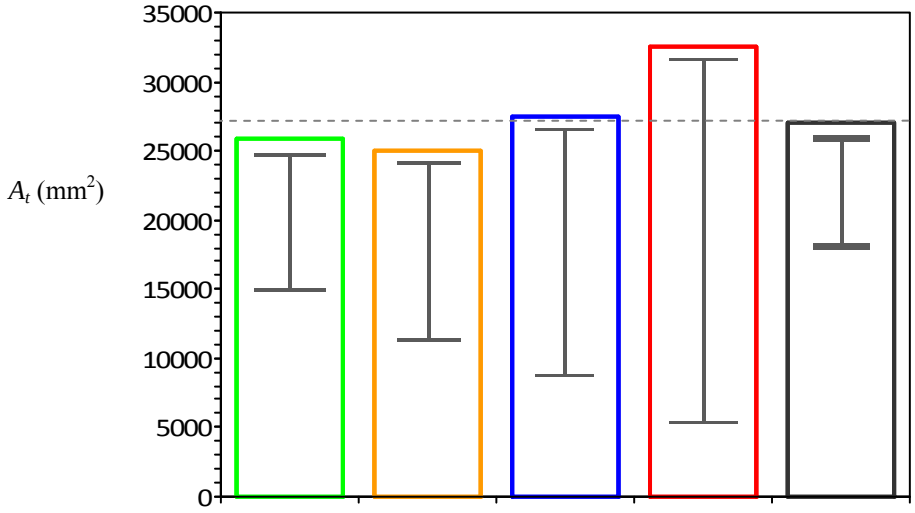

Optimal Solution	Class 1	Class 2	Class 3	Class 4	HEB 600
A_t (mm^2)	25850	**25058**	27507	32587	27000
b_f (mm)	375	335	313	363	300
t_f (mm)	20	16	12	4	30
d_w (mm)	700	925	1290	1915	540

Figure 10. Comparison between the dimensions of different optimal solutions for each Class and HEB 600, for strong axis bending moment. Scale of dimensions sketches: 1/400

In Figure 11 the obtained results from the optimization process imposing $t_f = 30$ mm (flange thickness of HEB600) have been represented for both welded and rolled sections. This figure shows that if welded sections are considered instead of rolled sections, areas slightly larger are obtained. These differences are due to the different values of the imperfection factors corresponding to the buckling curves that are different for both welded and rolled sections. For this example no welded solution exits with a cross-sectional area under 27000 mm^2 - HEB600 cross-section area- while if a rolled section is employed an area $A_t = 26098$ mm^2 is obtained (for $d_w = 805$ mm and $b_f = 227$ mm).

Figure 11 shows that the curve corresponding to rolled sections almost matches the solution corresponding to the HEB 600. These small differences are due to the fact that, as was explained earlier, in this work the fillets in rolled sections are not taken into account.

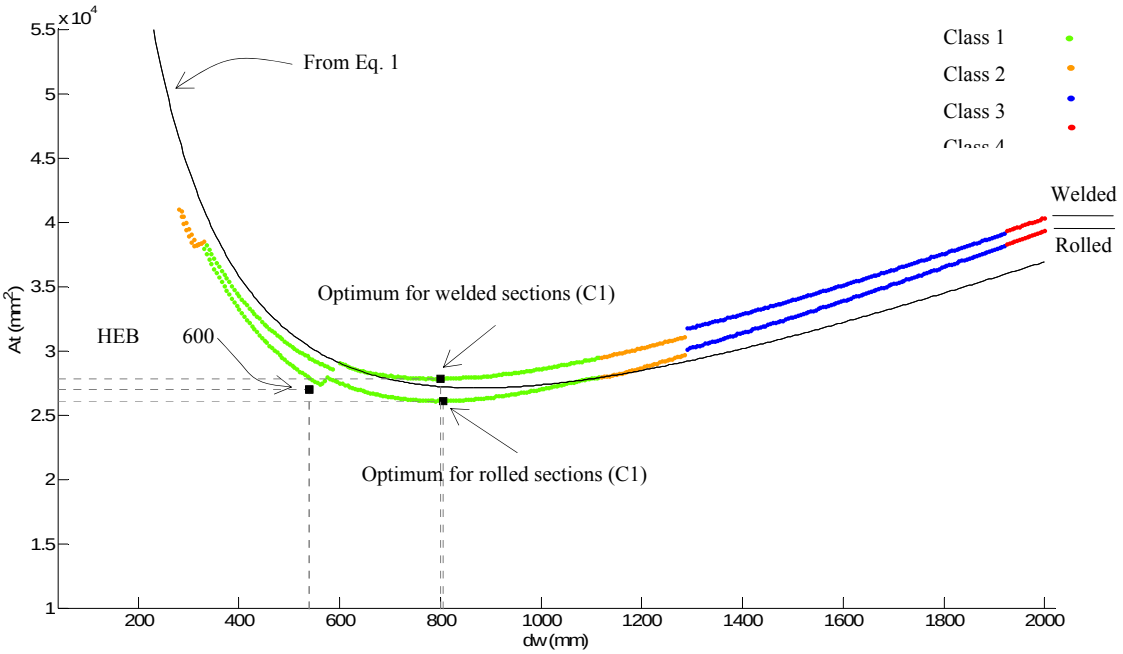

Figure 11. Cross-sectional area A_t of the solutions with t_f = 30 mm in terms of web depth d_w for strong axis bending moment employing welded and rolled sections imperfection factors

3.2. Combination B: N= -4180.80 kN (compression)

In this case, the steel section member is subject to a pure compression with a value of $N = -4180,80\ kN$. This load combination corresponds to point B in Figure 8, i.e. the buckling capacity of the considered HEB 600 member. The results for the different values of d_w, with a range from 50 mm to 800 mm with a step of 5 mm, are presented in Figure 12. Again, the HEB 600 web thickness ($t_w = 15,50\ mm$) is adopted for every solution. The adopted range of values for flange thicknesses, t_f, starts at 4 mm and finishes at 40 mm, with a step of 2 mm. The obtained optimal solution corresponds to $d_w = 215$ mm; $t_w = 15,50\ mm$ $t_f = 18$ mm; $b_{ft} = b_{fb} = 492$ mm; $A_t = 21045$ mm^2. This solution saves a 22,05 % of steel with respect to the HEB600. The cross-section Class is 3 due to the slenderness ratio for the flanges in compression: $10\varepsilon < \frac{c}{t} = 13.23 < 14\varepsilon$. The interaction factor for this solution is $\zeta = 0,9992$.

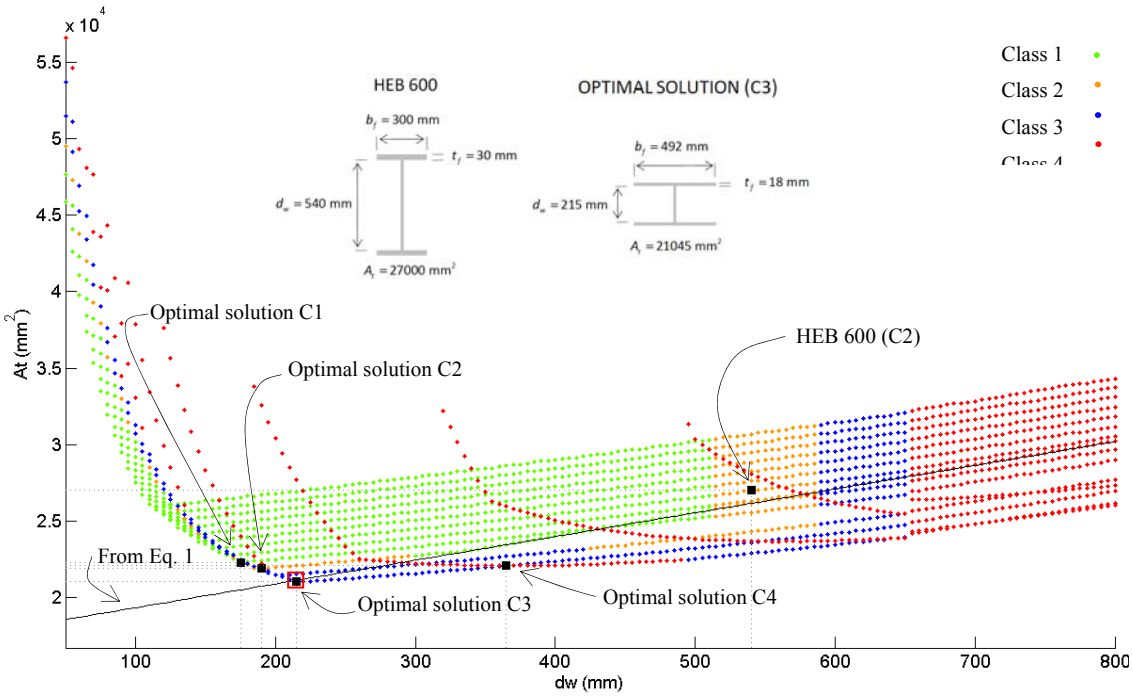

Figure 12. Cross-sectional area A_t of the solutions in terms of web depth d_w for pure compression

As in the former example, Figure 13 shows the optimal solution for each Class. In this particular case, all the optimal solutions have cross-sectional areas smaller that the one corresponding to the standard HEB600. As in the previous example, Eq. 1 provides symmetric solutions since, the only applied load there is now is the compressive axial load. Because the areas of the flanges are not affected by web depth, d_w , the flange widths, b_f, will be the same for every fixed value of the flange thickness, t_f. Figure 14 shows the evolution of the flange width, b_f, as function of

the depth of the web, d_w, for a fixed value of the flange thickness, $t_f = 30$ mm. The obtained optimal solution corresponds to a web depth $d_w = 145$ mm and a flange width $b_{ft} = b_{fb} = 357$ mm. The corresponding cross-sectional area is $A_t = 23668$ mm^2.

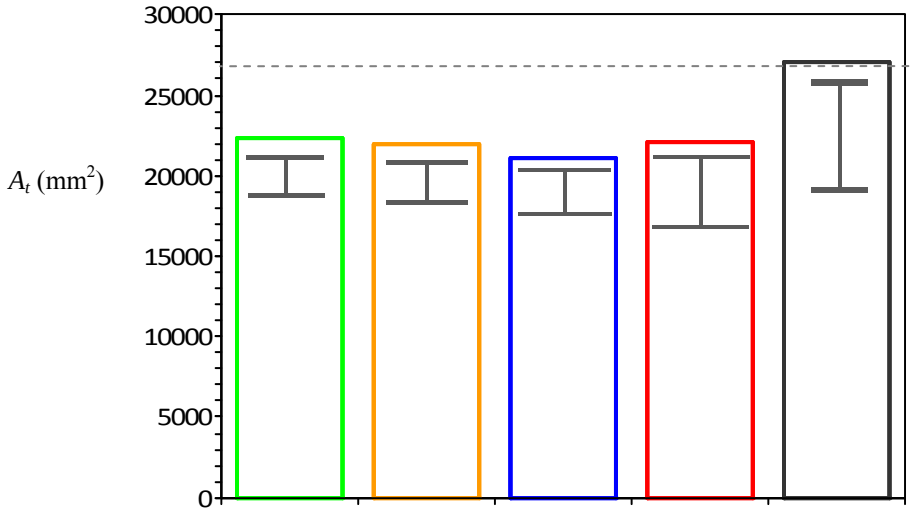

Optimal Solution	Class 1	Class 2	Class 3	Class 4	HEB 600
A_t (mm^2)	22297	21909	**21045**	22074	27000
b_f (mm)	408	431	492	513	300
t_f (mm)	24	22	18	16	30
d_w (mm)	175	190	215	365	540

Figure 13. Comparison between dimensions of different optimal solutions for each Class and HEB 600, for pure compression.

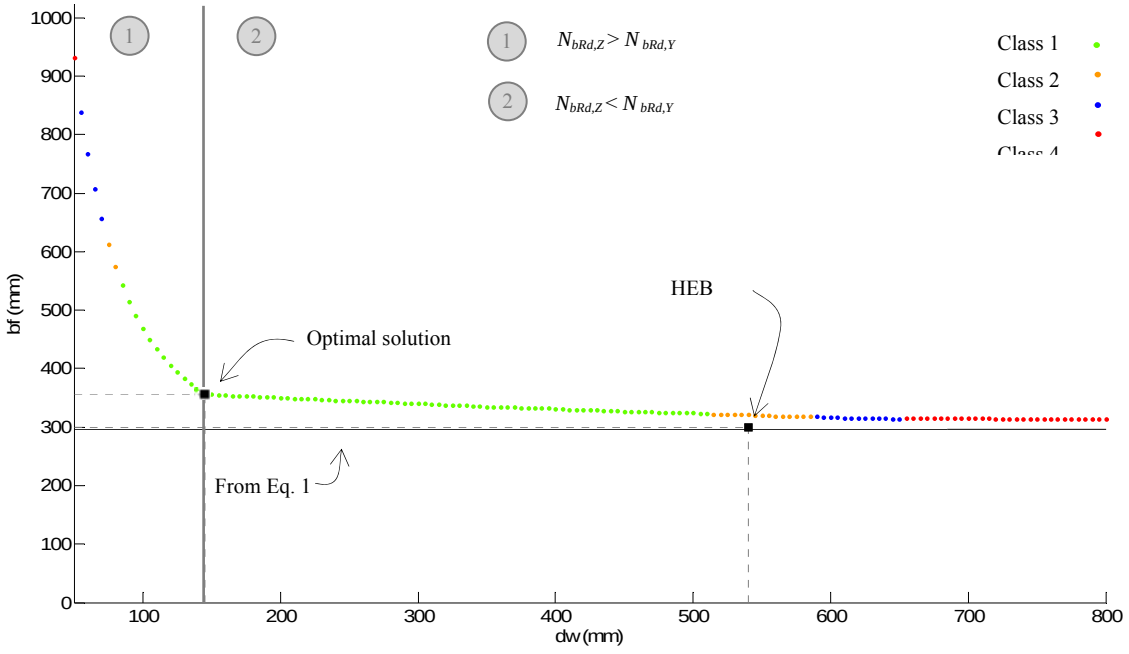

Figure 14. Flange width, b_f, for the solutions of flange thickness t_f = 30 mm in terms of web depth d_w for pure compression

In Figure 14 two regions appear. Region 1 corresponds to solutions where the relevant mode for lateral buckling under compression is flexural buckling (solutions are symmetric) about *y-y* axis. In this Region, solutions need to increase their preliminary proportioned flange width by an important amount before reaching stability, because the relevant mode is governed by the moment of inertia about *y-y*, which is proportional to b_f: $I_y \propto b_f$ ($\propto$ meaning being proportional). However, $I_y \propto d_w^3$, resulting in much less wider solutions as d_w becomes deeper. On the other hand, Region 2 corresponds to flexural buckling under *z-z* axis and solutions get quick stability since $I_z \propto b_f^3$, and solutions need to increase lightly their preliminary proportioned flanges. In this Region, the slope of the curve becomes much flatter as d_w increases since now $I_z \propto d_w$.

3.3. Combination C: M_y= 695.82 kN.m & N= -2090.41 *kN* (compression)

This case corresponds to a combination of simultaneous compression and bending moment about the strong axis. Point C in Figure 8 coincides with half compression and bending moment capacity of the standard HEB 600 adopted as a benchmark problem. Solutions have been obtained again for the same range of values for web depth, d_w, and flange thickness, t_f, as in the previous example. The value of the web thickness, t_f, is 15,5 mm. Figure 15 shows the results obtained and the optimal section, for which the dimensions are: $d_w = 585$ mm; $t_w = 15{,}50$ *mm* $t_f = 22$ mm; $b_{ft} = 433$ mm; $b_{fb} = 334$ mm; $A_t = 25942$ mm^2. For this section, both top flange and web are Class 2, and the entire cross-section results in that Class. The solution saves a 4 % of steel with regards to the standard HEB 600.

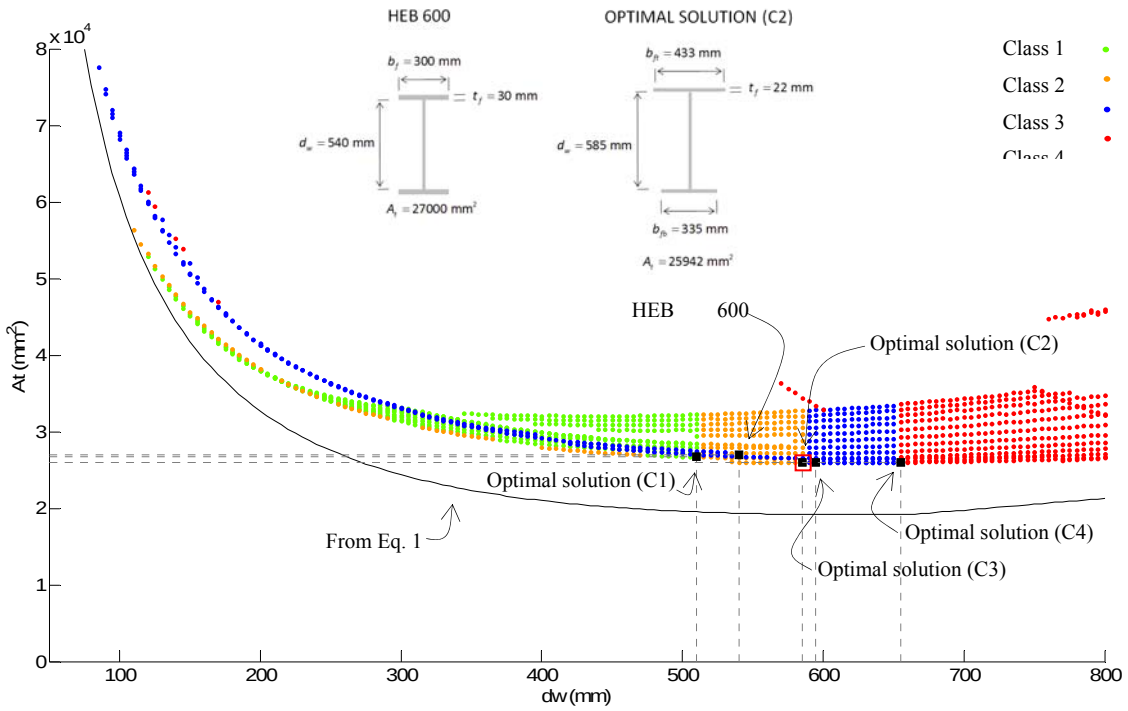

Figure 15. Cross-sectional area A_t of the solutions in terms of web depth d_w for simultaneous compression and bending moment about strong *y-y*

Figure 16 shows the obtained optimal results for each Class of sections. In this case, as in the former example, once again, all of them have a less cross-sectional area than the standard HEB600. There are two of them, solutions for Classes 2 and 3, which are almost the same area (slight differences in dimensions of flanges and web result in just 1 mm^2 less in cross-sectional area for solution in Class 2).

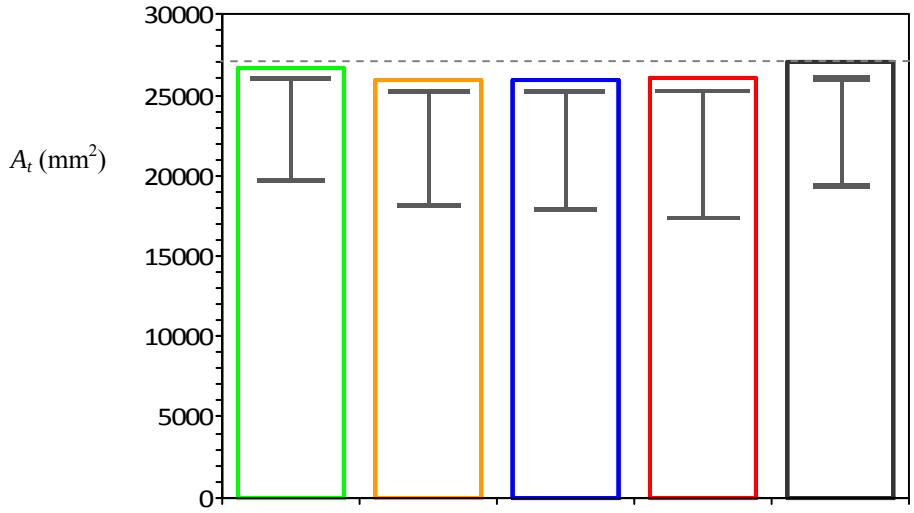

Optimal Solution	Class 1	Class 2	Class 3	Class 4	HEB 600
A_t (mm^2)	26721	**25942**	25943	26029	27000
b_{ft} (mm)	428	433	429	499	300
b_{fb} (mm)	356	334	331	383	300
t_f (mm)	24	22	22	18	30
d_w (mm)	510	585	595	655	540

Figure 16. Comparison between the dimensions of different optimal solutions for each Class and HEB 600, for simultaneous compression and bending moment about strong *y-y*.

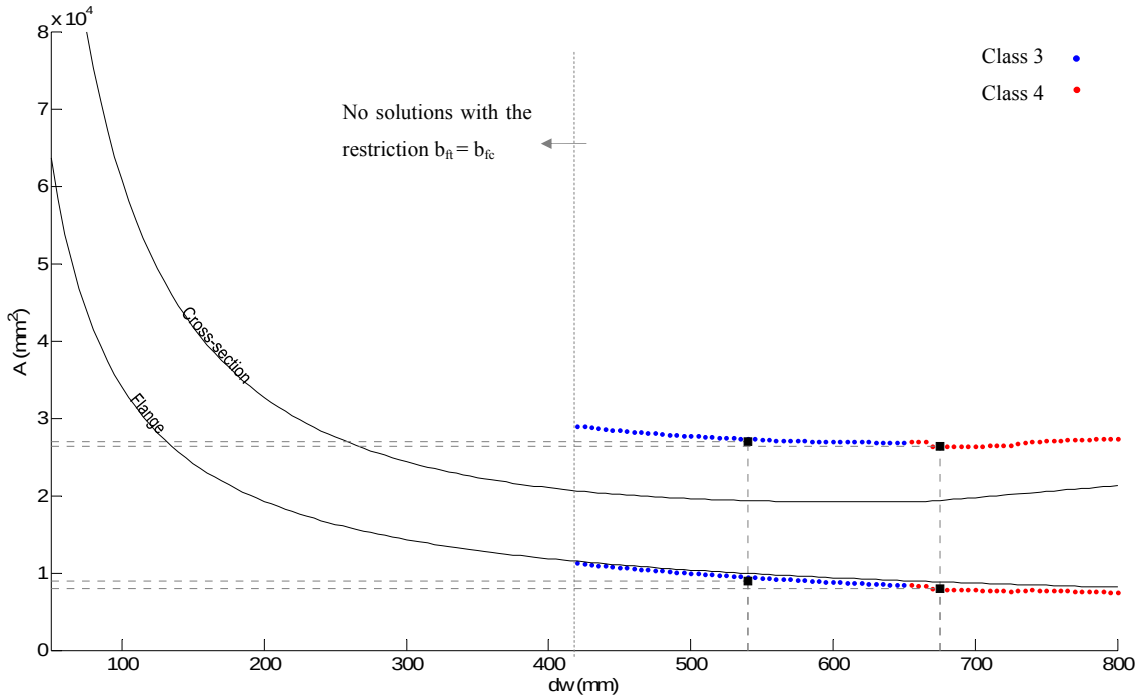

Figure 17. Cross-sectional and flange area in terms of d_w, for solutions of t_f = 20 mm and forcing both flanges to be equal (i.e. doubly-symmetrical cross-section) for simultaneous compression and bending moment about strong *y-y*.

As the procedure is completely general, the doubly-symmetrical cross-section may be extrapolated without loss of generality. If the width of both flanges are forced to be equal, the optimal solution corresponds to a flange thickness of $t_f = 20$ mm and $d_w = 625$ mm; $t_w = 15,50\ mm\ b_{ft} = 396$ mm; $b_{fb} = 396$ mm; $A_t = 26303$ mm^2. Figure 17 represents both the cross-sectional and flange areas for doubly-symmetrical cross-section with $t_f = 20$ mm in function of the height of the web. For this figure it is evident that solutions only exist for values of d_w from 420 mm, being the sections in Class 3 or 4. The standard HEB600 is included in the list of possible solutions in Class 2.

3.4. Global optimization

In order to extend the former optimization procedure to other values of web's thickness, t_w, the above process has been applied to several values of t_w between 6 mm and 19 mm for the axial compression and bending moment about the strong axis denoted as combination C (see Figure 8). The optimal cross-section (i.e., with minimum area) obtained for each class of cross-section [9] for each thickness of the web can be identify in Figure 18. This figure shows that the smallest area that fulfil all the EC3 [9] requirements corresponds to cross-section in class 4 with t_w = 8 mm. This optimal section needs to be stiffened because the slenderness of the web is too high. The optimum cross-section in class 3 and in Class 1 and 2 appears for t_w = 13,5 mm and t_w = 14,5 mm, respectively. In such cases the slenderness of the web is low enough that transverse stiffeners are not needed. In Figure 18, the optimal solutions obtained for the value of the thickness of the web adopted in the former sections (t_w of the standard HEB 600) have also been indicated.

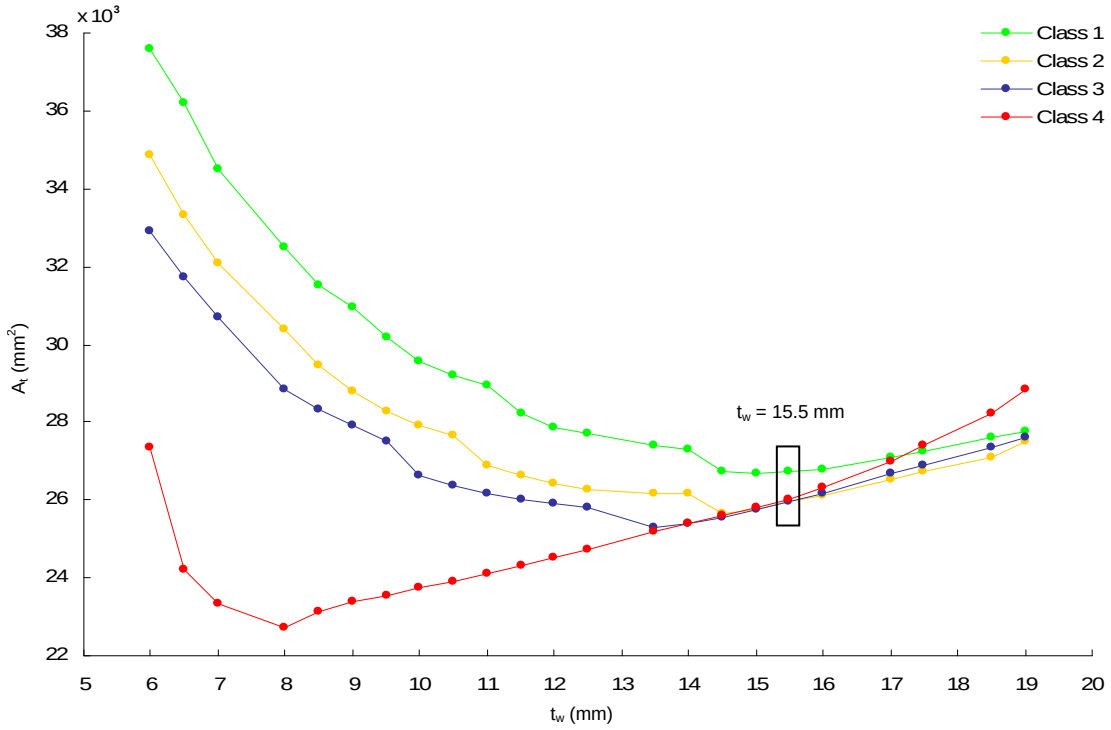

Figure 18. Optimal (i.e. minimum) cross-sectional area in terms of t_w obtained for each class of cross-section and for simultaneous compression and bending moment about strong *y-y*.

4. Conclusions

As has been explained and demonstrated in this work, employed symmetrical cross-sections are usually not, in most of the cases, the optimal solutions. This work presents an iterative procedure in order to get the optimal solution for the I-shaped cross-section of a steel beam-column member subject to an external axial load and bending about strong axis. The process is based on RSD diagrams for optimizing the longitudinal reinforcing steel in reinforced concrete sections and completes the procedure proposed by Gil-Martín et al. [1] for obtaining these optimal solutions with steel sections in Class 1 according to Eurocode 3. This method allows engineers to choose among all the possible solutions: compact, non-compact and slender sections, obtaining important savings in steel and hence leading to reductions in greenhouse gas emissions.

Acknowledgements

The present work was financed by the Spanish Ministry of Education. The first author is a Spanish Government PhD fellow (FPU grant AP 2010-3707). This support is gratefully acknowledged. As indicated, this work has been published by Journal of Steel Constructional Research. This publication is also gratefully acknowledged.

References

[1] Gil-Martín LM, Aschheim M, Hernández-Montes E. Proportioning of steel beam-column members based on RSD optimization methodology. Engineering Structures 2008; 30(11): 3003-11.

[2] Hernández-Montes E, Aschheim M, Gil-Martín LM. Impact of optimal longitudinal reinforcement on the curvature ductility capacity of reinforced concrete column sections. Magazine of Concrete Research 2004; 56(9): 499-14.

[3] Hernández-Montes E, Gil-Martín LM, Aschheim M. Design of concrete members subjected to uniaxial bending and compression using reinforcement sizing diagrams. ACI Structural Journal 2005; 102(1): 150-9.

[4] Hernández-Montes E, Gil-Martín LM. Hormigón armado y pretensado: concreto reforzado y preesforzado. Granada: Universidad de Granada, Grupo de Investigación TEP-190 Ingeniería e Infraestructuras; 2007.
(http://www.ugr.es/~emontes/prensa/HormigonEstructural.pdf)

[5] Comité Europeo de Normalización, Agencia Española de Normalización. UNE EN 1998-1: Eurocódigo 8: Proyecto de estructuras sismorresistentes. Parte 1: Reglas generales, acciones sísimicas y reglas para edificación. Madrid: Aenor; 2011b.

[6] Llago Acero R, García Rodríguez P. Composite twin-girder bridges: A competitive solution for medium span bridges. Revista de Obras Publicas 2010; 157(3516): 29-18.

[7] Brozzetti J. Design development of steel-concrete composite bridges in France. Journal of Constructional Steel Research 2000; 55(1–3): 229-15.

[8] Ryu H-K, Youn S-G, Bae D, Lee, Y-K. Bending capacity of composite girders with Class 3 section. Journal of Constructional Steel Research 2006; 62(9): 847-9.

[9] Dirección General de carreteras. Obras de paso de nueva construcción: conceptos generales. Madrid: Ministerio de Fomento; 2005.

[10] Comité Europeo de Normalización, Agencia Española de Normalización. UNE EN 1993-1-1: Eurocódigo 3: Proyecto de estructuras de acero. Parte 1-1: Reglas generales y reglas para edificios. Madrid: Aenor; 2008.

[11] Rugarli P. Classification of I- or H-shaped cross-sections under mixed internal actions. Journal of Constructional Steel Research 2009; 65(8-9): 159-8.

[12] Steel Construction Manual (AISC 325-11). 14th ed. Chicago: AISC American Institute of Steel Construction; 2009.

[13] Comité Europeo de Normalización, Agencia Española de Normalización. UNE EN 1993-1-5: Eurocódigo 3: Proyecto de estructuras de acero. Parte 1-5: Placas planas cargadas en su plano. Madrid: Aenor; 2011a.

Anexo 3

Eccentricity-based optimization procedure for strength design of RC sections under compression and in-plane bending moment

López-Martín D. [1], Carbonell-Márquez J.F. [2], Gil-Martín L.M. [3], Hernández-Montes, E. [4]

(Published in "Journal of Structural Engineering – ASCE", Volume 140, January 2014)
http://dx.doi.org/10.1061/(ASCE)ST.1943-541X.0000794)

Abstract. The strength design of reinforced concrete rectangular sections for combined compression and in-plane bending with two levels of reinforcement is indeterminate: three unknowns are to be solved with only two equilibrium equations; an additional condition is necessary in order to solve the problem. The additional condition leads to the solution of minimum reinforcement-concrete ratio. This paper proposes a new approach based on equivalent eccentricity of applied compressive load. Different domains are reported, each of them is associated with given values of eccentricity and axial load. Analytical expressions for the domain boundaries are established and a simple procedure is described in order to outline the conditions corresponding to the optimal reinforcement. The main advantage of this procedure is its simplicity, which allows for manual computations. Some examples employing reinforcement sizing diagrams illustrate the validity of the approach.

Keywords. Reinforced concrete; Optimal reinforcement; Strength design, Equivalent eccentricity

---

[1] Associate Professor, Department of Structural Mechanics, University of Granada (UGR). Campus Universitario de Fuentenueva s/n. 18072 Granada, Spain

[2] PhD Candidate, Department of Structural Mechanics, University of Granada (UGR). Campus Universitario de Fuentenueva s/n. 18072 Granada, Spain (corresponding author). Email jfcarbonell@ugr.es

[3]Associate Professor, Department of Structural Mechanics, University of Granada (UGR). Campus Universitario de Fuentenueva s/n. 18072 Granada, Spain

[4]Full Professor, Department of Structural Mechanics, University of Granada (UGR). Campus Universitario de Fuentenueva s/n. 18072 Granada, Spain

Notation

A_c	Concrete cross-section area
A_{s1}	Bottom reinforcement cross area
A_{s2}	Top reinforcement cross area
E_s	Steel elastic modulus
M	Externally applied in-plane bending moment
M_b	Maximum resisting moment of the section in simple bending without top reinforcement
N	Externally applied compressive axial load
N_c	Concrete compression block resultant
N_{s1}	Bottom steel reinforcement stress resultant
N_{s2}	Top steel reinforcement stress resultant
b	Cross-section width
d	Depth of centroid of bottom reinforcement, measured from top fiber
d_1	Distance between bottom fiber and centroid of bottom reinforcement
d_2	Depth of centroid of top reinforcement, measured from top fiber
e_0	Equivalent eccentricity
e_{0c}	Boundary eccentricity value for condition $A_{s1} = A_{s2} = 0$
$e_{0\lim}$	Boundary eccentricity value for $x = x_b$
e_{02}	Boundary eccentricity value for $A_{s2} = 0$
e_{0h}	Boundary eccentricity value for $x = +\infty$
f_{ck}	Characteristic compressive strength of concrete (according to EC2)
f_{cd}	Design compressive strength of concrete (according to EC2)
f_{yk}	Characteristic yield strength of reinforcement (according to EC2)
f_{yd}	Design yield strength of reinforcement (according to EC2)
h	Cross-section depth
x	Neutral axis depth
x_b	Neutral axis depth corresponding to a tensile strain of ε_y at bottom reinforcement and a compressive strain of ε_{cu} at top fiber
σ_c	Concrete compression
σ_{s1}	Bottom reinforcement stress
σ_{s2}	Top reinforcement stress
ε_c	Strain at section centroid
ε_{cu2}	Maximum concrete compressive strain employing parabolic and rectangular stress block (according to EC2)
ε_{cu3}	Maximum concrete compressive strain employing rectangular stress block (according to EC2)
ε_{c2}	Maximum concrete pure compression strain employing parabolic and rectangular stress block (according to EC2)
ε_{c3}	Maximum concrete pure compression strain employing rectangular stress block (according to EC2)
ε_{s1}	Bottom reinforcement centroid strain
ε_{s2}	Top reinforcement centroid strain
ε_y	Steel yield strain
ε_{ud}	Steel tensile strain limit

ϕ Curvature of the cross-section

α_{cc} Coefficient considering long term effects on the compressive strength and unfavorable effects resulting from the way the load is applied (according to EC2)

γ_s Partial safety factor for concrete (according to EC2)

λ Depth of equivalent rectangular compressive stress block relative to the neutral axis depth (according to EC2)

η Effective concrete strength factor

ν Reduced compression load

Introduction

One of the most commonly studied topics in schools of engineering is the ultimate strength proportioning of a reinforced concrete (RC) rectangular cross-section subjected to combined axial compressive load and bending moment. The widespread use of concrete and reinforcing steel in the buildings from the last century meant that this problem was dealt with in many books as well as being included in every concrete design code.

The referred problem is not of immediate resolution since numerous variables govern the equations and, usually, it is necessary iterate in order to find its solution. Therefore, the designer has to rely on his intuitive experience to fix some of these variables in order to obtain the most appropriate reinforcement. When experience is not enough, a wide range of existing literature also provides many simplified or trial and error procedures based on tables or abacuses which help in finding a solution for the design.

Recent studies provide many different approaches to get the optimal solution for the reinforcement design. Some try to find the optimum based on the cost of every component of the section, i.e. concrete and steel. M. H. F. M. Barros et al. (2005) investigated the cost optimization of rectangular RC sections using the non-linear MC90 equation. A. F. M. Barros et al. (2012) studied the minimal cost problem of a rectangular section in simple bending where the objective function is the cost of raw materials and the variables are the section depth and the steel reinforcement areas. Lee et al. (2003) and Camp et al. (2003) also employ genetic algorithms in order to perform a discrete optimization of the flexural design of RC frames, both of them including material and construction costs.

Other approaches assume that the rectangular dimensions of the cross-section are given and the optimal solution for the reinforcement in ultimate strength design needs to be found. Thereby, Hernández-Montes et al. (2004 and 2005) presented a new design approach called Reinforcement Sizing Diagrams (RSD), which shows the infinite number of solutions for top and bottom reinforcement that provide the required ultimate strength for sections subject to combined axial load and moment. Since RSD represents the infinite number of solutions, the

optimal (or minimum) reinforcement may be identified. Also, Aschheim et al. (2007) employed this RSD technique to define optimal domains with respect to axial-bending load coordinates according to provisions of Eurocode 2 (EC2) (CEN, 2004). Ultimately, the observation of the characteristics of optimal solutions has led Hernández-Montes et al. (2008) to the development of the Theorem of Optimal Section Reinforcement (TOSR). This work provides the additional conditions to be imposed in the equilibrium equations in order to achieve an optimal design of reinforcement.

Although Hernández-Montes et al. (2008) described and proved the additional conditions to be implemented, each of them has its special suitability depending on the applied loads. As a corollary to the mentioned theorem, Hernández-Montes et al. (2008) proposed to check every condition in the problem in question and select the one which provides the optimal solution.

In this work, a procedure similar to the one that Aschheim et al. (2007) exposed is to be given according to EC2 specifications facing the problem from the point of view of many traditional concrete textbooks: depending on the equivalent eccentricity of the applied compressive load, this approach will provide an additional condition to impose in order to obtain the optimal reinforcement. Some examples are presented in order to compare the results predicted by this approach with those obtained using the RSD technique. These examples test the validity of the procedure explained herein.

Flexural analysis and strength design assumptions

Bernouilli's Hypothesis

The compatibility conditions to be imposed within the problem make use of Bernouilli's hypothesis that plane sections remain plane after deformation and assume no slip of reinforcement at the critical section. Thus, the distribution of strain over the cross section may be defined by just two variables (Figure 1): the strain at the centroid (ε_c) of the cross section and the curvature (ϕ) of the cross-section. Therefore, strain at any fiber of concrete or steel located a distance *y* from centroid of the cross section will be:

$$\varepsilon\left(y,\varepsilon_c,\phi\right)=\varepsilon_c+\phi y \tag{1}$$

The formulation given in Eq. (1) considers the compression strain as positive and the curvature which produces tension in the bottom fiber.

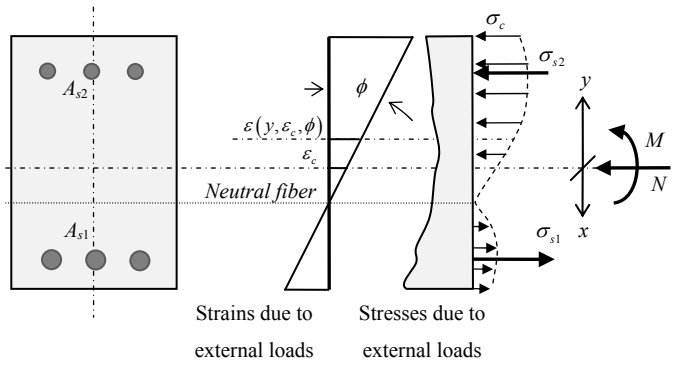

Figure 1. Strains and stresses diagrams at cross-section level

Section Ultimate Limit State according to EC2

Bending ultimate limit state is associated to failure of the section due to the limit of concrete compressive strength or, in some cases, the steel tension limit stress.

EC2 defines a series of possible ranges of ultimate strain distributions (Figure 2). Strain planes pivoting on point A are distributions in which steel fails in tension whereas the planes pivoting either on point B or C correspond to concrete failure in compression.

EC2 concrete model considers that concrete ultimate compression strain in flexural compression is different from the case of pure compression; this is the reason for the ultimate constant strain distribution at pure compression ε_{c2} or ε_{c3} (depending on consideration of parabolic-rectangular or rectangular concrete stress distribution) in Figure 2.

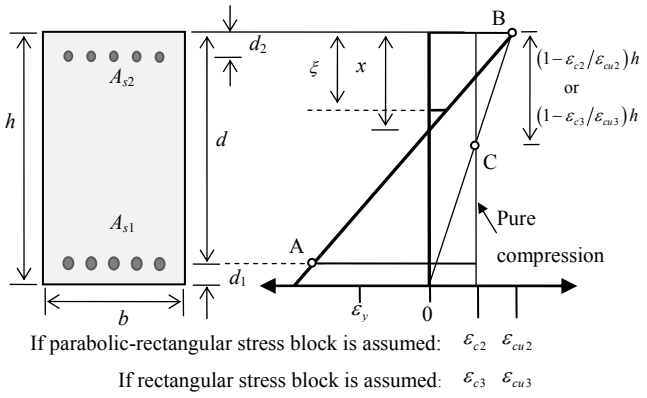

Figure 2. Possible strain distributions in the ultimate limit state according to EC2

Considering a stress bilinear model without strain hardening for reinforcing steel, EC2 allows no limitation of the steel tensile strain, so point A in Figure 2 disappears.

From the observation of the presented ultimate strain configurations in Figure 2, it can be noticed that the ultimate strain for any fiber in the cross-section may be expressed by means of

just one variable: neutral axis depth x (Eq. (2)). Considering the steel model without strain hardening condition, x takes values in the interval $[0,\infty)$.

$$\varepsilon(\xi,x)=\begin{cases}\varepsilon_{cu3}\dfrac{x-\xi}{x} & \text{if} \quad 0\le x<h\\ \varepsilon_{c3}\dfrac{x-\xi}{x-\Xi} & \text{if} \quad x\ge h\end{cases} \tag{2}$$

where $\Xi=h\left(1-\dfrac{\varepsilon_{c3}}{\varepsilon_{cu3}}\right)$ and ξ is the position where strain is to be measured.

Concrete ultimate state model

Concrete is a material whose stress-strain behavior is non-linear and changes with age and loading duration, among other factors. Due to the importance of the ultimate strength design, simplified schemes have been adopted in order to capture the behaviour of concrete. EC2 considers three different concrete stress-strain models: rectangular, parabolic-rectangular, and bilinear.

Within this work the rectangular model has been adopted with $\varepsilon_{c3}=2‰$ and $\varepsilon_{cu3}=3.5‰$. The resultant of compression in concrete, N_c, can be determined in the case of rectangular sections as a function of the neutral axis depth, x, as follows:

$$N_c(x)=\begin{cases}0 & \text{if } x\le 0\\ \eta f_{cd}\, b\, \lambda x & \text{if } 0\le x<h/\lambda\\ \eta f_{cd}\, b\, h & \text{if } x\ge h/\lambda\end{cases} \tag{3}$$

where $f_{cd}=\alpha_{cc}f_{ck}/\gamma_c$ is the concrete design strength according to EC2; f_{ck} is the characteristic compressive cylinder strength of concrete at 28 days; γ_c is the partial safety factor for concrete (1.5 for persistent and transient design situations and 1.2 for accidental situations); α_{cc} is the coefficient considering long term effects on the compressive strength and unfavorable effects resulting from the way the load is applied, should lie between 0.8 and 1.0, with a typical value of 0.85; h and b are depth and width of the rectangular cross-section, respectively. Values for η and λ are given by Eq. (4):

$$\lambda = \begin{cases} 0.8 & \text{for } f_{ck} \le 50 \text{ MPa} \\ 0.8 - (f_{ck} - 50)/400 & \text{for } 50 < f_{ck} \le 90 \text{ MPa} \end{cases}$$
$$\eta = \begin{cases} 1.0 & \text{for } f_{ck} \le 50 \text{ MPa} \\ 1.0 - (f_{ck} - 50)/200 & \text{for } 50 < f_{ck} \le 90 \text{ MPa} \end{cases} \quad (4)$$

Reinforcing steel ultimate state model

The steel model used herein is bilinear, without considering strain hardening and symmetric (i.e. the same expression for tension and compression is employed). Nevertheless, other non-symmetric models are possible. For the sake of simplicity, Eq. (3) does not consider the presence of reinforcement inside concrete cross-section. However, in order to take this into account, the steel model is formulated as follows:

$$\sigma_s(\varepsilon) = \begin{cases} f_{yd} - \eta f_{cd} & \text{if} \quad \varepsilon \ge \dfrac{f_{yd} - \eta f_{cd}}{E_s} \\ E_s \varepsilon & \text{if} \quad -\dfrac{f_{yd}}{E_s} < \varepsilon < \dfrac{f_{yd} - \eta f_{cd}}{E_s} \\ f_{yd} & \text{if} \quad \varepsilon \le -\dfrac{f_{yd}}{E_s} \end{cases} \quad (5)$$

As mentioned above, strain ε may be perfectly defined by means of just one variable: neutral axis depth, x. Therefore, expression for steel stress given in Eq. (5) can be also given as a function of x.

In the common case of a concrete cross-section with two layers of steel, A_{s1} (bottom) and A_{s2} (top), with mechanical covers of d_1 and d_2 respectively (considered equal in this work), ultimate strains and stresses in the reinforcements may be obtained from the composition of Eqs. (2) and (5) (Gil-Martín et al., 2012) as:

$$\begin{aligned} \varepsilon_{s1}(x) &= \varepsilon(h - d_1, x) \\ \varepsilon_{s2}(x) &= \varepsilon(d_2, x) \\ \sigma_{s1}(x) &= \sigma_{s1}(\varepsilon_{s1}(x)) = (\sigma_{s1} \circ \varepsilon_{s1})(x) \\ \sigma_{s2}(x) &= \sigma_{s2}(\varepsilon_{s2}(x)) = (\sigma_{s1} \circ \varepsilon_{s2})(x) \end{aligned} \quad (6)$$

where $\circ$ means composition of two mathematical functions.

Equilibrium equations

The stress distribution over the cross-section has to equilibrate the externally applied loads that, in this case, are an in-plane bending moment M and a compressive axial load N (Figure 1). Taking moment equilibrium at the centroid of the cross section, supposed rectangular with h height and b width, equilibrium equations may be presented as:

$$\begin{aligned} N &= N_c(x) + A_{s1}\sigma_{s1}(x) + A_{s2}\sigma_{s2}(x) \\ M &= N_c(x)\left(\frac{h}{2} - z_c(x)\right) - A_{s1}\sigma_{s1}(x)\left(\frac{h}{2} - d_1\right) + A_{s2}\sigma_{s2}(x)\left(\frac{h}{2} - d_2\right) \end{aligned} \tag{7}$$

where z_c is lever arm corresponding to the resultant of concrete compressions relative to the top fiber, defined as (Figure 3):

$$z_c(x) = \begin{cases} \dfrac{\lambda x}{2} & \text{if} \quad 0 \le x \le \dfrac{h}{\lambda} \\ \dfrac{h}{2} & \text{if} \quad x \ge \dfrac{h}{\lambda} \end{cases} \tag{8}$$

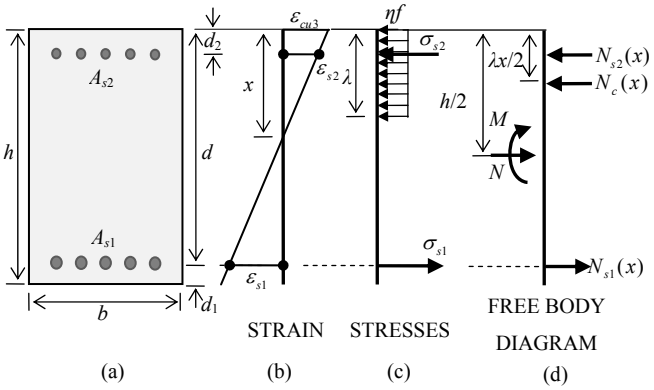

Figure 3. Terms for ultimate strength analysis according to EC2

The problem of optimum reinforcement

When faced with the problem of design of RC rectangular sections, once the dimensions h and b are preliminary fixed, the engineer has to provide a solution to the two equilibrium equations presented in Eq. (7). However, these equations have three unknowns: neutral axis depth, x, bottom, A_{s1}, and top, A_{s2}, reinforcing steel. Therefore, as the problem is indeterminate, it may be solved with an infinite set of values for x, A_{s1}, and A_{s2}.

As mentioned earlier, the RSD (Hernández-Montes et al., 2005) approach provides, in a graphical manner, all the possible combinations for x, A_{s1}, and A_{s2}. Employing this method,

Hernández-Montes et al., (2008) established the "Theorem of Optimal Section Reinforcement" (TOSR), where the authors stated that one of the following conditions imposed in Eq. (7) yields the optimal result for the reinforcing steel under combined compressive load and in-plane bending moment:

I. $A_{s1} = 0$

II. $A_{s2} = 0$

III. $A_{s1} = A_{s2} = 0$

IV. ε_s equal or slightly greater than $-\varepsilon_y$

V. $\varepsilon = \varepsilon_{s1} = \varepsilon_{s2} = \varepsilon_{c3}$

Above, conditions II and IV make the maximum usage of the steel capacity while conditions I, III, and V take advantage of the maximum concrete capacity. TOSR provides a sixth condition but it is not considered herein since it is related to the yielding of both layers of reinforcement in tension.

Although the conditions that lead to an optimum design are given, the designer still does not know which condition is to be imposed; it is necessary to evaluate the five abovementioned conditions (I to V) until the optimum solution is reached.

Eccentricity domains for optimal strength design

The externally applied compression load and bending moment, N and M, are equivalently expressed introducing the same compression load N acting at an eccentricity e_0 with respect to the centroid of the cross section (Nawy, 2003), so that (Figure 4):

$$e_0 = \frac{M}{N} \tag{9}$$

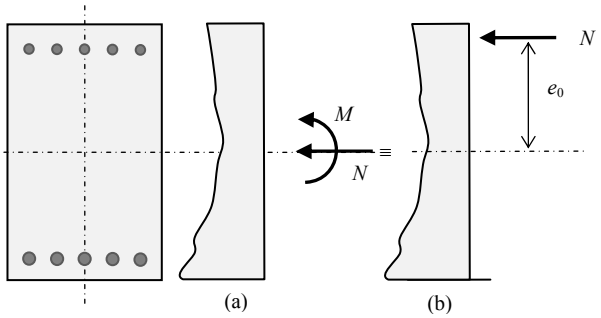

Figure 4. Combined compression and in-plane flexion. Both systems, (a) and (b), are equivalent if $e_0=M/N$

As will be shown, the former conditions for optimal proportioning of reinforcement in rectangular RC cross-sections may be explained in terms of the eccentricity e_0 and compression load N. Setting out moment equilibrium at different points of the section in several cases (Figure 5) different domain boundaries can be obtained. These domains and their boundaries will be deduced in the remainder of this section. The main advantage of these domains is that they may be graphically represented, which facilitates their application. Therefore, with only evaluation of pair $e_0 - N$, the designer will be able to identify the relevant domain and so, determine the optimal reinforcement for each loading case.

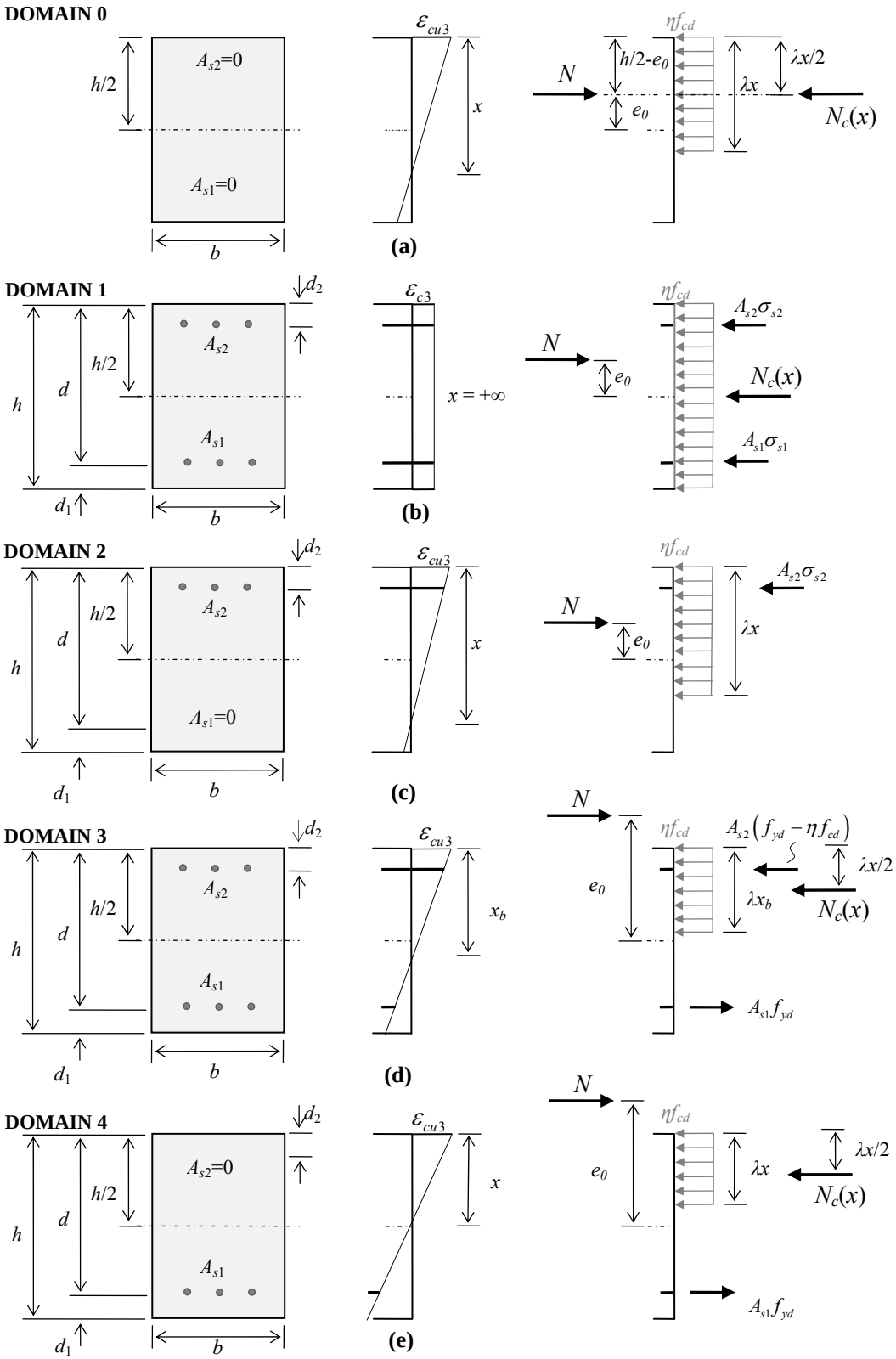

Figure 5. Ultimate limit states with optimal reinforcement for rectangular RC cross-sections subject to combined compression and in-plane bending moment

Domains and its boundaries.

The pair of values $e_0 - N$ for which concrete section is able to stand without any longitudinal reinforcement, that is, $A_{s1} = A_{s2} = 0$ (called domain 0) may be determined from Figure 5(a). For $N \le \eta f_{cd} \lambda x\, b$ and values of eccentricity in the range $0 \le e_0 < h/2$, the concrete cross-section is able to resist with no reinforcement to the applied loads, being the compression stress in concrete $\sigma_c = \eta f_{cd}$. From Figure 5(a) it can be noticed that, in the limit situation $\sigma_c = \eta f_{cd}$, the following conditions may be established:

$$N = \eta f_{cd}\, \lambda x\, b \tag{10}$$

$$e_0 = \frac{h}{2} - \frac{\lambda}{2} x \tag{11}$$

Combination of Eq. (10) and (11) leads to the eccentricity limit, e_{0c}, under which no reinforcement is necessary, $A_{s1} = A_{s2} = 0$. The value of e_{0c} is given by Eq. (12):

$$e_{0c} = \frac{1}{2}\left(h - \frac{N}{\eta f_{cd}\, b} \right) \tag{12}$$

Although the case above is theoretically possible, it is assumed that minimum reinforcement as prescribed in code provisions would be used, even for sections in domain 0.

Now, let us consider solutions in domain 1, where the condition of TOSR to be imposed is $x = +\infty$. In this domain, axial load N is applied with a low eccentricity value e_0 so that full compression of the cross-section is involved. In some cases, equilibrium makes the existence of compressed bottom reinforcement necessary ($A_{s1} \neq 0$). The boundary value of $e_0 = e_{0h}$ which separates the cases of $A_{s1} = 0$ and $A_{s1} \neq 0$, is deducted in Eq. (13). Setting up moment equilibrium at the top reinforcement level in the situation presented in Figure 5(b) (with $A_{s1} = 0$), in the situation of full compression of the cross-section (i.e. $\lambda x = h$):

$$e_{0h} = \left(\frac{h}{2} - d_2 \right) - \frac{\eta f_{cd}\, h\, b \left(\frac{h}{2} - d_2 \right)}{N} \tag{13}$$

For cases in domain 1, for which both top and bottom reinforcements are necessary (i.e. $A_{s1} \neq 0$ and $A_{s2} \neq 0$), the optimal reinforcement corresponds to the condition V of TOSR. Setting up

moment equilibrium at the top reinforcement level and equilibrium of axial loads (Figure 5 (b)), both bottom and top reinforcement areas A_{s1} and A_{s2} are given by Eqs. (14) and (15):

$$A_{s1} = \frac{\left(\frac{h}{2} - d_2 - e_0\right) N - \eta f_{cd} h\, b \left(\frac{h}{2} - d_2\right)}{\left(d - d_2\right) \sigma_{s1}\left(x = +\infty\right)} \tag{14}$$

$$A_{s2} = \frac{N - \left[\eta f_{cd} h\, b + A_{s1} \sigma_{s1}\left(x = +\infty\right)\right]}{\sigma_{s2}\left(x = +\infty\right)} \tag{15}$$

The eccentricity boundary e_{0h} separates domains 1 and 2. In domain 2 the additional condition to be imposed on Eq. (7) in order to get the optimal solution for reinforcement is $A_{s1} = 0$. In this domain, the section can be partially of fully compressed (i.e. $x \le h / \lambda$), and the area of top reinforcement is provided solving axial equilibrium in Figure 5(c):

$$A_{s2} = \frac{N - \eta f_{cd} \lambda x\, b}{f_{yd} - \eta f_{cd}} \tag{16}$$

In Eq. (16) $f_{yd} - \eta\, f_{cd} = \sigma_{s2}\left(x\right)$ and the neutral fiber position, x, can be obtained from equilibrium of moment at the top reinforcement level (Figure 5(c)):

$$\left(\frac{h}{2} - d_2 - e_0\right) N = \eta f_{cd} \lambda x\, b \left(\frac{\lambda x}{2} - d_2\right) \tag{17}$$

The strain limit for domain 3 is represented in Figure 5 (d). In this situation the optimal reinforcement corresponds to the condition IV of TOSR. Therefore, the optimal solution is located at balance point $x = x_b$, thus $N_c = \eta f_{cd} \lambda x_b b$ being

$$x_b = \frac{d_{s1}}{1 + \frac{f_{yd}}{\varepsilon_{cu3} E_s}} \tag{18}$$

The value of e_0 which separates domains 2 and 3, $e_{0\text{lim}}$, is deducted from Figure 5(d) imposing that $A_{s1} = 0$. Equilibrium of the free body diagram is considered with $A_{s1} = 0$ (domain 3) and $x = x_b$ (domain 4), leading to a boundary value of e_0 equals to:

$$e_{0\text{lim}} = \left(\frac{h}{2} - d_2\right) - \frac{\eta f_{cd}\, \lambda x_b b \left(\frac{\lambda x_b}{2} - d_2\right)}{N} \tag{19}$$

The value of $e_{0\lim}$ marks the classical boundary between large and small eccentricity problems (Nawy, 2003).

In domain 3 both bottom and top reinforcements are necessary. Taking moment at the bottom reinforcement level and setting up equilibrium of axial loads (Figure 5(d)) result in Eqs. (20) and (21) which provide the required reinforcements:

$$A_{s2} = \frac{\left(e_0 + \frac{h}{2} - d_1\right)N - \eta f_{cd} \lambda x_b b\left(d - \frac{\lambda x_b}{2}\right)}{\left(f_{yd} - \eta f_{cd}\right)\left(d - d_2\right)} \tag{20}$$

$$A_{s1} = \frac{\eta f_{cd} \lambda x_b b + A_{s2}\left(f_{yd} - \eta f_{cd}\right) - N}{f_{yd}} \tag{21}$$

The last domain to be considered is called domain 4 (Figure 5(e)); in this situation the top reinforcement is not needed ($A_{s2} = 0$). The boundary value of $e_0 = e_{02}$ which separates domains 3 and 4 is deducted considering equilibrium of the free body diagram in Figure 5(d) imposing $A_{s2} = 0$ (i.e. $A_{s2} = 0$ and $x = x_b$):

$$e_{02} = -\left(\frac{h}{2} - d_1\right) + \frac{\eta f_{cd}\, \lambda x_b b\left(d - \frac{\lambda x_b}{2}\right)}{N} \tag{22}$$

To obtain the required bottom reinforcement area in domain 4 it is necessary to know the value of the neutral axis depth x, which is computed setting up equilibrium of moments at the bottom reinforcement level (Eq. (23)). Once x is obtained, the equilibrium of axial loads provides bottom reinforcement area according to Eq. (24):

$$\left(e_0 + \frac{h}{2} - d_1\right)N = \eta f_{cd} \lambda x\, b\left(d - \frac{\lambda x}{2}\right) \tag{23}$$

$$A_{s1} = \frac{\eta f_{cd} \lambda x\, b - N}{f_{yd}} \tag{24}$$

An alternative and easier way to represent the former boundaries and domain that allow the engineer to obtain the optimal reinforcement of a rectangular RC cross-section is using a chart as presented in Figure 6. In this figure, the value of e_0 / h (i.e. ratio between eccentricity and the depth of the cross section) is represented in function of the non-dimensional parameter

$\nu = N/\left(\eta f_{cd} b\, h\right)$ for the studied section (i.e. the values of mechanical covers (d_1 = d_2 = h/10) and design strength of steel, f_{yd} (f_{yk} = 500 MPa) are known).

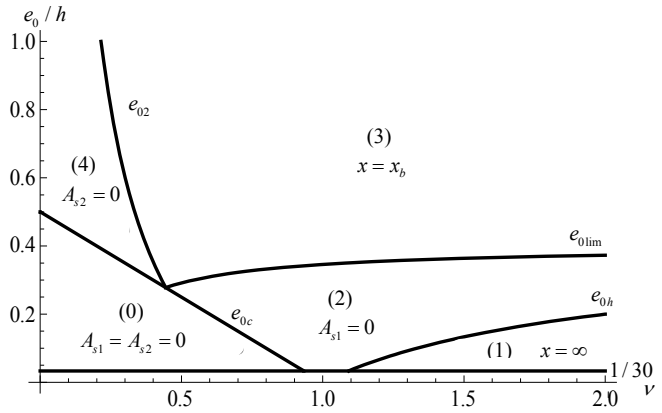

Figure 6. Chart $e_0 / h - \nu$ with $\nu = N/\eta f_{cd} h\, b$ corresponding to a rectangular RC cross section for steel B 500 S, and $d_1 = d_2 = h/10$

Since some boundary values of e_0 depend on x_b (see Eqs. (19) and (22) different charts will be obtained for different steel yield strain, $\varepsilon_y = f_{yd} / E_s$, being E_s the steel elasticity modulus ($E_s = 200.000$ MPa).

In Figure 6 the horizontal band for which $e_0 / h < 1/30$ has to be excluded according to prescriptions of EC2 § 6.1 (4) (CEN, 2004) relating minimum eccentricity concerns.

The former procedure has been summarized in the flow chart represented in Figure 7.

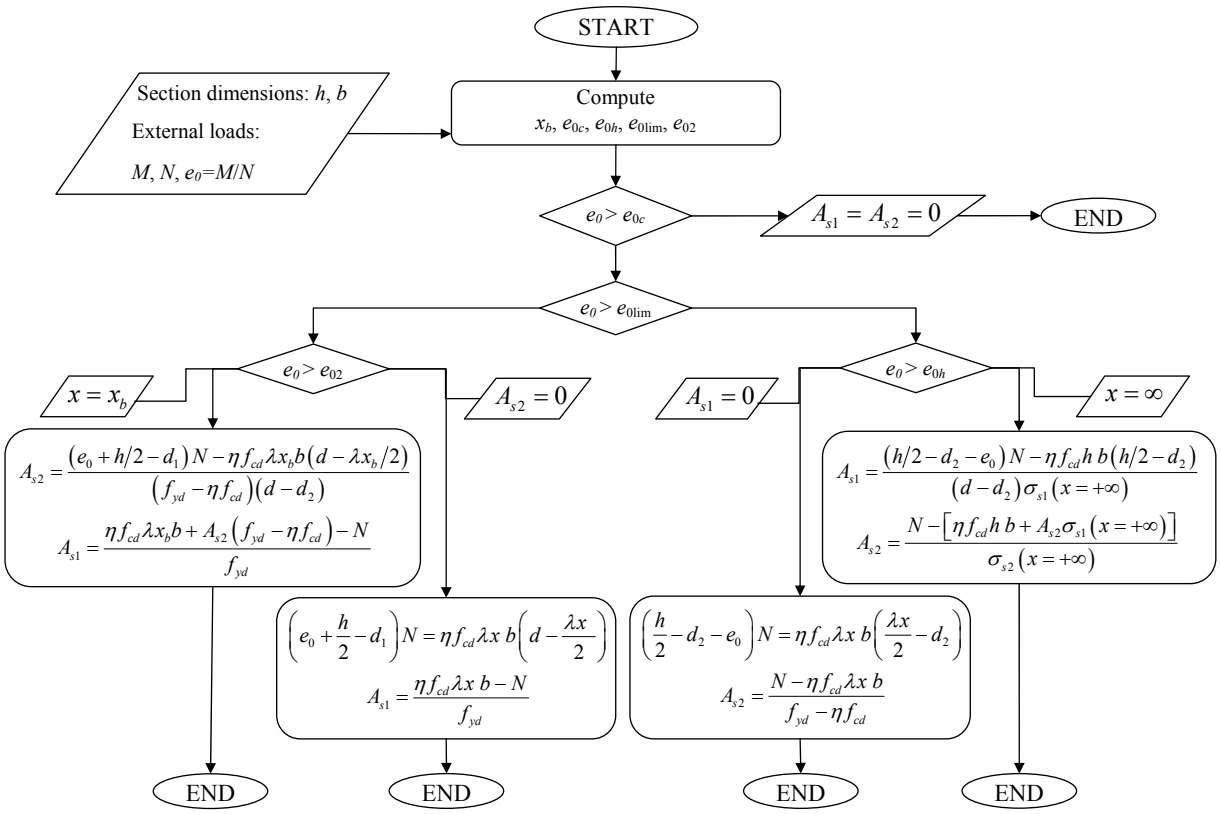

Figure 7. Flow chart: eccentricity-based process to optimize rectangular RC cross-sections subject to combined compression and in-plane bending moment

Examples

In this section some examples are presented in order to prove the validity of the approach proposed above. Several values of eccentricity e_0 and external compression load N have been considered and the additional condition to impose in order to get the optimal reinforcement is obtained from the chart presented in Figure 6. Results are verified using RSD representations of the required reinforcement areas since this technique shows in a graphical manner all the possible solutions for the reinforcement as a function of neutral axis depth x. Furthermore, the neutral axis depth x and the optimal reinforcement areas, A_{s1} and A_{s2}, are calculated.

In the following examples, the concrete has a strength resistance of $f_{ck} = 45$ MPa and the steel yield strength is $f_{yk} = 500$ MPa. The modulus of elasticity of the reinforcement is $E_s = 200000$ MPa. The dimensions of the studied cross section are: $h = 600$ mm, $b = 300$ mm, $d = 540$ mm, $d_1 = d_2 = 60$ mm.

In Figure 8 the chart ν-e_0/h for the former section has been represented. For a high value of the axial load, like $\nu = 1.5$ (vertical line 1 in Figure 8) three domains are possible depending on the

eccentricity e_0. For smaller values of e_0, i.e. for situations closer to centered compression, both top and bottom reinforcements are needed (segment a1 in domain 1 - Figure 8 -). As e_0 is increased, equilibrium may be set up without presence of bottom reinforcement (segment b1 in domain 2 - Figure 8 -). However, if eccentricity keeps on increasing, the applied moment M becomes great enough to require the presence of both reinforcements (segment c1 in domain 3 - Figure 8 -) and, in these circumstances, in order to take advantage of both concrete and bottom reinforcement the additional condition $x = x_b$ must be imposed.

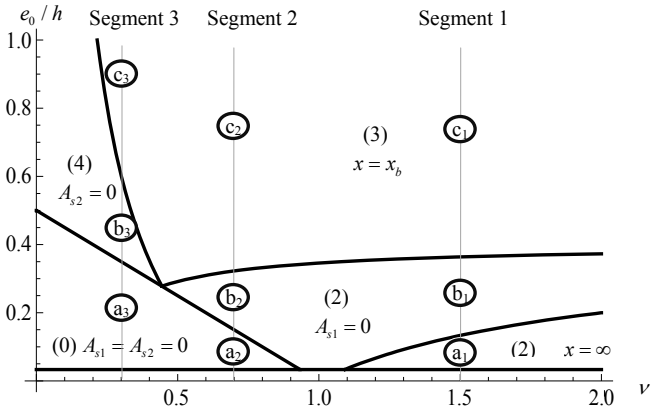

Figure 8. Chart $e_0 / h - \nu$ with $\nu = N / \eta f_{cd} h\, b$, with B 500 S and $d_1 = d_2 = h/10$

In Figures 9 and 10 the RSD diagrams corresponding to $e_0 / h = 0.1$ and $\nu = 1.5$ (a point in segment a_1) and $e_0 / h = 0.8$ and $\nu = 1.5$ (a point in segment c_1) have been represented respectively. The optimal reinforcements obtained from the RSDs confirm the validity of the results given in the chart in Figure 8.

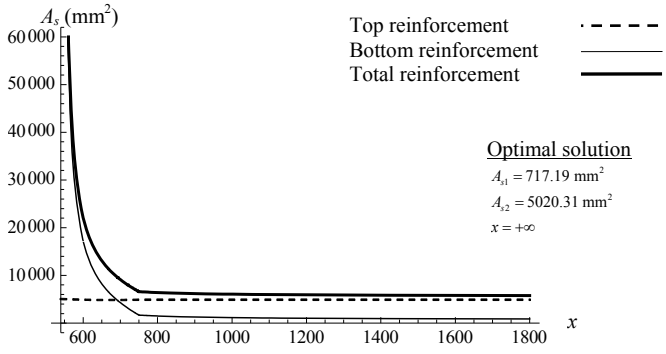

Figure 9. RSD diagram for a point in segment a_1 in Figure 8: $e_0 / h = 0.1$ & $\nu = 1.5$

If a smaller value of the axial load is considered, $\nu = 0.7$ (vertical line 2 in Figure 8), for low values of eccentricity the section is able to stand the external loads without reinforcement (segment a_2 in domain 0 - Figure 8 -).

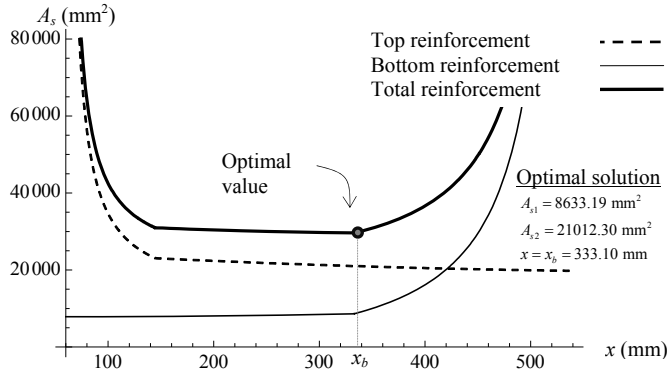

Figure 10. RSD diagram for a point in segment c_1 in Figure 8: $e_0 / h = 0.8$ & $\nu = 1.5$.

Figure 11 shows the RSD diagram for $\nu = 0.7$ and $e_0/h = 0.1$ (a point in segment a_2 in Figure 8); it is evident from Figure 11 that the equilibrium cannot be reached with $\sigma_c = \eta f_{cd}$, $A_{s1} \neq 0$, and $A_{s2} \neq 0$ and hence, for this situation, the optimal reinforcement corresponds to $\sigma_c < \eta f_{cd}$ and $A_{s1} = A_{s2} = 0$.

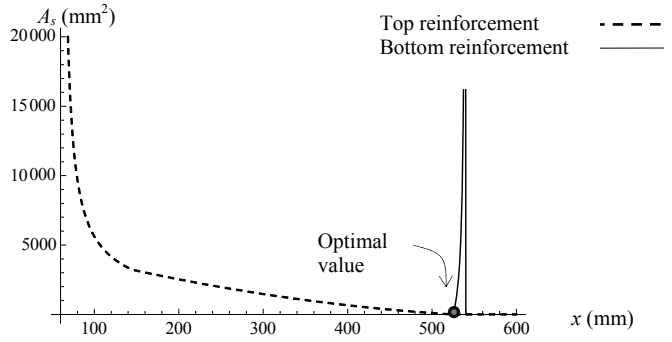

Figure 11. RSD diagram for a point in segment a_2 in Figure 8: $e_0 / h = 0.1$ & $\nu = 0.7$. Since either A_{s1} or A_{s2} are not positive for the same value of x, no solution is possible

As in the previous case, if the value of axial load stays constant but the value of the eccentricity increases then reinforcement is required. As mentioned above for $\nu = 1.5$, equilibrium may be reached without presence of bottom reinforcement (segment b_2 in domain 2 - Figure 8 -). The RSD for $e_0 / h = 0.25$ & $\nu = 0.7$ (a point in segment b_2 in Figure 8) represented in Figure 12 confirms the results obtained from the proposed chart.

A final case corresponding to the vertical line 3 in Figure 8 has also been analyzed. For the adopted value of axial load, $\nu = 0.3$, the optimal reinforcement corresponds to domain 0, domain 4 or domain 3 (segments a_3, b_3 and c_3 respectively in Figure 8) as e_0 increases. The RSD diagram for $\nu = 0.3$ and $e_0 = 0.45$ (a point in segment b_3 in Figure 8) represented in Figure 13 confirms that the optimal reinforcements corresponds to A_{s2}=0, that is the condition in domain 4.

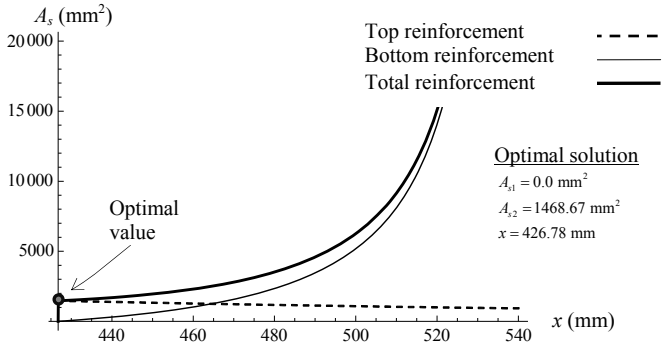

Figure 12. RSD diagram for a point in segment b_2 in Figure 8: $e_0 / h = 0.25$ & $\nu = 0.7$

As in the former cases, as eccentricity increases -and hence the bending moment- both reinforcements are required and for the biggest values of e_0 the optimal reinforcement is associated with $x = x_b$.

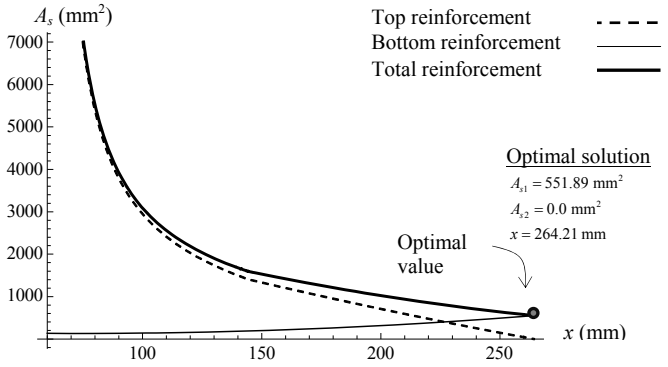

Figure 13. RSD diagram for a point in segment b_3 in Figure 8: $e_0 / h = 0.45$ & $\nu = 0.3$

Conclusions

The present work provides a geometric approach to optimum design of rectangular RC subject to combined compression N and in-plane bending moment M. The approach is said to be geometric since it is based on the evaluation of the resulting equivalent eccentricity of the pair of external loads, $e_0 = M / N$. A new formulation of boundary values for e_0 is presented in order to let the designer know which condition of the TOSR must be imposed in order to get optimal reinforcement (A_{s1} and A_{s2}). These conditions have been graphically represented in a non-dimensional chart $e_0/h - \nu$ with $\nu = N/\eta f_{cd} h\, b$. The main advantage of this chart is that allows the engineer to easily choose the optimal reinforcement. Some examples have proved the validity and compactness of the process.

Acknowledgements

Part of the present work was financed by the Spanish Ministry of Education. The second author is a Spanish Government PhD fellow (FPU grant AP 2010-3707). This support is gratefully acknowledged.

References

Aschheim, M., Hernández-Montes, E., and Gil-Martín, L. M. (2007). "Optimal domains for strength design of rectangular sections for axial load and moment according to Eurocode 2. " *Engineering Structures, 29*(8), 1752-1760.

Barros, A. F. M., Barros, M. H. F. M., and Ferreira, C. C. (2012). "Optimal design of rectangular RC sections for ultimate bending strength." *Structural and Multidisciplinary Optimization*, *45*(6), 845-860

Barros, M. H. F. M., Martins, R. A. F., and Barros, A. F. M. (2005). "Cost optimization of singly and doubly reinforced concrete beams with EC2-2001". *Structural and Multidisciplinary Optimization, 30*(3), 236-242.

Eurocode 2 (2001): Design of concrete structures—Part 1-1: General rules and rules for buildings. CEN European Committee for Standardization. EN 1992-1-1.

Camp, C.V., Pezeshk, S., Hansson, H. (2003). "Flexural design of reinforced concrete frames using a genetic algorithm". *Journal of Structural Engineering, 129*(1), 105-115.

Gil-Martín, L. M., López-Martín, D., Hernández-Montes, E., and Aschheim, M. (2012). "Dimensionamiento en rotura a flexión de secciones de hormigón armado." Un planteamiento compacto. *Informes de la Construcción* (in press). doi 10.3989/ic.11050

Hernández-Montes, E., Aschheim, M., and Gil-Martín, L. M. (2004). "Impact of optimal longitudinal reinforcement on the curvature ductility capacity of reinforced concrete column sections." *Magazine of Concrete Research, 56*(9), 499-512.

Hernández-Montes, E., Gil-Martín, L. M., and Aschheim, M. (2005). "Design of concrete members subjected to uniaxial bending and compression using reinforcement sizing diagrams." *ACI Structural Journal, 102*(1), 150-158.

Hernández-Montes, E., Gil-Martín, L. M., Pasadas-Fernández, M., and Aschheim, M. (2008). "Theorem of optimal reinforcement for reinforced concrete cross sections." *Structural and Multidisciplinary Optimization, 36*(5), 509-521.

Lee, C., Ahn, J. (2003). "Flexural design of reinforced concrete frames by genetic algorithm". *Journal of Structural Engineering, 129*(6), 762-774.

López-Martín, D., Gil-Martín, L. M., Hernández-Montes, E., and Aschheim, M. (2011). "Dominios de deformación referidos a la excentricidad de cálculo para el diseño óptimo de secciones rectangulares solicitadas a flexo-compresión." *1st International Congress on Mechanical Models in Structural Engineering*, Granada. 93-106.

Nawy, E. G. (2003). *Reinforced concrete: A fundamental approach* (5th ed.). Prentice-Hall, Upper Saddle River, NJ.

Anexo 4

Limits to the Strength Design of Reinforced Concrete Shells and Slabs

Enrique Hernández-Montes[1], Juan F. Carbonell-Márquez[2] and Luisa. M. Gil-Martín[3]

(Accepted for publication in "Engineering Structures")

http://dx.doi.org/10.1016/j.engstruct.2014.01.011

ABSTRACT

One of the most important works in the ultimate limit state design of reinforced concrete plates or shells subjected to flexure and membrane actions is the one provided by Brondum-Nielsen (Brondum-Nielsen, 1974). Therein, the author divides the shell element into three layers; the outer layers withstand a state of membrane forces located on their middle surfaces. The forces at the centroid of the reinforcement, in both directions, have been obtained from equilibrium, and the steel area needed is computed by dividing these tension forces by the steel yield stress, f_y. An extension to the strain plane hypothesis widely used in the strength design of RC beams and columns is presented, aiming at RC strength design of shells and slabs. As a result , limits to the application of the Bromdum-Nielsen procedure are given in this work since it cannot always be guaranteed that the stress in the steel is f_y as the original method proposes. A new method based on the computation of the balance point in the beam flexure design is developed to check the limits of application of Brondum-Nielsen's approach. The Upper Bound Theorem of plasticity guaranties that the obtained forces are on the safe side. Examples are provided.

[1] Professor, Department of Structural Mechanics, University of Granada (UGR). Campus Universitario de Fuentenueva s/n. 18072 Granada, Spain. emontes@ugr.es.

[2] PhD Candidate, Department of Structural Mechanics, University of Granada (UGR). Campus Universitario de Fuentenueva s/n. 18072 Granada, Spain. (corresponding author). Email jfcarbonell@ugr.es. Tel.: +34 958249965; fax: +34 958249959

[3] Associate Professor, Department of Structural Mechanics, University of Granada (UGR). Campus Universitario de Fuentenueva s/n. 18072 Granada, Spain. mlgil@ugr.es.

KEYWORDS: Reinforced Concrete; Shell; Slab; Optimization; Balance point;

Notation

a	Distance between the middle surfaces of the top and bottom layers
a_b, a_t	Distances between the middle surfaces of bottom and top layers to the middle surface of the shell, respectively
c_b, c_t	Depth of bottom and top layers , respectively
c_{b0}	First approximation of c_b
$c_{ki\lim}$	Limit depth of layer k ($k = t$ for top layer; $k = b$ for bottom layer) in order to yield the reinforcement in i direction (x or y) placed in the opposite layer j
d	depth of the reinforcement
f_c	Concrete compression strength
f_y	Yield stress of the reinforcement
E_s	Young's modulus of the steel
e_k	Distance between the middle layer of the shell element to the centroid of the reinforcement placed in layer k
h	Depth of the shell element
z_{ya}	Lever arm of $N_{yat}+N_{yab}$ related to the centre of gravity of the gross section
z_{yat}	Lever arm of N_{yat} related to the centre of gravity of the gross section
z_{yab}	Lever arm of N_{yab} related to the centre of gravity of the gross section
z_{xa}, z_{xat}, z_{xab}	Idem for $N_{xat}+N_{xab}$, N_{xat} and N_{xab}.
M_a	Flexural moment considered for the first estimation of c_b
M_x, M_y	Bending moments in x and y directions applied to the shell element
M_{xy}	Twisting moment applied to the shell element
N	Axial force
N_x, N_y	Normal forces in x and y directions applied to the shell element
N_{xy}	Shear force applied to the shell element
N_{xk}, N_{yk}	Membrane normal forces in x and y directions in layer k
N_{xyk}	Membrane shear force in layer k
N_{xak}, N_{yak}	Tension forces in reinforcement placed in x and y directions in layer k

N_{ck}	Concrete compression force in layer k
$N_{total,k}$	$N_{total,k} = N_{xak} + N_{yak}$. Summation of tension forces in the reinforcement placed in x and y directions in layer k
α_k	Angle between crack and x direction, in layer k
ε_{cu}	Concrete ultimate compressive strain
$\varepsilon_{j\text{-}i}$	Steel strain in i direction, placed in layer j, when the depth of compression block in layer k is c_k
$\varepsilon_{j\text{-}i\text{lim-}\alpha k}$	Strain measured, in the direction of the crack of layer k (α_k), at the level of centroid of reinforcement placed in layer j corresponding to the yield of the steel in i direction
ε_y	tension yield strain of the reinforcement
λ	Stress block factor of the rectangular stress distribution in concrete according Eurocode 2
σ	Stress
α_k	angle between the crack in layer k and x-direction
χ_{klim}	depth of the balance point

Subscript

a	Steel
b	bottom layer
i	x or y direction
j	layer j, opposite layer to layer k
k	layer k (top or bottom layer)
x	direction x
lim	balance conditions
y	direction y

Superscript

*	actual value

1. Introduction

Capacity of reinforced concrete (RC) shells and slabs has always been an interesting topic, e.g. [1][2][3]. The problem of designing the reinforcement for a concrete plate or shell in ultimate limit state to withstand membrane forces together with bending and torsion moments has not yet been universally solved. As a consequence, the main RC design codes – Eurocode 2 [4], AC1 318 [5] – do not provide a general method to deal with this problem as they do with the beam cross section design. Only the Model Code CEB-FIP 2010 (MC2010) [6] states, literally, that "shell elements may be modelled as comprising three layers. The outer layers provide resistance to the in-plane effects of both the bending and the in-plane axial loading, while the inner layer provides a shear transfer between the outer layers." But the designer would have difficulty finding further information on this issue.

You can find many different techniques in literature that try to obtain a generally accepted solution. One of the first practical approaches to this problem is the report by Brondum-Nielsen [7]. This work deals with the shell element as if it were a sandwich element composed of three layers, with the outer layers being responsible for withstanding the membrane force decomposition of the external bending, torsion, in-plane axial and in-plane shear loading. Each of these layers contains an orthogonal reinforcing net. Gupta [8] takes the work of Brondum-Nielsen as a reference to propose a general solution based on an iterative trial-and-error design method using the principle of minimum resistance by also dividing the shell into three layers containing the orthogonally provided reinforcement. Marti [9] assigns the out of plane shear to the middle layer, complementing the work of Brondum-Nielsen. Lourenço and Figueiras [10] [11] formulated the problem of reinforcing elements subjected to membrane and flexural forces based on equilibrium conditions and suggested a new iterative procedure. They have developed a consistent solution to the problem analyzing the shell element as a whole and not as two membrane outer layers. The information concerning this approach has been compiled by Fall et al. [12] in their revision of procedures of reinforcing methods in RC tailor-made structures. A similar approach to the one presented by Gupta is implemented in an iterative numerical computational algorithm by Min [13] and tested in several experimental examples. Furthermore,

nonlinear inelastic analyses are performed using the Mahmoud-Gupta's computer program [14][15][16][17] to prove the adequacy of the presented equations. A similar formulation of the problem is adopted by Tomás and Martí [18] in order to mathematically optimize the amount of reinforcement in each finite element of the mesh that models the geometry of the problem, employing the summation of the tensile forces in the reinforcement as the objective function. One of the most recent works in this field is the one proposed by Bertagnoli et al. [19] where the authors provide a method based on sandwich layers to optimize the amount of reinforcing steel to be placed in the two outer layers. The method considers non-orthogonal reinforcement layouts, and the optimization procedure is based on genetic algorithms.

It is extraordinary that, despite all the aforementioned works, one of the most powerful and popular commercial pieces of software in structural design, the SAP2000©, uses the very first of one of these methods (Brondum-Nielsen's approach) to design the reinforcement of concrete shells in ultimate limit state under bending and in-plane axial forces [20].

Apart from dividing the shell element into some layers, all the presented works have another aspect in common with respect to the stresses in the reinforcement and in the concrete. The compressive stress in concrete - compression struts – should be distributed uniformly throughout the depth of the layer and the steel in tension is assumed to be yielded, -i.e. with stress equal to f_y- the later hypothesis is also known as limit-analysis solution. Both the tensile stress in concrete and the compressive stress in the reinforcement are neglected.

The part concerning the yielding of the reinforcement is found to be questionable by the authors of this study. Similarly, as in the case of ultimate state of bending in beams, where the plane sections hypothesis has to be satisfied, the strain in the reinforcement of one of the outer layers in a slab element should be related to the depth of the compression stress block in the opposite one.

This paper presents a necessary hypothesis to the strength design of reinforced concrete shells and slabs. Furthermore Marti [9] expresses an attempt to limit the applicability of Brondum-

Nielsen's method "… these equations are only valid if the concrete compressive strength of the sandwich cover is not exceeded" –he calls cover to the thickness of the layer-. His attempt, although interesting, is an inaccurate observation that limits his design to small axial forces and he fails to provide a basic understanding of the behaviour of steel. Nonetheless an extension of the well established assumptions considered in the strength design of beams under bending is indeed a good advance in the reinforced concrete design of slabs and shells.

The present work draws on the formulation of the problem given in Brondum-Nielsen's procedure [7] to set the domains where this approach is valid. Firstly, Brondum-Nielsen's method is explained in a more compact fashion and the paper is therefore self-contained. Later, the beam balance point analogy is stated in order to determine reasonable limits to the application of Brondum-Nielsen's method. Finally, the original example given in Brondum-Nielsen's report is explained and the limits of application are checked.

2. Membrane forces decomposition of externally applied loads

The concrete shell element considered in this work has to withstand the established normal forces N_x and N_y, the shear force N_{xy}, the bending moments M_x and M_y and the twisting moment M_{xy}. These actions are given per unit of length. Actions are considered positive if they are directed as indicated in **Fig. 1**(a). The shell element has one or two parallel layers of orthogonal reinforcing net of which the position is known. The depth of the shell element is h.

Taking into account the state of the applied loads (**Fig. 1**(a)) and the geometry of the sandwich shell element (**Fig. 1**(b)), all forces and moments acting in the shell element may be resolved into membrane forces applied at the middle surface of top and bottom outer layers according to equilibrium equations: Eq. (1), as shown in **Fig. 2**. Sub-indexes t and b refer to the top and bottom layer, respectively. The terms c_t and c_b are the depth of the outer layers, a_t and a_b are the distances between their middle surfaces and the middle surface of the shell element and a is the distance between the top and bottom middle surfaces, as indicated in **Fig. 1**(b).

$$N_{xt} = N_x \frac{a_b}{a} - \frac{M_x}{a} \qquad N_{xb} = N_x \frac{a_t}{a} + \frac{M_x}{a}$$
$$N_{yt} = N_y \frac{a_b}{a} - \frac{M_y}{a} \qquad N_{yb} = N_y \frac{a_t}{a} + \frac{M_y}{a} \tag{1}$$
$$N_{xyt} = N_{xy} \frac{a_b}{a} - \frac{M_{xy}}{a} \quad N_{xyb} = N_{xy} \frac{a_t}{a} + \frac{M_{xy}}{a}$$

3. Limit analysis of each membrane layer

Consider now the layer *k* of the above sandwich element, it is cracked under the actions of the external forces, and layer *j* is the opposite outer layer. If *k* refers to top layer, then *k* = *t* and *j* = *b*, and vice versa. **Fig. 3** shows a portion of this layer, with two of its sides being parallel to the *x* and *y* directions and the third one corresponding to a crack in the membrane, which forms an angle α_k with *x* direction. The length of this crack is taken equal to 1.

From equilibrium in **Fig. 3**. (a), the forces in the reinforcement per unit of length in both *x* and *y* directions, N_{xak} and N_{yak}, can be obtained:

$$N_{xak} \sin\alpha_k = N_{xk} \sin\alpha_k + \left|N_{xyk}\right| \cos\alpha_k \rightarrow \boxed{N_{xak} = N_{xk} + \left|N_{xyk}\right| \cot\alpha_k} \tag{2}$$

$$N_{yak} \cos\alpha_k = N_{yk} \cos\alpha_k + \left|N_{xyk}\right| \sin\alpha_k \rightarrow \boxed{N_{yak} = N_{yk} + \left|N_{xyk}\right| \tan\alpha_k} \tag{3}$$

The direction of the principal compressive membrane force in the concrete, N_{ck}, is parallel to the crack and is, therefore, applied perpendicular to a section as indicated by the dashed line in **Fig. 3**. (a). The value of the principal compression in concrete N_{ck} is obtained in Eq. (4) from equilibrium in *x* direction in **Fig. 3**. (b) and considering Eq. (2):

$$N_{xak} \sin\alpha_k = N_{xk} \sin\alpha_k + N_{ck} \cos^2\alpha_k \sin\alpha_k \rightarrow \boxed{N_{ck} = \left|N_{xyk}\right| \left(\tan\alpha_k + \cot\alpha_k\right)} \tag{4}$$

There is a variable in the above presented equations, i.e. the crack direction α_k, that needs to be chosen by the designer. As it's in the designer's interest to find the optimum reinforcement, this variable α_k will have a specific value.

If it is assumed that the reinforcement placed at layer k has yielded, the total amount of steel needed will be proportional to the summation of tension forces in the reinforcement in this layer, $N_{total,k} = N_{xak} + N_{yak}$. So, the value of α_k that corresponds to the minimum reinforcement can be obtained by partial derivative of the summation of Eqs. (2) and (3):

$$\frac{\partial N_{total,k}}{\partial \alpha_k} = 0 \rightarrow \left|N_{xyk}\right|\left(-\frac{1}{\sin^2 \alpha_k} + \frac{1}{\cos^2 \alpha_k}\right) = 0 \rightarrow \sin \alpha_k = \cos \alpha_k \rightarrow \boxed{\alpha_k = 45^{\circ}} \tag{5}$$

Solutions given by Eqs. (2) to (4) are valid if $N_{xak} \geq 0$ and $N_{yak} \geq 0$, that is, both x and y reinforcements are subjected to tension forces, in this case $\alpha_k = 45^{o}$ is chosen for the reinforcement design. If this condition is not met, one of the following cases can be found. It is interesting to notice that the classification below has been made based on the limit of applicability of Equations 2 to 4, i.e.: $\alpha_k = 45^{o}$ and $N_{xak} \leq 0$ and/or $N_{yak} \leq 0$.

a) If $N_{xk} < -\left|N_{xyk}\right|$ and $N_{yk} \geq -\left|N_{xyk}\right|$, the reinforcement in the x direction is compressed. In this situation $N_{xak} = 0$ – no reinforcement in x direction is required – and the crack angle, α_k, can be obtained from Eq. (2) imposing $N_{xak} = 0$. In this situation, the angle that defines the orientation of the crack in the membrane is given by Eq. (6):

$$\alpha_k = \arctan\left(\frac{\left|N_{xyk}\right|}{-N_{xk}}\right) \tag{6}$$

b) If $N_{yk} < -\left|N_{xyk}\right|$ and $N_{xk} \geq -\left|N_{xyk}\right|$, the reinforcement in the y direction is compressed. In this situation $N_{yak} = 0$ – no reinforcement in y direction is required – and the crack angle, α_k, can be obtained from Eq. (3) imposing $N_{yak} = 0$. Now, the angle α_k can be obtained from Eq. (7):

$$\alpha_k = \arctan\left(\frac{-N_{yk}}{|N_{xyk}|}\right) \tag{7}$$

c) If $N_{xk} < -|N_{xyk}|$ and $N_{yk} < -|N_{xyk}|$, both reinforcements in the *x* and *y* directions are compressed. Therefore, $N_{xak} = N_{yak} = 0$ – no reinforcement in either *x* or *y* direction is required – and the maximum compression in concrete can be calculated from the Mohr's circle representation of the tensor of forces *N* in layer *k* (**Fig. 4**). Being:

$$N_{ck} = \frac{1}{2}\left(N_{xk} + N_{yk}\right) - \frac{1}{2}\sqrt{\left(N_{xk} - N_{yk}\right)^2 + 4N_{xyk}} \tag{8}$$

4. Concrete compression block

According to Eq. (1), the membrane forces acting on both top and bottom layers and, consequently, the forces in the concrete strut and in the reinforcement would be completely determined if the geometry of the sandwich shell element were defined, that is, if the values c_t and c_b are known.

Assuming that the middle surface of one of the layers corresponds to the centroid of the tension reinforcement required for the predominant bending, then, once this net is placed, the thickness of the corresponding layer is known. So, only the thickness of the opposite layer needs to be estimated.

As previously mentioned , the Brondum-Nielsen method [7] considers that the principal compressive force N_{ck} in the concrete is made resistant by a uniformly distributed stress in a depth equal to the thickness of the layer, c_k (Eq. (9) and **Fig. 5** for the case of the top layer, $k = t$). In Eq. (9) f_c is the compressive strength of the concrete.

$$c_k = \frac{N_{ck}}{f_c} \tag{9}$$

The former assumption resembles the Whitney's stress block used in the ultimate design of beams.

Imagine now that we are dealing with a beam whose cross section is A – A in **Fig. 5**; and this section is subjected to a bending moment M that comprises the upper part of the cross-section and to a tensile axial force N applied at the centroid of the section (**Fig. 6**). If moments are taken at the level of the tension reinforcement, the resultant moment M_a is:

$$M_a = M - N\, e_j \tag{10}$$

e_j being the distance between the centroids of the section and the tension reinforcement in layer j.

This moment M_a has to be balanced by the compression in the concrete in a depth equal to c_k. Therefore:

$$M_a = c_k f_c \left(d_j - \frac{c_k}{2} \right) \tag{11}$$

where d_j is the distance between the upper fibre in the cross-section (i.e. the most compressed one) and the level of the tension reinforcement placed in layer j opposite to k (**Fig. 6**). As indicated above, if the depth of the compression block is to be computed in the top layer, then $k = t$ and $j = b$, and vice versa.

The value of the depth of the compression block, c_k, is an unknown. Brondum-Nielsen adopts as a first estimation of c_k the one obtained from Eq. (11) M_a being the one obtained from Eq. (10) where M and N are the predominant bending moment and its corresponding axial force per unit of length, respectively, acting on the slab considered. Although a better approach to trigger the procedure may be obtained by using $M+|M_{xy}|$ instead of M –as used in the RC design of elements to bending plus torsion-, the authors have adopted Brondum-Nielsen's original approach in what follows, see Figure 7.

5. The application of the approach

According to Eq. (1), the geometry of the sandwich element – c_t and c_b – has to be known to compute the values of the membrane forces N_{xk}, N_{yk} and N_{xyk} . At the same time, this geometry depends on those membrane forces – Eq. (9) –. Thus, the problem has to be tackled in an iterative manner.

In all the above stated, it had been assumed that the reinforcement under tension due to the predominant bending is placed in the middle of the layer whereas a first estimation of the thickness of the opposite layer is obtained from Eq. (11). It is important to point out that the reinforcement placement is usually governed by the requirements of concrete cover.

Once the positions of the reinforcement in both layers, and as a result its thicknesses, are known, the external actions (N_x, N_y, N_{xy}, M_x, M_y and M_{xy}) can be resolved into membrane forces in the outer layers of the sandwich and the procedure proposed by Brondun-Nielsen [7] can be applied.

Fig. 7 shows a flow chart that explains in detail the entire process proposed by Brondun-Nielsen [7]. If predominant moment M compresses top fiber, then $k = t$ and $j = b$. On the other hand, if the bottom layer is compressed by M, then $k = b$ and $j = t$.

After the whole process has been completed, once the geometry of both layers is known and forces in the reinforcements of both outer layers have been obtained from Eqs. (2) and (3), it is necessary to resolve the forces at the centroids of the actual levels of the reinforcements if they have not already been computed at those levels.

6. Plane strain distribution for ultimate state of RC slabs in bending

Once the tension forces in both x and y reinforcement – N_{xat}, N_{yat}, N_{xab}, N_{xab} – have been calculated from Eqs. (2) and (3), it is necessary to compute the required areas of steel to withstand these tension forces in both directions – x and y – and in both layers – top and bottom –.

In the example given in Brondum-Nielsen's work [7] these areas are computed by dividing the obtained tension forces – N_{xa} and N_{ya} – by the prescribed steel design strength, taken as the steel yield stress, f_y. However, this procedure can be reconsidered because the actual state of steel stress should depend on the compression block depth, as it occurs in the ultimate design of beams.

Back to the shell element case, assuming that Kirchhoff's hypothesis of plane sections is satisfied, it is evident from comparison with the beam case that the tensile stress in the reinforcement cannot always be considered equal to f_y without paying attention to the value of c_k.

The beam section shown in **Fig. 6** is now subjected to the bending moment M and the axial force N, as presented in **Fig. 8**. Satisfying the plane sections hypothesis, if the applied actions cause a top fibre strain equal to concrete ultimate compression strain, ε_{cu}, and a strain at level of tensile reinforcement equal to steel yield strain, ε_y, then the section is said be in *balance conditions*, [21][22]. At this point, the compression block depth is $c_{k\text{lim}}$ and the distance from the uppermost fibre of the cross section to the neutral fibre is $\chi_{k\text{lim}}$. Both values are related by a coefficient λ taken as 0,8 according to EC2 [4] for $f_c \leq 50$ MPa. In the case of ultimate limit state of bending if the neutral fibre depth becomes greater than $\chi_{k\text{lim}}$ the strain at reinforcement level is lower than ε_y and, consequently, the steel stress is lower than f_y.

If the cross section given in **Fig. 8** corresponded to a RC shell element and it were positioned parallel to the direction of the principal compressive stress in the concrete (section A-A in **Fig. 5**), the compression block in one layer would lead to the yielding of the reinforcement in the opposite layer just under some circumstances as outlined below.

In the beam represented in **Fig. 8**, the direction of the reinforcement coincides with the direction of the compressive force in concrete. In this case, the depth of the compression block, $c_{k\text{lim}}$, corresponding to the balance point can be obtained from the expression:

$$c_{k\lim} = \lambda \cdot d_j \frac{\varepsilon_{cu}}{\varepsilon_y + \varepsilon_{cu}} \tag{12}$$

In the case of RC slabs, the orientation of the principal compressive force in the concrete in the outer layer *k*, α_k, does not generally coincide with the orientation of the reinforcement (*x* and *y* directions, respectively) in the opposite outer layer *j*, as presented in **Fig. 9**(a).

The hypotheses of the plane strain distribution for ultimate design of RC slabs in bending and torsion are:

1. Ultimate strength of RC slabs in bending and torsion with or without axial force behaves in accordance with an ultimate plane strain distribution.

2. The orientation of the ultimate plane strain distribution in the plane of the slab is defined by the principal direction of compression in concrete.

Since both hypotheses are to be used in a design process, the Upper Bound Theorem of plasticity guaranties that the forces obtained using these hypotheses are an upper value of the true collapse forces.

Stress-strain models of concrete and steel in ultimate strength design have to comply with those approved by Standards such as Eurocode 2 or ACI-318.

In line with both hypotheses, if a sandwich model is used, such as Brondum-Nielsen's [7] or Marti's [9], the principal compressive direction in one layer coincides with the principal tensile strain direction in the opposite one, as shown in **Fig. 9**(a) and 9(b). According to the second hypothesis, the principal direction is given by the principal compressive direction in the compressed layer (*k*). Therefore yielding of the steel placed in layer *j* and in each direction *x* or *y* of reinforcement corresponds to a yielding strain in the direction of the crack of the opposite layer α_k given by (**Fig. 9**(b)):

$$\varepsilon_{j-x\lim-\alpha k} = \frac{\varepsilon_y}{\cos\alpha_k}$$
$$\varepsilon_{j-y\lim-\alpha k} = \frac{\varepsilon_y}{\sin\alpha_k} \quad (13)$$

The maximum value of the thickness of layer *k* for which the yielding of the steel placed in the opposite layer *j* occurs, can be obtained from:

$$c_{ki\lim} = \lambda \cdot d_{ji} \cdot \frac{\varepsilon_{cu}}{\varepsilon_{j-i\lim-\alpha k} + \varepsilon_{cu}} \quad (14)$$

d_{ji} being the position of the reinforcement in *i* direction (*i*= *x or y*) placed in the *j* layer opposite the compressed layer *k* with respect to the furthest fibre of the cross section, as indicated in **Fig. 10**.

Once $c_{ki\lim}$ is known (i.e. $c_{kx\lim}$ and $c_{ky\lim}$), the designer has to compare the obtained value of c_k from the Brondum-Nielsen's approach with $c_{kx\lim}$ and $c_{ky\lim}$. If c_k is lower than the minimum $c_{ki\lim}$ then the stress in the tension reinforcement in *i* direction in the opposite layer *j* can be considered f_y. On the contrary, the geometry in the slab has to be altered in order to achieve the yielding of the reinforcement or if the stress of the reinforcement is smaller than f_y and has to be calculated.

7. Example 1

The example presented in the work of Brondum-Nielsen [7] is explained here again in order to check if the compression blocks in both outer layers are deep enough to guarantee that the tensile stress in the reinforcement is the yield stress, f_y. **Fig. 11** shows a section of the slab studied in [7], the actions acting on it and the material properties.

The example helps to clarify why the new hypotheses are needed. Figure 12 shows the 1×1 m slab of the example with the external forces and moments depicted. The signs are indicated by the directions of the arrows so the companion numbers only indicate the absolute value of the

forces and moments. If the axial forces N_x and N_y were of little importance, clearly the moment M_x (*-83 kN·m*) would command the behaviour of the slab. In this case we can deduce that in the top layer the steel in the x-direction can be considered at f_y while the steel in the y-direction will barely be at f_y.

The problem is solved following the flow chart given in **Fig. 7**. According to it, M_x is the predominant bending moment and it compresses the bottom fiber so $k = b$ and $j = t$. M_a obtained from Eq. (10) is:

$$M_a = 83000 - 67\left(\frac{-120000}{1000}\right) = 91040 \ \ N{\cdot}mm/mm$$

The first estimation of the thickness of the compressed layer, c_{b0}, is obtained from Eq. (11) with $d_j = d_t = 192$ mm (distance between the lowermost fibre of the cross section and the centroid of *x* reinforcement in the top layer), that is: $c_{b0} = 87,82$ mm.

For this first estimation of c_b, c_{b0}, the membrane forces in the bottom layer are obtained from Eq.(1):

$$a = 192 - \frac{87.82}{2} = 148.09\,mm$$
$$a_b = \frac{250 - 87.82}{2} = 81.09\,mm$$
$$N_{xb} = -120\frac{148.09 - 81.09}{148.09} + \frac{-83000}{148.09} = -614.76 \ N/mm$$
$$N_{yb} = 300\frac{148.09 - 81.09}{148.09} + \frac{12000}{148.09} = 216.76 \ N/mm$$
$$N_{xyb} = 170\frac{148.09 - 81.09}{148.09} + \frac{800}{148.09} = 82.31 \ N/mm$$

Since $N_{xb} < -\left|N_{xyb}\right|$ and $N_{yb} \geq -\left|N_{xyb}\right|$ no reinforcement is needed in *x* direction in the bottom layer.

The crack angle in this layer is obtained from Eq. (6):

$$\alpha_b = \arctan\left(\frac{82.31}{614.76}\right) = 7.63^{\circ}$$

The principal compression force on the concrete in the bottom layer is:

$$N_{cb} = 82.31\left[\tan(7.63^{\circ}) + \cot(7.63^{\circ})\right] = 625.78\ N/mm$$

Because $c_b = N_{cb}/f_c = 89.40\ mm$ is deeper than the first estimation – c_{b0} – , a value of c_b equal to 90 mm is adopted and the former values recalculated.

$$N_{xb} = -619.37\ N/mm$$
$$N_{yb} = 218.38\ N/mm$$
$$N_{xyb} = 82.93\ N/mm$$

In the bottom layer only reinforcement in y direction is required; the tension force on it is obtained from Eq. (3) as:

$$N_{yab} = 229.47\ N/mm$$

Assuming that the middle surface of the top layer coincides with the centroid of *x* reinforcement, the depth of this layer can be obtained:

$$c_t = 2\left(250 - 192\right) = 116\ \text{mm}$$

The values of the membrane forces acting upon it can be computed from Eq. (1):

$$N_{xt} = 499.32\ N/mm$$
$$N_{yt} = 81.63\ N/mm$$
$$N_{xyt} = 87.07\ N/mm$$

Since $N_{xt} \geq -\left|N_{xyt}\right|$ and $N_{yt} \geq -\left|N_{xyt}\right|$, then both *x* and *y* reinforcements are required in the top layer. The crack angle at this layer is 45º and the values of the tensile forces in *x* and *y* directions and the principal compression force in the concrete for the top layer are obtained from Eqs. (2) to (4) as:

$$N_{xat} = 586.39\ N/mm$$
$$N_{yat} = 168.71\ N/mm$$
$$N_{ct} = 174.16\ N/mm$$

It is verified that the corresponding principal compressive stress in the concrete is lower than f_c:

$$\frac{N_{ct}}{c_t} = \frac{174.16}{116} = 1.50\,N/mm^2 < 7N/mm^2$$

The next step is to relocate the tension forces of the reinforcement in both top and bottom layers. The resultant in *x* direction does not need to be computed since *x* reinforcement is not required in the bottom layer and the middle surface of the top layer coincides with the centroid of *x* reinforcement in this layer. Therefore, it is only necessary to calculate the resultant of tension forces in the *y* direction of reinforcement.

$$\sum N_{ya} = 398.18\ N/mm$$

If $z = 0$ is placed on the middle surface of the shell element (**Fig. 11**), the *z* coordinate of the point of application of $\sum N_{ya}$ is:

$$z_{ya} = \frac{N_{yat}z_{yat} + N_{yab}z_{yab}}{\sum N_{ya}} = \frac{168.71 \cdot 67 + 229.47(-80)}{398.18} = -17.72\ mm$$

The actual positions of *y* reinforcement in top and bottom layer are $z^*_{yat} = 53$ mm and $z^*_{yab} = -23$ mm, the corresponding tension forces at those levels, N^*_{yat} and N^*_{yab}, can be obtained from:

$$N^*_{yat} = \sum N_{ya}\frac{z_{ya} - z^*_{yab}}{z^*_{yat} - z^*_{yab}} = 398.18\frac{-17.72 + 23}{53 + 23} = 27.68\ N/mm$$
$$N^*_{yab} = \sum N_{ya}\frac{z^*_{yat} - z_{ya}}{z^*_{yat} - z^*_{yab}} = 398.18\frac{53 + 17.72}{53 + 23} = 370.50\ N/mm$$

Once the tensile forces in reinforcement have been determined, the necessary area of steel is obtained dividing by f_y:

$$A_{tx} = 2.17\, mm^2/mm$$
$$A_{ty} = 0.10\, mm^2/mm$$
$$A_{by} = 1.37\, mm^2/mm$$

The Brondum-Nielsen procedure ends here. According to the hypothesis discussed in this paper, it has to be verified that the steel has yielded, in the case that it has not, a different stress value must be considered.

The proposed procedure

In order to verify that reinforcement has yielded, the proposed methodology is applied. For the bottom layer, the angle of inclination of the cracks –i.e. the orientation of the principal compressive stress in concrete– is α_b= 7.63º. In the top layer both *x* and *y* reinforcements are required, their yielding strains and their corresponding maximum thickness in the opposite layer are –equations 13 and 14 respectively-:

- For *x* reinforcement:

$$\varepsilon_{t-x\,\lim-\alpha b} = \frac{\varepsilon_y}{\cos 7.63^o} = \frac{0.00135}{\cos 7.63^o} = 0.00136$$
$$c_{bx\,\lim} = \lambda \cdot d_{tx} \frac{\varepsilon_{cu}}{\varepsilon_{t-x\,\lim-\alpha b} + \varepsilon_{cu}} = 0.8 \cdot 192 \frac{0.0035}{0.00136 + 0.0035} = 110.62\ mm$$

- For *y* reinforcement:

$$\varepsilon_{t-y\,\lim-\alpha b} = \frac{\varepsilon_y}{\sin 7.63^o} = 0.010$$
$$c_{by\,\lim} = \lambda \cdot d_{ty} \frac{\varepsilon_{cu}}{\varepsilon_{t-y\,\lim-\alpha b} + \varepsilon_{cu}} = 0.8 \cdot 178 \frac{0.0035}{0.010 + 0.0035} = 36.45\ mm$$

From comparison of the thickness of the bottom layer (c_b= 90 mm) with $c_{bx\lim}$ and $c_{by\lim}$ it is clear that *x* reinforcement in the top layer is yielded but not, however, the *y* reinforcement. It was deduced in light of Figure 12 and commented at the beginning of the example. The area of steel in *x* direction per unit of length can be obtained as:

$$A_{tx} = \frac{N_{xat}}{f_y} = \frac{586.39\,\text{N/mm}}{270\,\text{N/mm}^2} = 2.17\ \text{mm}^2/\text{mm}$$

According to the hypotheses considered in the paper, for c_b= 90 mm steel in *y* direction is in the elastic domain and its strain and stress are:

$$\varepsilon_{t-y} = \frac{d_{ty} - c_b/0.8}{c_b/0.8}\varepsilon_{cu}\sin\alpha_b = \frac{178 - 90/0.8}{90/0.8}0.0035\sin 7.63^\text{o} = 0.00027$$

$$\sigma_{t-y} = E_s \cdot \varepsilon_{t-y} = 53.98\ MPa$$

The required area of steel in *y* direction per unit of length is:

$$A_{ty} = \frac{N^*_{yat}}{\sigma_{t-y}} = \frac{27.68\,\text{N/mm}}{53.98\,\text{N/mm}^2} = 0.513\,\text{mm}^2/\text{mm}$$

In the case of steel in the bottom layer, the orientation of the strain plane is defined by the principal direction of compression in the top layer. For the top layer, α_t= 45º. In the bottom layer only *y* reinforcement is required so the strain in the principal tensile direction is given by:

$$\varepsilon_{b-y\lim-\alpha t} = \frac{\varepsilon_y}{\sin 45^\text{o}} = 0.0019$$

If the compression block depth obtained as $c^*_t = N_{ct}/f_c = 24.9\ mm$ is considered for the top layer, as represented in Fig. 13(b), the maximum value of the compression block depth for which the *y* reinforcement yields can be obtained from Eq. (14) would be:

$$c_{ty\,\lim} = \lambda \cdot d_{by} \frac{\varepsilon_{cu}}{\varepsilon_{b-y\,\lim-\alpha t} + \varepsilon_{cu}} = 0.8 \cdot 148 \frac{0.0035}{0.0019 + 0.0035} = 76.61\ mm$$

This approach is safe because membrane forces were supposed to act with a smaller lever arm with respect to the lower reinforcement as Fig. 13 shows, so the calculated membrane forces are greater than the actual ones.

Because $c^*_t = 24.9\ mm < c_{tylim} = 76.61\ mm$ the y reinforcement in the bottom layer yields and therefore, the corresponding area of steel can be obtained dividing the tensile force between f_y:

$$A_{by} = \frac{N^*_{yab}}{f_y} = \frac{370.50\,\text{N/mm}}{270\,\text{N/mm}^2} = 1.37\ \text{mm}^2/\text{mm}$$

An alternative, in order to force the yielding of the y reinforcement in the top layer, is to change the geometry of the layers. This modification of the geometry may involve increasing the thickness of the slab and/or relocating the reinforcement.

8. Example 2

The previous slab is modified as indicated in Fig. 14, in this case all the reinforcement yield, i.e. the required cross-sectional areas of reinforcement per unit of length can be obtained dividing the tensile forces between f_y. These required areas of reinforcement are summarized in Fig. 14.

A detailed study of the stress of the top reinforcement in y-direction (σ_{ty}) relative to the thickness of the slab and the position of the steel for the same external loading as those considered in the previous example are shown in Fig. 15. The example of Fig. 14 can be observed in Fig. 15, if the thickness of the slab is reduced or if the lever arm of the y reinforcement of the top layer is reduced then the steel will not yield. The line of thickness equal to 250 mm and with the geometry of the slab considered in example 1 is also shown, this line contains the case analyzed in the example 1.

9. Example 3

Figure 16 shows the values corresponding to strength design of one slab as function of the flexural moment, M_y. The geometry of the slab is defined by, thickness=325 mm, z_{yat}=80 mm, and is represented in Figure 15 with the label Example 3. It is made with concrete $f_c = 7\ MPa$ and steel $f_y = 270\ MPa$.

Beside M_y, which is considered as variable, the rest of forces and moments acting on the slab are kept constants:

N_x=-120000 N/m, N_y=300000 N/m, N_{xy}=170000 N/m, M_x=-83000 Nm/m and M_{xy}=800 Nm/m.

As is observed in Fig. 15 and in Fig.16 the y-reinforcement in the top layer is not yielded for the value of M_y considered in the previous example (M_y=12000 Nm/m).

Figure 16 (a) represents stresses in the reinforcement in the y-direction for both top and bottom layers, (b) the tension forces in the y-reinforcement for both top and bottom layers, (c) the angle of the crack with respect to the x-direction for both top and bottom layers and (d) the depth of the bottom layer.

Figure 17 represents the areas of steel as M_y increases, as can be observed as M_y increases bottom steel in y-direction increases and the upper steel in y-direction decreases.

10. Conclusions

The Sandwich element analogy is the most relevant hypothesis used in the bending ultimate limit design of shells and slabs. Once the geometry of the outer layers and the membrane forces acting on them are determined, the tension forces in the reinforcement and the principal compressive force in the concrete can easily be obtained from equilibrium conditions. Finally, Brondum-Nielsen's work [7] aims to compute the necessary amount of reinforcing steel per unit length dividing these tension forces by the steel yield stress, f_y.

In the present work, the Brondum-Nielsen approach has been summarized in detail and it has been shown that this procedure needs to be applied under some restrictions since reinforcement yielding cannot always be guaranteed. Taking as reference the determination of the balance point concept widely used in beams and columns, a procedure has been developed in order to determine the limits of application of Brondum-Nielsen's method. If these limits are exceeded, either the geometry of the slab or the reinforcement stresses and areas need to be modified.

Acknowledgements

The present work was financed by the Spanish Ministry of Education. The second author is a Spanish Government PhD fellow (FPU grant AP 2010-3707). This support is gratefully acknowledged.

References

[1] Schladitz F, Frenzel M, Ehlig D, Curbach M. Bending load capacity of reinforced concrete slabs strengthened with textile reinforced concrete. Engineering Structures 2012; 40: 317-10

[2] Smith ST, Hu S, Kim SJ, Seracino R. FRP-strengthened RC slabs anchored with FRP anchors. Engineering Structures 2011; 33(4): 1075-13

[3] Jia, X. Revisiting the failure mode of a RC hyperbolic cooling tower, considering changes of material and geometric properties. Engineering Structures 2013; 47: 148-7

[4] EC 2. Eurocode 2: Design of concrete structures_Part 1-1: General rules and rules for buildings EN 1992-1-1. Brussels: European Committee for Standarization, 2004.

[5] ACI Committee 318. Building code requirements for structural concrete (ACI 318-08). Farmington Hills (MI): American Concrete Institute; 2008

[6] FIB. Model Code 2010. Model Code 2010 - Final draft, Volume 1. Fib Bulletin No. 65. Lausanne: International Federation for Structural Concrete; 2012

[7] Broundum-Nielsen T. Optimum Design of Reinforced Concrete Shells and Slabs. Report No R44. Copenhagen: Structural Research Laboratory, University of Denmark; 1974

[8] Gupta AK. Combined membrane and flexural reinforcement in plates and shells. ASCE Journal of Structural Division 1986; 112(3): 550-7

[9] Marti P. Design of Concrete Slabs for Transerse Shear. ACI Structural Journal, V.87, No2, March-April 1990.

[10] Lourenço PB, Figuerias JA. Automatic design of reinforcement in concrete plates and shells. Engineering Computations 1993; 10(6): 519-23

[11] Lourenço PB, Figueiras JA. Solution for the design of reinforcement concrete plates and shells. Journal of Structural Engineering ASCE 1995; 121(5): 815-9

[12] Fall D, Lundgren K, Rempling R, Gylltof K. Reinforcing tailor-made concrete structures: alternatives and challenges. Engineering Structures 2012; 44: 372-7

[13] Min CS. Design and ultimate behaviour of RC plates and shells. Nuclear Engineering and Design 2004; 228: 207-17

[14] Min CS, Gupta AK. A study of inelastic behaviour of reinforced concrete shells using supercomputers. Technical Report. Raileigh (NC): North Carolina State University; 1992

[15] Min CS, Gupta AK. Vector algorithm for layered reinforced concrete shell element stiffness matrix. Structural Engineering and Mechanics 1995; 3(2): 172-12

[16] Min CS, Gupta AK. Inelastic vector finite element analysis of RC shells. Structural Engineering and Mechanics 1996; 4(2): 139-10

[17] Mahmoud BEH, Gupta AK. Inelastic large displacement behaviour and buckling of hyperbolic cooling tower shells. Technical Report. Raileigh (NC): North Carolina State University; 1993

[18] Tomás A, Martí P. Design of reinforcement for concrete co-planar shell structures using optimization techniques. Meccanica 2010; 45: 657-13

[19] Bertagnoli G, Giordano L, Mancini S. Design and optimization of skew reinforcement in concrete shells. Structural Concrete 2012; 13(4): 248-11

[20] https://wiki.csiberkeley.com/display/kb/Shell+reinforcement+design

[21] Hernández-Montes E, Gil-Martín LM, Pasadas M, Aschheim M. “Theorem of Optimal Section Reinforcement”. Structural and Multidisciplinary Optimization 2008; 36(5): 509-13

[22] Aschheim M, Hernández-Montes E, Gil-Martín LM. “Optimal Domains for Strength Design of Rectangular Sections for Axial Load and Moment according to Eurocode 2”. Engineering Structures 2007; 29(8): 1752-9

FIGURES

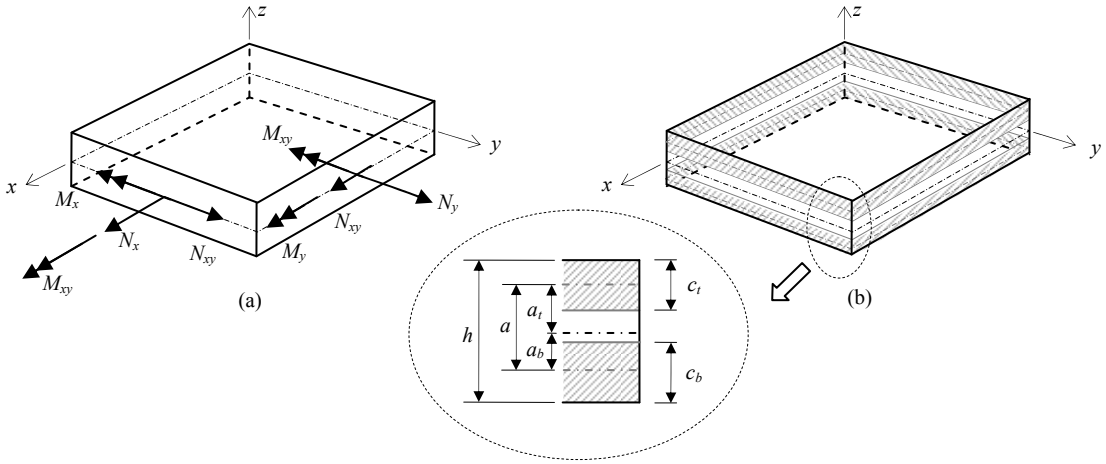

Fig. 1. (a) Applied actions to the shell element; (b) Sandwich layers geometry

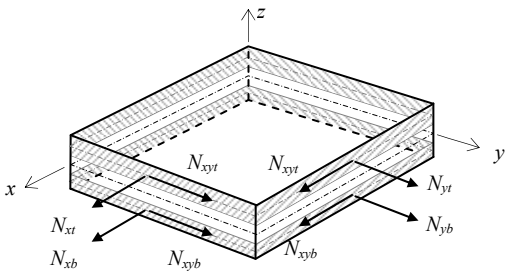

Fig. 2. Membrane forces decomposition of the state of actions applied to the shell element

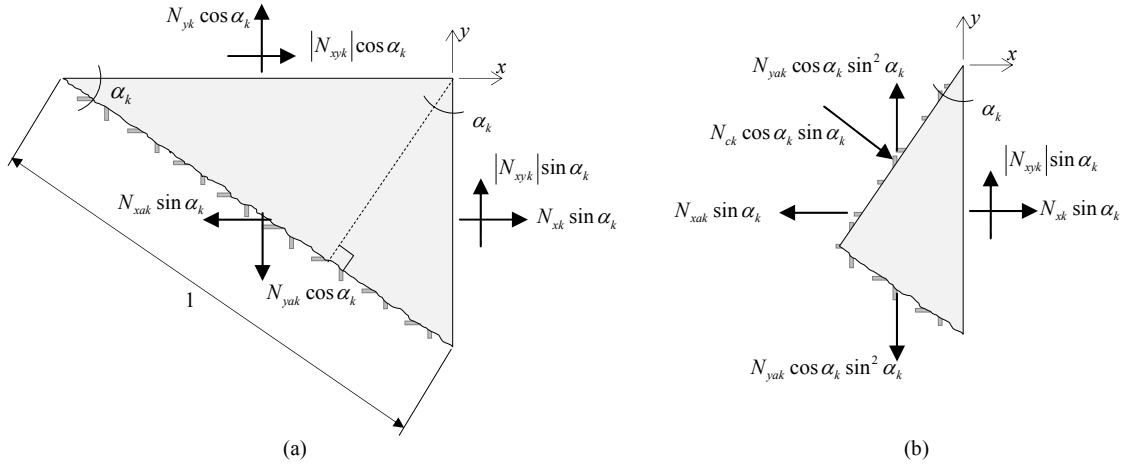

Fig. 3. Equilibrium of forces in a cracked membrane element: (a) Forces in the reinforcement to equilibrate normal and shear forces; (b) Principal compressive concrete force

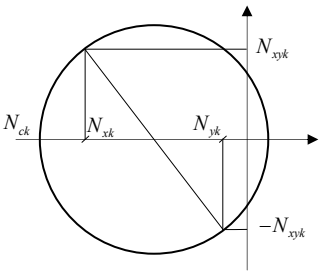

Fig. 4. Mohr's circle of forces for the case $N_{xk} < -|N_{xyk}|$ and $N_{yk} < -|N_{xyk}|$.

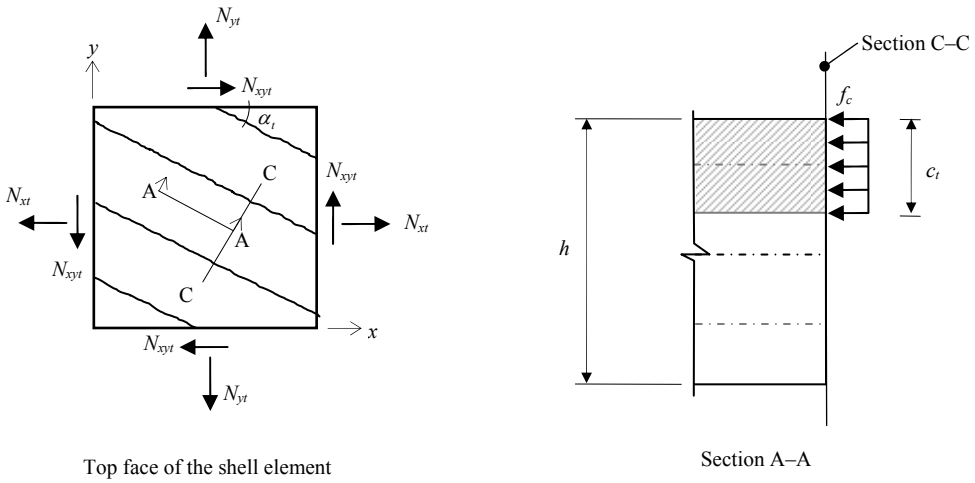

Fig. 5. Compressive stress in top layer

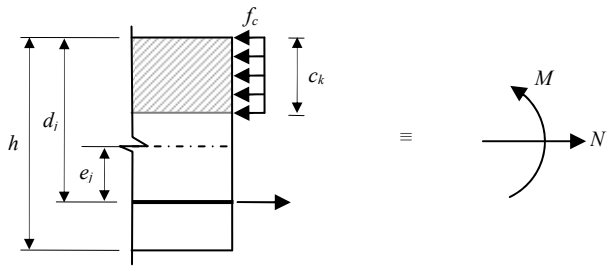

Fig. 6. Combined flexure and axial action in a beam

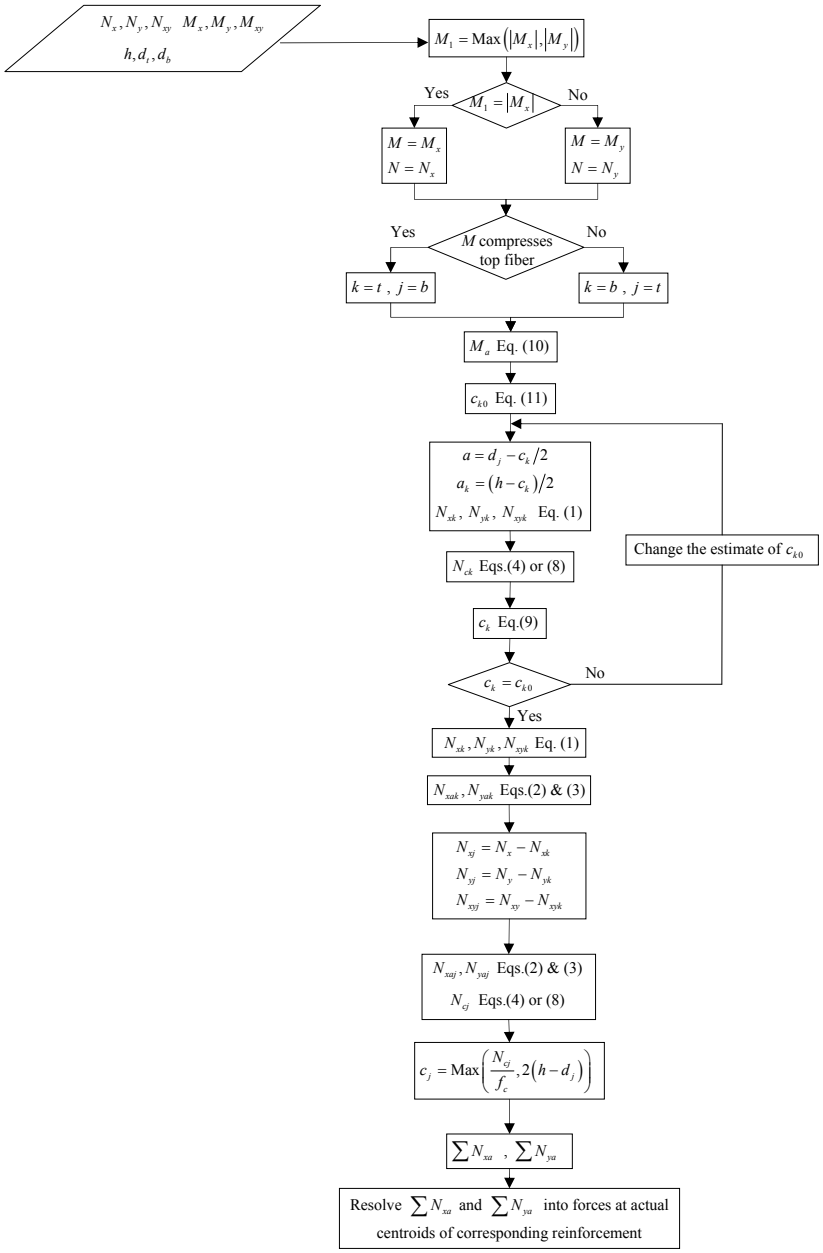

Fig. 7. Flow chart detailing the Brondum-Nielsen approach

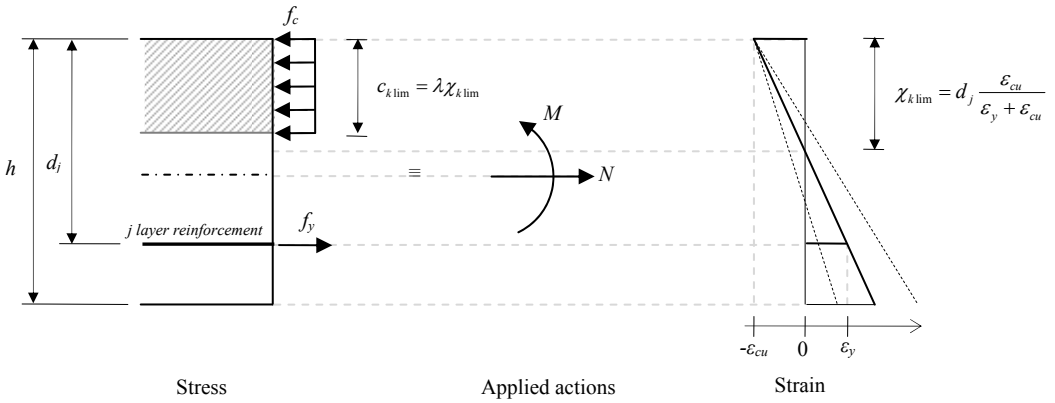

Fig. 8. Combined flexure and axial action in a beam: balance point determination

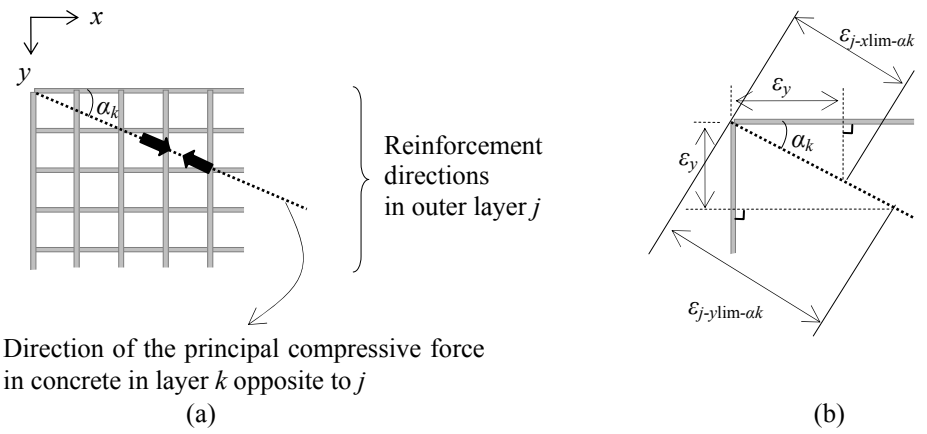

Fig. 9. Strain decomposition

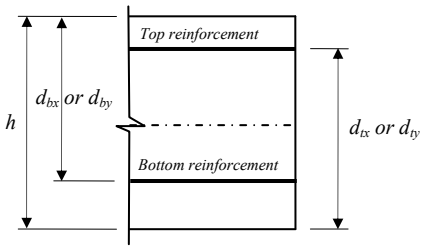

Fig. 10. Nomenclature

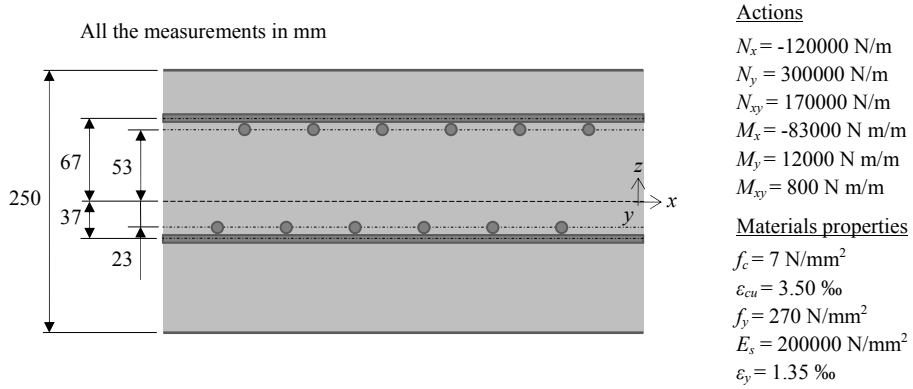

Fig. 11. Section of the slab studied by Brondum-Nielsen and external loads. Adapted from [7]

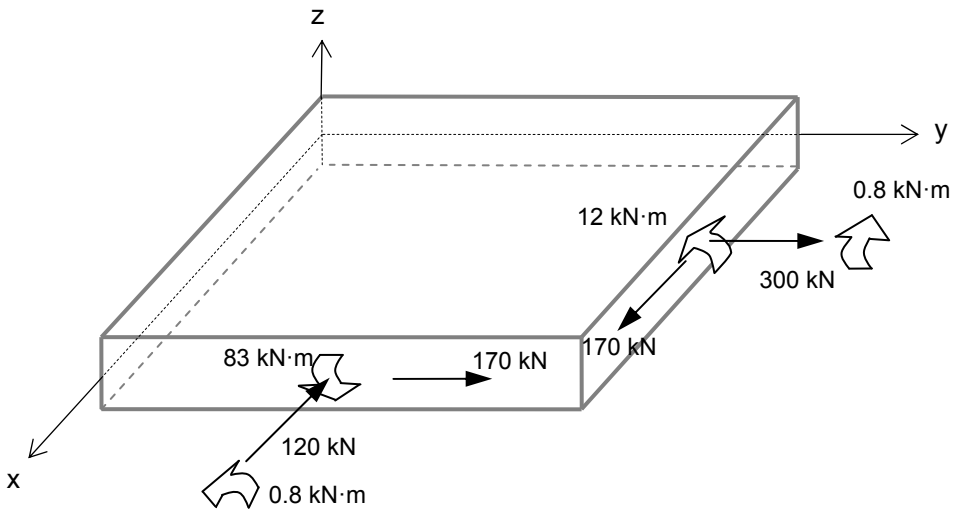

Figure 12. Orientation of the external actions on the slab.

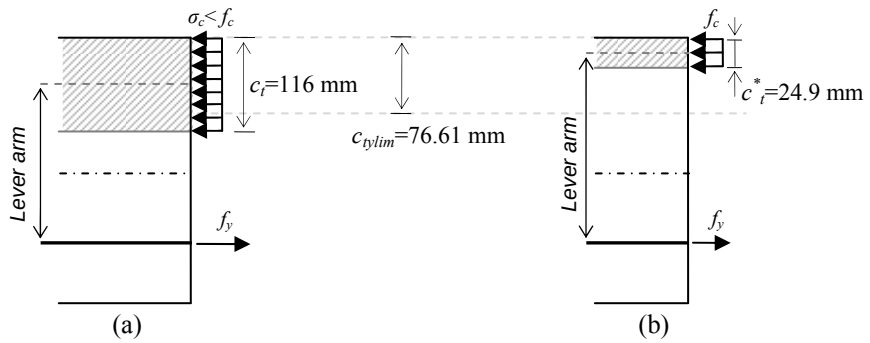

Figure 13. Compression block for the upper layer. Comparison between the resulting depth (a) assuming that level of top reinforcement is the middle surface of the layer and (b) the resulting depth applying Eq. (9)

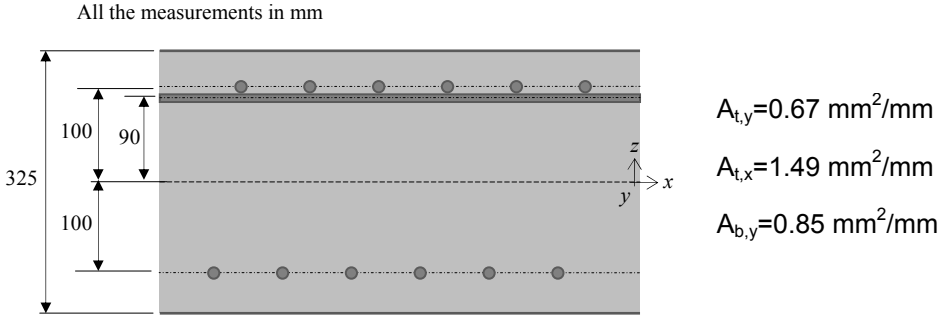

Figure 14. Modified slab of the example of Brondum-Nielsen and required areas of reinforcement per unit of length

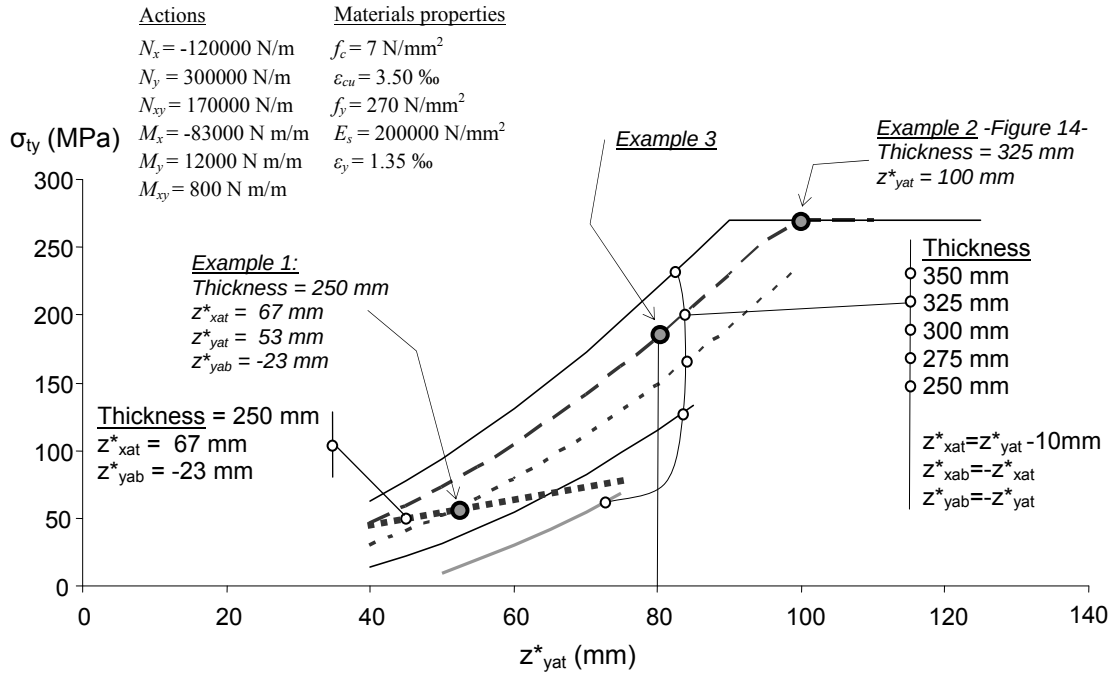

Figure 15: Stress in the reinforcement in the y-direction of the top layer of the slab as function of the location of the reinforcement for several thicknesses.

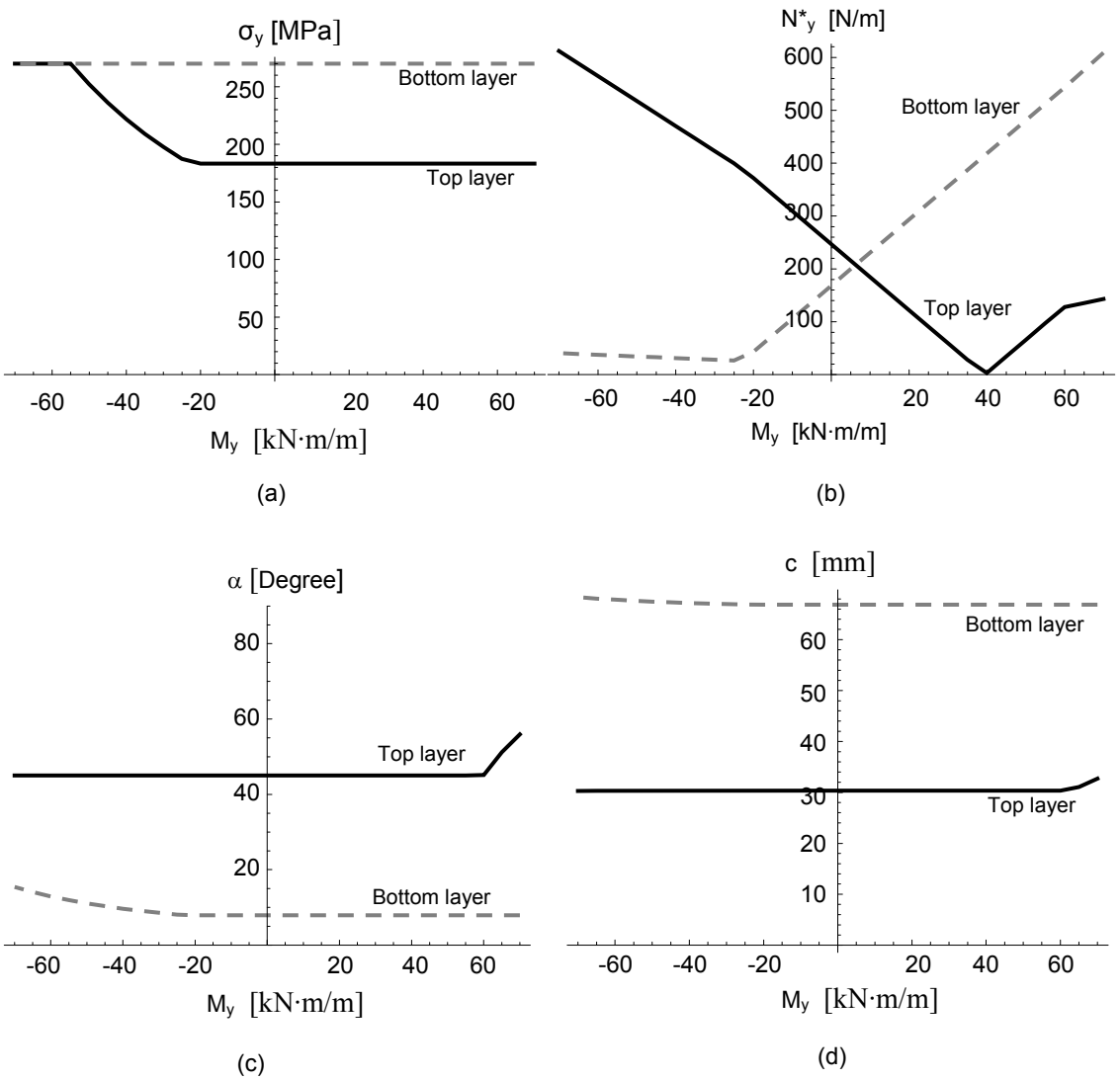

Figure 16. Example 3.

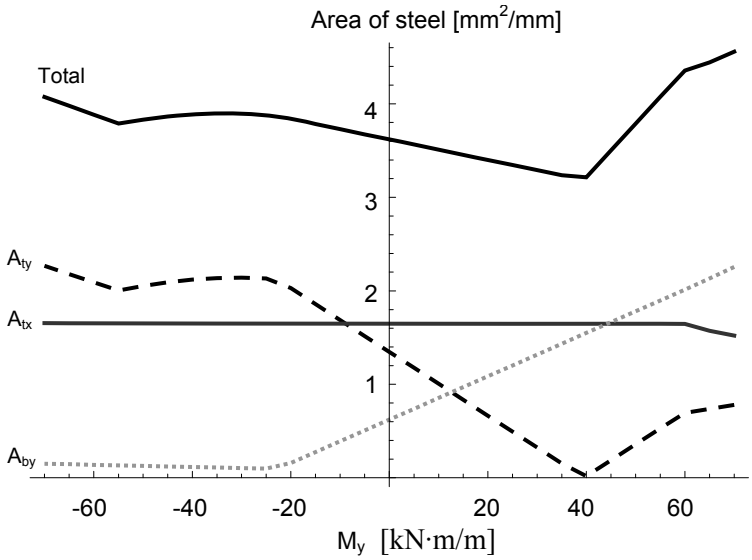

Figure 17. Steel areas

Journal of Constructional Steel Research 80 (2013) 213–223

Contents lists available at SciVerse ScienceDirect

Journal of Constructional Steel Research

Strength design optimization of structural steel members according to Eurocode 3

Juan Francisco Carbonell-Márquez, Luisa María Gil-Martín, Enrique Hernández-Montes *

University of Granada, Campus de Fuentenueva, 18072 Granada, Spain

ARTICLE INFO

Article history:
Received 27 February 2012
Accepted 25 July 2012
Available online xxxx

Keywords:
Steel structures
Structural optimization
Cross-section class
Local buckling
Eurocode 3

ABSTRACT

In order to design a steel member subjected to a bending moment and an axial load, there are an infinite number of possible solutions of I- or H-steel cross-sections, the doubly-symmetric solution being just one of them. This paper presents a procedure to obtain the optimal steel cross-section from the infinite number of possible solutions. The process is based on the Reinforcement Sizing Diagrams employed in reinforced concrete strength design. The procedure looks for any type of solution regarding compact or non-compact steel sections. All aspects related to local instabilities are taken into account, as well as some special considerations in order to address the global instabilities associated with the slenderness of the steel element.

1. Introduction

Typical sections for steel beam–column members are usually I- or H-rolled sections. However, in other fields of steel constructions such as civil bridges, the selected cross-sections may be welded, since the higher loadings to be supported by the structure demand larger dimensions than the usual tabulated rolled sections. Whether edification or civil construction, designers tend to proportion their structures using symmetric sections, these being just one of the multiple solutions. Nevertheless, the optimal solution may not coincide with the symmetric one and important savings in the amount of steel used could be achieved. In this respect, environmental concerns constitute an important factor because savings in steel consumption may be translated into significant reductions in greenhouse gas emissions.

The present work studies the optimal design of beam–column members subject to an external in-plane bending moment, M_y, and to an axial load, N, initially considered to be applied at the centroid of the web of the section (Fig. 1). Fig. 2 shows the employed nomenclature for the cross-section of the element and the sign criteria for the applied external loads. Bending moment, M_y, acting on the strong axis of the cross-section will be considered positive when compressing the top flange of the section. The applied axial load, N, will be considered positive in tension. For the sake of simplicity, the filets in rolled sections and throat thickness in welded sections have been ignored in the process. The different elements of the section are proportioned to provide sufficient strength and stiffness to resist the external actions and avoid premature buckling of the member. For non-compact sections, the plastic capacity will not be reached, so elastic capacity will be employed.

The problem studied in this work has already been solved by Gil-Martín et al. [1] for Class 1 sections. Optimization was completed by using the RSD design approaches [2,3]. This methodology, originally conceived for reinforced concrete, represents the required reinforcement area for supporting a determined external loading as a function of depth of neutral axis in the concrete section (Fig. 3). RSD is the representation in one graph of the infinite solutions in strength design of a reinforced concrete section when the infinity is of grade one, i.e. the number of unknowns are equal to the number of equations plus one. When applying RSD design approaches to optimization in steel sections, minor changes need to be made. Thereby, the graphics represent the cross-section area, A_t, as a function of the web height, d_w, and the optimal solution corresponds to the one with the lowest value for A_t (Fig. 4).

The present paper explains the well-developed process that was followed to obtain the optimal solution for any pair of (M_y, N,). This process makes it possible for the designer to choose the Class of the adopted cross-section; this is either compact or non-compact. Selecting the Class of the section is very important, for example, when designing a building for earthquake resistance according to Eurocode 8 (EC8) [5]. EC8 states that, for any given building subjected to an earthquake, the relationship between its resistance and capacity for dissipating energy is related to the section classification (see Table 6.3 in EC8). Generally speaking, the more ductility needed the more compactness is required for the cross-section.

In contrast to the previous case is a composite roadway or highway bridge. These kinds of bridges, also called "twin-girder bridges", are composed of two longitudinal steel girders connected to the concrete slab of the deck by shear connectors. Twin-girder bridges are

* Corresponding author. Tel.: +34 958249965; fax: +34 958249959.
E-mail addresses: jfcarbonell@ugr.es (J.F. Carbonell-Márquez), mlgil@ugr.es (L.M. Gil-Martín), emontes@ugr.es (E. Hernández-Montes).

0143-974X/$ – see front matter © 2012 Elsevier Ltd. All rights reserved.
http://dx.doi.org/10.1016/j.jcsr.2012.07.019

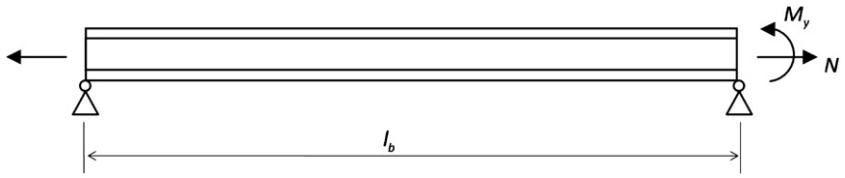

Fig. 1. Conditions of the problem to be analyzed.

the most economical solution when covering span lengths in the range of 30 and 100 m [6], with special suitability between 60 and 80 m [7]. Considering these span lengths, self-weight becomes an important action to be withstood. Under this load, and beyond the complexity involving a composite section, cross-sections under positive moment at mid-span regions of composite bridges are usually in Class 1 or 2, since compression is carried out mainly by the concrete deck. However, on internal supports, under negative moment, sections tend to be designed in Class 3 or 4 in order to avoid the excessive amount of steel that would be needed if those compressed sections were to be in Class 1 or 2 [8].

The typical section for these kinds of bridges is shown in Fig. 5. The most usual range for H/L, H being the height of the I-section and L the covered span, is between 1/25 and 1/20 for highway or roadway bridges and 1/15 for railway bridges [6,7,9]. For a highway bridge with a span of 60 m, H would be between 2.5 and 3.0 m. These large dimensions in cross sections do not allow the designer to choose them from the standard rolled sections and therefore welded cross sections are used. For these types of girders, the algorithm developed within this work lets the designer impose any constraint related to the dimensions of a particular element of the section, in this case, web height or anything related to the Class of the cross-section.

The algorithm used to optimize the sections has been implemented in a computer program and some examples are presented here. The results obtained will be analyzed in order to test the validity of the process.

2. The optimization procedure

As explained above, the optimization procedure to be presented in the current work is based on RSD methodology. This approach consists of the consideration of all the possible solutions for a design problem through a graphical representation that allows us to choose the optimal one. In reinforced concrete members, usually the reinforcement area is represented as a function of the neutral axis depth [2,3].

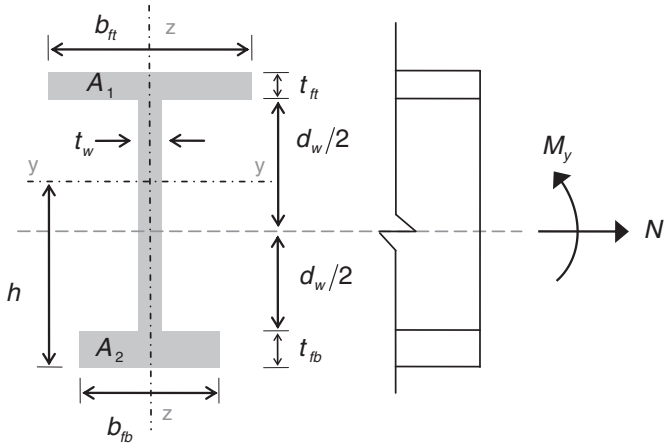

Fig. 2. Nomenclature and sign criteria.

In steel construction, as was observed with reinforced concrete, an infinite number of solutions exist for the design of a steel cross-section subjected to combined loads N and M. These solutions can be presented using graphics similar to those used in the reinforced concrete RSD representation. In this case, the area of structural steel has been represented as a function of the height of the web [1]. The main advantage of this procedure is that the engineer knows all the possible cross-sections that resist a given combination of axial load and moment (N, M) making possible the choice among all the possible solutions: minimum weight, availability of steel shapes, simplicity on the job site, Class of the cross-section and so on.

The process followed during the optimization procedure is shown in the flow chart in Fig. 6.

2.1. Section initial proportioning

The first step in the process is the selection of a fixed value for the web thickness, t_w, and a range of values for the height of the web, d_w. The range of d_w is obtained accounting for both shear strength and shear buckling requirements. The preliminary proportions of the flanges are provided by equilibrium of forces acting on the cross-section, applying the axial load at the centroid of the web. The equilibrium is established ignoring the web contribution and assuming that the forces carried by the top and bottom flanges act at the ends of the web and drive the flanges to the yield stress. Therefore, the sum of moments on either ends of the web results in Eq. (1):

$$\begin{aligned} A_1 \cdot f_y \cdot d_w + M_y - N \cdot \frac{d_w}{2} = 0 \\ A_2 \cdot f_y \cdot d_w + M_y + N \cdot \frac{d_w}{2} = 0. \end{aligned} \tag{1}$$

Once A_1 and A_2 are known for each value of d_w, the next step is to choose another range of values for the flange thicknesses, t_{ft} and t_{fb}. Therefore, for each value of t_{ft} and t_{fb} the values of the flange widths can be obtained from Eq. (2):

$$b_{ft} = \frac{A_1}{t_{ft}} \text{and} b_{fb} = \frac{A_2}{t_{fb}}. \tag{2}$$

In the following, without loss of generality, the same thickness of both flanges has been considered, being, $t_{ft} = t_{fb} = t_f$.

2.2. Section classification

As described in Eurocode 3 (EC3) [10], the role of cross-section classification is to identify the extent to which the resistance and rotation capacity of the cross-section is limited by its local buckling resistance. The classification of a determined cross-section will depend on the slenderness, i.e. the width to thickness ratio, of the parts subjected to compression.

According to EC3, there are four classes for steel sections: Class 1, which can form a plastic hinge with the rotation capacity required from plastic analysis without reduction of the resistance; Class 2, similar to Class 1 but with limited rotation capacity due to local buckling; Class 3, those sections in which local buckling appears before forming a plastic hinge and are assumed to work with an elastic distribution of stresses reaching the yield strength; and Class 4, in which local

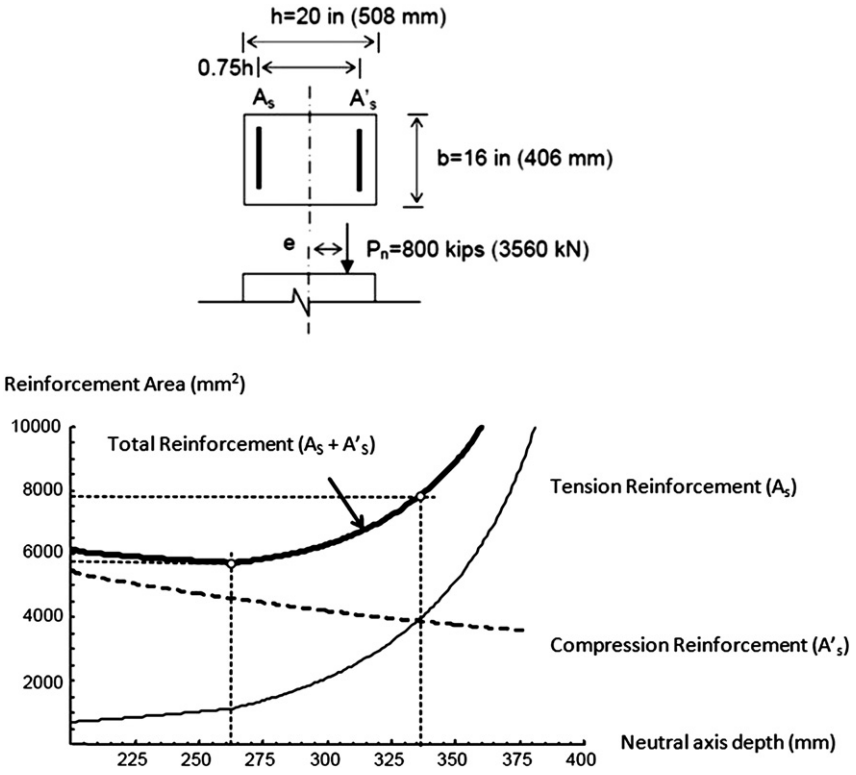

Fig. 3. Example of RSD in a reinforced concrete section.
From (Hernández-Montes and Gil-Martín [4]).

buckling is reached before elastic limit [11]. This classification may also be found in other codes as AISC Steel Construction Manual [12] with other terminology and slenderness limit values. Thereby, according to AISC, Class 1 and 2 sections are called compact sections; Class 3 sections are equivalent to non-compact sections; and Class 4 sections are similar to slender sections.

The limit values for the slenderness of each component of the section are given in Tables 5.2-1 and 5.2-2, presented in section 5 of Part 1-1 in EC3. According to these standard codes, the cross-section is classified according to the highest (least favorable) class of its compression parts.

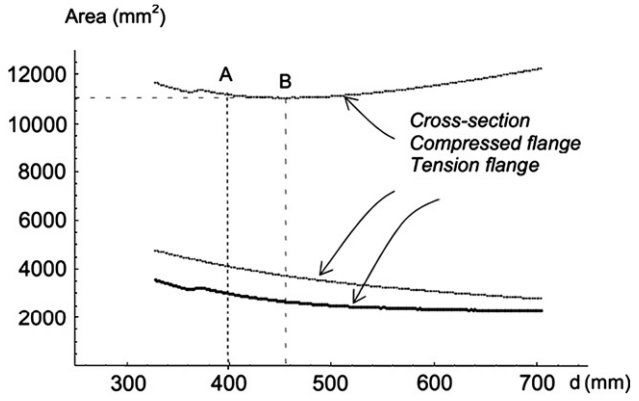

Fig. 4. Example of RSD in a steel section: optimization of IPE500 under $M_{y,Ed}=$ 288 kN m and $N_{Ed}=-483$ kN with $t_f=16$ mm and $t_w=100.2$ mm. Point A represents the optimal solution and point B corresponds to IPE500.
Taken from (Gil-Martín et al. [1]).

Widths of the elements of the cross-section in Class 4 have to be reduced in order to assign their effective dimensions according to Part 1-5 of EC3.

2.3. Global instabilities at member level

Once the class of the cross-section is determined, it is necessary to calculate the resistance of the beam–column member to lateral buckling and lateral-torsional buckling due to axial load and bending moment, respectively. Following the formulas given in EC3 [9], the design buckling resistance of a compression member should be taken as:

$$N_{b,Rd}=\frac{\chi\cdot A\cdot f_y}{\gamma_{M1}} \tag{3}$$

where $A=A_t$ for cross-sections in Class 1, 2, or 3, and $A=A_{teff}$ for cross-sections in Class 4 when subjected to uniform compression. The parameter χ is the reduction factor for the relevant buckling mode, computed as indicated in section 6.3.1. in Part 1-1 of EC3.

On the other hand, section 6.3.2 of EC3 [9] provides the formula to calculate the parameter χ_{LT}, i.e. the reduction factor for lateral-torsional buckling. According to this, the design buckling resistance moment of a laterally unrestrained beam should be taken as:

$$M_{b,Rd}=\frac{\chi_{LT}\cdot W_y\cdot f_y}{\gamma_{M1}}. \tag{4}$$

Here, W_y is the appropriate section modulus, taken as $W_{pl,y}$ for Class 1 or 2 cross-sections, $W_{el,y}$ for Class 3 cross-sections, and $W_{eff,y}$ for Class 4 cross-sections when only the moment about the relevant axis is applied.

When the buckling resistances of the member are calculated, the General Method for lateral and lateral torsional buckling of structural components is applied. This method, explained in section 6.3.4 of EC3

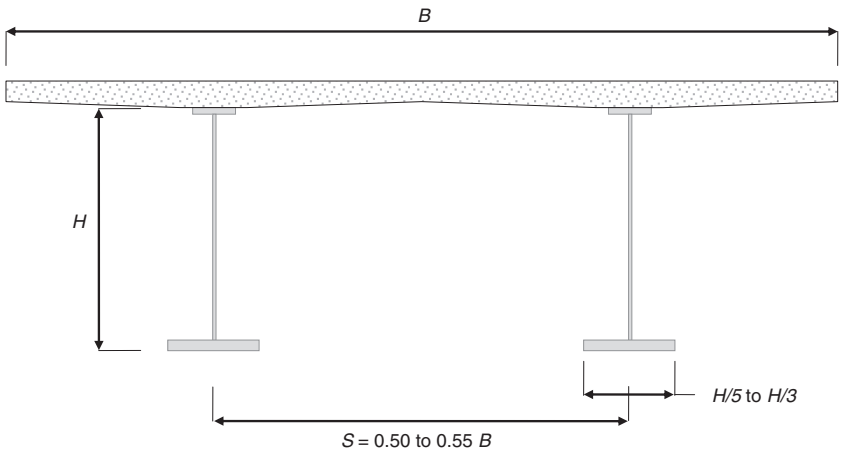

Fig. 5. Typical section for a twin-girder composite bridge.

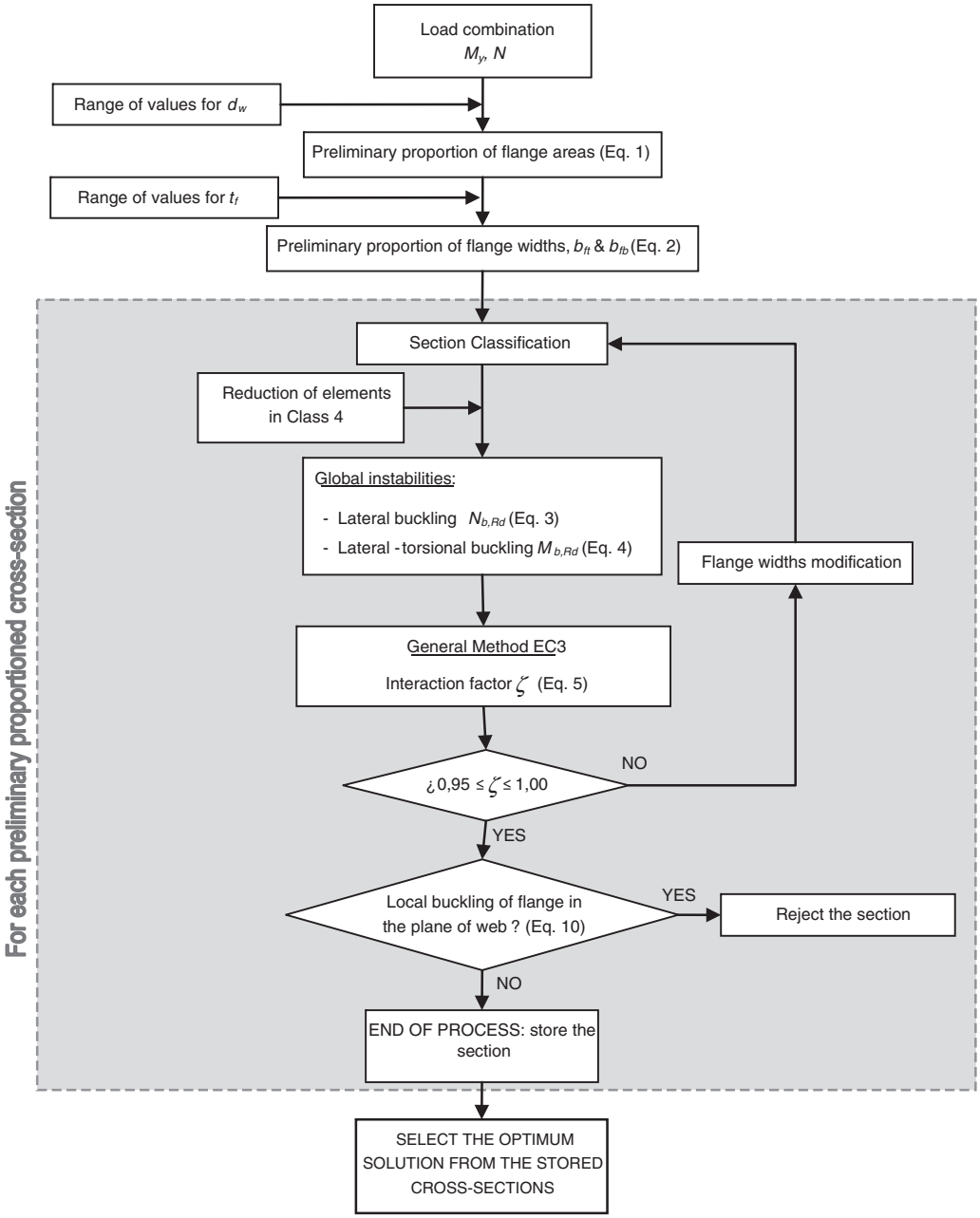

Fig. 6. Flow chart explaining the entire process.

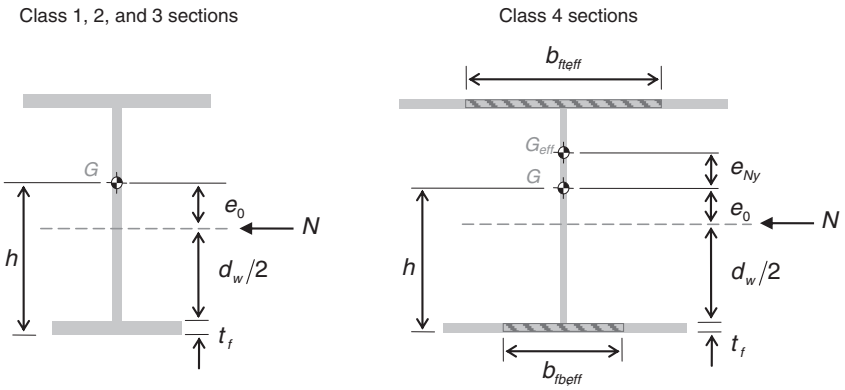

Fig. 7. Values for the eccentricities e_0 and e_{Ny}.

[9], allows the verification of the resistance to the former global instabilities of single members subjected to compression and mono-axial bending in the plane. The member must fulfill Eq. (5) in order to achieve stability.

$$\frac{N_{Ed}}{\chi \cdot N_{Rk}/\gamma_{M1}} + \frac{M_{y,Ed}}{\chi_{LT} \cdot M_{y,Rk}/\gamma_{M1}} \leq 1 \tag{5}$$

where N_{Rk} and $M_{y,Rk}$ are the critical cross-section characteristic resistance to normal force and moment resistance about the y–y axis. In this work, applied loads N_{Ed} and $M_{y,Ed}$ are:

$$M_{y,Ed} = M_y + \left(e_0 + e_{N_y}\right)N \tag{6}$$

$$N_{Ed} = N \tag{7}$$

e_{Ny} being the shift of the relevant centroidal axis of the cross-section due to the width reduction in Class 4 when the member is subjected to uniform compression and e_0 the distance between the mid-height of the web — where the axial load is supposedly initially applied at the gravity center of the gross-section (Fig. 7), calculated as:

$$e_0 = h - \left(d_w/2 + t_f\right). \tag{8}$$

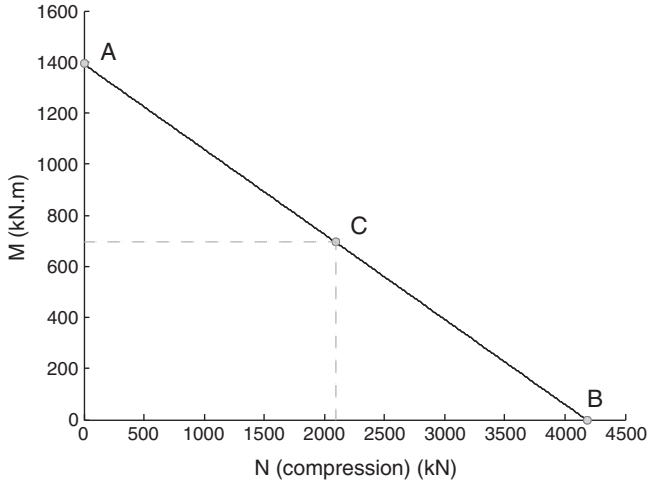

Fig. 8. Interaction equation corresponding to HEB600, for $f_y = 235$ N/mm^2, $l_b = 6$ m and $\psi = 0$.

In the above expression, h is the height of the gravity center of the cross-section.

In this work, the value for the sum presented in Eq. (5) has been called "interaction factor" and is represented by $\zeta = {}^{N_{Ed}}/_{\chi} \cdot N_{Rk}/\gamma_{M1} + {}^{M_{y,Ed}}/_{\chi_{LT}} \cdot M_{y,Rk}/\gamma_{M1}$.

2.4. Design adjustments

It is clear from the flow chart presented in Fig. 6 that the proposed procedure is iterative. The dimensions of the cross-section are preliminary proportioned and classified. Afterwards, the General Method is applied to evaluate the stability of the member; because in most of the cases the preliminary cross-section will not be able to withstand the applied loads without buckling, dimensions need to be modified. In this work, for each pair of values $d_w - t_f$, the widths of the flanges, b_{ft} and b_{fb}, are adjusted until the member does not buckle, i.e. $\zeta \leq 1$. However, in order to gain optimal results, a lower limit has been imposed to ζ, so that the adjustments will be completed when $0.95 \leq \zeta \leq 1$. The adopted procedure for providing a cross-section of minimum cross-sectional area, fulfilling all the stability considerations, is similar to the one followed by [1], and is explained below:

1. If $\zeta < 0.95$ the section provides excess capacity. In order to reduce the cross-sectional area, the widths of both flanges are reduced until:

$$0.95 \leq \zeta \leq 1. \tag{9}$$

2. If $\zeta > 1$ the section behavior is governed by instability. To provide sufficient strength, the flange areas must be increased. The approach to increase one flange or another depends on axial force and bending moment:

   a. If $M_y = 0$ or $N = 0$, the section is symmetric from the initial proportioning given by Eq. (1). The areas of both flanges are increased by the same amount until the condition given by Eq. (9) is reached.
   b. If $M_y \neq 0$ and $N \neq 0$, the section obtained from Eq. (1) is initially asymmetric. In this case, one of the flange areas is increased in

Table 1
Studied load combinations (negative axial load indicates compression).

Load combination	$M_{y,Ed}$ (kN m)	N_{Ed} (kN)
A	1391.60	0.00
B	0.00	−4180.80
C	695.82	−2090.41

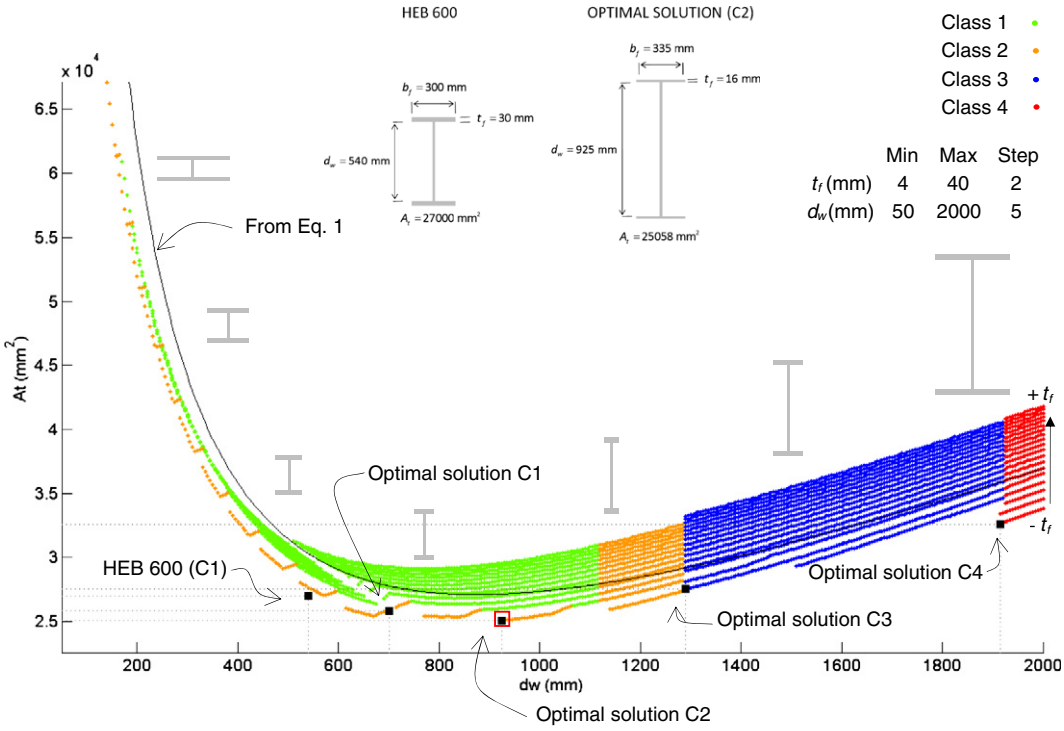

Fig. 9. Cross-sectional area A_t of the solutions in terms of web depth d_w for strong axis bending moment. (For interpretation of the references to color in this figure legend, the reader is referred to the web version of this article.)

order to reduce the eccentricity given by Eq. (8) until the limitation given by Eq. (9) is reached:

i. If M_y and N have equal signs, the top flange width will increase.
ii. If M_y and N have different signs, the bottom flange width will increase.

Once Eq. (9) is fulfilled for certain values of $d_w - t_{ft} - t_{fc}$ (in this example $t_f = t_{ft} = t_{fc}$), the cross-section will be stored if the dimensions of the flanges in compression are sufficient to prevent local buckling in the plane of the web. According to section 8 in Part 1-5 of EC3 [13], the following criterion should be met:

$$\frac{d}{t_w} \le k\frac{E}{f_y}\sqrt{\frac{d_w \cdot t_w}{A_{fcomp}}} \Rightarrow b_{fcomp} \le \frac{k^2 \cdot E^2 \cdot t_w^3}{f_y^2 \cdot t_f \cdot d_w}. \quad (10)$$

The value of k should be taken as follows:

— Plastic rotation utilized $k = 0.3$
— Plastic moment resistance utilized $k = 0.4$
— Elastic moment resistance utilized $k = 0.55$.

All the cross-sections with their corresponding pairs $d_w - t_f$ are stored. These solutions are sorted by cross-sectional area and the minimum is identified as the optimal solution. It is important to notice that the process may provide some solutions with the same optimal cross-sectional area. In this case, the final selected solution will be the one with the minimum value of interaction factor ζ.

Furthermore, the procedure provides an infinite number of solutions (depending on the established constraints). The optimum (i.e. minimum cross-sectional area) or the symmetric solution is just one of the possible cross-sections that may be chosen [1–3].

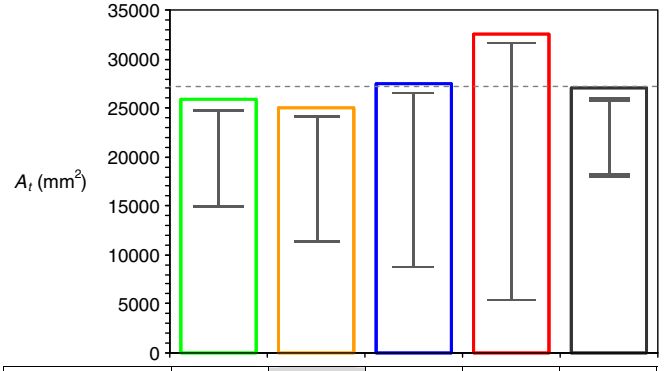

Optimal Solution	Class 1	Class 2	Class 3	Class 4	HEB 600
A_t (mm²)	25850	**25058**	27507	32587	27000
b_f (mm)	375	335	313	363	300
t_f (mm)	20	16	12	4	30
d_w (mm)	700	925	1290	1915	540

Fig. 10. Comparison between the dimensions of different optimal solutions for each class and HEB 600, for strong axis bending moment. Scale of dimensions sketches: 1/400. (For interpretation of the references to color in this figure legend, the reader is referred to the web version of this article.)

3. Examples

The validity and effectiveness of the process have been tested and this can be seen in the following three examples; in order to obtain minimum cross-sectional solutions for three combinations of M_y and N with the conditions represented in Fig. 1: a simple supported beam with end-fork conditions (i.e. pin supported end and free warping). The applied load combinations correspond to three points in the interaction equation (Fig. 8) corresponding to a specimen made out of steel Grade 235 ($f_y = 235$ N/mm^2) with a cross-section HEB600 ($d_w = 540$ mm; $t_w = 15.50$ mm; $t_f = 30$ mm; $b_{ft} = b_{fb} = 300$ mm; $A_t = 27{,}000$ mm^2)

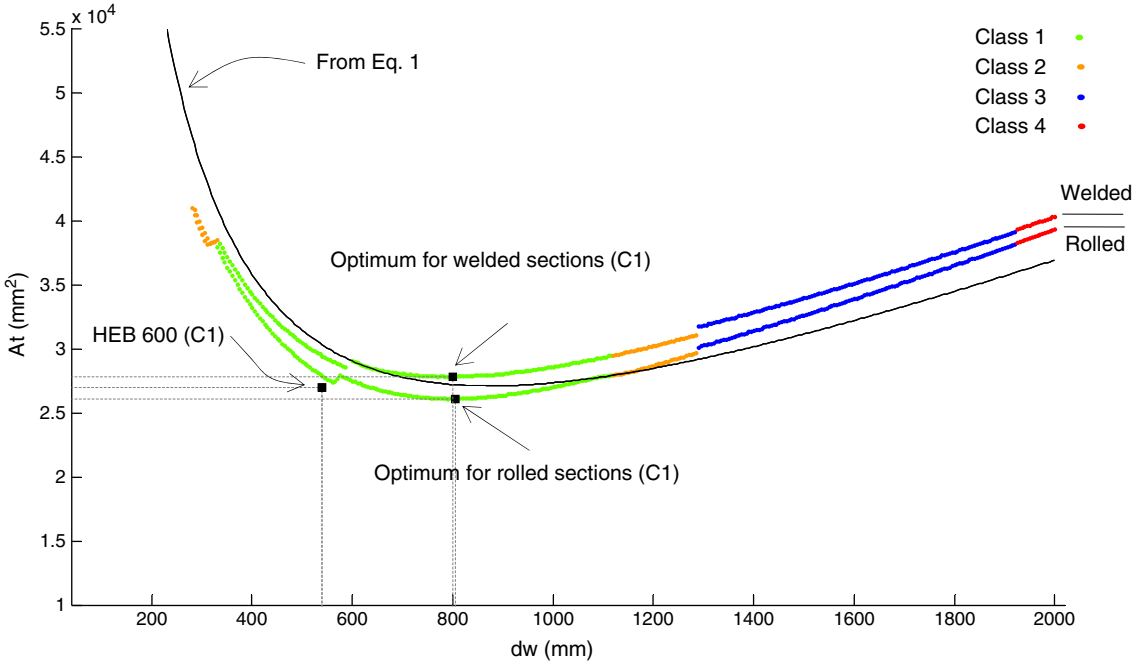

Fig. 11. Cross-sectional area A_t of the solutions with $t_f = 30$ mm in terms of web depth d_w for strong axis bending moment employing welded and rolled sections imperfection factors. (For interpretation of the references to color in this figure legend, the reader is referred to the web version of this article.)

and an unbraced length, l_b, equals to 6.00 m. The load combinations are presented in Table 1.

3.1. Combination A: $M_y = 1391.60$ kN m — bending moment applied on the right support of the beam

The first combination of loads corresponds to point A in Fig. 8, simple strong axis bending with a value of $M_y = 1391.60$ kN m. Fig. 9 shows the obtained design solutions for different web depths, d_w, with a range from 50 mm to 2000 mm in steps of 5 mm. The adopted range of values for flange thicknesses, t_f, varies from 4 mm to 40 mm, in steps of 2 mm. The HEB 600 web thickness ($t_w = 15.500$ mm) is adopted for every solution. According to Eq. (1), if $t_f = t_{ft} = t_{fc}$ all the obtained solutions are doubly-symmetric (i.e. $b_{ft} = b_{fb}$). The results from Eq. (1) are presented as a continuous line. Dots in Fig. 9 correspond to the solutions obtained after the adjustment process for the four different classes of cross-sections. In order to distinguish between each class, different colors (in the on-line version) and grayscale (in the printed version) have been used, respectively. In Fig. 9, the solution corresponding to the HEB section and the optimal ones obtained for each class using the optimization procedure have been identified. As may be observed in Fig. 9, the initially proportioned dimensions for the elements of the cross-section given by

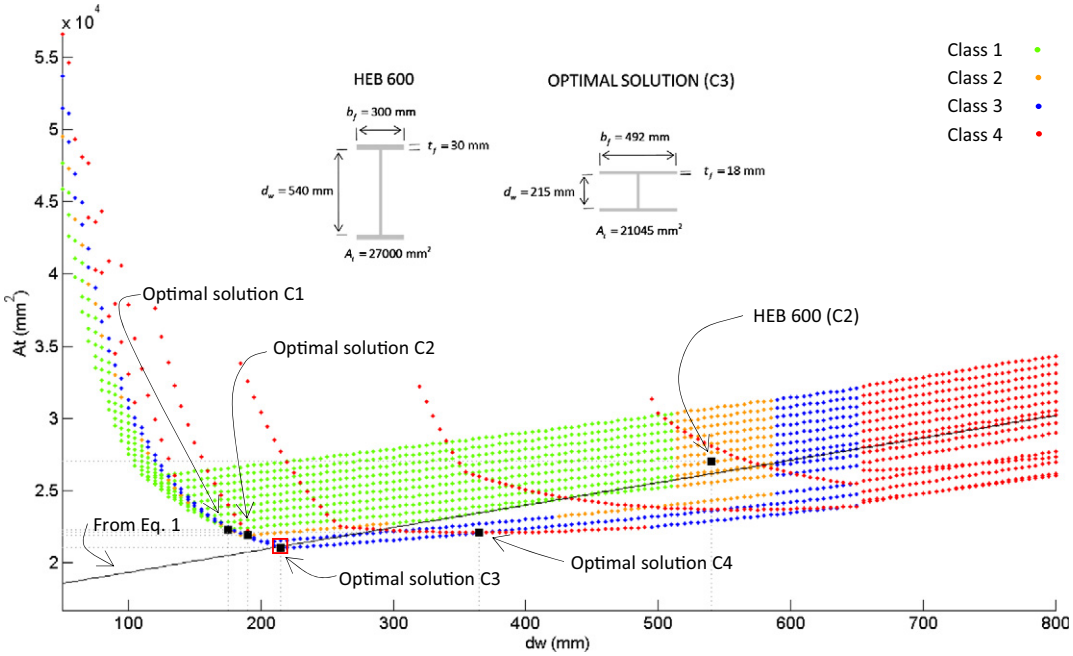

Fig. 12. Cross-sectional area A_t of the solutions in terms of web depth d_w for pure compression. (For interpretation of the references to color in this figure legend, the reader is referred to the web version of this article.)

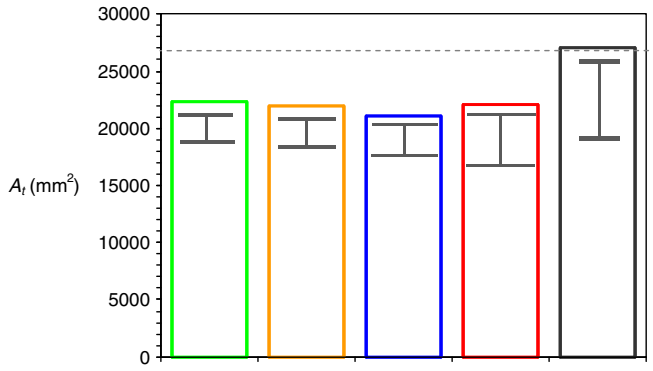

Optimal Solution	Class 1	Class 2	Class 3	Class 4	HEB 600
A_t (mm^2)	22297	21909	**21045**	22074	27000
b_f (mm)	408	431	492	513	300
t_f (mm)	24	22	18	16	30
d_w (mm)	175	190	215	365	540

Fig. 13. Comparison between dimensions of different optimal solutions for each Class and HEB 600, for pure compression. (For interpretation of the references to color in this figure legend, the reader is referred to the web version of this article.)

Eq. (1) are subsequently modified by the adjustment process. In some cases, those dimensions have been overestimated since the contribution of the web was ignored in Eq. (1). However, many solutions present cross-sectional areas greater than those initially estimated due to the fact that members turned out unstable and therefore dimensions needed to be modified in order to get sufficient strength to withstand the applied loads.

The solution with the lowest cross-sectional area corresponds to:

$$d_w = 925 \text{ mm}; \quad t_w = 15.50 \text{ mm}; \quad t_f = 16 \text{ mm};$$
$$b_{ft} = b_{fb} = 335 \text{ mm}; \quad A_t = 25,058 \text{ mm}^2$$

The web and top flange Classes are 1 and 2 respectively, leading to cross-section Class 2. The interaction factor is $\zeta = 0.9989$.

Fig. 10 shows the optimal solution for each class according to EC3 and compares their cross-sectional area with the one of HEB 600. The table in Fig. 10 provides the dimensions for these optimal solutions. Class 1, 2, and 3 sections reduce the flange width, b_f, when increasing web depth, d_w, while in Class 4 b_f increases since the web is reduced due to local buckling. In this case, only compact solutions (Classes 1 and 2) provide less cross-sectional area rather than the standard HEB600. Fig. 9 shows that a saving of 7.2% with respect to the area of HEB600 can be obtained.

In Fig. 11, the obtained results from the optimization process imposing $t_f = 30$ mm (flange thickness of HEB600) have been represented for both welded and rolled sections. This figure shows that if welded sections are considered instead of rolled sections, areas slightly larger are obtained. These differences are due to the different values of the imperfection factors corresponding to the buckling curves that are different for both welded and rolled sections. For this example no welded solution exits with a cross-sectional area under 27,000 mm^2 – HEB600 cross-section area – while if a rolled section is employed an area $A_t = 26,098$ mm^2 is obtained (for $d_w = 805$ mm and $b_f = 227$ mm).

Fig. 11 shows that the curve corresponding to rolled sections almost matches the solution corresponding to the HEB 600. These small differences are due to the fact that, as explained earlier in this work, the filets in rolled sections are not taken into account.

3.2. Combination B: $N = -4180.80$ kN (compression)

In this case, the steel member is subject to a pure compression of $N = -4180.80$ kN. This load combination corresponds to point B in Fig. 8, i.e. the buckling capacity of the considered HEB 600 member. The results for the different values of d_w, with a range from 50 mm to 800 mm in steps of 5 mm, are presented in Fig. 12. Again, the HEB 600 web thickness ($t_w = 15.50$ mm) is adopted for every solution. The adopted range of values for flange thicknesses, t_f, starts at 4 mm and finishes at 40 mm, in steps of 2 mm. The obtained optimal solution corresponds to $d_w = 215$ mm; $t_w = 15.50$ mm; $t_f = 18$ mm; $b_{ft} = b_{fb} = 492$ mm; $A_t = 21,045$ mm^2. The final solution saves 22.05% of steel with respect to the HEB600. The cross-section Class is 3 due to the slenderness ratio of the flanges in compression: $10\varepsilon < \frac{c}{t} = 13.23 < 14\varepsilon$. The interaction factor for this solution is $\zeta = 0.9992$. As in the former example, Fig. 13 shows the optimal solution for each Class. In this particular case, all the optimal solutions have cross-sectional areas smaller than the one corresponding to the standard HEB600. As in the previous example,

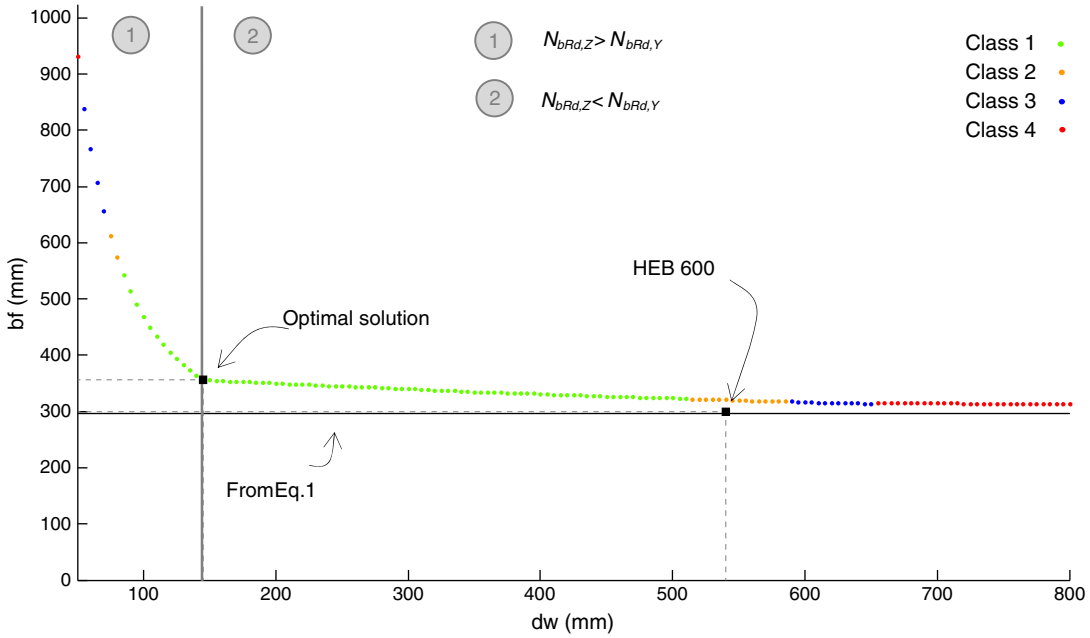

Fig. 14. Flange width, b_f, for the solutions of flange thickness $t_f = 30$ mm in terms of web depth d_w for pure compression. (For interpretation of the references to color in this figure legend, the reader is referred to the web version of this article.)

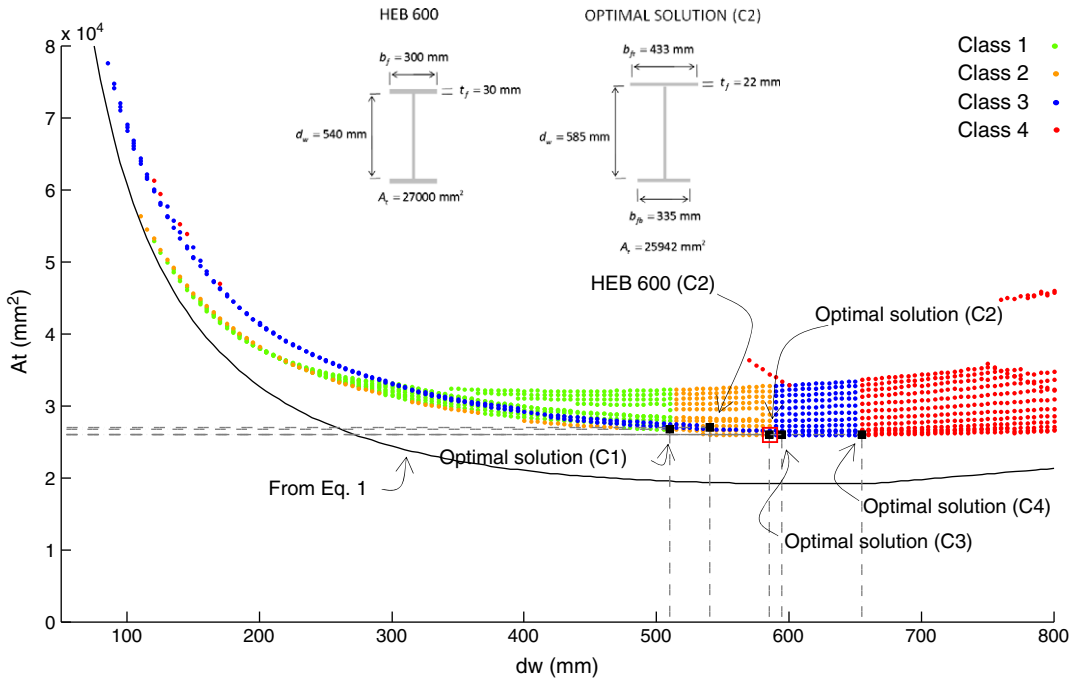

Fig. 15. Cross-sectional area A_t of the solutions in terms of web depth d_w for simultaneous compression and bending moment about strong y–y. (For interpretation of the references to color in this figure legend, the reader is referred to the web version of this article.)

Eq. (1) provides symmetric solutions since, the only applied load is the compressive axial load. Because the areas of the flanges are not affected by web depth, d_w, the flange widths, b_f, will be the same for every fixed value of the flange thickness, t_f. Fig. 14 shows the evolution of the flange width, b_f, as a function of the depth of the web, d_w, for a fixed value of the flange thickness, $t_f = 30$ mm. The obtained optimal solution corresponds to a web depth $d_w = 145$ mm and a flange width $b_{ft} = b_{fb} = 357$ mm. The corresponding cross-sectional area is $A_t = 23{,}668$ mm^2. In Fig. 14 two regions appear. Region 1 corresponds to solutions in which the relevant mode for lateral buckling under compression is the flexural buckling (solutions are symmetric) about the y–y axis. In this Region, solutions need to increase their preliminary proportioned flange width by an important amount before reaching stability, because the relevant mode is governed by the moment of inertia about y–y, which is proportional to b_f: $I_y \propto b_f$ ($\propto$ meaning being proportional). However, $I_y \propto d_w^3$, resulting in much less wider solutions as d_w becomes deeper. On the other hand, Region 2 corresponds to flexural buckling under the z–z axis and solutions get quick stability since $I_z \propto b_f^3$, and solutions need to increase lightly their preliminary proportioned flanges. In this Region, the slope of the curve becomes much flatter as d_w increases since $I_z \propto d_w$.

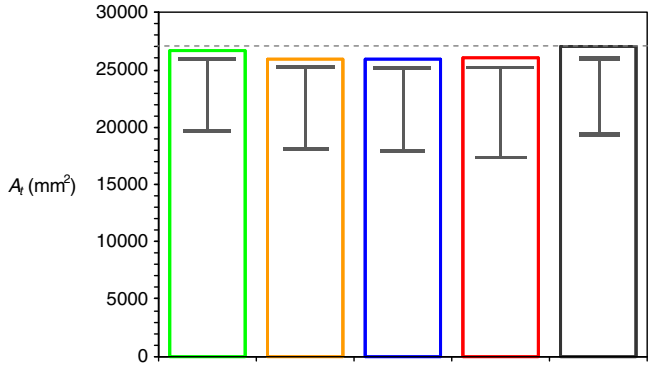

Optimal Solution	Class 1	Class 2	Class 3	Class 4	HEB 600
A_t (mm^2)	26721	**25942**	25943	26029	27000
b_{ft} (mm)	428	433	429	499	300
b_{fb} (mm)	356	334	331	383	300
t_f (mm)	24	22	22	18	30
d_w (mm)	510	585	595	655	540

Fig. 16. Comparison between the dimensions of different optimal solutions for each class and HEB 600, for simultaneous compression and bending moment about strong y–y. (For interpretation of the references to color in this figure legend, the reader is referred to the web version of this article.)

3.3. Combination C: $M_y = 695.82$ kN m and $N = -2090.41$ kN (compression)

This case, point C in Fig. 8, corresponds to a combination of simultaneous compression and bending moment about the strong axis. Solutions have been obtained using the same range of values for web depth, d_w, and flange thickness, t_f, as in the previous example. The value of the web thickness, t_w, is 15.5 mm. Fig. 15 shows the results obtained and the optimal section, for which the dimensions are: $t_f = 22$ mm; $t_w = 15.50$ mm; $t_f = 22$ mm; $b_{ft} = 433$ mm $b_{fb} = 334$ mm; $A_t = 25{,}942$ mm^2. For this section, both top flange and web are Class 2, and the entire cross-section results in this class. The solution saves 4% of steel with regards to the standard HEB 600.

Fig. 16 shows the obtained optimal results for each Class. In this case, as in the former example, once again, all of them have a smaller cross-sectional area than the HEB600. There are two of them, solutions for Classes 2 and 3, which have almost the same area (slight differences in dimensions of flanges and web result in a difference of just 1 mm^2).

Due to the fact that the procedure is completely general, the condition of doubly-symmetric may be imposed without loss of generality. If the width of both flanges are forced to be equal, the optimal solution corresponds to a flange thickness of $t_f = 20$ mm and $d_w = 625$ mm; $t_w = 15.50$ mm; $b_{ft} = 396$ mm; $b_{fb} = 396$ mm; $A_t = 26{,}303$mm^2. Fig. 17 represents both the cross-sectional and flange areas for doubly-symmetrical cross-section with $t_f = 20$ mm as a function of the height of the web. It can be observed that solutions are possible only if d_w is greater than 420 mm, found in the sections of Class 3 or 4. The standard HEB600 is included in the list of possible solutions in Class 2.

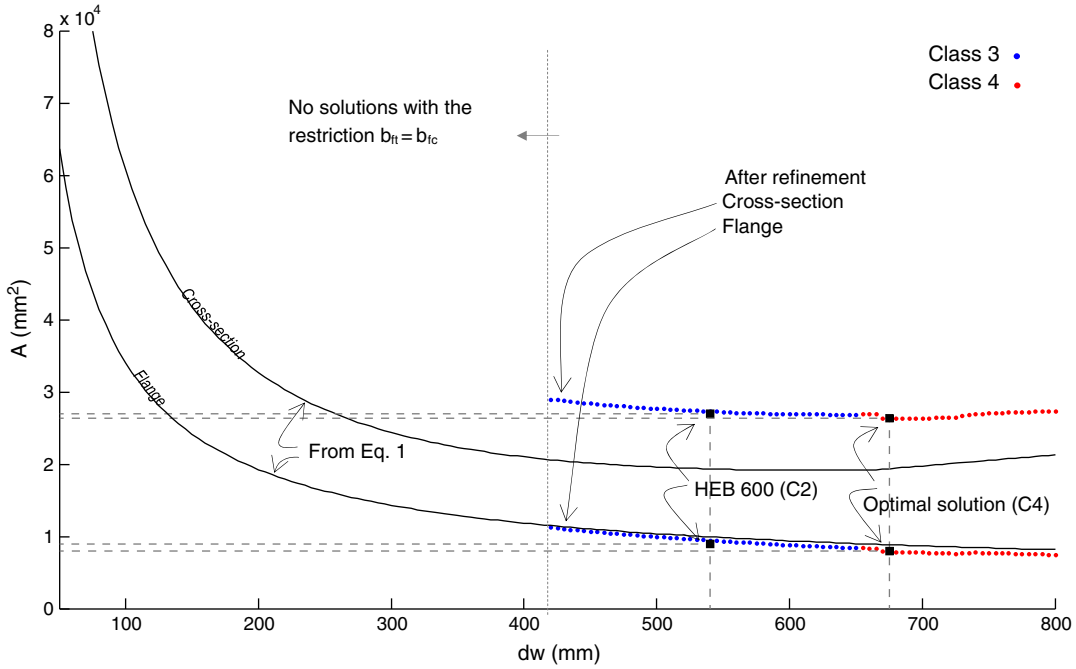

Fig. 17. Cross-sectional and flange areas in terms of d_w, for solutions of $t_f = 20$ mm and forcing both flanges to be equal (i.e. doubly-symmetrical cross-section) for simultaneous compression and bending moment about strong y–y. (For interpretation of the references to color in this figure legend, the reader is referred to the web version of this article.)

3.4. Global optimization

In order to extend the former optimization procedure to other values of the web's thickness, t_w, the above process has been applied to several values of t_w between 6 mm and 19 mm for the axial compression and bending moment about the strong axis denoted as combination C (see Fig. 8). The optimal cross-section (i.e., with minimum area) obtained for each class of cross-section [9] for each thickness of the web can be identify in Fig. 18. This figure shows that the smallest area that fulfills all the EC3 [9] requirements corresponds to the cross-section in Class 4 with $t_w = 8$ mm. This optimal section needs to be stiffened because the slenderness of the web is too big. The optimum cross-sections in Class 3 and in Classes 1 and 2 appear for $t_w =$ 13.5 mm and $t_w = 14.5$ mm, respectively. In such cases the slenderness of the web is low enough that transverse stiffeners are not needed. In Fig. 18, the optimal solutions obtained for the value of the thickness of the web adopted in the former sections (t_w of the standard HEB 600) have also been indicated.

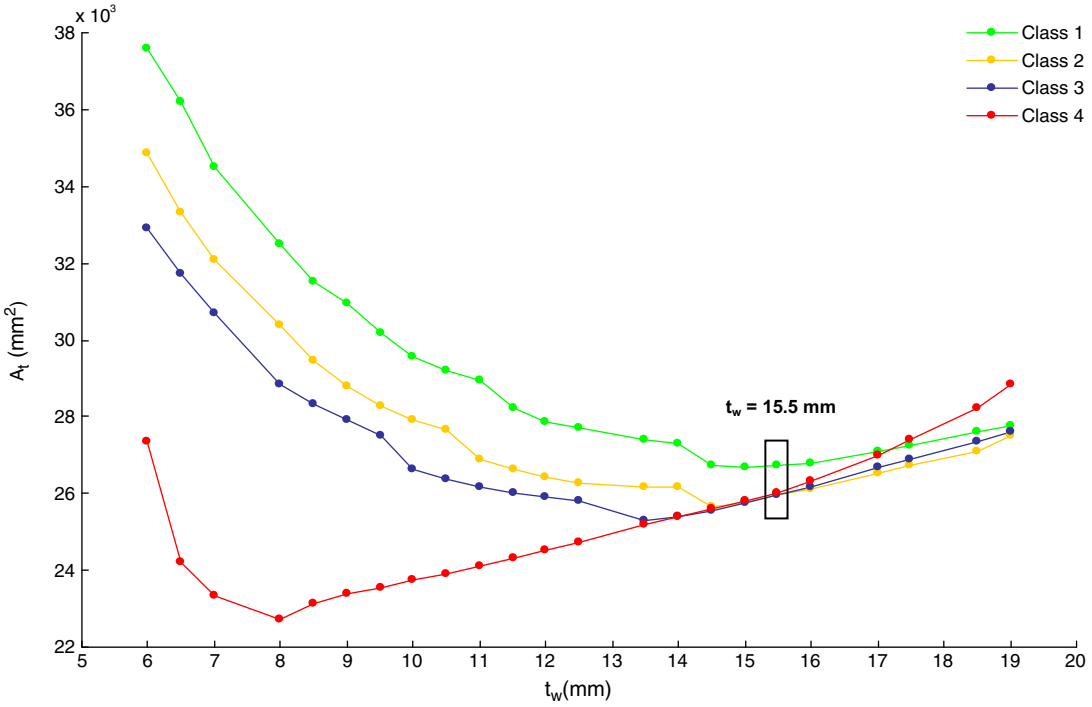

Fig. 18. Optimal (i.e. minimum) cross-sectional area in terms of t_w obtained for each class of cross-section and for simultaneous compression and bending moment about strong y–y. (For interpretation of the references to color in this figure legend, the reader is referred to the web version of this article.)

4. Conclusions

As explained and demonstrated in this work, employed symmetrical cross-sections are usually not, in most cases, the optimal solutions. This work presents an iterative procedure in order to get the optimal solution for the I-shaped cross-section of a steel beam–column member subject to an external axial load and bending about the strong axis. The process is based on RSD diagrams for optimizing the longitudinal reinforcing steel in reinforced concrete sections and completes the procedure proposed by Gil-Martín et al. [1] for obtaining these optimal solutions with steel sections in Class 1 according to Eurocode 3. This method allows engineers to choose from all the possible solutions: compact, non-compact and slender sections, obtaining important savings in steel and hence leading to reductions in greenhouse gas emissions.

Notation

A	cross-section area employed to compute $N_{b,Rd}$
A_t	cross-section area
A_{teff}	effective cross-section area for cross-sections in Class 4
A_1	top flange area
A_2	bottom flange area
E	steel elastic modulus
M_y	external in-plane bending moment
$M_{b,Rd}$	design buckling resistance moment of a laterally unrestrained beam
$M_{y,Ed}$	external in-plane bending moment applied to the section
$M_{y,Rk}$	critical cross-section characteristic moment resistance about y–y axis
N	external axial load
$N_{b,Rd}$	design buckling resistance of a compression member
N_{Ed}	external axial load applied to the section
N_{Rk}	critical cross-section characteristic resistance to normal force
$W_{eff,y}$	effective section modulus about y–y axis, for Class 4 sections
$W_{el,y}$	elastic section modulus about y–y axis
$W_{pl,y}$	plastic section modulus about y–y axis
W_y	appropriate section modulus employed in the computation of $M_{b,Rd}$
b_{fcomp}	compressed flange width
b_{fb}	bottom flange width
b_{ft}	top flange width
d_w	Web height
h	centroid height
f_y	specified steel yield strength
k	factor employed in the computation of the criterion to prevent the compression flange buckling in the plane of the web
l_b	unbraced length of the beam–column member
t_{fb}	bottom flange thickness
t_{ft}	top flange thickness
t_w	web thickness
χ	reduction factor for the relevant buckling mode in compression
χ_{LT}	reduction factor for lateral-torsional buckling
γ_{M1}	partial safety factor for the building ζ Interaction factor

Acknowledgments

The present work was financed by the Spanish Ministry of Education. The first author is a Spanish Government PhD fellow (FPU grant AP 2010-3707). This support is gratefully acknowledged.

References

[1] Gil-Martín LM, Aschheim M, Hernández-Montes E. Proportioning of steel beam–column members based on RSD optimization methodology. Eng Struct 2008;30(11):3003-11.
[2] Hernández-Montes E, Aschheim M, Gil-Martín LM. Impact of optimal longitudinal reinforcement on the curvature ductility capacity of reinforced concrete column sections. Mag Concr Res 2004;56(9):499-14.
[3] Hernández-Montes E, Gil-Martín LM, Aschheim M. Design of concrete members subjected to uniaxial bending and compression using reinforcement sizing diagrams. ACI Struct J 2005;102(1):150-8.
[4] Hernández-Montes E, Gil-Martín LM. Hormigón armado y pretensado: concreto reforzado y preesforzado. TEP-190 Ingeniería e Infraestructuras. Granada: Universidad de Granada, Grupo de Investigación; 2007 [(http://www.ugr.es/~emontes/prensa/HormigonEstructural.pdf)].
[5] Comité Europeo de Normalización, Agencia Española de Normalización. UNE EN 1998-1: Eurocódigo 8: Proyecto de estructuras sismorresistentes. Parte 1: Reglas generales, acciones sísimicas y reglas para edificación. Madrid: Aenor; 2011.
[6] Llago Acero R, García Rodríguez P. Composite twin-girder bridges: a competitive solution for medium span bridges. Rev Obras Publicas 2010;157(3516):29-46.
[7] Brozzetti J. Design development of steel–concrete composite bridges in France. J Constr Steel Res 2000;55(1–3):229-43.
[8] Ryu H-K, Youn S-G, Bae D, Lee Y-K. Bending capacity of composite girders with Class 3 section. J Constr Steel Res 2006;62(9):847-9.
[9] Dirección General de carreteras. Obras de paso de nueva construcción: conceptos generales. Madrid: Ministerio de Fomento; 2005.
[10] Comité Europeo de Normalización, Agencia Española de Normalización. UNE EN 1993-1-1: Eurocódigo 3: Proyecto de estructuras de acero. Parte 1-1: Reglas generales y reglas para edificios. Madrid: Aenor; 2008.
[11] Rugarli P. Classification of I- or H-shaped cross-sections under mixed internal actions. J Constr Steel Res 2009;65(8–9):1597-6.
[12] Steel Construction Manual (AISC 325-11). 14th ed. Chicago: AISC American Institute of Steel Construction; 2009.
[13] Comité Europeo de Normalización, Agencia Española de Normalización. UNE EN 1993-1-5: Eurocódigo 3: Proyecto de estructuras de acero. Parte 1-5: Placas planas cargadas en su plano. Madrid: Aenor; 2011.

ISI Web of Knowledge℠

Journal Citation Reports®

WELCOME HELP RETURN TO JOURNAL

2012 JCR Science Edition

Rank in Category: JOURNAL OF CONSTRUCTIONAL STEEL RESEARCH

Journal Ranking

For **2012**, the journal **JOURNAL OF CONSTRUCTIONAL STEEL RESEARCH** has an Impact Factor of **1.327**.

This table shows the ranking of this journal in its subject categories based on Impact Factor.

Category Name	Total Journals in Category	Journal Rank in Category	Quartile in Category
CONSTRUCTION & BUILDING TECHNOLOGY	57	14	Q1
ENGINEERING, CIVIL	122	30	Q1

Category Box Plot

For **2012**, the journal **JOURNAL OF CONSTRUCTIONAL STEEL RESEARCH** has an Impact Factor of **1.327**.

This is a box plot of the subject category or categories to which the journal has been assigned. It provides information about the distribution of journals based on Impact Factor values. It shows median, 25th and 75th percentiles, and the extreme values of the distribution.

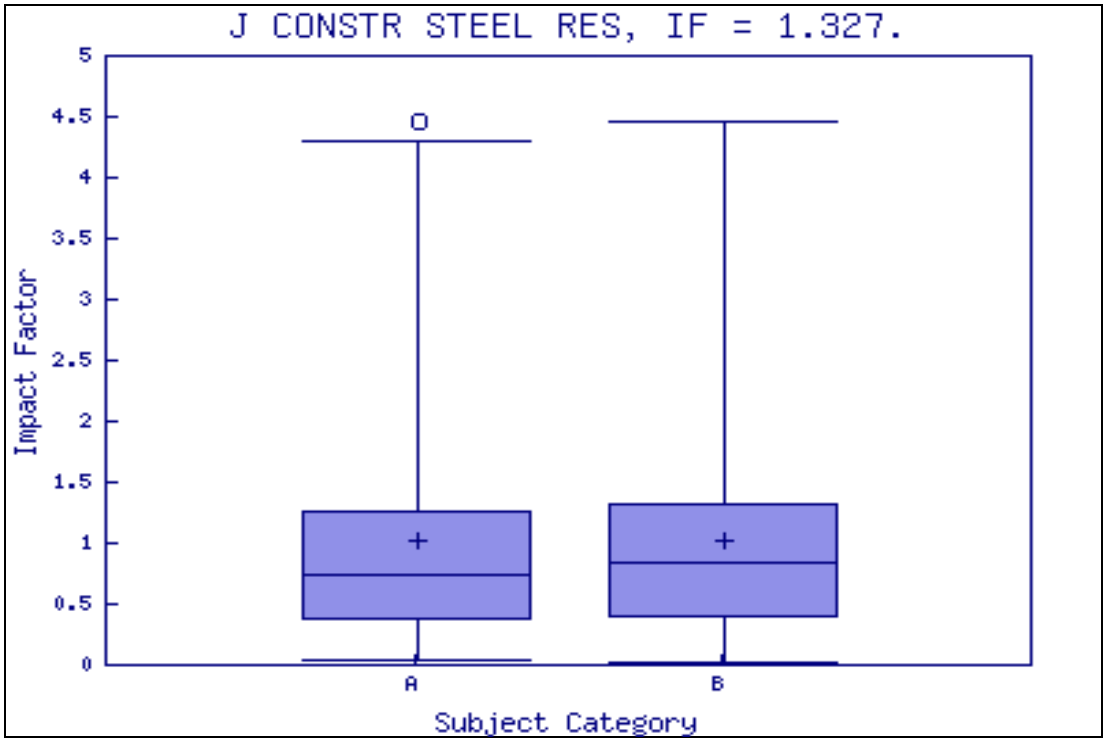

Key

A - CONSTRUCTION & BUILDING TECHNOLOGY

B - ENGINEERING, CIVIL

Eccentricity-Based Optimization Procedure for Strength Design of RC Sections under Compression and In-Plane Bending Moment

D. López-Martín[1]; J. F. Carbonell-Márquez[2]; L. M. Gil-Martín[3]; and E. Hernández-Montes[4]

Abstract: The strength design of reinforced concrete (RC) rectangular sections for combined compression and in-plane bending with two levels of reinforcement is indeterminate: three unknowns are to be solved, but with only two equilibrium equations; an additional condition is necessary to solve the problem. The additional condition leads to the finding of a minimum reinforcement-concrete ratio. This paper proposes a new approach based on the equivalent eccentricity of the applied compressive load. Different domains are reported, each of which is associated with given values of eccentricity and axial load. Analytical expressions for the domain boundaries are established, and a simple procedure is described to outline the conditions corresponding to the optimal reinforcement. The main advantage of this procedure is its simplicity, which allows manual computations. Some examples employing reinforcement sizing diagrams illustrate the validity of this approach. **DOI: 10.1061/(ASCE)ST.1943-541X.0000794.**

Author keywords: Reinforced concrete; Optimal reinforcement; Strength design; Equivalent eccentricity; Structural optimization.

Introduction

One of the most commonly studied topics in schools of engineering is the ultimate strength proportioning of a reinforced concrete (RC) rectangular cross section subjected to a combination of axial compressive load and bending moment. The widespread use of concrete and reinforcing steel in buildings constructed in the twentieth century meant that this problem has been dealt with in many books, as well as being included in every concrete design code.

The problem is difficult to resolve because numerous variables govern the equations, and it is usually necessary to iterate in order to find its solution. Therefore, the designer has to rely on intuitive experience to fix some of these variables to obtain the most appropriate reinforcement. When experience is not enough, a wide range of existing literature also provides many simplified or trial-and-error procedures based on tables or abacuses, which help in finding a design solution.

Recent studies provide many different approaches to getting the optimal solution for the reinforcement design. Some researchers have tried to find the optimum based on the cost of every component of the section (i.e., concrete and steel). Barros et al. (2005) investigated the cost optimization of rectangular RC sections using the nonlinear MC90 equation. Barros et al. (2012) studied the minimal cost problem of a rectangular section in simple bending where the objective function is the cost of raw materials and the variables are the section depth and the steel reinforcement areas. Lee and Ahn (2003) and Camp et al. (2003) also employed genetic algorithms to perform a discrete optimization of the flexural design of RC frames, both of which included material and construction costs.

Other approaches assume that the rectangular dimensions of the cross section are given and the optimal solution for the reinforcement in ultimate strength design needs to be found. Thereby, Hernández-Montes et al. (2004, 2005) presented a new design approach called Reinforcement Sizing Diagrams (RSD), which shows the infinite number of solutions for top and bottom reinforcement that provide the required ultimate strength for sections subject to combined axial load and moment. Because RSD represents an infinite number of solutions, the optimal (or minimum) reinforcement may be identified. Also, Aschheim et al. (2007) employed this RSD technique to define optimal domains with respect to axial-bending load coordinates according to provisions of Eurocode 2 (EC2) (CEN 2001). Ultimately, the observation of the characteristics of optimal solutions led Hernández-Montes et al. (2008) to the development of the Theorem of Optimal Section Reinforcement (TOSR). This work provides the additional conditions to be imposed in the equilibrium equations to achieve an optimal design of reinforcement.

Although Hernández-Montes et al. (2008) described and proved the additional conditions to be implemented, each of which has a special suitability depending on the applied loads. As a corollary to the mentioned theorem, Hernández-Montes et al. (2008) proposed to check every condition in the problem in question and select the one that provides the optimal solution.

In this paper, a procedure similar to the one that Aschheim et al. (2007) exposed is given according to EC2 specifications that address the problem from the point of view of many traditional concrete textbooks: depending on the equivalent eccentricity of the applied compressive load, this approach will provide an additional

[1]Associate Professor, Dept. of Structural Mechanics, Univ. of Granada (UGR), Campus Universitario de Fuentenueva, 18072 Granada, Spain.

[2]Ph.D. Candidate, Dept. of Structural Mechanics, Univ. of Granada (UGR), Campus Universitario de Fuentenueva, 18072 Granada, Spain (corresponding author). E-mail: jfcarbonell@ugr.es

[3]Associate Professor, Dept. of Structural Mechanics, Univ. of Granada (UGR), Campus Universitario de Fuentenueva, 18072 Granada, Spain.

[4]Full Professor, Dept. of Structural Mechanics, Univ. of Granada (UGR), Campus Universitario de Fuentenueva, 18072 Granada, Spain.

Note. This manuscript was submitted on July 3, 2012; approved on December 17, 2012; published online on December 19, 2012. Discussion period open until February 23, 2014; separate discussions must be submitted for individual papers. This paper is part of the ***Journal of Structural Engineering***, © ASCE, ISSN 0733-9445/04013029(9)/$25.00.

condition to impose in order to obtain the optimal reinforcement. Some examples are presented to compare the results predicted by this approach with those obtained using the RSD technique. These examples test the validity of the procedure explained herein.

Flexural Analysis and Strength Design Assumptions

Bernoulli's Hypothesis

The compatibility conditions to be imposed within the problem use Bernoulli's hypothesis that plane sections remain planed after deformation and assume that no slip of reinforcement occurs at the critical section. Thus, the distribution of strain over the cross section may be defined by just two variables (Fig. 1): the strain at the centroid (ε_c) of the cross section and the curvature (ϕ) of the cross section. Therefore, the strain at any fiber of concrete or steel located a distance y from the centroid of the cross section will be

$$\varepsilon(y, \varepsilon_c, \phi) = \varepsilon_c + \phi y \tag{1}$$

The formulation given in Eq. (1) considers the compression strain as positive and the curvature that produces tension in the bottom fiber.

Section Ultimate Limit State according to EC2

Bending the ultimate limit state is associated with failure of the section due to the limit of concrete compressive strength, or in some cases, the steel tension limit stress.

EC2 defines a series of possible ranges of ultimate strain distributions (Fig. 2). Strain planes pivoting on point A are distributions in which steel fails in tension, whereas planes pivoting either on point B or C correspond to concrete failure in compression.

The EC2 concrete model considers that concrete ultimate compression strain in flexural compression is different from the case of pure compression. This is the reason for the ultimate constant strain distribution at pure compression ε_{c2} or ε_{c3} (depending on consideration of parabolic-rectangular or rectangular concrete stress distribution), as shown in Fig. 2. Considering a stress bilinear model without)] for reinforcing steel, EC2 allows no limitation of the steel tensile strain, so point A in Fig. 2 disappears.

From observing the ultimate strain configurations presented in Fig. 2, it can be seen that the ultimate strain for any fiber in the cross section may be expressed by means of just one variable: neutral axis depth x [Eq. (2)]. Considering the steel model without the strain-hardening condition, x takes values in the interval $(0, \infty)$:

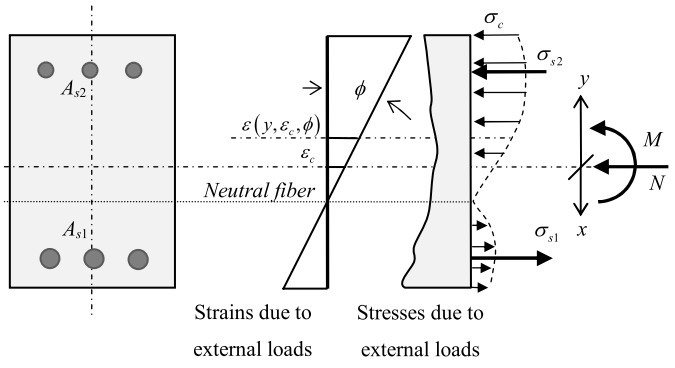

Fig. 1. Strains and stresses diagrammed at the cross-section level

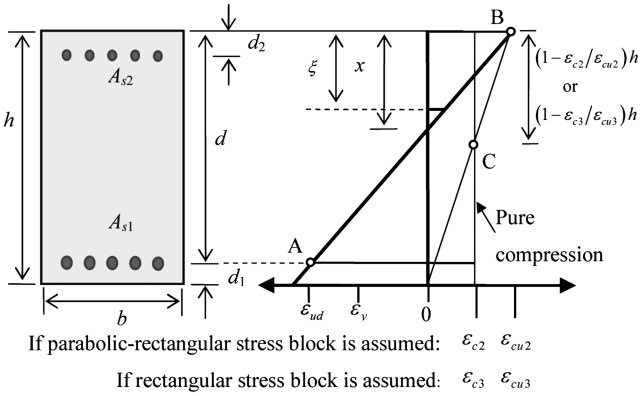

Fig. 2. Possible strain distributions in the ultimate limit state according to EC2

$$\varepsilon(\xi, x) = \begin{cases} \varepsilon_{cu3}\frac{x-\xi}{x} & \text{if } 0 \le x < h \\ \varepsilon_{c3}\frac{x-\xi}{x-\Xi} & \text{if } x \ge h \end{cases} \tag{2}$$

where $\Xi = h[1 - (\varepsilon_{c3}/\varepsilon_{cu3})]$ and ξ is the position where the strain is to be measured.

Concrete Ultimate State Model

Concrete is a material whose stress-strain behavior is nonlinear and changes with age and loading duration, among other factors. Due to the importance of the ultimate strength design, simplified schemes have been adopted to capture the behavior of concrete. EC2 considers three different concrete stress-strain models: rectangular, parabolic-rectangular, and bilinear.

Within this work, the rectangular model has been adopted with $\varepsilon_{c3} = 2‰$ and $\varepsilon_{cu3} = 3.5‰$. The resultant of compression in concrete, N_c, can be determined in the case of rectangular sections as a function of the neutral axis depth x as follows:

$$N_c(x) = \begin{cases} 0 & \text{if } x \le 0 \\ \eta f_{cd} b \lambda x & \text{if } 0 \le x < h/\lambda \\ \eta f_{cd} b h & \text{if } x \ge h/\lambda \end{cases} \tag{3}$$

where $f_{cd} = \alpha_{cc} f_{ck}/\gamma_c$ is the concrete design strength according to EC2; f_{ck} is the characteristic compressive cylinder strength of concrete at 28 days; γ_c is the partial safety factor for concrete (1.5 for persistent and transient design situations and 1.2 for accidental situations); α_{cc} is the coefficient considering long-term effects on the compressive strength and unfavorable effects resulting from the way the load is applied, should lie between 0.8 and 1.0, with a typical value of 0.85; and h and b are the depth and width of the rectangular cross section, respectively. Values for η and λ are given by Eq. (4):

$$\lambda = \begin{cases} 0.8 & \text{for } f_{ck} \le 50 \text{ MPa} \\ 0.8 - (f_{ck} - 50)/400 & \text{for } 50 < f_{ck} \le 90 \text{ MPa} \end{cases}$$
$$\eta = \begin{cases} 1.0 & \text{for } f_{ck} \le 50 \text{ MPa} \\ 1.0 - (f_{ck} - 50)/200 & \text{for } 50 < f_{ck} \le 90 \text{ MPa} \end{cases} \tag{4}$$

Reinforcing the Steel Ultimate State Model

The steel model used herein is bilinear, without considering strain hardening, and symmetric (i.e., the same expression for tension and compression is employed). Nevertheless, other nonsymmetric models are possible. For the sake of simplicity, Eq. (3) does not consider

the presence of reinforcement inside a concrete cross section. However, to take this into account, the steel model is formulated as follows:

$$\sigma_s(\varepsilon) = \begin{cases} f_{yd} - \eta f_{cd} & \text{if } \varepsilon \geq \frac{f_{yd}-\eta f_{cd}}{E_s} \\ E_s \varepsilon & \text{if } -\frac{f_{yd}}{E_s} < \varepsilon < \frac{f_{yd}-\eta f_{cd}}{E_s} \\ f_{yd} & \text{if } \varepsilon \leq -\frac{f_{yd}}{E_s} \end{cases} \tag{5}$$

As mentioned previously, strain ε may be defined perfectly by means of just one variable: neutral axis depth x. Therefore, the expression of steel stress given in Eq. (5) also can be given as a function of x.

In the common case of a concrete cross section with two layers of steel, A_{s1} (bottom) and A_{s2} (top), with mechanical covers of d_1 and d_2 respectively (considered equal in this work), ultimate strains and stresses in the reinforcements may be obtained from the composition of Eqs. (2) and (5) (Gil-Martín et al. 2012) as

$$\begin{aligned} \varepsilon_{s1}(x) &= \varepsilon(h - d_1, x) \\ \varepsilon_{s2}(x) &= \varepsilon(d_2, x) \\ \sigma_{s1}(x) &= \sigma_{s1}[\varepsilon_{s1}(x)] = (\sigma_{s1} \circ \varepsilon_{s1})(x) \\ \sigma_{s2}(x) &= \sigma_{s2}[\varepsilon_{s2}(x)] = (\sigma_{s1} \circ \varepsilon_{s2})(x) \end{aligned} \tag{6}$$

where $\circ$ means the composition of two mathematical functions.

Equilibrium Equations

The stress distribution over the cross section has to equilibrate the externally applied loads that, in this case, are an in-plane bending moment M and a compressive axial load N (Fig. 1). Taking moment equilibrium at the centroid of the cross section, which is a supposed rectangular with h height and b width, equilibrium equations may be presented as

$$\begin{aligned} N &= N_c(x) + A_{s1}\sigma_{s1}(x) + A_{s2}\sigma_{s2}(x) \\ M &= N_c(x)\left[\frac{h}{2} - z_c(x)\right] - A_{s1}\sigma_{s1}(x)\left(\frac{h}{2} - d_1\right) \\ &\quad + A_{s2}\sigma_{s2}(x)\left(\frac{h}{2} - d_2\right) \end{aligned} \tag{7}$$

where z_c is the lever arm corresponding to the resultant of concrete compressions relative to the top fiber, defined as (Fig. 3)

$$z_c(x) = \begin{cases} \frac{\lambda x}{2} & \text{if } 0 \leq x \leq \frac{h}{\lambda} \\ \frac{h}{2} & \text{if } x \geq \frac{h}{\lambda} \end{cases} \tag{8}$$

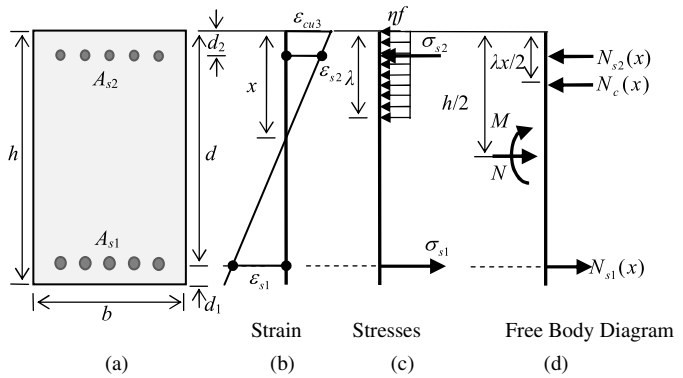

Fig. 3. Terms for ultimate strength analysis according to EC2: (a) cross section; (b) strain; (c) stresses; (d) free body diagram

Problem of Optimum Reinforcement

When faced with the problem of designing RC rectangular sections, once the dimensions h and b are preliminarily fixed, the engineer has to provide a solution to the two equilibrium equations presented in Eq. (7). However, these equations have three unknowns: neutral axis depth, x; bottom, A_{s1}; and top, A_{s2}, reinforcing steel. Therefore, as the problem is indeterminate, it may be solved with an infinite set of values for x, A_{s1}, and A_{s2}.

As mentioned earlier, the RSD (Hernández-Montes et al. 2005) approach provides, in a graphical manner, all the possible combinations for x, A_{s1}, and A_{s2}. Employing this method, Hernández-Montes et al. (2008) established the TOSR, where the authors stated that one of the following conditions imposed in Eq. (7) yields the optimal result for the reinforcing steel under the combined compressive load and in-plane bending moment:

1. $A_{s1} = 0$
2. $A_{s2} = 0$
3. $A_{s1} = A_{s2} = 0$
4. ε_s equal to or slightly greater than $-\varepsilon_y$
5. $\varepsilon = \varepsilon_{s1} = \varepsilon_{s2} = \varepsilon_{c3}$

Conditions 2 and 4 make maximum use of the steel capacity, while conditions 1, 3, and 5 take advantage of the maximum concrete capacity. TOSR provides a sixth condition, but it is not considered herein because it is related to the yielding of both layers of reinforcement in tension.

Although the conditions that lead to an optimum design are given, the designer still does not know which condition is to be imposed; it is necessary to evaluate the five abovementioned conditions (1 to 5) until the optimum solution is reached.

Eccentricity Domains for Optimal Strength Design

The externally applied compression load and bending moment, N and M, are equivalently expressed, introducing the same compression load N acting at an eccentricity e_0 with respect to the centroid of the cross section (Nawy 2003), so that (Fig. 4)

$$e_0 = \frac{M}{N} \tag{9}$$

As will be shown later in this paper, the former conditions for the optimal proportioning of reinforcement in rectangular RC cross sections may be explained in terms of the eccentricity e_0 and

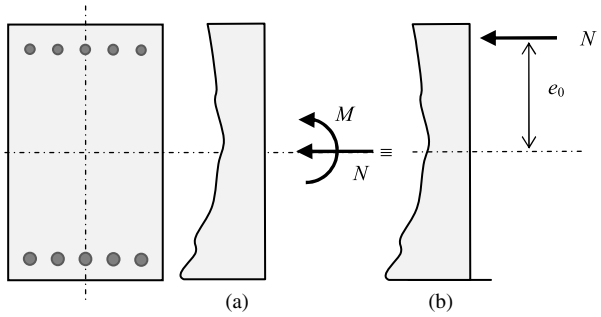

Fig. 4. Combined compression and in-plane flexion. Both systems, (a) and (b), are equivalent if $e_0 = M/N$

compression load N. Setting out the moment equilibrium at different points of the cross section in several cases (Fig. 5), different domain boundaries can be obtained. These domains and their boundaries will be deduced in the remainder of this section. The main advantage of these domains is that they may be represented graphically, which facilitates their application. Therefore, with only the evaluation of pair $e_0 - N$, the designer will be able to identify the relevant domain and thus determine the optimal reinforcement for each loading case.

Domains and Their Boundaries

The pair of values $e_0 - N$ for which a concrete section is able to stand without any longitudinal reinforcement [that is, $A_{s1} = A_{s2} = 0$ (called domain 0)] may be determined from Fig. 5(a). For $N \le \eta f_{cd} \lambda x b$ and values of eccentricity in the range $0 \le e_0 < h/2$, the concrete cross section is able to resist with no reinforcement to the applied loads, with the compression stress in concrete expressed as $\sigma_c = \eta f_{cd}$. From Fig. 5(a), it can be seen that, in the limit situation $\sigma_c = \eta f_{cd}$, the following conditions may be established:

$$N = \eta f_{cd} \lambda x b \tag{10}$$

$$e_0 = \frac{h}{2} - \frac{\lambda}{2} x \tag{11}$$

The combination of Eqs. (10) and (11) leads to eccentricity limit, e_{0c}, under which no reinforcement is necessary ($A_{s1} = A_{s2} = 0$). The value of e_{0c} is given by Eq. (12):

$$e_{0c} = \frac{1}{2}\left(h - \frac{N}{\eta f_{cd} b}\right) \tag{12}$$

Although this case is theoretically possible, it is assumed that a minimum level of reinforcement, as prescribed in code provisions, would be used, even for sections in domain 0.

Now, consider solutions in domain 1, where the condition of TOSR to be imposed is $x = +\infty$. In this domain, axial load N is applied with a low eccentricity value e_0 so that full compression of the cross section is involved. In some cases, equilibrium makes the existence of compressed bottom reinforcement necessary ($A_{s1} \neq 0$). The boundary value of $e_0 = e_{0h}$, which separates the cases of $A_{s1} = 0$ and $A_{s1} \neq 0$, is calculated in Eq. (13). Setting up the moment equilibrium at the top reinforcement level in the situation presented in Fig. 5(b) (with $A_{s1} = 0$), and in the situation of full compression of the cross section (i.e., $\lambda x = h$)

$$e_{0h} = \left(\frac{h}{2} - d_2\right) - \frac{\eta f_{cd} h b (\frac{h}{2} - d_2)}{N} \tag{13}$$

For cases in domain 1, for which both top and bottom reinforcements are necessary (i.e., $A_{s1} \neq 0$ and $A_{s2} \neq 0$), the optimal reinforcement corresponds to condition 5 of TOSR. The moment equilibrium at the top reinforcement level and the equilibrium of axial loads [Fig. 5(b)] at both the bottom and top reinforcement areas A_{s1} and A_{s2} are given by Eqs. (14) and (15):

$$A_{s1} = \frac{(\frac{h}{2} - d_2 - e_0)N - \eta f_{cd} h b (\frac{h}{2} - d_2)}{(d - d_2)\sigma_{s1}(x = +\infty)} \tag{14}$$

$$A_{s2} = \frac{N - [\eta f_{cd} h b + A_{s1}\sigma_{s1}(x = +\infty)]}{\sigma_{s2}(x = +\infty)} \tag{15}$$

The eccentricity boundary e_{0h} separates domains 1 and 2. In domain 2, the additional condition to be imposed on Eq. (7) to get the optimal solution for reinforcement is $A_{s1} = 0$. In this domain, the section can be partially or fully compressed (i.e., $x \le h/\lambda$), and the area of top reinforcement is provided to solve the axial equilibrium in Fig. 5(c):

$$A_{s2} = \frac{N - \eta f_{cd} \lambda x b}{f_{yd} - \eta f_{cd}} \tag{16}$$

In Eq. (16), $f_{yd} - \eta f_{cd} = \sigma_{s2}(x)$ and the neutral fiber position x can be obtained from the equilibrium of moment at the top reinforcement level [Fig. 5(c)]:

$$\left(\frac{h}{2} - d_2 - e_0\right)N = \eta f_{cd} \lambda x b \left(\frac{\lambda x}{2} - d_2\right) \tag{17}$$

The strain limit for domain 3 is represented in Fig. 5(d). In this situation, the optimal reinforcement corresponds to condition 4 of TOSR. Therefore, the optimal solution is located at balance point $x = x_b$; thus, $N_c = \eta f_{cd} \lambda x_b b$ is

$$x_b = \frac{d_{s1}}{1 + \frac{f_{yd}}{\varepsilon_{cu3} E_s}} \tag{18}$$

The value of e_0 that separates domains 2 and 3, $e_{0\,\mathrm{lim}}$, is calculated from Fig. 5(d), imposing that $A_{s1} = 0$. Equilibrium of the free body diagram is considered with $A_{s1} = 0$ (domain 3) and $x = x_b$ (domain 4), leading to a boundary value of e_0 equal to

$$e_{0\,\mathrm{lim}} = \left(\frac{h}{2} - d_2\right) - \frac{\eta f_{cd} \lambda x_b b (\frac{\lambda x_b}{2} - d_2)}{N} \tag{19}$$

The value of $e_{0\,\mathrm{lim}}$ marks the classical boundary between large and small eccentricity problems (Nawy 2003).

In domain 3, both bottom and top reinforcements are necessary. Taking the moment at the bottom reinforcement level and setting up the equilibrium of axial loads [Fig. 5(d)] result in Eqs. (20) and (21), which provide the required reinforcements:

$$A_{s2} = \frac{(e_0 + \frac{h}{2} - d_1)N - \eta f_{cd} \lambda x_b b (d - \frac{\lambda x_b}{2})}{(f_{yd} - \eta f_{cd})(d - d_2)} \tag{20}$$

$$A_{s1} = \frac{\eta f_{cd} \lambda x_b b + A_{s2}(f_{yd} - \eta f_{cd}) - N}{f_{yd}} \tag{21}$$

The last domain to be considered is called domain 4 [Fig. 5(e)]; in this situation, the top reinforcement is not needed ($A_{s2} = 0$). The boundary value of $e_0 = e_{02}$, which separates domains 3 and 4, is calculated considering the equilibrium of the free body diagram in Fig. 5(d), imposing $A_{s2} = 0$ (i.e., $A_{s2} = 0$ and $x = x_b$):

$$e_{02} = -\left(\frac{h}{2} - d_1\right) + \frac{\eta f_{cd} \lambda x_b b (d - \frac{\lambda x_b}{2})}{N} \tag{22}$$

To obtain the required bottom reinforcement area in domain 4, it is necessary to know the value of the neutral axis depth x, which is computed by setting up the equilibrium of moments at the bottom reinforcement level [Eq. (23)]. Once x is obtained, the equilibrium of axial loads provides the bottom reinforcement area according to Eq. (24):

$$\left(e_0 + \frac{h}{2} - d_1\right)N = \eta f_{cd} \lambda x b \left(d - \frac{\lambda x}{2}\right) \tag{23}$$

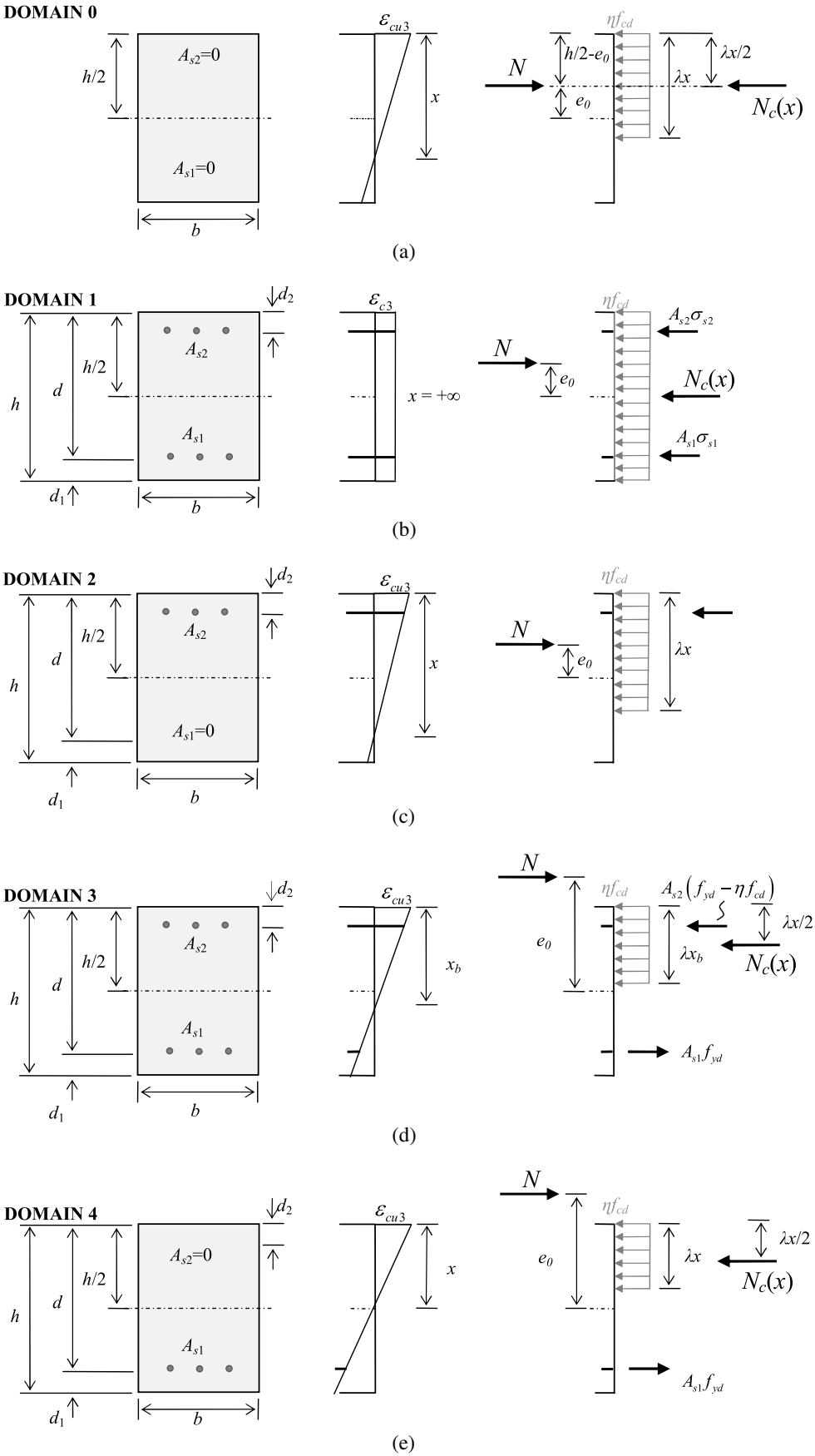

Fig. 5. Ultimate limit states with optimal reinforcement for rectangular RC cross sections subject to combined compression and in-plane bending moment

$$A_{s1} = \frac{\eta f_{cd} \lambda x b - N}{f_{yd}} \tag{24}$$

An alternative and easier way to represent the former boundaries and domain that allow the engineer to obtain the optimal reinforcement of a rectangular RC section (López-Martín et al. 2011) is using a chart like the one presented in Fig. 6. In this chart, the value of e_0/h (i.e., the ratio between eccentricity and the depth of the cross section) is represented as a function of the nondimensional parameter $\nu = N/(\eta f_{cd} bh)$ for the studied section [i.e., the values of mechanical covers ($d_1 = d_2 = h/10$) and the design strength of steel f_{yd} ($f_{yk} = 500$ MPa) are known].

Because some boundary values of e_0 depend on x_b [see Eqs. (19) and (22)] different charts will be obtained for different steel yield strains, $\varepsilon_y = f_{yd}/E_s$, with E_s being the steel elasticity modulus ($E_s = 200.000$ MPa).

In Fig. 6, the horizontal band for which $e_0/h < 1/30$ has to be excluded according to prescriptions of EC2 § 6.1 (4) (CEN 2001) relating minimum eccentricity concerns.

This procedure is summarized in the flowchart shown in Fig. 7.

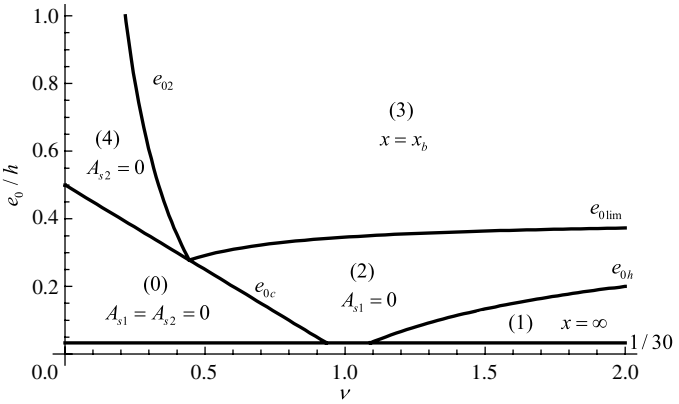

Fig. 6. Chart $e_0/h - \nu$ with $\nu = N/\eta f_{cd} hb$ corresponding to a rectangular RC cross section for steel B 500 S, and $d_1 = d_2 = h/10$

Examples

In this section, some examples are presented to prove the validity of the approach proposed in this paper. Several values of eccentricity e_0 and external compression load N have been considered, and the additional condition to impose to get the optimal reinforcement is obtained from the chart presented in Fig. 6. Results have been verified using RSD representations of the required reinforcement areas because this technique shows in a graphical manner all the possible solutions for the reinforcement as a function of neutral axis depth x. Furthermore, the neutral axis depth x and the optimal reinforcement areas, A_{s1} and A_{s2}, are calculated.

In the following examples, the concrete has strength resistance of $f_{ck} = 45$ MPa and steel yield strength of $f_{yk} = 500$ MPa. The modulus of elasticity of the reinforcement is $E_s = 200{,}000$ MPa. The dimensions of the studied cross section are as follows: $h = 600$ mm, $b = 300$ mm, $d = 540$ mm, $d_1 = d_2 = 60$ mm.

In Fig. 8, the chart $\nu - e_0/h$ for the former section has been represented. For a high value of the axial load, like $\nu = 1.5$ (shown as the vertical line 1 in Fig. 8), three domains are possible depending on eccentricity e_0. For smaller values of e_0 (i.e., for situations closer to centered compression), both top and bottom reinforcements are needed (segment a_1 in domain 1 in Fig. 8). As e_0 is increased, equilibrium may be set up without the presence of bottom reinforcement (segment b_1 in domain 2 in Fig. 8). However, if eccentricity continues to increase, the applied moment M becomes

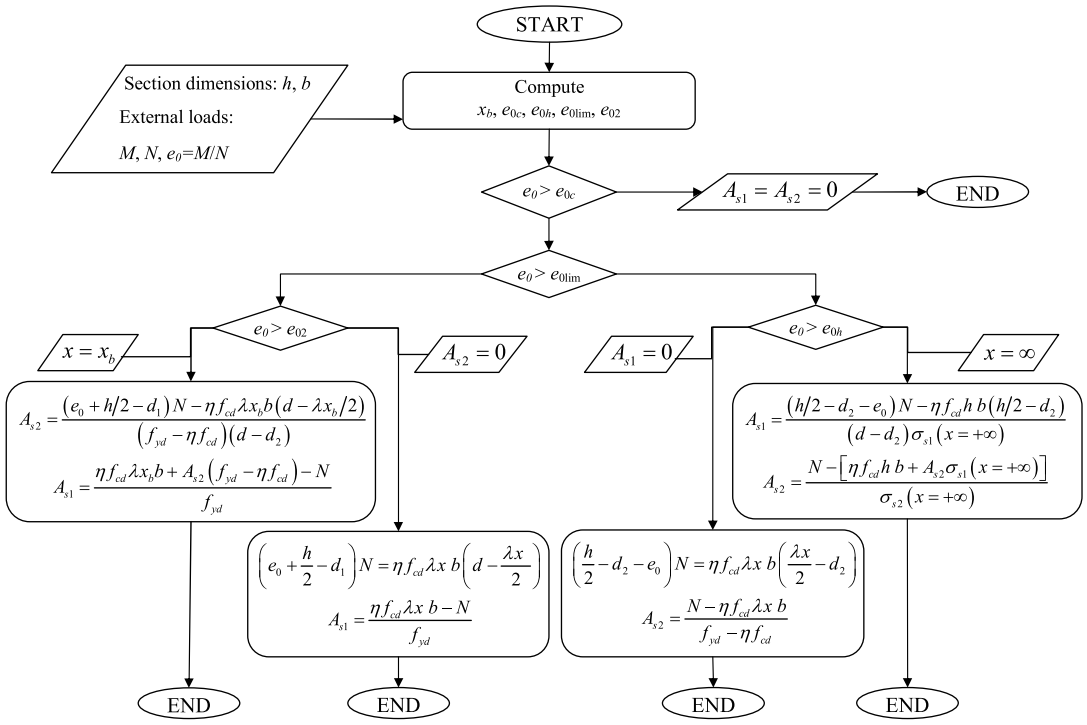

Fig. 7. Flowchart: Eccentricity-based process to optimize rectangular RC cross sections subject to combined compression and in-plane bending moment

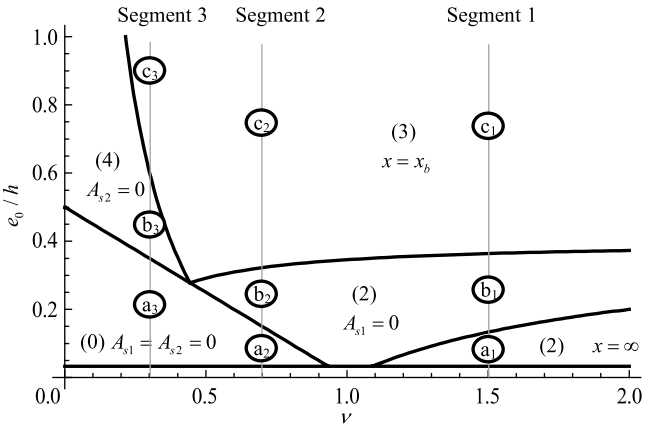

Fig. 8. Chart $e_0/h-\nu$ with $\nu=N/\eta f_{cd}hb$, with B 500 S

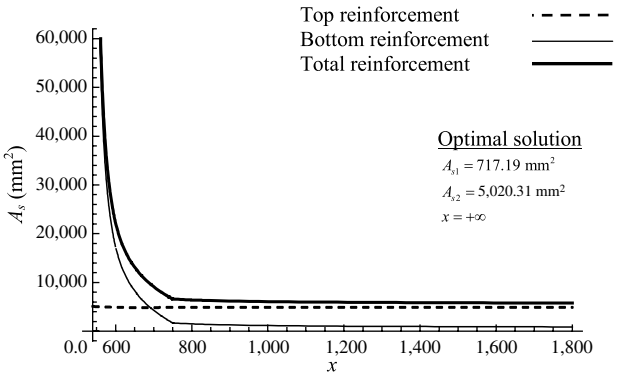

Fig. 9. RSD diagram for a point in segment a_1 in Fig. 8: $e_0/h=0.1$ and $\nu=1.5$

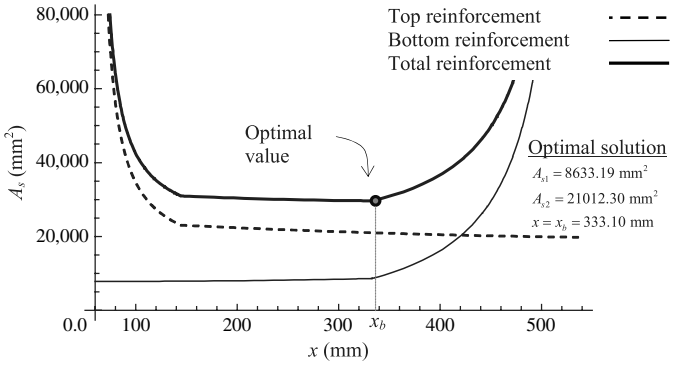

Fig. 10. RSD diagram for a point in segment c_1 in Fig. 8: $e_0/h=0.8$ and $\nu=1.5$

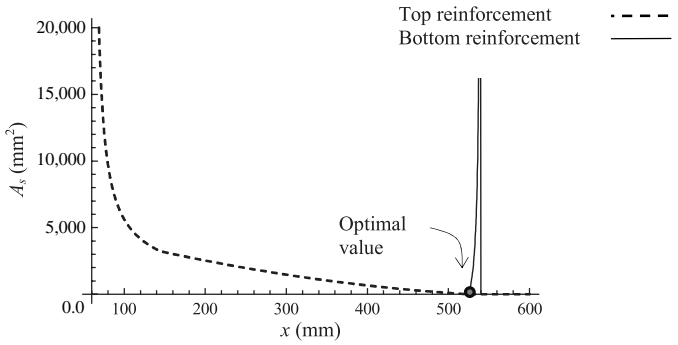

Fig. 11. RSD diagram for a point in segment a_2 in Fig. 8: $e_0/h=0.1$ and $\nu=0.7$; because either A_{s1} or A_{s2} are not positive for the same value of x, no solution is possible

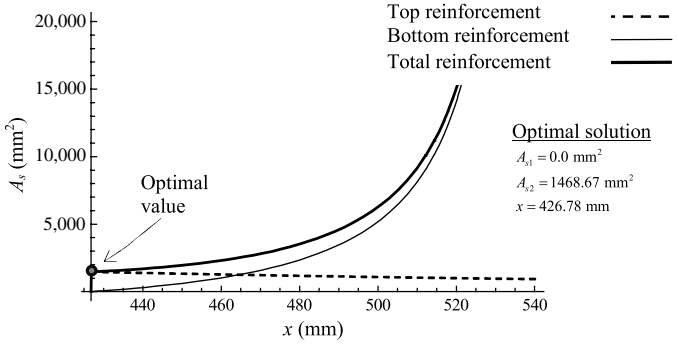

Fig. 12. RSD diagram for a point in segment b_2 in Fig. 8: $e_0/h=0.25$ and $\nu=0.7$

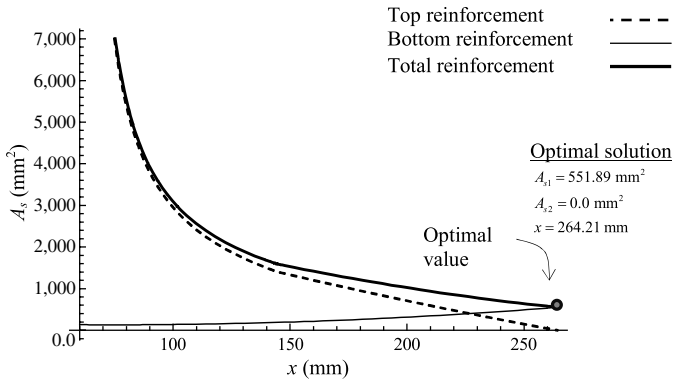

Fig. 13. RSD diagram for a point in segment b_3 in Fig. 8: $e_0/h=0.45$ and $\nu=0.3$

great enough to require the presence of both reinforcements (segment c_1 in domain 3 in Fig. 8), and in these circumstances, the additional condition $x=x_b$ must be imposed in order to take advantage of both concrete and bottom reinforcement.

The RSD diagrams corresponding to $e_0/h=0.1$ and $\nu=1.5$ (a point in segment a_1), and $e_0/h=0.8$ and $\nu=1.5$ (a point in segment c_1) have been represented in Figs. 9 and 10, respectively. The optimal reinforcements obtained from the RSDs confirm the validity of the results given in the chart in Fig. 8.

If a smaller value of the axial load is considered [$\nu=0.7$ (the vertical line 2 in Fig. 8)] for low values of eccentricity, the section is able to stand the external loads without reinforcement (segment a_2 in domain 0 in Fig. 8). Fig. 11 shows the RSD diagram for $\nu=0.7$ and $e_0/h=0.1$ (a point in segment a_2 in Fig. 8); it is evident from this figure that the equilibrium cannot be reached with $\sigma_c=\eta f_{cd}$, $A_{s1}\neq 0$, and $A_{s2}\neq 0$, and hence, for this situation, the optimal reinforcement corresponds to $\sigma_c<\eta f_{cd}$ and $A_{s1}=A_{s2}=0$.

As in the previous case, if the value of the axial load stays constant but the value of the eccentricity increases, then reinforcement

is required. As mentioned previously for $\nu = 1.5$, equilibrium may be reached without the presence of bottom reinforcement (segment b_2 in domain 2 in Fig. 8). The RSD for $e_0/h = 0.25$ and $\nu = 0.7$ (a point in segment b_2 in Fig. 8), represented in Fig. 12, confirms the results obtained from the proposed chart.

A final case, corresponding to the vertical line 3 in Fig. 8, also was analyzed. For the adopted value of axial load, $\nu = 0.3$, the optimal reinforcement corresponds to domain 0, domain 4, or domain 3 (segments a_3, b_3, and c_3, respectively, in Fig. 8) as e_0 increases. The RSD diagram for $\nu = 0.3$ and $e_0 = 0.45$ (a point in segment b_3 in Fig. 8), represented in Fig. 13, confirms that the optimal reinforcements corresponds to $A_{s2} = 0$, which is the condition in domain 4.

As in the former cases, as eccentricity—and hence the bending moment—increase, both reinforcements are required; and for the biggest values of e_0, the optimal reinforcement is associated with $x = x_b$.

Conclusions

This paper provides a geometric approach to determining the optimum design of rectangular RC subject to combined compression N and in-plane bending moment M. The solution is said to be geometric because it is based on the evaluation of the resulting equivalent eccentricity of the pair of external loads, $e_0 = M/N$. A new formulation of boundary values for e_0 is presented to let the designer know which condition of the TOSR must be imposed to get optimal reinforcement (A_{s1} and A_{s2}). These conditions have been represented graphically in a nondimensional chart as $e_0/h - \nu$ with $\nu = N/\eta f_{cd} hb$. The main advantage of this chart is that it allows the engineer to choose the optimal reinforcement easily. Some examples have proved the validity and compactness of the process.

Acknowledgments

Part of the present work was financed by the Spanish Ministry of Education. The second author is a Spanish government Ph.D. fellow (FPU grant AP 2010-3707). This support is gratefully acknowledged.

Notation

The following symbols are used in this paper:

A_c = concrete cross-section area;
A_{s1} = bottom reinforcement cross-section area;
A_{s2} = top reinforcement cross-section area;
b = cross-section width;
d = depth of centroid of bottom reinforcement, measured from top fiber;
d_1 = distance between bottom fiber and centroid of bottom reinforcement;
d_2 = depth of centroid of top reinforcement, measured from top fiber;
E_s = steel elastic modulus;
e_0 = equivalent eccentricity;
e_{0c} = boundary eccentricity value for condition $A_{s1} = A_{s2} = 0$;
e_{0h} = boundary eccentricity value for $x = +\infty$;
$e_{0\,\mathrm{lim}}$ = boundary eccentricity value for $x = x_b$;
e_{02} = boundary eccentricity value for $A_{s2} = 0$;
f_{cd} = design compressive strength of concrete (according to EC2);
f_{ck} = characteristic compressive strength of concrete (according to EC2);
f_{yd} = design yield strength of reinforcement (according to EC2);
f_{yk} = characteristic yield strength of reinforcement (according to EC2);
h = cross-section depth;
M = externally applied in-plane bending moment;
M_b = maximum resisting moment of the section in simple bending without top reinforcement;
N = externally applied compressive axial load;
N_c = concrete compression block resultant;
N_{s1} = bottom steel reinforcement stress resultant;
N_{s2} = top steel reinforcement stress resultant;
x = neutral axis depth;
x_b = neutral axis depth corresponding to a tensile strain of ε_y at bottom reinforcement and a compressive strain of ε_{cu} at top fiber;
α_{cc} = coefficient considering long-term effects on the compressive strength and unfavorable effects resulting from the way the load is applied (according to EC2);
γ_s = partial safety factor for concrete (according to EC2);
ε_c = strain at section centroid;
ε_{c2} = maximum concrete pure compression strain employing a parabolic and rectangular stress block (according to EC2);
ε_{c3} = maximum concrete pure compression strain employing a rectangular stress block (according to EC2);
ε_{cu2} = maximum concrete compressive strain employing a parabolic and rectangular stress block (according to EC2);
ε_{cu3} = maximum concrete compressive strain employing a rectangular stress block (according to EC2);
ε_{s1} = bottom reinforcement centroid strain;
ε_{s2} = top reinforcement centroid strain;
ε_{ud} = steel tensile strain limit;
ε_y = steel yield strain;
η = effective concrete strength factor;
λ = depth of an equivalent rectangular compressive stress block relative to the neutral axis depth (according to EC2);
σ_c = concrete compression;
σ_{s1} = bottom reinforcement stress;
σ_{s2} = top reinforcement stress;
ν = reduced compression load; and
ϕ = curvature of the cross section.

References

Aschheim, M., Hernández-Montes, E., and Gil-Martín, L. M. (2007). "Optimal domains for strength design of rectangular sections for axial load and moment according to Eurocode 2." *Eng. Struct.*, 29(8), 1752–1760.

Barros, A. F. M., Barros, M. H. F. M., and Ferreira, C. C. (2012). "Optimal design of rectangular RC sections for ultimate bending strength." *Struct. Multidisciplin. Optim.*, 45(6), 845–860.

Barros, M. H. F. M., Martins, R. A. F., and Barros, A. F. M. (2005). "Cost optimization of singly and doubly reinforced concrete beams with EC2-2001." *Struct. Multidisciplin. Optim.*, 30(3), 236–242.

Camp, C. V., Pezeshk, S., and Hansson, H. (2003). "Flexural design of reinforced concrete frames using a genetic algorithm." *J. Struct. Eng.*, 10.1061/(ASCE)0733-9445(2003)129:1(105), 105–115.

Comité Européen de Normalisation (CEN) Eurocode 2. (2001). "Design of concrete structures—Part 1-1: General rules and rules for buildings." *EN 1992-1-1*, CEN European Committee for Standardization, Brussels.

Gil-Martín, L. M., López-Martín, D., Hernández-Montes, E., and Aschheim, M. (2012). "Dimensionamiento en rotura a flexión de secciones de hormigón armado. Un planteamiento compacto." *Informes de la Construcción*, 64, 497–505.10.3989/ic.11050

Hernández-Montes, E., Aschheim, M., and Gil-Martín, L. M. (2004). "Impact of optimal longitudinal reinforcement on the curvature ductility capacity of reinforced concrete column sections." *Mag. Concr. Res.*, 56(9), 499–512.

Hernández-Montes, E., Gil-Martín, L. M., and Aschheim, M. (2005). "Design of concrete members subjected to uniaxial bending and compression using reinforcement sizing diagrams." *ACI Struct. J.*, 102(1), 150–158.

Hernández-Montes, E., Gil-Martín, L. M., Pasadas-Fernández, M., and Aschheim, M. (2008). "Theorem of optimal reinforcement for reinforced concrete cross sections." *Struct. Multidisciplin. Optim.*, 36(5), 509–521.

Lee, C., and Ahn, J. (2003). "Flexural design of reinforced concrete frames by genetic algorithm." *J. Struct. Eng.*, 10.1061/(ASCE)0733-9445(2003)129:6(762), 762–774.

López-Martín, D., Gil-Martín, L. M., Hernández-Montes, E., and Aschheim, M. (2011). "Dominios de deformación referidos a la excentricidad de cálculo para el diseño óptimo de secciones rectangulares solicitadas a flexo-compresión." *1st Intl. Cong. Mech. Models Struct. Eng.*, Godel Impresiones Digitales, Granada, Spain, 93–106.

Nawy, E. G. (2003). *Reinforced concrete: A fundamental approach*. 5th Ed., Prentice-Hall, Upper Saddle River, NJ.

ISI Web of Knowledge℠

Journal Citation Reports®

WELCOME HELP RETURN TO JOURNAL

2012 JCR Science Edition

Rank in Category: JOURNAL OF STRUCTURAL ENGINEERING-ASCE

Journal Ranking

For **2012**, the journal **JOURNAL OF STRUCTURAL ENGINEERING-ASCE** has an Impact Factor of **1.206**.

This table shows the ranking of this journal in its subject categories based on Impact Factor.

Category Name	Total Journals in Category	Journal Rank in Category	Quartile in Category
CONSTRUCTION & BUILDING TECHNOLOGY	57	16	Q2
ENGINEERING, CIVIL	122	39	Q2

Category Box Plot

For **2012**, the journal **JOURNAL OF STRUCTURAL ENGINEERING-ASCE** has an Impact Factor of **1.206**.

This is a box plot of the subject category or categories to which the journal has been assigned. It provides information about the distribution of journals based on Impact Factor values. It shows median, 25th and 75th percentiles, and the extreme values of the distribution.

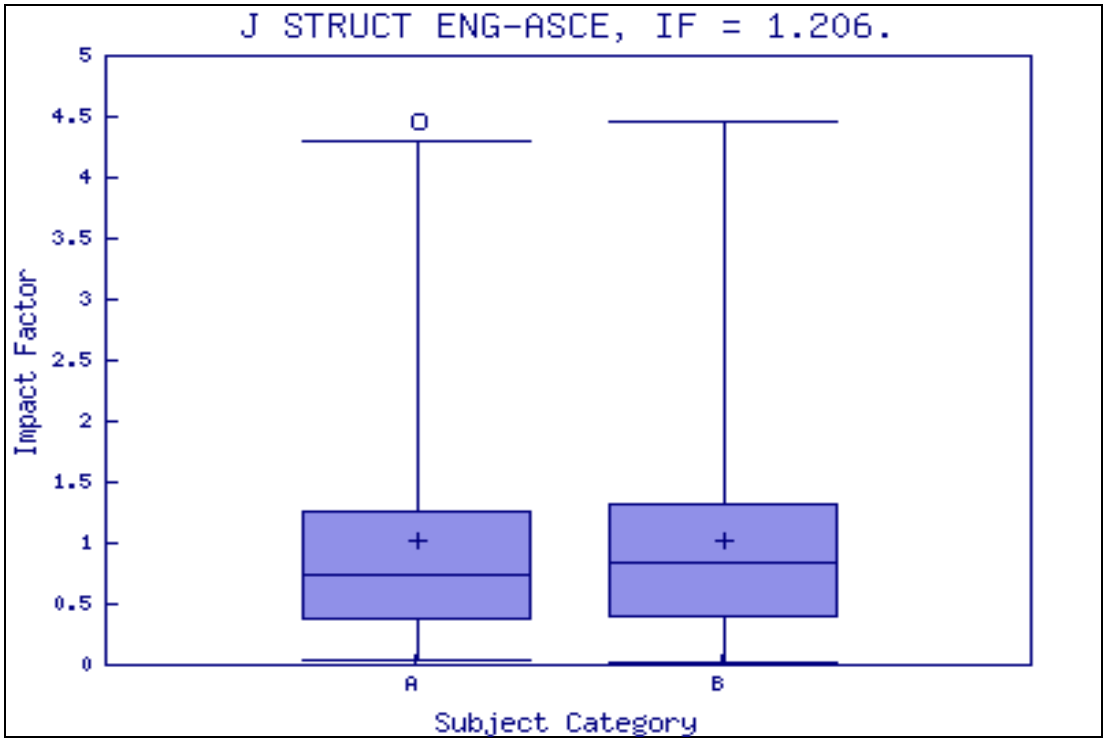

Key

A - CONSTRUCTION & BUILDING TECHNOLOGY

B - ENGINEERING, CIVIL

AUTHOR QUERY FORM

ELSEVIER

Journal: JEST

Article Number: 4771

Please e-mail or fax your responses and any corrections to:

E-mail: corrections.esch@elsevier.sps.co.in

Fax: +31 2048 52799

Dear Author,

Please check your proof carefully and mark all corrections at the appropriate place in the proof (e.g., by using on-screen annotation in the PDF file) or compile them in a separate list. Note: if you opt to annotate the file with software other than Adobe Reader then please also highlight the appropriate place in the PDF file. To ensure fast publication of your paper please return your corrections within 48 hours.

For correction or revision of any artwork, please consult http://www.elsevier.com/artworkinstructions.

Any queries or remarks that have arisen during the processing of your manuscript are listed below and highlighted by flags in the proof. Click on the 'Q' link to go to the location in the proof.

Location in article	Query / Remark: click on the Q link to go Please insert your reply or correction at the corresponding line in the proof
Q1	Please confirm that given name(s) and surname(s) have been identified correctly.
Q2	The decimal comma has been changed to a decimal point for the value '0,8' globally. Please check, and correct if necessary.
Q3	Please check the hierarchy of the section headings.
Q4	Please check the page range in all references.

Please check this box if you have no corrections to make to the PDF file ☐

Thank you for your assistance.

Highlights

• Slabs in a similar way to beams present a hypothesis related to plane deformation. • The plane section hypothesis is used in strength design of beams. • No deformation hypothesis is used in strength design of slabs. • This paper presents a deformation hypothesis for strength design of RC slabs.

Engineering Structures xxx (2014) xxx–xxx

Contents lists available at ScienceDirect

Engineering Structures

journal homepage: www.elsevier.com/locate/engstruct

Limits to the strength design of reinforced concrete shells and slabs

Enrique Hernández-Montes, Juan F. Carbonell-Márquez*, Luisa M. Gil-Martín

Department of Structural Mechanics, University of Granada (UGR), Campus Universitario de Fuentenueva s/n, 18072 Granada, Spain

ARTICLE INFO

Article history:
Received 4 May 2013
Revised 25 October 2013
Accepted 8 January 2014
Available online xxxx

Keywords:
Reinforced concrete
Shell
Slab
Optimization
Balance point

ABSTRACT

One of the most important works in the ultimate limit state design of reinforced concrete plates or shells subjected to flexure and membrane actions is the one provided by Brondum-Nielsen (1974). Therein, the author divides the shell element into three layers; the outer layers withstand a state of membrane forces located on their middle surfaces. The forces at the centroid of the reinforcement, in both directions, have been obtained from equilibrium, and the steel area needed is computed by dividing these tension forces by the steel yield stress, f_y. An extension to the strain plane hypothesis widely used in the strength design of RC beams and columns is presented, aiming at RC strength design of shells and slabs. As a result, limits to the application of the Bromdum-Nielsen procedure are given in this work since it cannot always be guaranteed that the stress in the steel is f_y as the original method proposes. A new method based on the computation of the balance point in the beam flexure design is developed to check the limits of application of Brondum-Nielsen's approach. The Upper Bound Theorem of plasticity guaranties that the obtained forces are on the safe side. Examples are provided.

1. Introduction

Capacity of reinforced concrete (RC) shells and slabs has always been an interesting topic, e.g. [1–3]. The problem of designing the reinforcement for a concrete plate or shell in ultimate limit state to withstand membrane forces together with bending and torsion moments has not yet been universally solved. As a consequence, the main RC design codes – Eurocode 2 [4], AC1 318 [5] – do not provide a general method to deal with this problem as they do with the beam cross section design. Only the Model Code CEB-FIP 2010 (MC2010) [6] states, literally, that "shell elements may be modelled as comprising three layers. The outer layers provide resistance to the in-plane effects of both the bending and the in-plane axial loading, while the inner layer provides a shear transfer between the outer layers." But the designer would have difficulty finding further information on this issue.

You can find many different techniques in literature that try to obtain a generally accepted solution. One of the first practical approaches to this problem is the report by Brondum-Nielsen [7]. This work deals with the shell element as if it were a sandwich element composed of three layers, with the outer layers being responsible for withstanding the membrane force decomposition of the external bending, torsion, in-plane axial and in-plane shear loading. Each of these layers contains an orthogonal reinforcing net. Gupta [8] takes the work of Brondum-Nielsen as a reference to propose a general solution based on an iterative trial-and-error design method using the principle of minimum resistance by also dividing the shell into three layers containing the orthogonally provided reinforcement. Marti [9] assigns the out of plane shear to the middle layer, complementing the work of Brondum-Nielsen. Lourenço and Figueiras [10,11] formulated the problem of reinforcing elements subjected to membrane and flexural forces based on equilibrium conditions and suggested a new iterative procedure. They have developed a consistent solution to the problem analyzing the shell element as a whole and not as two membrane outer layers. The information concerning this approach has been compiled by Fall et al. [12] in their revision of procedures of reinforcing methods in RC tailor-made structures. A similar approach to the one presented by Gupta is implemented in an iterative numerical computational algorithm by Min [13] and tested in several experimental examples. Furthermore, nonlinear inelastic analyses are performed using the Mahmoud-Gupta's computer program [14–17] to prove the adequacy of the presented equations. A similar formulation of the problem is adopted by Tomás and Martí [18] in order to mathematically optimize the amount of reinforcement in each finite element of the mesh that models the geometry of the problem, employing the summation of the tensile forces in the reinforcement as the objective function. One of the most recent works in this field is the one proposed by Bertagnoli et al. [19] where the authors provide a method based on sandwich layers to optimize the amount of reinforcing steel to be placed in the two outer layers. The method considers non-orthogonal reinforcement layouts, and the optimization procedure is based on genetic algorithms.

* Corresponding author. Tel.: +34 958249965; fax: +34 958249959.
E-mail addresses: emontes@ugr.es (E. Hernández-Montes), jfcarbonell@ugr.es (J.F. Carbonell-Márquez), mlgil@ugr.es (L.M. Gil-Martín).

0141-0296/$ - see front matter © 2014 Published by Elsevier Ltd.
http://dx.doi.org/10.1016/j.engstruct.2014.01.011

Nomenclature

a	distance between the middle surfaces of the top and bottom layers
a_b, a_t	distances between the middle surfaces of bottom and top layers to the middle surface of the shell, respectively
c_b, c_t	depth of bottom and top layers, respectively
c_{b0}	first approximation of c_b
$c_{ki\mathrm{lim}}$	limit depth of layer k ($k = t$ for top layer; $k = b$ for bottom layer) in order to yield the reinforcement in i direction (x or y) placed in the opposite layer j
d	depth of the reinforcement
f_c	concrete compression strength
f_y	yield stress of the reinforcement
E_s	Young's modulus of the steel
e_k	distance between the middle layer of the shell element to the centroid of the reinforcement placed in layer k
h	depth of the shell element
z_{ya}	lever arm of $N_{yat} + N_{yab}$ related to the center of gravity of the gross section
z_{yat}	lever arm of N_{yat} related to the center of gravity of the gross section
z_{yab}	lever arm of N_{yab} related to the center of gravity of the gross section
z_{xa}, z_{xat}, z_{xab}	idem for $N_{xat} + N_{xab}$, N_{xat} and N_{xab}
M_a	flexural moment considered for the first estimation of c_b
M_x, M_y	bending moments in x and y directions applied to the shell element
M_{xy}	twisting moment applied to the shell element
N	axial force
N_x, N_y	normal forces in x and y directions applied to the shell element
N_{xy}	shear force applied to the shell element
N_{xk}, N_{yk}	membrane normal forces in x and y directions in layer k
N_{xyk}	membrane shear force in layer k
N_{xak}, N_{yak}	tension forces in reinforcement placed in x and y directions in layer k
N_{ck}	concrete compression force in layer k
$N_{total,k}$	$N_{total,k} = N_{xak} + N_{yak}$. Summation of tension forces in the reinforcement placed in x and y directions in layer k
α_k	angle between crack and x direction, in layer k
ε_{cu}	concrete ultimate compressive strain
$\varepsilon_{j\text{-}i}$	steel strain in i direction, placed in layer j, when the depth of compression block in layer k is c_k
$\varepsilon_{j\text{-}i\mathrm{lim}\text{-}\alpha k}$	strain measured, in the direction of the crack of layer k (α_k), at the level of centroid of reinforcement placed in layer j corresponding to the yield of the steel in i direction
ε_y	tension yield strain of the reinforcement
λ	stress block factor of the rectangular stress distribution in concrete according Eurocode 2
σ	stress
α_k	angle between the crack in layer k and x-direction
χ_{klim}	depth of the balance point

Subscript

a	steel
b	bottom layer
i	x or y direction
j	layer j, opposite layer to layer k
k	layer k (top or bottom layer)
x	direction x
lim	balance conditions
y	direction y

Superscript

$*$	actual value

It is extraordinary that, despite all the aforementioned works, one of the most powerful and popular commercial pieces of software in structural design, the SAP2000©, uses the very first of one of these methods (Brondum-Nielsen's approach) to design the reinforcement of concrete shells in ultimate limit state under bending and in-plane axial forces [20].

Apart from dividing the shell element into some layers, all the presented works have another aspect in common with respect to the stresses in the reinforcement and in the concrete. The compressive stress in concrete – compression struts – should be distributed uniformly throughout the depth of the layer and the steel in tension is assumed to be yielded, – i.e. with stress equal to f_y – the later hypothesis is also known as limit-analysis solution. Both the tensile stress in concrete and the compressive stress in the reinforcement are neglected.

The part concerning the yielding of the reinforcement is found to be questionable by the authors of this study. Similarly, as in the case of ultimate state of bending in beams, where the plane sections hypothesis has to be satisfied, the strain in the reinforcement of one of the outer layers in a slab element should be related to the depth of the compression stress block in the opposite one.

This paper presents a necessary hypothesis to the strength design of reinforced concrete shells and slabs. Furthermore Marti [9] expresses an attempt to limit the applicability of Brondum-Nielsen's method "... these equations are only valid if the concrete compressive strength of the sandwich cover is not exceeded" – he calls cover to the thickness of the layer. His attempt, although interesting, is an inaccurate observation that limits his design to small axial forces and he fails to provide a basic understanding of the behavior of steel. Nonetheless an extension of the well established assumptions considered in the strength design of beams under bending is indeed a good advance in the reinforced concrete design of slabs and shells.

The present work draws on the formulation of the problem given in Brondum-Nielsen's procedure [7] to set the domains where this approach is valid. Firstly, Brondum-Nielsen's method is explained in a more compact fashion and the paper is therefore self-contained. Later, the beam balance point analogy is stated in order to determine reasonable limits to the application of Brondum-Nielsen's method. Finally, the original example given in Brondum-Nielsen's report is explained and the limits of application are checked.

2. Membrane forces decomposition of externally applied loads

The concrete shell element considered in this work has to withstand the established normal forces N_x and N_y, the shear force N_{xy}, the bending moments M_x and M_y and the twisting moment M_{xy}. These actions are given per unit of length. Actions are considered positive if they are directed as indicated in Fig. 1(a). The shell element has one or two parallel layers of orthogonal reinforcing net of which the position is known. The depth of the shell element is h.

Please cite this article in press as: Hernández-Montes E et al. Limits to the strength design of reinforced concrete shells and slabs. Eng Struct (2014), http://dx.doi.org/10.1016/j.engstruct.2014.01.011

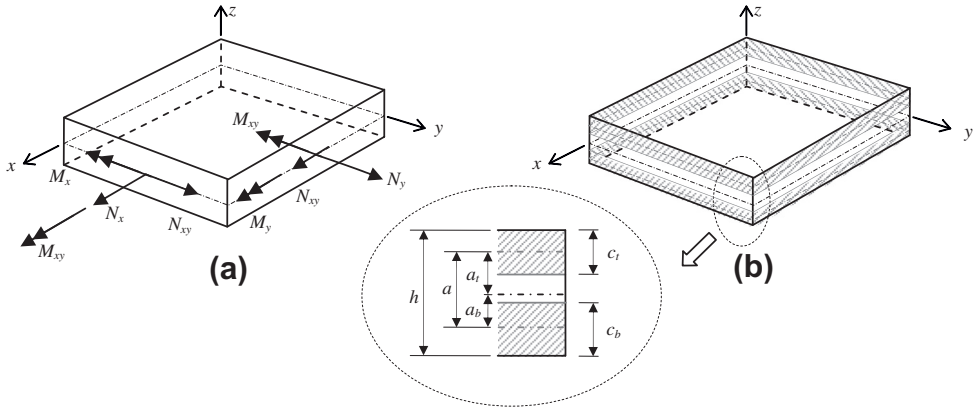

Fig. 1. (a) Applied actions to the shell element; (b) Sandwich layers geometry.

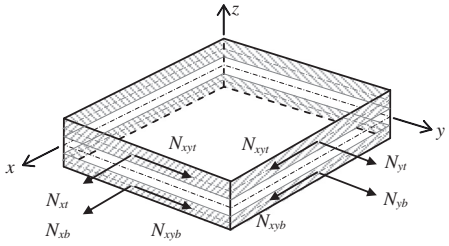

Fig. 2. Membrane forces decomposition of the state of actions applied to the shell element.

Taking into account the state of the applied loads (Fig. 1(a)) and the geometry of the sandwich shell element (Fig. 1(b)), all forces and moments acting in the shell element may be resolved into membrane forces applied at the middle surface of top and bottom outer layers according to equilibrium equations: Eq. (1), as shown in Fig. 2. Sub-indexes t and b refer to the top and bottom layer, respectively. The terms c_t and c_b are the depth of the outer layers, a_t and a_b are the distances between their middle surfaces and the middle surface of the shell element and a is the distance between the top and bottom middle surfaces, as indicated in Fig. 1(b).

$$N_{xt} = N_x \frac{a_b}{a} - \frac{M_x}{a} \quad N_{xb} = N_x \frac{a_t}{a} + \frac{M_x}{a}$$
$$N_{yt} = N_y \frac{a_b}{a} - \frac{M_y}{a} \quad N_{yb} = N_y \frac{a_t}{a} + \frac{M_y}{a} \qquad (1)$$
$$N_{xyt} = N_{xy} \frac{a_b}{a} - \frac{M_{xy}}{a} \quad N_{xyb} = N_{xy} \frac{a_t}{a} + \frac{M_{xy}}{a}$$

3. Limit analysis of each membrane layer

Consider now the layer k of the above sandwich element, it is cracked under the actions of the external forces, and layer j is the opposite outer layer. If k refers to top layer, then $k = t$ and $j = b$, and vice versa. Fig. 3 shows a portion of this layer, with two of its sides being parallel to the x and y directions and the third one corresponding to a crack in the membrane, which forms an angle α_k with x direction. The length of this crack is taken equal to 1.

From equilibrium in Fig. 3(a), the forces in the reinforcement per unit of length in both x and y directions, N_{xak} and N_{yak}, can be obtained:

$$N_{xak} \sin\alpha_k = N_{xk} \sin\alpha_k + |N_{xyk}| \cos\alpha_k \rightarrow \boxed{N_{xak} = N_{xk} + |N_{xyk}| \cot\alpha_k} \qquad (2)$$

$$N_{yak} \cos\alpha_k = N_{yk} \cos\alpha_k + |N_{xyk}| \sin\alpha_k \rightarrow \boxed{N_{yak} = N_{yk} + |N_{xyk}| \tan\alpha_k} \qquad (3)$$

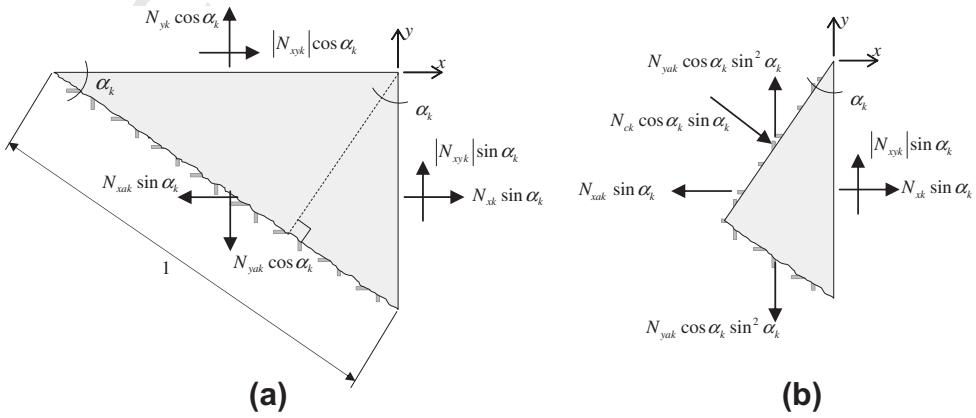

Fig. 3. Equilibrium of forces in a cracked membrane element: (a) Forces in the reinforcement to equilibrate normal and shear forces; (b) Principal compressive concrete force.

The direction of the principal compressive membrane force in the concrete, N_{ck}, is parallel to the crack and is, therefore, applied perpendicular to a section as indicated by the dashed line in Fig. 3(a). The value of the principal compression in concrete N_{ck} is obtained in Eq. (4) from equilibrium in x direction in Fig. 3(b) and considering Eq. (2):

$$N_{xak}\sin\alpha_k = N_{xk}\sin\alpha_k + N_{ck}\cos^2\alpha_k\sin\alpha_k \rightarrow \boxed{N_{ck} = |N_{xyk}|\left(\tan\alpha_k + \cot\alpha_k\right)} \tag{4}$$

There is a variable in the above presented equations, i.e. the crack direction α_k, that needs to be chosen by the designer. As it is in the designer's interest to find the optimum reinforcement, this variable α_k will have a specific value.

If it is assumed that the reinforcement placed at layer k has yielded, the total amount of steel needed will be proportional to the summation of tension forces in the reinforcement in this layer, $N_{total,k} = N_{xak} + N_{yak}$. So, the value of α_k that corresponds to the minimum reinforcement can be obtained by partial derivative of the summation of Eqs. (2) and (3):

$$\frac{\partial N_{total,k}}{\partial \alpha_k} = 0 \rightarrow |N_{xyk}|\left(-\frac{1}{\sin^2\alpha_k} + \frac{1}{\cos^2\alpha_k}\right) = 0 \rightarrow \sin\alpha_k = \cos\alpha_k \rightarrow \boxed{\alpha_k = 45^\circ} \tag{5}$$

Solutions given by Eqs. (2)–(4) are valid if $N_{xak} \geqslant 0$ and $N_{yak} \geqslant 0$, that is, both x and y reinforcements are subjected to tension forces, in this case $\alpha_k = 45^\circ$ is chosen for the reinforcement design. If this condition is not met, one of the following cases can be found. It is interesting to notice that the classification below has been made based on the limit of applicability of Eqs. (2)–(4), i.e.: $\alpha_k = 45^\circ$ and $N_{xak} \leqslant 0$ and/or $N_{yak} \leqslant 0$.

a. If $N_{xk} < -|N_{xyk}|$ and $N_{yk} \geqslant -|N_{xyk}|$, the reinforcement in the x direction is compressed. In this situation $N_{xak} = 0$ – no reinforcement in x direction is required – and the crack angle, α_k, can be obtained from Eq. (2) imposing $N_{xak} = 0$. In this situation, the angle that defines the orientation of the crack in the membrane is given by the following equation:

$$\alpha_k = \arctan\left(\frac{|N_{xyk}|}{-N_{xk}}\right) \tag{6}$$

b. If $N_{yk} < -|N_{xyk}|$ and $N_{xk} \geqslant -|N_{xyk}|$, the reinforcement in the y direction is compressed. In this situation $N_{yak} = 0$ – no reinforcement in y direction is required – and the crack angle, α_k, can be obtained from Eq. (3) imposing $N_{yak} = 0$. Now, the angle α_k can be obtained from the following equation:

$$\alpha_k = \arctan\left(\frac{-N_{yk}}{|N_{xyk}|}\right) \tag{7}$$

c. If $N_{xk} < -|N_{xyk}|$ and $N_{yk} < -|N_{xyk}|$, both reinforcements in the x and y directions are compressed. Therefore, $N_{xak} = N_{yak} = 0$ – no reinforcement in either x or y direction is required – and the maximum compression in concrete can be calculated from the Mohr's circle representation of the tensor of forces N in layer k (Fig. 4). Being:

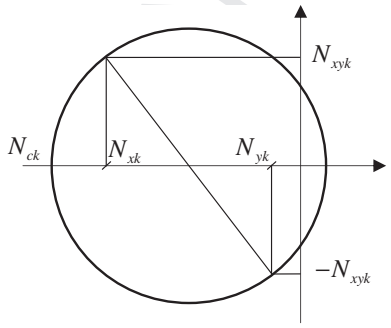

Fig. 4. Mohr's circle of forces for the case $N_{xk} < -|N_{xyk}|$ and $N_{yk} < -|N_{xyk}|$.

$$N_{ck} = \frac{1}{2}(N_{xk} + N_{yk}) - \frac{1}{2}\sqrt{(N_{xk} - N_{yk})^2 + 4N_{xyk}} \tag{8}$$

4. Concrete compression block

According to Eq. (1), the membrane forces acting on both top and bottom layers and, consequently, the forces in the concrete strut and in the reinforcement would be completely determined if the geometry of the sandwich shell element were defined, that is, if the values c_t and c_b are known.

Assuming that the middle surface of one of the layers corresponds to the centroid of the tension reinforcement required for the predominant bending, then, once this net is placed, the thickness of the corresponding layer is known. So, only the thickness of the opposite layer needs to be estimated.

As previously mentioned, the Brondum-Nielsen method [7] considers that the principal compressive force N_{ck} in the concrete is made resistant by a uniformly distributed stress in a depth equal to the thickness of the layer, c_k (Eq. (9) and Fig. 5 for the case of the top layer, $k = t$). In Eq. (9) f_c is the compressive strength of the concrete.

$$c_k = \frac{N_{ck}}{f_c} \tag{9}$$

The former assumption resembles the Whitney's stress block used in the ultimate design of beams.

Imagine now that we are dealing with a beam whose cross section is A–A in Fig. 5; and this section is subjected to a bending

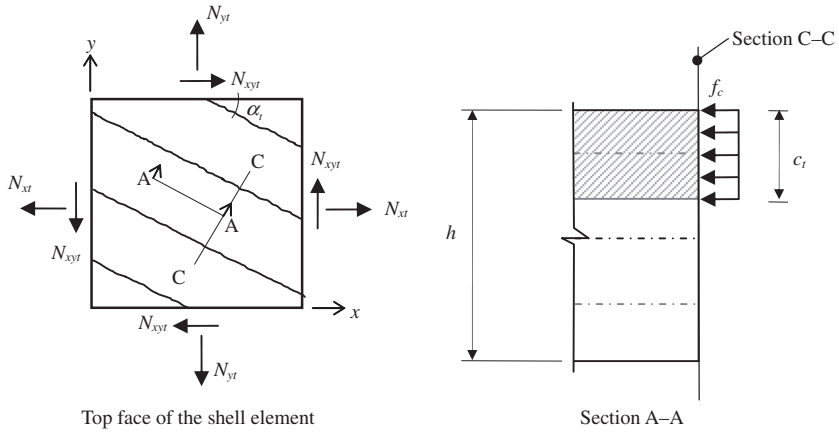

Fig. 5. Compressive stress in top layer.

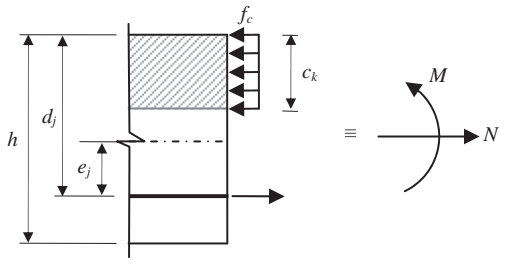

Fig. 6. Combined flexure and axial action in a beam.

moment M that comprises the upper part of the cross-section and to a tensile axial force N applied at the centroid of the section (Fig. 6). If moments are taken at the level of the tension reinforcement, the resultant moment M_a is:

$$M_a = M - Ne_j \tag{10}$$

e_j being the distance between the centroids of the section and the tension reinforcement in layer j.

This moment M_a has to be balanced by the compression in the concrete in a depth equal to c_k. Therefore:

$$M_a = c_k f_c \left(d_j - \frac{c_k}{2}\right) \tag{11}$$

where d_j is the distance between the upper fiber in the cross-section (i.e. the most compressed one) and the level of the tension reinforcement placed in layer j opposite to k (Fig. 6). As indicated above, if the depth of the compression block is to be computed in the top layer, then $k = t$ and $j = b$, and vice versa.

The value of the depth of the compression block, c_k, is an unknown. Brondum-Nielsen adopts as a first estimation of c_k the one obtained from Eq. (11) M_a being the one obtained from Eq. (10) where M and N are the predominant bending moment and its corresponding axial force per unit of length, respectively, acting on the slab considered. Although a better approach to trigger the procedure may be obtained by using $M + |M_{xy}|$ instead of M – as used in the RC design of elements to bending plus torsion, the authors have adopted Brondum-Nielsen's original approach in what follows, see Fig. 7.

5. The application of the approach

According to Eq. (1), the geometry of the sandwich element – c_t and c_b – has to be known to compute the values of the membrane forces N_{xk}, N_{yk} and N_{xyk}. At the same time, this geometry depends on those membrane forces – Eq. (9). Thus, the problem has to be tackled in an iterative manner.

In all the above stated, it had been assumed that the reinforcement under tension due to the predominant bending is placed in the middle of the layer whereas a first estimation of the thickness of the opposite layer is obtained from Eq. (11). It is important to point out that the reinforcement placement is usually governed by the requirements of concrete cover.

Once the positions of the reinforcement in both layers, and as a result its thicknesses, are known, the external actions (N_x, N_y, N_{xy}, M_x, M_y and M_{xy}) can be resolved into membrane forces in the outer layers of the sandwich and the procedure proposed by Brondun-Nielsen [7] can be applied.

Fig. 7 shows a flow chart that explains in detail the entire process proposed by Brondun-Nielsen [7]. If predominant moment M compresses top fiber, then $k = t$ and $j = b$. On the other hand, if the bottom layer is compressed by M, then $k = b$ and $j = t$.

After the whole process has been completed, once the geometry of both layers is known and forces in the reinforcements of both outer layers have been obtained from Eqs. (2) and (3), it is necessary to resolve the forces at the centroids of the actual levels of the reinforcements if they have not already been computed at those levels.

6. Plane strain distribution for ultimate state of RC slabs in bending

Once the tension forces in both x and y reinforcement – N_{xat}, N_{yat}, N_{xab}, N_{xab} – have been calculated from Eqs. (2) and (3), it is necessary to compute the required areas of steel to withstand these tension forces in both directions – x and y – and in both layers – top and bottom.

In the example given in Brondum-Nielsen's work [7] these areas are computed by dividing the obtained tension forces – N_{xa} and N_{ya} by the prescribed steel design strength, taken as the steel yield stress, f_y. However, this procedure can be reconsidered because the actual state of steel stress should depend on the compression block depth, as it occurs in the ultimate design of beams.

Back to the shell element case, assuming that Kirchhoff's hypothesis of plane sections is satisfied, it is evident from comparison with the beam case that the tensile stress in the reinforcement cannot always be considered equal to f_y without paying attention to the value of c_k.

The beam section shown in Fig. 6 is now subjected to the bending moment M and the axial force N, as presented in Fig. 8. Satisfying the plane sections hypothesis, if the applied actions cause a top

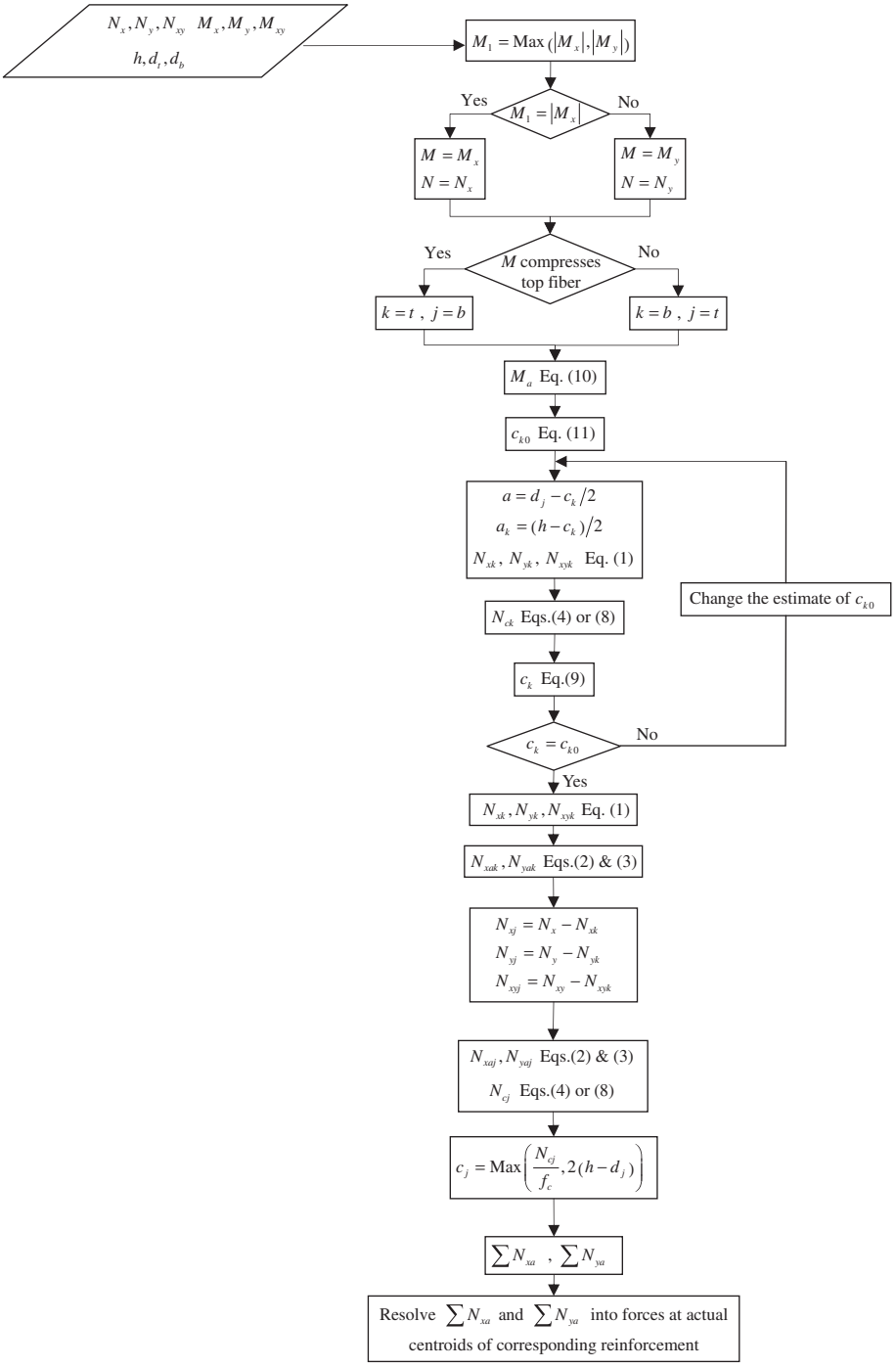

Fig. 7. Flow chart detailing the Brondum-Nielsen approach.

fiber strain equal to concrete ultimate compression strain, ε_{cu}, and a strain at level of tensile reinforcement equal to steel yield strain, ε_y, then the section is said be in *balance conditions*, [21,22]. At this point, the compression block depth is $c_{k\text{lim}}$ and the distance from the uppermost fiber of the cross section to the neutral fiber is $\chi_{k\text{lim}}$. Both values are related by a coefficient λ taken as 0.8 according to EC2 [4] for $f_c \leqslant 50$ MPa. In the case of ultimate limit state of bending if the neutral fiber depth becomes greater than $\chi_{k\text{lim}}$ the strain at reinforcement level is lower than ε_y and, consequently, the steel stress is lower than f_y.

If the cross section given in Fig. 8 corresponded to a RC shell element and it were positioned parallel to the direction of the principal compressive stress in the concrete (section A–A in Fig. 5), the compression block in one layer would lead to the yielding of the reinforcement in the opposite layer just under some circumstances as outlined below.

In the beam represented in Fig. 8, the direction of the reinforcement coincides with the direction of the compressive force in concrete. In this case, the depth of the compression block, $c_{k\text{lim}}$, corresponding to the balance point can be obtained from the expression:

$$c_{k\,\text{lim}} = \lambda \cdot d_j \frac{\varepsilon_{cu}}{\varepsilon_y + \varepsilon_{cu}} \tag{12}$$

Please cite this article in press as: Hernández-Montes E et al. Limits to the strength design of reinforced concrete shells and slabs. Eng Struct (2014), http://dx.doi.org/10.1016/j.engstruct.2014.01.011

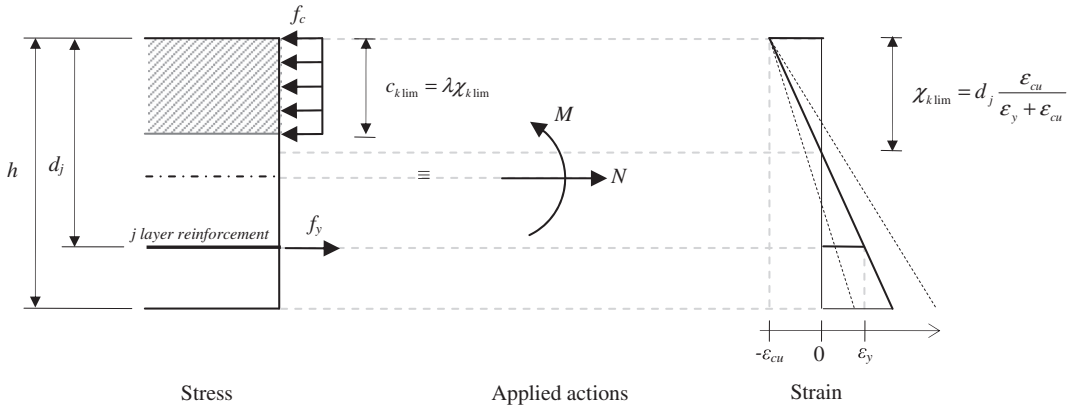

Fig. 8. Combined flexure and axial action in a beam: balance point determination.

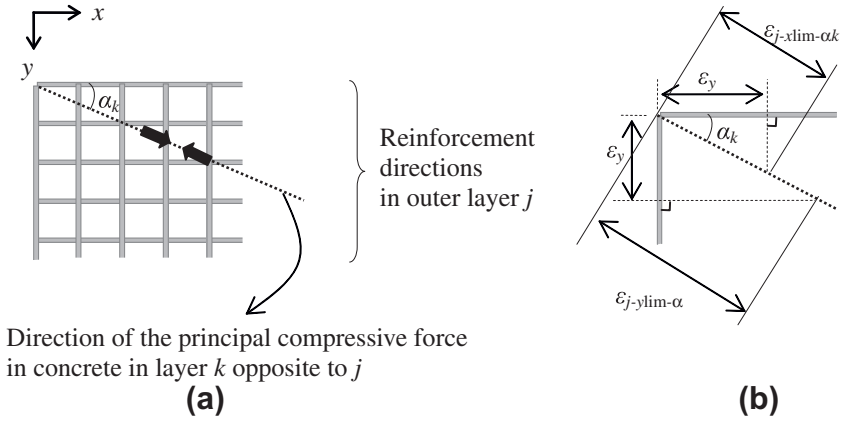

Fig. 9. Strain decomposition.

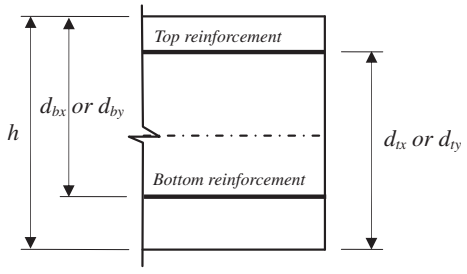

Fig. 10. Nomenclature.

In the case of RC slabs, the orientation of the principal compressive force in the concrete in the outer layer k, α_k, does not generally coincide with the orientation of the reinforcement (x and y directions, respectively) in the opposite outer layer j, as presented in Fig. 9(a).

The hypotheses of the plane strain distribution for ultimate design of RC slabs in bending and torsion are:

1. Ultimate strength of RC slabs in bending and torsion with or without axial force behaves in accordance with an ultimate plane strain distribution.
2. The orientation of the ultimate plane strain distribution in the plane of the slab is defined by the principal direction of compression in concrete.

Since both hypotheses are to be used in a design process, the Upper Bound Theorem of plasticity guaranties that the forces obtained using these hypotheses are an upper value of the true collapse forces.

Stress–strain models of concrete and steel in ultimate strength design have to comply with those approved by Standards such as Eurocode 2 or ACI-318.

In line with both hypotheses, if a sandwich model is used, such as Brondum-Nielsen's [7] or Marti's [9], the principal compressive direction in one layer coincides with the principal tensile strain direction in the opposite one, as shown in Fig. 9(a) and (b). According to the second hypothesis, the principal direction is given by the principal compressive direction in the compressed layer (k). Therefore yielding of the steel placed in layer j and in each direction x or y of reinforcement corresponds to a yielding strain in the direction of the crack of the opposite layer α_k given by (Fig. 9(b)):

$$\varepsilon_{j-x\,\mathrm{lim}-\alpha k} = \frac{\varepsilon_y}{\cos\,\alpha_k}$$
$$\varepsilon_{j-y\,\mathrm{lim}-\alpha k} = \frac{\varepsilon_y}{\sin\,\alpha_k} \qquad (13)$$

The maximum value of the thickness of layer k for which the yielding of the steel placed in the opposite layer j occurs, can be obtained from:

$$c_{ki\,\mathrm{lim}} = \lambda \cdot d_{ji} \cdot \frac{\varepsilon_{cu}}{\varepsilon_{j-i\,\mathrm{lim}-\alpha k} + \varepsilon_{cu}} \qquad (14)$$

d_{ji} being the position of the reinforcement in i direction ($i = x$ or y) placed in the j layer opposite the compressed layer k with respect to the furthest fiber of the cross section, as indicated in Fig. 10.

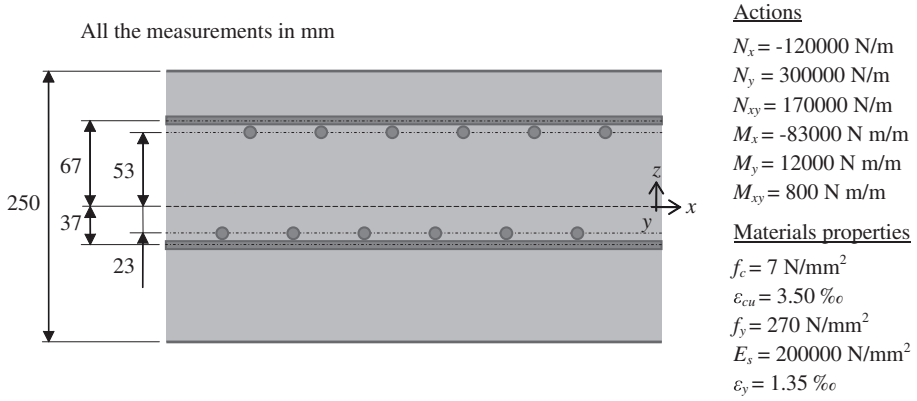

Fig. 11. Section of the slab studied by Brondum-Nielsen and external loads. Adapted from [7].

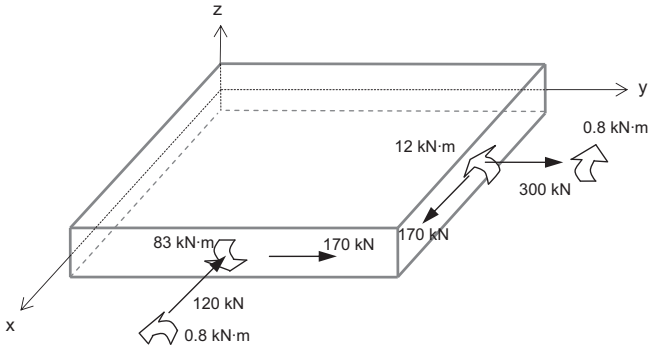

Fig. 12. Orientation of the external actions on the slab.

Once $c_{ki\lim}$ is known (i.e. $c_{kx\lim}$ and $c_{ky\lim}$), the designer has to compare the obtained value of c_k from the Brondum-Nielsen's approach with $c_{kx\lim}$ and $c_{ky\lim}$. If c_k is lower than the minimum $c_{ki\lim}$ then the stress in the tension reinforcement in i direction in the opposite layer j can be considered f_y. On the contrary, the geometry in the slab has to be altered in order to achieve the yielding of the reinforcement or if the stress of the reinforcement is smaller than f_y and has to be calculated.

7. Example 1

The example presented in the work of Brondum-Nielsen [7] is explained here again in order to check if the compression blocks in both outer layers are deep enough to guarantee that the tensile stress in the reinforcement is the yield stress, f_y. Fig. 11 shows a section of the slab studied in [7], the actions acting on it and the material properties.

The example helps to clarify why the new hypotheses are needed. Fig. 12 shows the 1 × 1 m slab of the example with the external forces and moments depicted. The signs are indicated by the directions of the arrows so the companion numbers only indicate the absolute value of the forces and moments. If the axial forces N_x and N_y were of little importance, clearly the moment M_x (−83 kN m) would command the behavior of the slab. In this case we can deduce that in the top layer the steel in the x-direction can be considered at f_y while the steel in the y-direction will barely be at f_y.

The problem is solved following the flow chart given in Fig. 7. According to it, M_x is the predominant bending moment and it compresses the bottom fiber so $k = b$ and $j = t$. M_a obtained from Eq. (10) is:

$$M_a = 83{,}000 - 67\left(\frac{-120{,}000}{1000}\right) = 91{,}040 \text{ N mm/mm}$$

The first estimation of the thickness of the compressed layer, c_{b0}, is obtained from Eq. (11) with $d_j = d_t = 192$ mm (distance between the lowermost fiber of the cross section and the centroid of x reinforcement in the top layer), that is: $c_{b0} = 87,82$ mm. For this first estimation of c_b, c_{b0}, the membrane forces in the bottom layer are obtained from Eq. (1):

$$a = 192 - \frac{87.82}{2} = 148.09 \text{ mm}$$

$$a_b = \frac{250 - 87.82}{2} = 81.09 \text{ mm}$$

$$N_{xb} = -120\frac{148.09 - 81.09}{148.09} + \frac{-83{,}000}{148.09} = -614.76 \text{ N/mm}$$

$$N_{yb} = 300\frac{148.09 - 81.09}{148.09} + \frac{12{,}000}{148.09} = 216.76 \text{ N/mm}$$

$$N_{xyb} = 170\frac{148.09 - 81.09}{148.09} + \frac{800}{148.09} = 82.31 \text{ N/mm}$$

Since $N_{xb} < -|N_{xyb}|$ and $N_{yb} \geqslant -|N_{xyb}|$ no reinforcement is needed in x direction in the bottom layer.

The crack angle in this layer is obtained from Eq. (6):

$$\alpha_b = \arctan\left(\frac{82.31}{614.76}\right) = 7.63^\circ$$

The principal compression force on the concrete in the bottom layer is:

$$N_{cb} = 82.31[\tan(7.63^\circ) + \cot(7.63^\circ)] = 625.78 \text{ N/mm}$$

Because $c_b = N_{cb}/f_c = 89.40$ mm is deeper than the first estimation – c_{b0}, a value of c_b equal to 90 mm is adopted and the former values recalculated.

$$N_{xb} = -619.37 \text{ N/mm}$$
$$N_{yb} = 218.38 \text{ N/mm}$$
$$N_{xyb} = 82.93 \text{ N/mm}$$

In the bottom layer only reinforcement in y direction is required; the tension force on it is obtained from Eq. (3) as:

$$N_{yab} = 229.47 \text{ N/mm}$$

Assuming that the middle surface of the top layer coincides with the centroid of x reinforcement, the depth of this layer can be obtained:

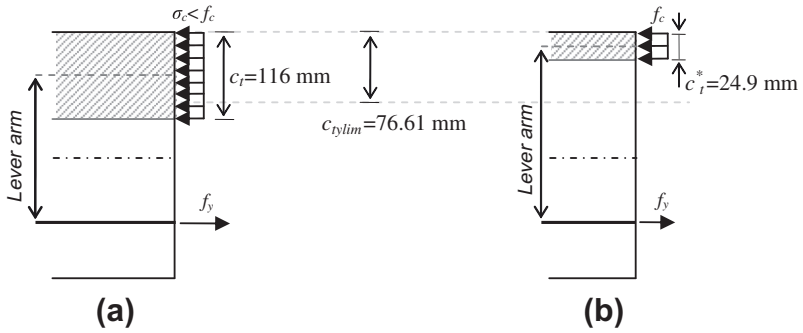

Fig. 13. Compression block for the upper layer. Comparison between the resulting depth (a) assuming that level of top reinforcement is the middle surface of the layer and (b) the resulting depth applying Eq. (9).

$$c_t = 2(250 - 192) = 116 \text{ mm}$$

The values of the membrane forces acting upon it can be computed from Eq. (1):

$$N_{xt} = 499.32 \text{ N/mm}$$

$$N_{yt} = 81.63 \text{ N/mm}$$

$$N_{xyt} = 87.07 \text{ N/mm}$$

Since $N_{xt} \geqslant -|N_{xyt}|$ and $N_{yt} \geqslant -|N_{xyt}|$, then both x and y reinforcements are required in the top layer. The crack angle at this layer is 45° and the values of the tensile forces in x and y directions and the principal compression force in the concrete for the top layer are obtained from Eqs. (2)–(4) as:

$$N_{xat} = 586.39 \text{ N/mm}$$

$$N_{yat} = 168.71 \text{ N/mm}$$

$$N_{ct} = 174.16 \text{ N/mm}$$

It is verified that the corresponding principal compressive stress in the concrete is lower than f_c:

$$\frac{N_{ct}}{c_t} = \frac{174.16}{116} = 1.50 \text{ N/mm}^2 < 7 \text{ N/mm}^2$$

The next step is to relocate the tension forces of the reinforcement in both top and bottom layers. The resultant in x direction does not need to be computed since x reinforcement is not required in the bottom layer and the middle surface of the top layer coincides with the centroid of x reinforcement in this layer. Therefore, it is only necessary to calculate the resultant of tension forces in the y direction of reinforcement.

$$\sum N_{ya} = 398.18 \text{ N/mm}$$

If $z = 0$ is placed on the middle surface of the shell element (Fig. 11), the z coordinate of the point of application of $\sum N_{ya}$ is:

$$z_{ya} = \frac{N_{yat} z_{yat} + N_{yab} z_{yab}}{\sum N_{ya}} = \frac{168.71 \cdot 67 + 229.47(-80)}{398.18} = -17.72 \text{ mm}$$

The actual positions of y reinforcement in top and bottom layer are $z^*_{yat} = 53$ mm and $z^*_{yab} = -23$ mm, the corresponding tension forces at those levels, N^*_{yat} and N^*_{yab}, can be obtained from:

$$N^*_{yat} = \sum N_{ya} \frac{z_{ya} - z^*_{yab}}{z^*_{yat} - z^*_{yab}} = 398.18 \frac{-17.72 + 23}{53 + 23} = 27.68 \text{ N/mm}$$

$$N^*_{yab} = \sum N_{ya} \frac{z^*_{yat} - z_{ya}}{z^*_{yat} - z^*_{yab}} = 398.18 \frac{53 + 17.72}{53 + 23} = 370.50 \text{ N/mm}$$

Once the tensile forces in reinforcement have been determined, the necessary area of steel is obtained dividing by f_y:

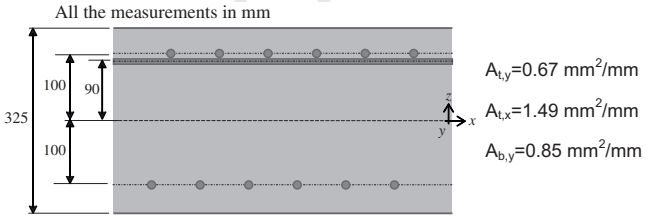

Fig. 14. Modified slab of the example of Brondum-Nielsen and required areas of reinforcement per unit of length.

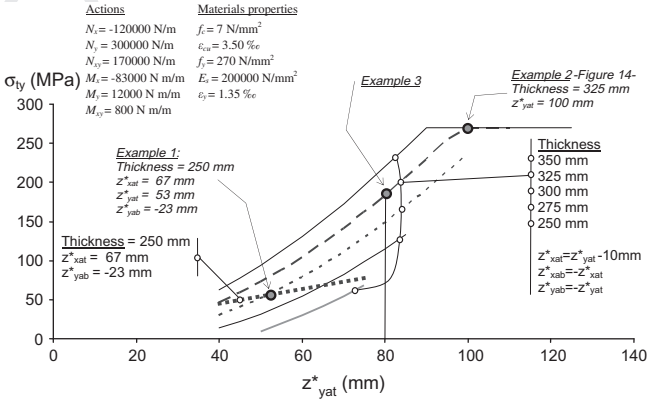

Fig. 15. Stress in the reinforcement in the y-direction of the top layer of the slab as function of the location of the reinforcement for several thicknesses.

$$A_{tx} = 2.17 \text{ mm}^2/\text{mm}$$

$$A_{ty} = 0.10 \text{ mm}^2/\text{mm}$$

$$A_{by} = 1.37 \text{ mm}^2/\text{mm}$$

The Brondum-Nielsen procedure ends here. According to the hypothesis discussed in this paper, it has to be verified that the steel has yielded, in the case that it has not, a different stress value must be considered.

7.1. The proposed procedure

In order to verify that reinforcement has yielded, the proposed methodology is applied. For the bottom layer, the angle of inclination of the cracks – i.e. the orientation of the principal compressive stress in concrete – is $\alpha_b = 7.63°$. In the top layer both x and y reinforcements are required, their yielding strains and their corresponding maximum thickness in the opposite layer are – Eqs. (13) and (14) respectively:

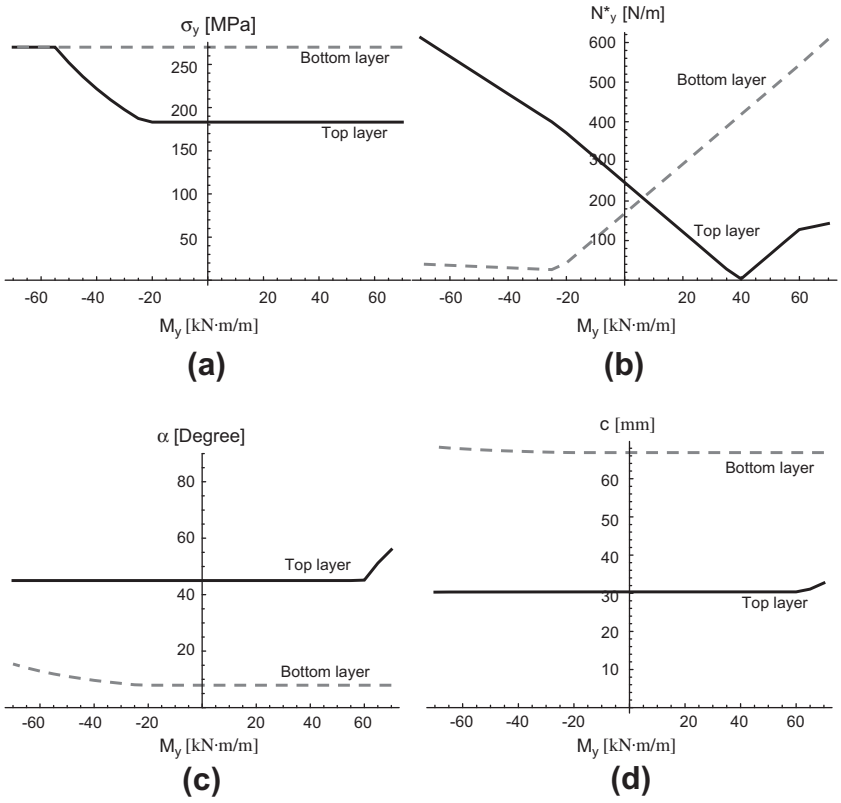

Fig. 16. Example 3.

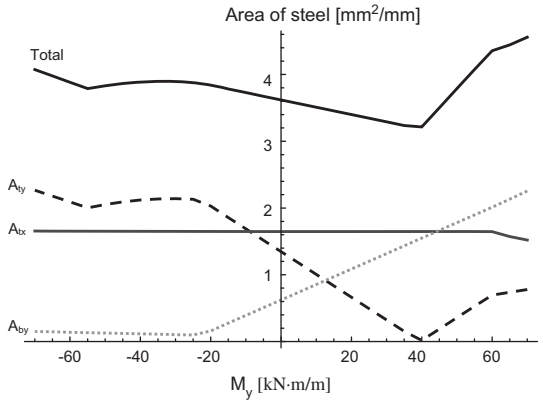

Fig. 17. Steel areas.

– For x reinforcement:

$$\varepsilon_{t-x\lim-\alpha b} = \frac{\varepsilon_y}{\cos 7.63^\circ} = \frac{0.00135}{\cos 7.63^\circ} = 0.00136$$

$$c_{bx\lim} = \lambda \cdot d_{tx} \frac{\varepsilon_{cu}}{\varepsilon_{t-x\lim-\alpha b} + \varepsilon_{cu}} = 0.8 \cdot 192 \frac{0.0035}{0.00136 + 0.0035} = 110.62\,\text{mm}$$

– For y reinforcement:

$$\varepsilon_{t-y\lim-\alpha b} = \frac{\varepsilon_y}{\sin 7.63^\circ} = 0.010$$

$$c_{by\lim} = \lambda \cdot d_{ty} \frac{\varepsilon_{cu}}{\varepsilon_{t-y\lim-\alpha b} + \varepsilon_{cu}} = 0.8 \cdot 178 \frac{0.0035}{0.010 + 0.0035} = 36.45\,\text{mm}$$

From comparison of the thickness of the bottom layer (c_b = 90 mm) with $c_{bx\lim}$ and $c_{by\lim}$ it is clear that x reinforcement in the top layer is yielded but not, however, the y reinforcement. It was deduced in light of Fig. 12 and commented at the beginning of the example. The area of steel in x direction per unit of length can be obtained as:

$$A_{tx} = \frac{N_{xat}}{f_y} = \frac{586.39\ \text{N/mm}}{270\ \text{N/mm}^2} = 2.17\ \text{mm}^2/\text{mm}$$

According to the hypotheses considered in the paper, for c_b = 90 mm steel in y direction is in the elastic domain and its strain and stress are:

$$\varepsilon_{t-y} = \frac{d_{ty} - c_b/0.8}{c_b/0.8} \varepsilon_{cu} \sin\alpha_b = \frac{178 - 90/0.8}{90/0.8} 0.0035 \sin 7.63^\circ = 0.00027$$

$$\sigma_{t-y} = E_s \cdot \varepsilon_{t-y} = 53.98\,\text{MPa}$$

The required area of steel in y direction per unit of length is:

$$A_{ty} = \frac{N^*_{yat}}{\sigma_{t-y}} = \frac{27.68\ \text{N/mm}}{53.98\ \text{N/mm}^2} = 0.513\ \text{mm}^2/\text{mm}$$

In the case of steel in the bottom layer, the orientation of the strain plane is defined by the principal direction of compression in the top layer. For the top layer, α_t = 45°. In the bottom layer only y reinforcement is required so the strain in the principal tensile direction is given by:

$$\varepsilon_{b-y\lim-\alpha t} = \frac{\varepsilon_y}{\sin 45} = 0.0019$$

If the compression block depth obtained as $c^*_t = N_{ct}/f_c$ = 24.9 mm is considered for the top layer, as represented in Fig. 13(b), the maximum value of the compression block depth for which the y reinforcement yields can be obtained from Eq. (14) would be:

$$c_{ty\lim} = \lambda \cdot d_{by} \frac{\varepsilon_{cu}}{\varepsilon_{b-y\lim-\alpha t} + \varepsilon_{cu}} = 0.8 \cdot 148 \frac{0.0035}{0.0019 + 0.0035} = 76.61\,\text{mm}$$

This approach is safe because membrane forces were supposed to act with a smaller lever arm with respect to the lower reinforcement as Fig. 13 shows, so the calculated membrane forces are greater than the actual ones.

Because $c_t^* = 24.9\ \text{mm} < c_{tylim} = 76.61\ \text{mm}$ the y reinforcement in the bottom layer yields and therefore, the corresponding area of steel can be obtained dividing the tensile force ~~between~~ f_y:

$$A_{by} = \frac{N_{yab}^*}{f_y} = \frac{370.50\ \text{N/mm}}{270\ \text{N/mm}^2} = 1.37\ \text{mm}^2/\text{mm}$$

An alternative, in order to force the yielding of the y reinforcement in the top layer, is to change the geometry of the layers. This modification of the geometry may involve increasing the thickness of the slab and/or relocating the reinforcement.

8. Example 2

The previous slab is modified as indicated in Fig. 14, in this case all the reinforcement yield, i.e. the required cross-sectional areas of reinforcement per unit of length can be obtained dividing the tensile forces ~~between~~ f_y. These required areas of reinforcement are summarized in Fig. 14.

A detailed study of the stress of the top reinforcement in y-direction (σ_{ty}) relative to the thickness of the slab and the position of the steel for the same external loading as those considered in the previous example are shown in Fig. 15. The example of Fig. 14 can be observed in Fig. 15, if the thickness of the slab is reduced or if the lever arm of the y reinforcement of the top layer is reduced then the steel will not yield. The line of thickness equal to 250 mm and with the geometry of the slab considered in example 1 is also shown, this line contains the case analyzed in the example 1.

9. Example 3

Fig. 16 shows the values corresponding to strength design of one slab as function of the flexural moment, M_y. The geometry of the slab is defined by, thickness = 325 mm, z_{yat} = 80 mm, and is represented in Fig. 15 with the label Example 3. It is made with concrete f_c = 7 MPa and steel f_y = 270 MPa.

Beside M_y, which is considered as variable, the rest of forces and moments acting on the slab are kept constants:

$$N_x = -120{,}000\ \text{N/m},\ N_y = 300{,}000\ \text{N/m},$$
$$N_{xy} = 170{,}000\ \text{N/m},\ M_x = -83{,}000\ \text{N m/m and}$$
$$M_{xy} = 800\ \text{N m/m}.$$

As is observed in Figs. 15 and 16 the y-reinforcement in the top layer is not yielded for the value of M_y considered in the previous example (M_y = 12,000 Nm/m).

Fig. 16(a) represents stresses in the reinforcement in the y-direction for both top and bottom layers, (b) the tension forces in the y-reinforcement for both top and bottom layers, (c) the angle of the crack with respect to the x-direction for both top and bottom layers and (d) the depth of the bottom layer.

Fig. 17 represents the areas of steel as M_y increases, as can be observed as M_y increases bottom steel in y-direction increases and the upper steel in y-direction decreases.

10. Conclusions

The Sandwich element analogy is the most relevant hypothesis used in the bending ultimate limit design of shells and slabs. Once the geometry of the outer layers and the membrane forces acting on them are determined, the tension forces in the reinforcement and the principal compressive force in the concrete can easily be obtained from equilibrium conditions. Finally, Brondum-Nielsen's work [7] aims to compute the necessary amount of reinforcing steel per unit length dividing these tension forces by the steel yield stress, f_y.

In the present work, the Brondum-Nielsen approach has been summarized in detail and it has been shown that this procedure needs to be applied under some restrictions since reinforcement yielding cannot always be guaranteed. Taking as reference the determination of the balance point concept widely used in beams and columns, a procedure has been developed in order to determine the limits of application of Brondum-Nielsen's method. If these limits are exceeded, either the geometry of the slab or the reinforcement stresses and areas need to be modified.

Acknowledgements

The present work was financed by the Spanish Ministry of Education. The second author is a Spanish Government PhD fellow (FPU grant AP 2010-3707). This support is gratefully acknowledged.

References

[1] Schladitz F, Frenzel M, Ehlig D, Curbach M. Bending load capacity of reinforced concrete slabs strengthened with textile reinforced concrete. Eng Struct Q4 2012;40:317–~~26~~.
[2] Smith ST, Hu S, Kim SJ, Seracino R. FRP-strengthened RC slabs anchored with FRP anchors. Eng Struct 2011;33(4):1075–~~87~~.
[3] Jia X. Revisiting the failure mode of a RC hyperbolic cooling tower, considering changes of material and geometric properties. Eng Struct 2013;47. 148-7.
[4] EC 2. Eurocode 2: Design of concrete structures_Part 1–1: General rules and rules for buildings EN 1992-1-1. Brussels: European Committee for Standarization; 2004.
[5] ACI Committee 318. Building code requirements for structural concrete (ACI 318-08). Farmington Hills (MI): American Concrete Institute; 2008.
[6] FIB. Model Code 2010. Model Code 2010 – Final draft, vol. 1. Fib Bulletin No. 65. Lausanne: International Federation for Structural Concrete; 2012.
[7] Broundum-Nielsen T. Optimum design of reinforced concrete shells and slabs. Report No R44. Copenhagen: Structural Research Laboratory, University of Denmark; 1974.
[8] Gupta AK. Combined membrane and flexural reinforcement in plates and shells. ASCE J Struct Div 1986;112(3):550–~~7~~.
[9] Marti P. Design of concrete slabs for transverse shear. ACI Struct J 1990;87(2).
[10] Lourenço PB, Figuerias JA. Automatic design of reinforcement in concrete plates and shells. Eng Comput 1993;10(6):519–23.
[11] Lourenço PB, Figueiras JA. Solution for the design of reinforcement concrete plates and shells. J Struct Eng ASCE 1995;121(5):815–9.
[12] Fall D, Lundgren K, Rempling R, Gylltof K. Reinforcing tailor-made concrete structures: alternatives and challenges. Eng Struct 2012;44:372–7.
[13] Min CS. Design and ultimate behaviour of RC plates and shells. Nucl Eng Des 2004;228:207–17.
[14] Min CS, Gupta AK. A study of inelastic behaviour of reinforced concrete shells using supercomputers. Technical Report. Raileigh (NC): North Carolina State University; 1992.
[15] Min CS, Gupta AK. Vector algorithm for layered reinforced concrete shell element stiffness matrix. Struct Eng Mech 1995;3(2):~~12–172~~.
[16] Min CS, Gupta AK. Inelastic vector finite element analysis of RC shells. Struct Eng Mech 1996;4(2):~~10–139~~.
[17] Mahmoud BEH, Gupta AK. Inelastic large displacement behaviour and buckling of hyperbolic cooling tower shells. Technical Report. Raileigh (NC): North Carolina State University; 1993.
[18] Tomás A, Martí P. Design of reinforcement for concrete co-planar shell structures using optimization techniques. Meccanica 2010;45. 657-13.
[19] Bertagnoli G, Giordano L, Mancini S. Design and optimization of skew reinforcement in concrete shells. Struct Concr 2012;13(4):~~248–58~~.
[20] <https://wiki.csiberkeley.com/display/kb/Shell±reinforcement±design>.
[21] Hernández-Montes E, Gil-Martín LM, Pasadas M, Aschheim M. Theorem of optimal section reinforcement. Struct Multidiscip Optim 2008;36(5):509–13.
[22] Aschheim M, Hernández-Montes E, Gil-Martín LM. Optimal domains for strength design of rectangular sections for axial load and moment according to Eurocode 2. Eng Struct 2007;29(8):1752–9.

ISI Web of Knowledge℠

Journal Citation Reports®

WELCOME HELP RETURN TO JOURNAL

2012 JCR Science Edition

Rank in Category: ENGINEERING STRUCTURES

Journal Ranking

For **2012**, the journal **ENGINEERING STRUCTURES** has an Impact Factor of **1.713**.

This table shows the ranking of this journal in its subject categories based on Impact Factor.

Category Name	Total Journals in Category	Journal Rank in Category	Quartile in Category
ENGINEERING, CIVIL	122	18	Q1

Category Box Plot

For **2012**, the journal **ENGINEERING STRUCTURES** has an Impact Factor of **1.713**.

This is a box plot of the subject category or categories to which the journal has been assigned. It provides information about the distribution of journals based on Impact Factor values. It shows median, 25th and 75th percentiles, and the extreme values of the distribution.

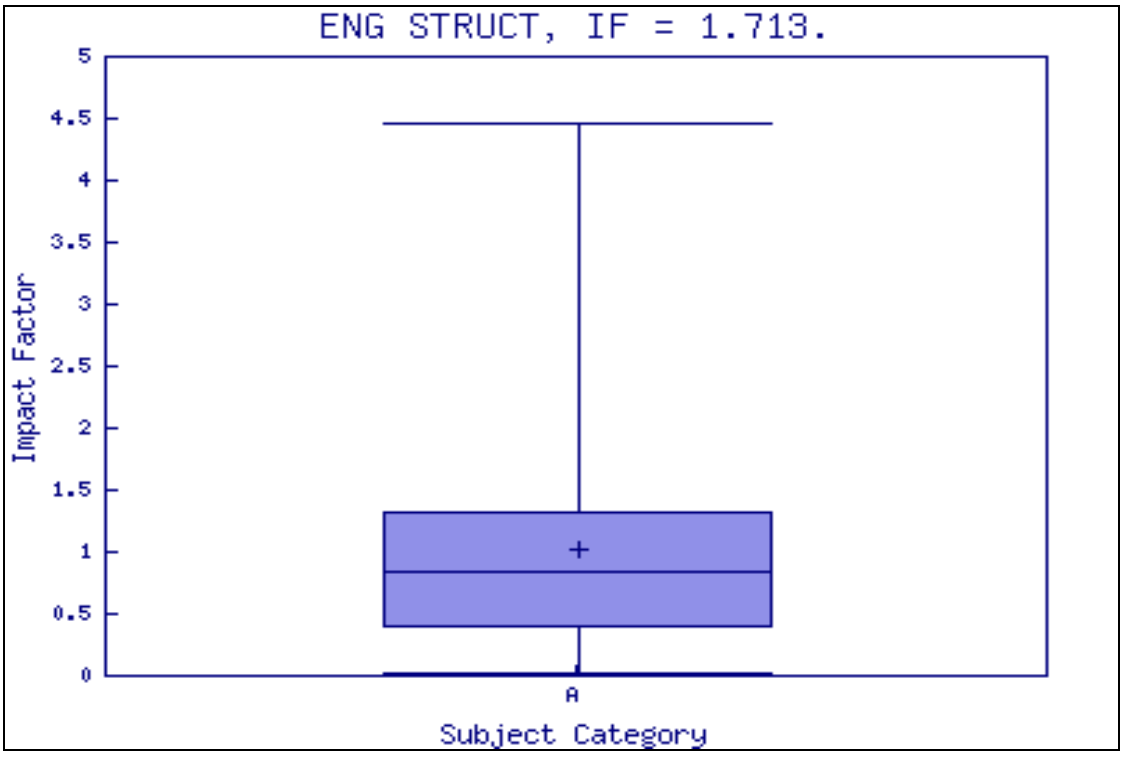

Key

A - ENGINEERING, CIVIL